FRACTAL-LIKE FINITE ELEMENT METHOD AND STRAIN ENERGY APPROACH FOR COMPUTATIONAL MODELLING AND ANALYSIS OF GEOMETRICALLY V-NOTCHED PLATES

A THESIS SUBMITTED TO THE UNIVERSITY OF MANCHESTER FOR THE DEGREE OF DOCTOR OF PHILOSOPHY IN THE FACULTY OF ENGINEERING AND PHYSICAL SCIENCE

2012

MUHAMMAD TREIFI

SCHOOL OF MECHANICAL, AEROSPACE AND CIVIL ENGINEERING

Table of Contents[1]

[1] Word Count: 60000.

Nomenclature

a	Crack/Notch length
a, c	Set of generalised co-ordinates
B	strain-displacement operator
A, B, a, b	Constants
C_1, C_2, C_3, C_4	Constants
d	Nodal displacement vector
$\mathbf{d}_r$, $\mathbf{d}_m$, and $\mathbf{d}_s$	Nodal displacement vectors of nodes in regular region, master nodes, and in singular region
$\mathbf{d}_s^{1st,2nd,...}$	Nodal displacements of the nodes in the first layer, second layer, … in the singular region
D	Material property matrix
E	Young's modulus
$E^{(e)}$	Strain energy
f	Nodal force vector
$\mathbf{f}_r$, $\mathbf{f}_m$, and $\mathbf{f}_s$	Nodal force vectors of nodes in regular region, master nodes, and in singular region
$\bar{\mathbf{f}}_s^{1st,inn}$	Transformed nodal force vectors of the first layer and the inner layers in the singular region
G	Shear modulus
H, h	Plate height
h_c	distance between crack/notch tip and bottom boundary of plate
H	constitutive matrix

$\mathbf{k}$	Element stiffness matrix
$\mathbf{K}$	Stiffness matrix
$\mathbf{K}_{rr}$, $\mathbf{K}_{mr}$, $\mathbf{K}_{mm}$, $\mathbf{K}_{ss,\ \ldots}$	Partitioned stiffness matrices (r refers to regular region, m to master nodes, and s to slave nodes)
$\mathbf{K}_s^n$	partitioned stiffness matrix of the n^{th} layer in the singular region
$\overline{\mathbf{K}}_s^{1st}$, $\overline{\mathbf{K}}_s^{inn}$	Transformed partitioned stiffness matrices of the first layer and the inner layers in the singular region
K_I, K_{II}, K_{III}	Stress intensity factors of mode I, II, III
K_c	Complex stress intensity factor
K_{Ic}	Fracture toughness
i	Complex unit $\left(\sqrt{-1}\right)$; integer variable
j	Integer variable
$\mathbf{J}$	Jacobian Matrix
J	Determinant of the Jacobian Matrix
m, n	Integer variables
$\mathbf{N}$	shape function matrix
NL, nl	Number of layers in the singular region
NT, nt	Number of terms of eigenfunction series expansion
P_x, P_y	Resultant forces
R_0	Radius of region meshed using a similarity ratio
R_c	Radius of control volume
R_s	Radius of singular region
r, θ	Polar co-ordinates

t	Plate thickness
$\mathbf{T}$	Transformation matrix
$\mathbf{T}_s^n$	Transformation matrix of the nodal displacements of the nth layer in the singular region
$\mathbf{T}_s^{1st}$	Transformation matrix of the nodal displacements of the first layer in the singular region
$\mathbf{T}_c$	Matrix of direction cosines
$\mathbf{u}$	Displacement field
u_x, u_y	Displacements in x and y directions
V	Volume
w	Displacement in z directions
W	Width of single-edge-notched plate or half width of double-edge-/centre- notched plate
$W^{(e)}$	Strain energy density
x, y, z	Cartesian co-ordinates
z	Complex variable
α	Angle between notch face and x-axis
β	Angle between notch bisector and x-axis
$[\delta]$	Diagonal matrix
Δ_x, Δ_y	Relative displacements in x and y directions
ε	Normal strain
$\boldsymbol{\varepsilon}$	strain vector
γ	Notch opening angle; shear strain
$\Gamma_1, \Gamma_2, \Gamma_3, ...$	Curves labels

ϕ, ω, Ω	Complex potentials
Φ	Airy stress function
λ	Eigenvalue
ν	Poisson's ratio
ρ	Similarity ratio
σ	Normal stress
$\boldsymbol{\sigma}$	Stress vector
σ_t	Ultimate tensile strength
τ	Shear stress
ξ , η	Natural coordinates
∇^2	The Laplacian operator

Abstract

Fractal-like Finite Element Method and Strain Energy Approach for Computational Modelling and Analysis of Geometrically V-notched Plates

Muhammad Treifi
Doctor of Philosophy
The University of Manchester
December 2012

The fractal-like finite element method (FFEM) is developed to compute stress intensity factors (SIFs) for isotropic homogeneous and bi-material V-notched plates. The method is semi-analytical, because analytical expressions of the displacement fields are used as global interpolation functions (GIFs) to carry out a transformation of the nodal displacements within a singular region to a small set of generalised coordinates. The concept of the GIFs in reducing the number of unknowns is similar to the concept of the local interpolation functions of a finite element. Therefore, the singularity at a notch-tip is modelled accurately in the FFEM using a few unknowns, leading to reduction of the computational cost.

The analytical expressions of displacements and stresses around a notch tip are derived for different cases of notch problems: in-plane (modes I and II) conditions and out-of-plane (mode III) conditions for isotropic and bi-material notches. These expressions, which are eigenfunction series expansions, are then incorporated into the FFEM to carry out the transformation of the displacements of the singular nodes and to compute the notch SIFs directly without the need for post-processing. Different numerical examples of notch problems are presented and results are compared to available published results and solutions obtained by using other numerical methods.

A strain energy approach (SEA) is also developed to extract the notch SIFs from finite element (FE) solutions. The approach is based on the strain energy of a control volume around the notch-tip. The strain energy may be computed using commercial FE packages, which are only capable of computing SIFs for crack problems and not for notch problems. Therefore, this approach is a strong tool for enabling analysts to compute notch SIFs using current commercial FE packages. This approach is developed for comparison of the FFEM results for notch problems where available published results are scarce especially for the bi-material notch cases.

A very good agreement between the SEA results and the FFEM results is illustrated. In addition, the accuracy of the results of both procedures is shown to be very good compared to the available results in the literature. Therefore, the FFEM as a stand-alone procedure and the SEA as a post-processing technique, developed in this research, are proved to be very accurate and reliable numerical tools for computing the SIFs of a general notch in isotropic homogeneous and bi-material plates.

Declaration

No portion of the work referred to in the thesis has been submitted in support of an application for another degree or qualification of this or any other university or other institute of learning.

Copyright

i. The author of this thesis (including any appendices and/or schedules to this thesis) owns certain copyright or related rights in it (the "Copyright") and s/he has given The University of Manchester certain rights to use such Copyright, including for administrative purposes.

ii. Copies of this thesis, either in full or in extracts and whether in hard or electronic copy, may be made only in accordance with the Copyright, Designs and Patents Act 1988 (as amended) and regulations issued under it or, where appropriate, in accordance with licensing agreements which the University has from time to time. This page must form part of any such copies made.

iii. The ownership of certain Copyright, patents, designs, trade marks and other intellectual property (the "Intellectual Property") and any reproductions of copyright works in the thesis, for example graphs and tables ("Reproductions"), which may be described in this thesis, may not be owned by the author and may be owned by third parties. Such Intellectual Property and Reproductions cannot and must not be made available for use without the prior written permission of the owner(s) of the relevant Intellectual Property and/or Reproductions.

iv. Further information on the conditions under which disclosure, publication and commercialisation of this thesis, the Copyright and any Intellectual Property and/or

Reproductions described in it may take place is available in the University IP Policy (see http://www.campus.manchester.ac.uk/medialibrary/policies/intellectual-property.pdf), in any relevant Thesis restriction declarations deposited in the University Library, The University Library's regulations (see http://www.manchester.ac.uk/library/aboutus/regulations) and in The University's policy on presentation of Theses.

Acknowledgement

I would like to express my gratitude to the academic and administrative staff of the School of Mechanical, Aerospace and Civil Engineering for their understanding and support, especially during the hardship I had been through during the course of this research. I would like to specifically thank Dr Oyadiji, my supervisor, for his continuous guidance and supervision. I would also like to thank Dr Tsang for his academic support at the start of this research project. I would also like to thank Miss Beverley Knight from the administrative team for her help and support.

Finally, I would like to thank my wife, Susanne, for her continuous support and encouragement and my little sons, Karim and Jonas, for their “patience and understanding”. My heart also goes to my parents, brother and sisters back in Syria hoping you are always safe.

Chapter 1

Introduction

1. Introduction

1.1. Background and Motivation

The presence of cracks in structural elements leads to stress intensities at the crack tips. This may lead to a catastrophic sudden failure of those structures. Therefore, a lot of research has been dedicated to finding parameters to characterise the fracture caused by cracks. Some of those parameters, that are used today, are the stress intensity factors (SIFs), the J-integral, and the crack tip opening displacement, which are used as failure criteria. Relationships between these parameters exist in linear elastic fracture mechanics.

The presence of notches, too, leads to stress intensities at the notch tips. A crack is a special case of a notch (a notch with an opening angle of zero is basically a crack). Therefore, developing new methods and/or extending existing methods of computing fracture parameters of a crack to compute general fracture parameters of a notch is of high relevance. This is because it would allow interested designers and analysts to compute fracture parameters of any general case of stress intensity.

The usefulness is greater if a method can be developed or extended to compute fracture parameters for notches and cracks in two different materials joined together. This is important, because of the use of components made up of different materials joined together in different engineering fields. Those fracture parameters help the designer and the operator to understand the mechanical integrity of such bi-material components. This could also be used to assess the bonding strength of an adhesive between the different joined materials.

Many researchers have dedicated a lot of research to attempt to treat notches along the interface of a bi-material component. However, because of the complicated nature of such cases, they only produced results for stress singularities of bi-material notches without producing results of the more useful parameters, such as the SIFs.

The fractal-like finite element method (FFEM) is a semi-analytical method that was initially developed in the 1980s in Hong Kong to compute the SIFs of crack problems. Its results are of good accuracy and it is easy to implement in a finite element (FE) code as only matrix multiplication is involved, provided that "good" global interpolation functions (GIFs) are used. From the late 1990s, researchers at Manchester have extended the FFEM to multiple penny-shaped cracks, thermoelastic crack problems and dynamic crack problems. However, none of the researchers in Hong Kong or Manchester have investigated notch problems. Therefore, the main objective of this thesis is to extend the FFEM to compute the SIFs of general notch cases of isotropic and bi-material cases, along with attempts to develop other approaches to extract the SIFs for a general notch from commercial FE packages. This is because most FE commercial packages are capable of computing the SIFs for cracks but not for general notches.

1.2. Aims and Objectives

The specific objectives of this study are:

1. Derivation of global interpolation functions for an isotropic notch under mode I, II and III loading conditions.

2. Extending the FFEM to compute the SIFs for symmetric isotropic notch under mode I, II and III loading conditions.
3. Dealing with asymmetric isotropic notch using FFEM.
4. Derivation of global interpolation functions for a bi-material notch under mode I, II and III loading conditions.
5. Extending the FFEM to compute the SIFs for bi-material notch under mode I, II and III loading conditions.
6. Developing a technique for extracting SIFs values from commercial FE packages based on the strain energy for comparison.

1.3. Contributions to Knowledge

This research provides a means to compute the SIFs for general notch problems. It develops the FFEM to compute notch SIFs as a stand-alone method. To evaluate the accuracy of the predicted notch SIFs values by the FFEM, comparison with available published results is carried out. However, for many cases considered there are no available published results to compare with especially in the cases of bi-material notch problems. Therefore, a comparison is carried out with crack cases for which published results exist or numerical results are obtainable using commercial FE packages, as a crack is simply a special case of a notch. Although this comparison proves partially and, to a certain degree, sufficiently that the FFEM provides accurate results, the necessity to compare FFEM results, especially for the bi-material cases, with another method seems in order as it will enable the validation of the newly developed FFEM for analysing bi-material notches. Therefore, a lot of effort and research has been devoted to overcome this, and an approach based on the strain energy of a singular region around the notch tip

to compute the notch SIFs is developed. The strain energy can be easily computed using a commercial FE package. This makes this approach quite appealing, as it makes it easy to extract notch SIFs using commercial FE packages, which to my knowledge are not capable of computing SIFs of a general notch.

In addition, the many examples of different notch shapes and locations subjected to different loading conditions give a valuable insight into the behaviour of the SIFs values as the notch gets closer to the boundaries or as the material properties of a bi-material notch vary. Many of those results are new.

In list form, the contributions to knowledge are as follows:

1. Development of the FFEM to compute mode I and II SIFs for isotropic notch problems.
2. Development of the FFEM to compute mode I and II SIFs for isotropic asymmetric notch problems.
3. Development of the FFEM to compute mode III SIFs for isotropic notch problems.
4. Development of the FFEM to compute mode III SIFs for bi-material notch problems.
5. Development of the FFEM to compute mode I and II SIFs for bi-material notch problems.
6. Development of the SEA to extract mode I, II and III SIFs for isotropic and bi-material notch problems from FE solutions produced using commercial FE packages.

1.4. Layout of Thesis

This thesis is presented in an Alternative Format, meaning that its core context is presented in the form of research papers that have been published in externally refereed contexts. Therefore, this thesis is divided into twelve chapters. ***Chapter one*** defines the aims and objectives, justifies the undertaking and highlights the contributions to knowledge of the study. ***Chapter two*** provides a literature review of the methods that have been developed and used to compute SIFs for cracks and notches. ***Chapter three*** provides a general theoretical background of the FFEM and the mathematical derivations of the global interpolation functions. ***Chapter four*** provides a research overview and a summary of the papers included in the thesis. The following seven chapters, ***Chapter five to Chapter eleven***, are the published research papers that demonstrate the methods and findings of the research undertaken. The sections of these papers are listed in the Table of Contents. However, the pagination of the thesis does not include the pages numbers of the papers. Hence, ***Chapters five to eleven*** appear at pages 110, 111, 112, etc.

Chapter five presents a copy of a journal paper entitled "*Computation of the stress intensity factors of sharp notched plates by the fractal-like finite element method*" that has been published in the International Journal for Numerical Methods in Engineering. In this paper the FFEM is developed to compute SIFs values for the in-plane problem (mode I and II) under tension. ***Chapter six*** presents a copy of a journal paper entitled "*Computations of modes I and II stress intensity factors of sharp notched plates under in-plane shear and bending loading by the fractal-like finite element method*" that has been published in the International Journal of Solids and Structures. In this paper, the FFEM code is extended to compute the notch SIFs for plates subjected to in-plane shear and

bending loading conditions. ***Chapter seven*** presents a copy of a conference paper entitled "*Computations of SIFs for non-symmetric v-notched plates by the FFEM*" that has been published in the Proceedings of the ASME 2009 International Design Engineering Technical Conferences & Computers and Information in Engineering Conference IDETC/CIE 2009 August 30 - September 2, 2009, San Diego, CA, USA. In this paper the method is extended to compute the SIFs for non-symmetric notch cases. ***Chapter eight*** presents a copy of a journal paper entitled "*Computations of the stress intensity factors of double-edge and centre V-notched plates under tension and anti-plane shear by the fractal-like finite element method*" that has been published in the journal Engineering Fracture Mechanics. In this paper, the FFEM is developed to compute mode III SIFs for notches subjected to out-of-plane loading conditions. All the aforementioned work was on developing the FFEM to compute SIFs for isotropic homogeneous cases.

Chapter nine presents a copy of a journal paper entitled "*Evaluation of mode III stress intensity factors for bi-material notched bodies using the fractal-like finite element method*" that has been published (early view) in the journal Computers and Structures. In this paper, the FFEM is developed to compute the mode III SIFs for bi-material notches. ***Chapter ten*** presents a copy of a journal paper entitled "*Strain Energy Approach to Compute Stress Intensity Factors for Isotropic Homogeneous and Bi-material V-notches*" that has been published (early view) in the International Journal of Solids and Structures. In this paper, an approach to compute SIFs for general notches in isotropic homogeneous or bi-material plates based on the strain energy is developed. ***Chapter eleven*** presents a copy of a journal paper entitled "*Bi-material V-notch Stress Intensity Factors by the Fractal-like Finite Element Method*" that has been published (early view) in the journal Engineering Fracture Mechanics. In this paper, the FFEM is developed to compute the

mode I and II SIFs for bi-material notches. ***Chapter twelve*** concludes the thesis, summarises the findings and makes suggestions for future work.

Chapter 2

Literature Review

2. Literature Review

2.1. Historical Background of Fracture Mechanics

Structures were traditionally designed so that the internal stresses would be below certain limiting values, which were usually taken as the yield stress values of the materials used. This approach is insufficient, because materials may have defects such as cracks, dislocations or impurities, etc, or a structure may have sharp corners, notches, or holes. All of these may cause the stresses to rise and are considered stress raisers. As a result the structure might fail at much lower values of the stresses. Many historic catastrophic failures of major structures such as bridges, ships, aircraft, pipelines, and tanks have happened as a result of not only inadequate design but also because of the pre-existence of flaws in the materials, leading not only to financial losses but also to the loss of many lives. An example is the failure sustained by the World War II Liberty ships. Of about 2700 ships built during World War II, roughly 400 sustained fractures, of which 90 were serious. Twenty ships sustained complete failure; ten of them basically broke in two (Anderson, 1995). Most of the fractures initiated on the deck at square hatch corners. The investigations of the fracture problem that occurred during the decade after the War led to the development of the field which we now know as Fracture Mechanics.

Griffith (1920) carried out one the earliest systematic investigation of fracture problems based on the existing development of the stress analysis of an elliptical hole performed by Inglis (1913). Griffith's theory is based on energy balance. He noted that in case of the presence of a crack in a loaded plate, a balance must be attained between the decrease in potential energy and the increase in surface energy resulting from the presence of the

crack. However, his approach was too primitive for engineering applications and was only good for brittle materials. Subsequent efforts to make it applicable to metals were not successful, until a breakthrough was achieved by Irwin (1948) to extend Griffith approach to metals by including the energy dissipated by local plastic flow. He also developed the concept of *strain energy release rate* (Irwin, 1957) which was related to Griffith's approach but was more useful for engineering problems. Irwin's work was based on the assumption that solutions to crack problems could be obtained using elastic considerations if the plastic zone around the crack tip was small. Utilising Westergaard's (1939) solutions for a cracked body, Irwin showed that the displacements and stresses near a crack tip could be described by a single constant related to the strain energy rate. This constant later became known as the Stress Intensity Factor.

During the same period, Williams (1952, 1957) derived the stress and displacement expressions for the singular region around a notch/crack tip under generalised in-plane loading. The expressions were shown to be eigenfunction series expansions, which are referred to in the literature as Williams' eigenfunction series expansions to acknowledge his effort. He was the first to demonstrate the $r^{-\frac{1}{2}}$ singularity for elastic crack problems, which has offered substantial understanding of the type of singularity near the crack tip, and paved the way forward for future research.

Around the 1960s, the fundamentals of Linear Elastic Fracture Mechanics (LEFM) were fairly well established, and scientists began to give attention to crack-tip plasticity, since LEFM ceases to be valid when there is a significant plastic zone around the crack tip. Many researchers suggested a yielding correction at the crack tip. Irwin (1961) suggested a correction that was a very simple extension of LEFM. Dugdale (1960) and Barenblatt

(1962) independently developed more detailed models based on a narrow strip of yielded material at the crack tip. Wells (1961) recognised that the crack faces moved apart with plastic deformation, which led to the development of the concept called the crack-tip-opening displacement (CTOD). Rice (1968) was able to generalise the energy release rate to nonlinear materials by idealising the plastic deformation behaviour as nonlinear elastic. He explained that the nonlinear energy release rate can be expressed as a path-independent line integral, called the J-integral (or domain integral), evaluated along an arbitrary contour around the crack tip.

Recent research trends have been related to dynamic and time-dependent fracture mechanics of linear and nonlinear materials, and to the development of microstructural models for fracture and models to relate local and global fracture behaviour of materials.

2.2. Stress Intensity Factors (SIFs):

In LEFM, the stress intensity factors (SIFs) characterise the stress, strain, and displacement fields in the crack/notch tip region and have a significant function in virtually all fracture problems. For example, in failure design studies, it is necessary to accurately evaluate SIFs in order to determine fracture parameters such as the critical crack length, the fracture loads and the service life of a structural component. Fast, reliable and accurate computations of SIFs are often necessary in practical applications such as in the design of new structures or in the assessment of the integrity of existing structures. This is especially true for high integrity structures such as nuclear reactor cores, aircraft, submarines and spacecraft. Another area of major application is in welded structures.

The general solutions for the stresses and displacements near the crack tip can be expressed in terms of the three SIFs related to three basic cracking modes as illustrated in Figure 2.1: the opening mode referred to as mode I (K_I), the sliding (or in-plane shear) mode referred to as mode II (K_{II}), and the tearing (or out-of-plane shear) mode referred to as mode III (K_{III}). When a SIF value, for example the value of K_I, reaches a critical value, rapid crack growth occurs. The critical value is a material property and is known as the fracture toughness (K_{IC}). The fracture toughness of a material is determined experimentally.

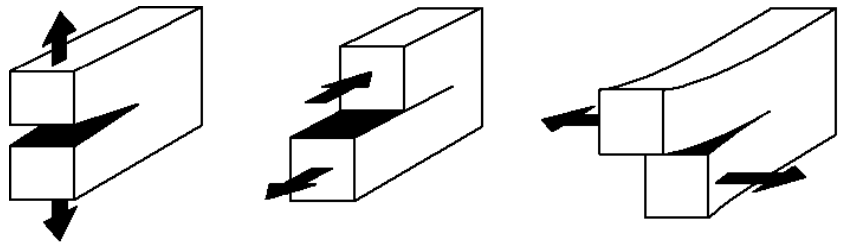

(a) (b) (c)

Figure 2.1. Basic Modes of Fracture: (a) mode I; (b) mode II; and (c) mode III.

Similarly, as notch or sharp corners lead to stress intensities at the notch tip, notch SIFs could be used to characterise the notch tip conditions. Therefore, the study of stress intensities at a corner/notch is of high importance, because the presence of corners in a structure may result in crack initiation leading to a structural failure or shortening of the service life of the structure (recall the Liberty ships where the crack initiated at the corners of square hatches). The importance is even higher in the case of composite bodies, which comprise isotropic materials jointed together, because it could be used, for example, to evaluate the adhesive strength. Therefore, much effort and research has been

devoted to the analysis of sharp notch problems and computation of notch SIFs. By analogy to the fracture criterion for cracks, Seweryn (1994) proposed a general fracture criterion for notches; i.e. Failure occurs when the notch SIFs reach critical values. Other researchers who tried to establish a failure criterion for a notch are Knésl (1991), Gómez and Elices (2003), and Carpinteri et al. (2008). Knésl (1991) extended the stability criterion of a crack to the general case of a notch. Gómez and Elices (2003) showed the advantages of the cohesive crack model for predicting fracture of notched components, and recently Carpinteri et al. (2008) presented an expression for the generalised fracture toughness which is a function of the material tensile strength, the fracture toughness and the notch opening angle.

Many researchers have developed various methods and procedures to compute the SIFs using experimental, analytical, numerical or semi-analytical methods. Experimental methods such as photoelasticity, moire′, or caustics could be used to obtain SIFs (Sih, 1981). The SIFs cannot be measured directly in an experiment, but they can be found via relations between SIFs and measurable quantities like strains or displacements.

The most common analytical methods used to determine SIFs are the Integral Transformation Method by Sneddon (1946, 1969), the Complex Variable Method by Westergaard (1939) and Muskhelishvili (1953), and Williams' Eigenfunction Series Expansion by Williams (1952). These methods have been used to determine the distribution of the stresses and the displacements near the crack tip. Williams (1952) was the first to investigate the analytical form of singularities resulting at a notch tip. He found that the stresses in a homogeneous notched body become infinite at the notch tip under any boundary conditions. Analytical methods give accurate solutions, but they can

only be applied to simple cases. Some of these methods are used in this thesis to derive the stress and displacement expressions near the notch tip that are used as GIFs in the FFEM.

For most realistic problems with finite geometrical boundaries and complex loading conditions, numerical and semi-analytical procedures are the only means to determine the SIFs. There are many numerical methods, such as the Finite Element Method (FEM), the Boundary Element Method, the Finite Difference Method, the Weight Residue Method, the Boundary Collocation Method, etc. Details of these methods can be found in many references such as Atluri (1986) and Aliabadi et al. (1991). Most numerical procedures in the literature are based on modified versions of those methods.

Among the aforementioned methods, the FEM is the most established approach in engineering. It has been proven to be capable of dealing with crack problems. However, computationally speaking, it is quite costly because of the unavoidable fine mesh required around the crack tip, which leads to a very large number of unknowns. Some singular elements have been developed to eliminate some of the FEM's problems, such as the widely used quarter-point element Barsoum (1976a, 1976b). This type of elements can generate the $1/\sqrt{r}$ singularity at the crack tip. There has been some criticism of this element such as the discussion raised by Dhondt (1994). He proved that the quarter-point element is an unstable equilibrium configuration, meaning a small geometric modification of the quarter-point element to match the body geometry, for example, will lead to a totally degenerated element. Another issue is that the quarter-point element can only be degenerated from specific finite element types. However, the singular quarter-point element was an important development, and it is widely incorporated into commercial FE

packages. Moreover, the SIFs cannot be obtained using the FEM directly, but some post-processing is required, such as using the domain integral (or J-integral) techniques by Rice (1968) or the virtual crack extension by Hellen (1975).

Semi-analytical methods that have been developed to compute the SIFS are among others the hybrid crack element (HCE), the scaled boundary finite element method (SBFEM), and the fractal-like finite element method (FFEM). Semi-analytical methods appear promising for fracture mechanics because they combine the accuracy of analytical solutions with the practicality of numerical procedures. The HCE was developed by Tong et al. (1973) to compute the SIFs for plane cracks. Karihaloo and Xiao (2001) presented a simplified variational principle using truncated asymptotic crack tip displacement and stress series expansions was used to formulate the HCE. Despite the good accuracy of the numerical results obtained by the HCE, the element was incompatible with the surrounding finite elements because of the exclusion of coefficients of the Williams series expansion that do not contribute to the stresses and strains in the formulation of the HCE (Xiao and Karihaloo, 2004). To minimise the incompatibility, Xiao and Karihaloo (2007) recovered these coefficients by an indirect method that involves the application of a least-squares method. Wolf (2003) developed the SBFEM, which is a numerical finite element-based procedure in the circumferential directions and an analytical procedure in the radial direction. In the SBFEM, the governing partial differential equations are transformed to a scaled boundary co-ordinate system. By introducing shape functions in the circumferential directions, these equations are reduced to a set of second-order ordinary differential equations. These ordinary differential equations are solved analytically in the radial direction after determining their coefficients by a finite element approximation in the circumferential directions. However, the mathematics of the SBFEM compared to the

FEM is rather complicated (Chidgzey and Deeks, 2005). A brief history about the FFEM is presented in the next section.

For notch cases, researchers have developed various methods and procedures to compute the SIFs for a notch based on methods used to predict crack SIFs. Gross and Mendelson (1972) calculated the SIFs for many notch cases of modes I and II by means of a boundary collocation method based on the stress functions derived by Williams (1952). Tong and Pian (1973) concluded that in order to improve the convergence rate of finite element solutions of problems with a singularity, the interpolation functions of a finite element formulation must include terms that can account for the analytical form of the singularity. In addition, these interpolation functions should be used for elements within a finite region, and not only for those around the singular point. Lin and Tong (1980) developed singular finite elements for the analysis of v-notched plates. Carpenter (1984) presented a collocation procedure to compute SIFs for notch problems based on the contour integral of Stern et al. (1976). Babuška and Miller (1984) developed post-processing approaches to extract the generalised SIFs near corner points from a finite element solution using Green's function or the energy release principle. Portela et al. (1991) proposed a boundary element singularity subtraction technique to compute the SIFs of notch problems. Their method requires extra boundary conditions that they referred to as ''singularity conditions of the regularisation procedure". Zhao and Hahn (1992) predicted the SIFs of a notch problem from the SIFs of a crack problem. Chen (1995) computed the SIFs of notched plates by means of the body force method.

Results of mode III SIFs of cracked plates were reported by some authors such as Zhang (1988) who presented results for off-centre single-edge-cracked plates with the aid of the

basic theorem of the Fourier transform and Fourier series. Noda and Takase (2003) calculated the generalised SIFs for a V-shaped notched round bar under tension, bending, and torsion using the singular integral equation of the body force method.

Most of the aforementioned research work was concerned only with isotropic homogeneous crack and/or notch problems. For bi-material cases, which are more complicated, researchers such as Theocaris (1974), Dempsey and Sinclair (1981), and Hein and Erdogan (1971), among others, studied the stress and displacement fields and investigated the behaviour of the singular eigenvalues for bi-material notches. The case of an interfacial crack problem, which is a special case of a bi-material notch problem, has been investigated by many researchers, such as Lin and Mar (1976) constructed a hybrid crack element to compute SIFs for cracks in bi-materials. Yau and Wang (1984) used a procedure that involves known auxiliary solutions and evaluation of conservation integrals along a suitably selected remote path. Lee and Choi (1988) computed the SIFs for interfacial cracks using a boundary element method which employed the multi-region technique and the double-point concept. Matsumto et al. (2000) evaluated the SIFs of interface cracks using a concept based on the interaction energy release rates.

Results for stress intensities for bi-material notch problems were reported by few researchers, due to their complexity. Carpenter and Byers (1987) investigated bi-material notch problems by using the reciprocal work contour integral method. Tan and Meguid (1997) presented a singular finite element to compute the SIFs of a notch formulated by using explicit expressions for the singular stress and displacement fields of a general bi-material wedge. Chen and Sze (2001) developed a hybrid-stress finite element model in which the asymptotic stress and displacement fields embedded into the wedge-tip element

were numerically obtained. All of this research work was concerned with only the in-plane problems, i.e. modes I and II.

For the case of anti-plane shear, i.e. mode III, in bi-material crack/notch problems Wu and Chiu (1991) computed the SIFs for interface cracks in bi-materials under anti-plane shear by using a complex-variable formulation based on the solutions of a dislocation and a body force in an infinite composite body. Other researchers who studied the case of a bi-material crack under anti-plane shear loading conditions are, among others, Lee and Earmme (2000), Li (2001), and Li and Duan (2006). The general case of anti-plane notch was investigated by Jun and Yuqiu (1992) by using a Sub-Region Mixed FEM. They provided very limited examples of a notch in a disk. Liu and Chue (2006) examined the stress singularity orders in dissimilar anisotropic wedges.

2.3. The Fractal-like Finite Element Method (FFEM)

The idea of the Fractal-like Finite Element Method goes back to the work of Leung and Cheung (1981). Originally they proposed a two-level finite element technique of constructing a frame super-element to reduce the computational cost for solving dynamic problems of a large scale frame. The idea was based on the concept of global-local interpolation functions introduced by Mote (1971). The concept was that while local interpolation functions (shape functions) reduce the infinite number of degrees of freedom of a continuum to a finite number of degrees of freedom related to the nodes of the continuous element, the global finite element interpolation functions can be used to reduce the number of unknowns significantly.

The study was extended to model two-dimensional plates subject to concentrated static and harmonic loads by Leung and Wong (1988, 1992) and two-dimensional crack problems by Leung and Wong (1989). Leung and Su extended the method further to include many two-dimensional crack problems. They applied the method to mode I (Leung and Su, 1994), mixed mode (Leung and Su, 1995a), and body force crack problems (Leung and Su, 1995b), as well as to cracked Kirchhoff's plates (Leung and Su, 1996a), cracked Reissner's plates (Leung and Su, 1996b) and further to penny-shaped and circumferential cracks and axisymmetric cracks (Leung and Su, 1998). Leung and Tsang (2000) studied mode III crack problems. Xie el al. (2003) carried out a parametric study of the FFEM for the computations of SIFs for crack problems. Tsang et al. (2004) extended the method to penny shaped and circumferential cracks. It has been shown that the Fractal-like Finite Element Method gives very accurate results for many different crack problems. Reddy and Rao (2008a) carried out a stochastic fracture mechanics analysis of linear-elastic cracked structures subjected to mixed-mode (I and II) loading conditions using the FFEM. They also developed a fractal finite element based method for continuum-based shape sensitivity analysis for a crack in a homogeneous, isotropic body subject to mixed-mode (I and II) loading conditions (Reddy and Rao, 2008b).

Recently, during the course of this research Treifi el al. (2008, 2009a, 2009b, 2009c, 2013a, 2013b, 2013c) have developed the FFEM to compute the SIFs for notch problems in isotropic homogeneous and bi-material plates subjected to mode I, II, or III loading conditions. These research papers make up the core contents of this thesis.

As a semi-analytical method, the FFEM brings together the agility of the finite element method (FEM) and the accuracy of the exact analytical solutions. It is well known that in order to improve the convergence of FE solutions for problems with singularities, it is

necessary to discretise the singular regions around the singular points using very fine meshes. This leads to a large number of unknowns and a considerable increase of the computational cost. In the FFEM, the employment of the exact analytical expressions of a displacement field as global interpolation functions to transform the large number of nodal displacements into a small set of generalised co-ordinates reduces the computational cost significantly. Also, the SIFs and the coefficients of the higher order terms of the notch tip asymptotic field are the generalised co-ordinates and are computed directly. Therefore, no post-processing is required to extract them. Moreover, no special singular finite elements are needed to model the singular region around a notch tip—conventional finite elements can be used to model the whole of the cracked/notched body (singular and regular regions). The implementation of the FFEM involves simple matrix multiplication. No complicated mathematics is involved. Therefore, it is easy to be implemented into an existing FE code.

The FFEM is based on the FEM. Therefore, the FFEM results are mesh dependent as is the case in the FEM. Following the general advice given for the FEM on how to generate good meshes is sufficient to produce good results in the FFEM. The only limitation to the use of the FFEM is the availability of "good" global interpolation functions, whether they be exact analytical or not.

2.4. The Strain Energy Approach (SEA)

The idea of using the strain energy to compute the SIFs goes back to the work of Sih (1974a, 1974b), who proposed a strain energy density factor for cracks. Lazzarin et al. (2001, 2007, 2010) have established an approach based on the averaged strain energy

density over a control volume around a notch tip to compute the SIFs for sharp and rounded notches. They dealt only with isotropic homogeneous notches subject to pure mode I, II or III conditions. For mixed mode I and II cases, they usually neglected the effect of mode II SIF (Lazzarin and Zambardi, 2001) where they used examples with non-singular mode II stress components, but in a recent publication (Lazzarin et al., 2010) they suggested using two concentric volumes to compute mode I and II notch SIFs. However, this approach does not always work as will be discussed later in Chapter 10. In Chapter 10, a strain energy approach is developed to compute the SIFs for isotropic homogeneous and bi-material notches under mode I, II and III. The case of mixed modes I and II is dealt with differently to what Lazzarin et al. (2010) proposed. The approach is based on the strain energy of a control volume around a singular point such as a notch tip. The formulae are simple and easy to implement. The strain energy can easily be computed using commercial finite element packages. Thus, enabling analysts to compute the notch SIFs using commercial FE packages, which are generally not capable of computing the SIFs of a general notch (they are only capable of computing the SIFs of a crack). Because the SEA depends on the strain energy computed using the FEM, the results are mesh dependent. Also, fine meshes around the singular points are recommended especially for mixed mode cases.

2.5. Conclusion

In this chapter, a literature review about the methods used to compute the SIFs, the FFEM, and the SEA was presented. In addition, the advantages of the FFEM and SEA were highlighted together with their limitations.

Chapter 3

Theoretical Background

3. Theoretical Background

3.1. Introduction

In this chapter, a detailed background of the work, techniques and methods developed and used in this research is presented for completeness. Firstly, the theoretical formulation of the FFEM is presented, followed by the derivations of the GIFs employed in the FFEM in the subsequent chapters. The numerical techniques developed to carry out the analysis in the FFEM and the SEA are also described. The sections of this chapter correspond to work and techniques developed and used in the upcoming chapters which contain materials published in externally refereed contexts.

3.2. Formulation of the FFEM

In the FFEM, a body containing singular points, such as, a tip of a notch or a crack, is divided into singular and regular regions delineated by curves such as $\Gamma_0^1, \Gamma_0^2, \ldots$ as illustrated in Figure 3.1. Conventional finite elements are used to model the singular and regular regions. However, a very fine mesh of conventional finite elements is used within the singular regions. This mesh is generated layer by layer in a self-similar fractal-like process. In the conventional FEM, the nodal displacements are the unknowns of a problem. In the FFEM, the unknowns are the nodal displacements of the nodes in the regular region and the coefficients of the GIFs, called generalised coordinates. The GIFs are used to transform the nodal displacements of the nodes in the singular region into a small set of generalised co-ordinates. The generalised co-ordinates associated with the singular eigenvalues are related to the stress intensity factors for modes I, II and III. The

other coordinates are the coefficients of the higher order terms. The first non-singular stress term of the eigenfunction series expansion which is called the "T-stress" is related to the coefficient of the first higher order term of the series. The "T-stress" coefficient is the most important coefficient as it plays an important role in the directional stability of the crack propagation (Cotterell and Rice, 1980). In addition, it is understood that using more terms of the series expansion of the stresses and displacement expressions lead to more accurate results (Hui and Ruina, 1995). As those generalised coordinates are computed directly in the FFEM, no post-processing is necessary to extract the SIFs. Analytical solutions for the displacements around the notch tip are used as GIFs to perform the transformation.

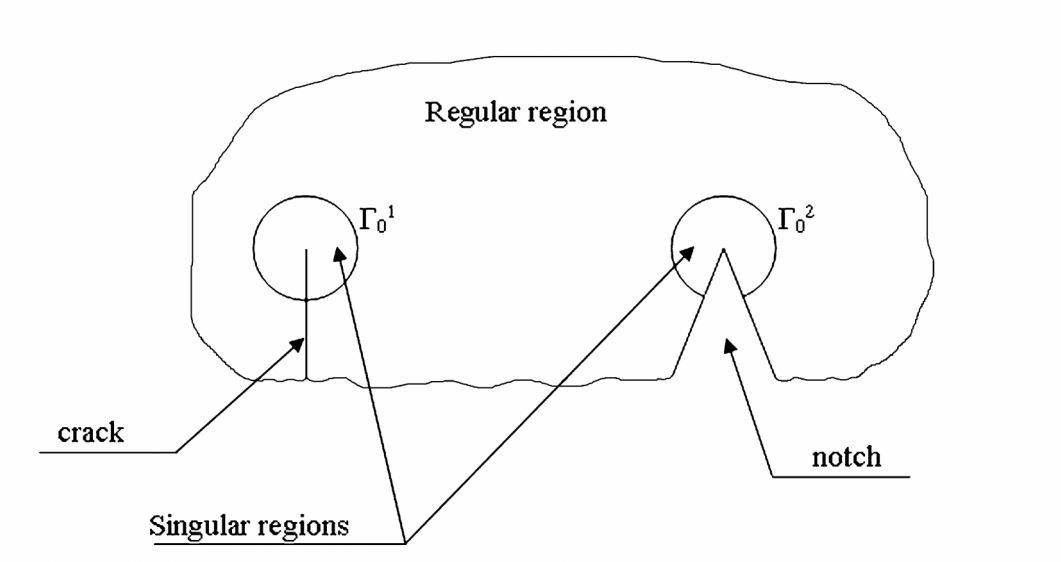

Figure 3.1. Singular and regular regions of a cracked and notched plate.

Using ρ as a similarity ratio and the crack tip as a centre of similarity, a set of curves $\{\Gamma_1, \Gamma_2, \Gamma_3, ...\}$, similar to Γ_0, is generated within the singular region. The layer between the curves Γ_{n-1} and Γ_n is called the *nth* layer. All nodes on Γ_0 are considered master nodes, while the nodes inside Γ_0 are considered slave nodes as shown in Figure 3.2.

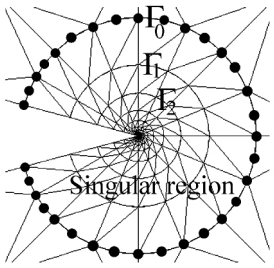

Figure 3.2. An illustration of a singular region (master nodes are highlighted).

In the conventional finite element method, the displacements can be expressed as follows:

$$\mathbf{u} = \mathbf{N}.\mathbf{d} \tag{3.1}$$

where $\mathbf{u}$ is the displacement field, $\mathbf{d}$ is the nodal displacement vector, and $\mathbf{N}$ is the shape function matrix. The strain can be obtained using

$$\boldsymbol{\varepsilon} = \mathbf{B}.\mathbf{d} \tag{3.2}$$

where: $\boldsymbol{\varepsilon}$ is the strain vector, and $\mathbf{B}$ is the strain-displacement operator. For linearly elastic conditions, the stress-strain relations can be stated as

$$\boldsymbol{\sigma} = \mathbf{H}.\boldsymbol{\varepsilon} \tag{3.3}$$

where $\boldsymbol{\sigma}$ is the stress vector, and $\mathbf{H}$ is the material properties matrix (constitutive matrix).

The static equilibrium equation, in the FEM, is

$$\mathbf{K}.\mathbf{d} = \mathbf{f} \tag{3.4}$$

where $\mathbf{f}$ is the nodal force vector and $\mathbf{K}$ is the global stiffness matrix

In the FFEM, the static equilibrium equation of the regular region can be written as

$$\begin{bmatrix} \mathbf{K}_{rr} & \mathbf{K}_{rm} \\ \mathbf{K}_{mr} & \mathbf{K}_{mm} \end{bmatrix} \begin{Bmatrix} \mathbf{d}_r \\ \mathbf{d}_m \end{Bmatrix} = \begin{Bmatrix} \mathbf{f}_r \\ \mathbf{f}_m \end{Bmatrix} \tag{3.5}$$

where $\mathbf{d}_r$ are the displacements of the nodes in the regular region and $\mathbf{d}_m$ are the displacements of the master nodes. Similarly, for the first layer in the singular region, the static equilibrium equation can be written as

$$\begin{bmatrix} \mathbf{K}_{mm}^{1st} & \mathbf{K}_{ms}^{1st} \\ \mathbf{K}_{sm}^{1st} & \mathbf{K}_{ss}^{1st} \end{bmatrix} \begin{Bmatrix} \mathbf{d}_m \\ \mathbf{d}_s^{1st} \end{Bmatrix} = \begin{Bmatrix} \mathbf{f}_m^{1st} \\ \mathbf{f}_s^{1st} \end{Bmatrix} \tag{3.6}$$

where $\mathbf{d}_s^{1st}$ are the displacements of the slave nodes in the first layer. $\mathbf{d}_s^{1st}$ can be expressed in terms of a set of generalised co-ordinates $\mathbf{c} = \{C_1, C_2, C_3, ...\}^T$, which are the coefficients of the GIFs, as follows:

$$\mathbf{d}_s^{1st} = \mathbf{T}_s^{1st} \mathbf{c} \tag{3.7}$$

$\mathbf{T}_s^{1st}$ is the transformation matrix in terms of polar co-ordinates (r, θ) for the slave nodes in the first layer. Therefore, Eq. (3.6) can be written as

$$\begin{bmatrix} \mathbf{I} & 0 \\ 0 & \mathbf{T}_s^{1st} \end{bmatrix}^T \begin{bmatrix} \mathbf{K}_{mm}^{1st} & \mathbf{K}_{ms}^{1st} \\ \mathbf{K}_{sm}^{1st} & \mathbf{K}_{ss}^{1st} \end{bmatrix} \begin{bmatrix} \mathbf{I} & 0 \\ 0 & \mathbf{T}_s^{1st} \end{bmatrix} \begin{Bmatrix} \mathbf{d}_m \\ \mathbf{c} \end{Bmatrix} = \begin{bmatrix} \mathbf{I} & 0 \\ 0 & \mathbf{T}_s^{1st} \end{bmatrix}^T \begin{Bmatrix} \mathbf{f}_m^{1st} \\ \mathbf{f}_s^{1st} \end{Bmatrix} \tag{3.8}$$

or

$$\begin{bmatrix} \mathbf{K}_{mm}^{1st} & \mathbf{K}_{ms}^{1st} \mathbf{T}_s^{1st} \\ \mathbf{T}_s^{1st\,T} K_{sm}^{1st} & \mathbf{T}_s^{1st\,T} \mathbf{K}_{ss}^{1st} \mathbf{T}_s^{1st} \end{bmatrix} \begin{Bmatrix} \mathbf{d}_m \\ \mathbf{c} \end{Bmatrix} = \begin{Bmatrix} \mathbf{f}_m^{1st} \\ \mathbf{T}_s^{1st\,T} \mathbf{f}_s^{1st} \end{Bmatrix} \tag{3.9}$$

In order to provide the continuity between the singular and the regular region, $\mathbf{d}_m$ are not transformed.

Now, the static equilibrium equation of the *nth* layer in the singular region, $n > 1$, is

$$\mathbf{K}_s^n \mathbf{d}_s^n = \mathbf{f}_s^n \tag{3.10}$$

By applying the transformation and pre-multiplying by the transpose of $\mathbf{T}_s^n$, we get

$$\mathbf{T}_s^{n\,T} \mathbf{K}_s^n \mathbf{T}_s^n \mathbf{c} = \mathbf{T}_s^{n\,T} \mathbf{f}_s^n \tag{3.11}$$

where $\mathbf{K}_s^n = \begin{bmatrix} \mathbf{K}_{s11}^n & \mathbf{K}_{s12}^n \\ \mathbf{K}_{s21}^n & \mathbf{K}_{s22}^n \end{bmatrix}$

Because $\mathbf{d}_m$ are not transformed, the size of the transformation matrix of the first layer $\mathbf{T}_s^{1st}$ is smaller than that of the transformation matrix of the n^{th} layer $\mathbf{T}_s^n$.

The global equilibrium equation can now be written as

$$\begin{bmatrix} \mathbf{K}_{rr} & \mathbf{K}_{rm} & & & & & \\ \mathbf{K}_{mr} & \mathbf{K}_{mm}+\mathbf{K}_{mm}^{1st} & \mathbf{K}_{ms}^{1st} & & & & \\ & \mathbf{K}_{sm}^{1st} & \mathbf{K}_{ss}^{1st}+\mathbf{K}_{s11}^{2nd} & \mathbf{K}_{s12}^{2nd} & & & \\ & & \mathbf{K}_{s21}^{2nd} & \mathbf{K}_{s22}^{2nd}+\mathbf{K}_{s11}^{3rd} & \mathbf{K}_{s12}^{3rd} & & \\ & & & \ddots & \ddots & \ddots & \\ & & & & \mathbf{K}_{s21}^{nl} & \mathbf{K}_{s22}^{nl} \end{bmatrix} \begin{Bmatrix} \mathbf{d}_r \\ \mathbf{d}_m \\ \mathbf{d}_s^{1st} \\ \mathbf{d}_s^{2nd} \\ \vdots \\ \mathbf{d}_s^{nl} \end{Bmatrix} = \begin{Bmatrix} \mathbf{f}_r \\ \mathbf{f}_m \\ \mathbf{f}_s^{1st} \\ \mathbf{f}_s^{2nd} \\ \vdots \\ \mathbf{f}_s^{nl} \end{Bmatrix} \tag{3.12}$$

where nl is the number of layers used to model the singular region. Eq. (3.12) can be rewritten after applying the transformation as follows

$$\begin{bmatrix} \mathbf{K}_{rr} & \mathbf{K}_{rm} & 0 \\ \mathbf{K}_{mr} & \mathbf{K}_{mm}+\mathbf{K}_{mm}^{1st} & \mathbf{K}_{ms}^{1st}\mathbf{T}_s^{1st} \\ 0 & \mathbf{T}_s^{1st\,T}\mathbf{K}_{sm}^{1st} & \mathbf{T}_s^{1st\,T}\mathbf{K}_{ss}^{1st}\mathbf{T}_s^{1st}+\sum_{n=2}^{nl}\mathbf{T}_s^{n\,T}\mathbf{K}_s^n\mathbf{T}_s^n \end{bmatrix} \begin{Bmatrix} \mathbf{d}_r \\ \mathbf{d}_m \\ \mathbf{c} \end{Bmatrix} = \begin{Bmatrix} \mathbf{f}_r \\ \mathbf{f}_m+\mathbf{f}_m^{1st} \\ \mathbf{T}_s^{1st\,T}\mathbf{f}_s^{1st}+\sum_{n=2}^{nl}\mathbf{T}_s^{n\,T}\mathbf{f}_s^n \end{Bmatrix} \tag{3.13}$$

Or

$$\begin{bmatrix} \mathbf{K}_{rr} & \mathbf{K}_{rm} & 0 \\ \mathbf{K}_{mr} & \mathbf{K}_{mm}+\mathbf{K}_{mm}^{1st} & \overline{\mathbf{K}}_{ms}^{1st} \\ 0 & \overline{\mathbf{K}}_{sm}^{1st} & \overline{\mathbf{K}}_{ss}^{1st}+\overline{\mathbf{K}}_s^{inn} \end{bmatrix} \begin{Bmatrix} \mathbf{d}_r \\ \mathbf{d}_m \\ \mathbf{c} \end{Bmatrix} = \begin{Bmatrix} \mathbf{f}_r \\ \mathbf{f}_m+\mathbf{f}_m^{1st} \\ \bar{\mathbf{f}}_s^{1st}+\bar{\mathbf{f}}_s^{inn} \end{Bmatrix} \tag{3.14}$$

where $\overline{\mathbf{K}}_{ms}^{1st} = \mathbf{K}_{ms}^{1st}\mathbf{T}_s^{1st}$, $\overline{\mathbf{K}}_{sm}^{1st} = \mathbf{T}_s^{1st\,T}\mathbf{K}_{sm}^{1st}$, $\overline{\mathbf{K}}_{ss}^{1st} = \mathbf{T}_s^{1st\,T}\mathbf{K}_{ss}^{1st}\mathbf{T}_s^{1st}$, $\overline{\mathbf{K}}_s^{inn} = \sum_{n=2}^{nl}\overline{\mathbf{K}}_s^n$, $\overline{\mathbf{K}}_s^n = \mathbf{T}_s^{n\,T}\mathbf{K}_s^n\mathbf{T}_s^n$, $\bar{\mathbf{f}}_s^{1st} = \mathbf{T}_s^{1st\,T}\mathbf{f}_s^{1st}$, $\bar{\mathbf{f}}_s^{inn} = \sum_{n=2}^{nl}\bar{\mathbf{f}}_s^n$, and $\bar{\mathbf{f}}_s^n = \mathbf{T}_s^{n\,T}\mathbf{f}_s^n$. Only the parts with the subscript s are transformed. The unknowns of the problem are now the nodal

displacements $(\mathbf{d}_r \,\&\, \mathbf{d}_m)$ of the nodes in the regular region and the generalised co-ordinates $\mathbf{c}$.

If we consider $\mathbf{d}_s$ as the vector of displacements in the singular region except for those on Γ_0, the size of the vector $\mathbf{d}_s$ is much bigger than the vector of the generalised co-ordinates $\mathbf{c}$. Therefore, solving the system of equations (3.14) is much more efficient than solving the system of equations (3.12). Figure 3.3 shows the essential steps of the FFEM. They are similar to the FEM steps. The differences are highlighted in *Italics*.

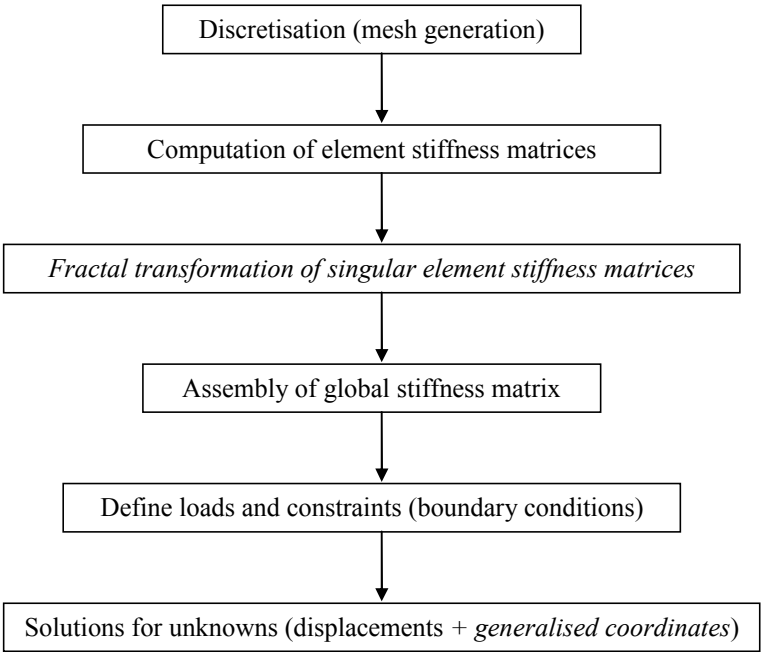

Figure 3.3. Essential steps in FFEM (differences between FFEM and FEM are in *Italics*)

3.3. Fractal Transformation

In the FFEM, the singular region is modelled using layers of elements of similar shapes. The layers are constructed using a similarity ratio ρ. The property of the stiffness

matrices of two dimensional iso-parametric finite elements of similar shapes is utilised to compute the stiffness matrix of the inner layers $(n \geq 2)$ of the singular region, $\overline{\mathbf{K}}_s^{inn}$. The element stiffness matrix can be computed using

$$\mathbf{k} = \int_V \mathbf{B}^T \mathbf{H} \mathbf{B} dV \tag{3.15}$$

where V is the volume of an element. For an iso-parametric finite element, Eq. (3.15) can be written as

$$\mathbf{k} = \int_{-1}^{1}\int_{-1}^{1} \mathbf{B}^T \mathbf{H} \mathbf{B} J d\xi d\eta \tag{3.16}$$

where ξ and η are natural coordinates, and J is the determinant of the Jacobian Matrix $\mathbf{J}$. Assuming two 3-node triangular elements (1 and 2) of similar shape, where element 2 nodal coordinates can be written in terms of those of element 1 using a similarity ratio ρ as

$$\mathbf{X}^{(2)} = \rho \mathbf{X}^{(1)} \tag{3.17}$$

The matrices $\mathbf{B}$ and $\mathbf{J}$ of a triangular element are

$$\mathbf{B} = \left[\mathbf{B}_i, \mathbf{B}_j, \mathbf{B}_k\right] \tag{3.18}$$

$$\mathbf{J} = \begin{bmatrix} \dfrac{\partial x}{\partial \xi} & \dfrac{\partial y}{\partial \xi} \\ \dfrac{\partial x}{\partial \eta} & \dfrac{\partial y}{\partial \eta} \end{bmatrix} \tag{3.19}$$

where a typical $\mathbf{B}_i$ is defined as

$$\mathbf{B}_i = \begin{bmatrix} \dfrac{\partial N_i}{\partial x} & 0 \\ 0 & \dfrac{\partial N_i}{\partial y} \\ \dfrac{\partial N_i}{\partial y} & \dfrac{\partial N_i}{\partial x} \end{bmatrix} \tag{3.20}$$

The matrix $\mathbf{B}^{(2)}$ and the determinant $J^{(2)}$ for element 2 can be written in terms of those of element 1 as

$$\mathbf{B}^{(2)} = \frac{1}{\rho}\mathbf{B}^{(1)} \tag{3.21}$$

$$J^{(2)} = \rho^2 J^{(1)} \tag{3.22}$$

Substituting Eqs. (3.21) and (3.22) into Eq. (3.16) leads to

$$\mathbf{k}^{(2)} = \mathbf{k}^{(1)} \tag{3.23}$$

Eq. (3.23) demonstrates that iso-parametric elements of similar shapes have the same stiffness matrix. In other words, the stiffness matrices of all the layers in the singular region are the same.

The stiffness matrix $\overline{\mathbf{K}}_s^{inn}$ of the inner layers $(n \geq 2)$ in the singular region is

$$\overline{\mathbf{K}}_s^{inn} = \sum_{n=2}^{nl} \overline{\mathbf{K}}_s^n = \sum_{n=2}^{nl} \mathbf{T}_s^{nT} \mathbf{K}_s^n \mathbf{T}_s^n \tag{3.24}$$

The stiffness matrix of every layer in the singular region is the same because the stiffness matrices of the two-dimensional iso-parametric finite elements of similar shapes are the same as proven above. Therefore,

$$\mathbf{K}_s^n = \mathbf{K}_s^{1st} \tag{3.25}$$

The transformation matrix of the *nth* layer can be written in terms of that of the first layer as

$$\mathbf{T}_s^n = \mathbf{T}_s^f \left[\delta\right] \tag{3.26}$$

where $\mathbf{T}_s^f$ is the transformation matrix of the nodal displacements of all the nodes (slave and master) in the first layer and it is different from the aforementioned $\mathbf{T}_s^{1st}$, and $\left[\delta\right]$ is a diagonal matrix where

$$\delta_{ii} = \rho^{(n-1)\lambda_i} \tag{3.27}$$

where λ_i are the eigenvalues of the terms considered in the GIFs. Substituting equations (3.25)-(3.27) into equation (3.24) gives

$$\overline{\mathbf{K}}_s^{inn} = \sum_{n=2}^{nl} [\delta]^T \mathbf{T}_s^{f\,T} \mathbf{K}_s^{1st} \mathbf{T}_s^f [\delta] = \left[\overline{\delta}_{ij}\, \overline{k}_{ij}\right] \tag{3.28}$$

where

$$\left[\overline{k}_{ij}\right] = \mathbf{T}_s^{f\,T} \mathbf{K}_s^{1st} \mathbf{T}_s^f \tag{3.29}$$

and

$$\begin{aligned} \overline{\delta}_{ij} &= \sum_{n=2}^{nl} \rho^{(n-1)\lambda_i} \rho^{(n-1)\lambda_j} = \sum_{n=2}^{nl} \rho^{(n-1)(\lambda_i+\lambda_j)} \\ &= \rho^{(\lambda_i+\lambda_j)} + \rho^{2(\lambda_i+\lambda_j)} + ... + \rho^{(nl-1)(\lambda_i+\lambda_j)} \end{aligned} \tag{3.30}$$

This sum is a geometric series. For a finite number of layers, $\overline{\delta}_{ij}$ can be written as

$$\overline{\delta}_{ij} = \frac{\rho^{(\lambda_i+\lambda_j)}\left(1-\rho^{(nl-1)(\lambda_i+\lambda_j)}\right)}{1-\rho^{(\lambda_i+\lambda_j)}} \tag{3.31}$$

and for an infinite number of layers $(nl \to \infty)$ as

$$\overline{\delta}_{ij} = \frac{\rho^{(\lambda_i+\lambda_j)}}{1-\rho^{(\lambda_i+\lambda_j)}} \tag{3.32}$$

A similar procedure can be followed to compute the generalised force vector of the inner layers in the singular region

$$\overline{\mathbf{f}}_s^{inn} = \left\{ ... \quad \overline{\delta}_i \overline{f}_i^{\,f} \quad ... \right\}^T \tag{3.33}$$

where

$$\overline{\delta}_i = \frac{\rho^{(\lambda_i+2)}}{1-\rho^{(\lambda_i+2)}} \tag{3.34}$$

for an infinite number of layers $(nl \to \infty)$.

3.4. General Form of Global Interpolation Functions (GIFs)

The GIFs play a very important role in the FFEM. They are used to perform the fractal-like transformation of the large number of nodal displacements of the singular region into a small set of generalised coordinates. The generalised coordinates are basically the coefficients of the terms used as GIFs. Therefore, analytical expressions for the displacement field are used as GIFs. Because of this choice, the SIFs and the higher order terms become direct unknowns in the FFEM, because they are simply the generalised coordinates as will be shown in the subsequent sections.

Assuming the displacement field is expressed as

$$u = \sum_{i=1}^{NT} c_i f_i(r,\theta) \tag{3.35}$$

where c_i are the generalised coordinates, $f_i(r,\theta)$ are the GIFs, and NT is the number of terms considered, the transformation matrix $\mathbf{T}$ can be written in an explicit form as

$$\mathbf{T} = \begin{bmatrix} f_{11}(r,\theta) & f_{12}(r,\theta) & \cdots & f_{1NT}(r,\theta) \\ f_{21}(r,\theta) & f_{22}(r,\theta) & \cdots & f_{2NT}(r,\theta) \\ \vdots & \vdots & \cdots & \vdots \\ f_{n1}(r,\theta) & f_{n2}(r,\theta) & \cdots & f_{nNT}(r,\theta) \end{bmatrix} \tag{3.36}$$

where n refers to the number of nodes in a layer of elements.

The analytical displacement and stress expressions around a notch tip for the different cases presented in the coming chapters are presented in the next sections of this chapter. The displacement expressions are used as GIFs, while the stress expressions are used to obtain the SIF expressions.

3.5. GIFs for Homogenous Isotropic Notch under In-plane Loading (modes I and II)

The displacement and stress expressions around a notch tip of an isotropic plate can be derived using an eigenfunction expansion method or a complex variable method. Both methods are presented. The expressions derived using the two methods are equivalent and produce the same results, although they look different symbolically.

3.5.1. Airy Stress Function Method

Stress Analysis

The Airy stress function approach can be used to derive the displacement and stress expansions around a notch tip in the manner of Williams (1952). Let Φ be the Airy stress function in a polar co-ordinate system (r,θ) centred at the tip of an infinite notch as illustrated in Figure 3.4. The $\theta = 0$ axis and the Cartesian x-axis coincide with the bisector of the notch angle. In the absence of body forces, the elasticity equations of equilibrium are satisfied if the stresses are expressed as follows (Coker and Filon, 1931):

$$\sigma_\theta = \frac{\partial^2 \Phi}{\partial r^2} \tag{3.37}$$

$$\sigma_r = \nabla^2 \Phi - \sigma_\theta \tag{3.38}$$

$$\sigma_{r\theta} = -\frac{\partial}{\partial r}\left(\frac{1}{r}\frac{\partial \Phi}{\partial \theta}\right) = \frac{1}{r^2}\frac{\partial \Phi}{\partial \theta} - \frac{1}{r}\frac{\partial^2 \Phi}{\partial r \partial \theta} \tag{3.39}$$

The Airy stress function $\Phi(r,\theta)$ satisfies the bi-harmonic equation:

$$\nabla^2\left(\nabla^2 \Phi\right) = 0 \tag{3.40}$$

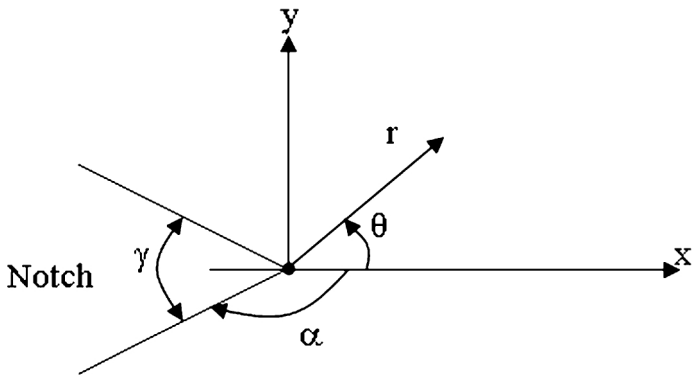

Figure 3.4. Notch geometry and the co-ordinate systems.

where

$$\nabla^2 = \frac{\partial^2}{\partial r^2} + \frac{1}{r}\frac{\partial}{\partial r} + \frac{1}{r^2}\frac{\partial^2}{\partial \theta^2} \tag{3.41}$$

Following Williams (1952), the Airy stress function for a notch problem can be taken as

$$\Phi(r,\theta) = r^{\lambda+1}F(\theta) \tag{3.42}$$

and its first and second partial derivatives are

$$\frac{\partial}{\partial r}\left(r^{\lambda+1}F\right) = (\lambda+1)r^{\lambda}F, \qquad \frac{\partial^2}{\partial r^2}\left(r^{\lambda+1}F\right) = (\lambda+1)\lambda r^{\lambda-1}F$$

$$\frac{\partial}{\partial \theta}\left(r^{\lambda+1}F\right) = r^{\lambda+1}F', \qquad \frac{\partial^2}{\partial \theta^2}\left(r^{\lambda+1}F\right) = r^{\lambda+1}F''$$

where the prime denotes differentiation with respect to θ. F is also used instead of $F(\theta)$ for convenience.

Now, substituting Eq. (3.42) into Eq. (3.40) gives

$$\nabla^2\left(\left(\lambda^2+\lambda\right)r^{\lambda-1}F + \frac{1}{r}(\lambda+1)r^{\lambda}F + \frac{1}{r^2}r^{\lambda+1}F''\right) = 0$$

$$\therefore \nabla^2\left(\left(\lambda^2+2\lambda+1\right)r^{\lambda-1}F + r^{\lambda-1}F''\right) = 0$$

or

$$\nabla^2\left((\lambda+1)^2 r^{\lambda-1}F + r^{\lambda-1}F''\right)=0 \tag{3.43}$$

Expanding Eq. (3.43) using the following partial derivatives

$$\frac{\partial}{\partial r}\left((\lambda+1)^2 r^{\lambda-1}F + r^{\lambda-1}F''\right)=(\lambda+1)^2(\lambda-1)r^{\lambda-2}F+(\lambda-1)r^{\lambda-2}F''$$

$$\frac{\partial^2}{\partial r^2}\left((\lambda+1)^2 r^{\lambda-1}F + r^{\lambda-1}F''\right)=$$
$$(\lambda+1)^2(\lambda-1)(\lambda-2)r^{\lambda-3}F+(\lambda-1)(\lambda-2)r^{\lambda-3}F''$$

$$\frac{\partial}{\partial \theta}\left((\lambda+1)^2 r^{\lambda-1}F + r^{\lambda-1}F''\right)=(\lambda+1)^2 r^{\lambda-1}F'+r^{\lambda-1}F'''$$

$$\frac{\partial^2}{\partial \theta^2}\left((\lambda+1)^2 r^{\lambda-1}F + r^{\lambda-1}F''\right)=(\lambda+1)^2 r^{\lambda-1}F''+r^{\lambda-1}F''''$$

gives

$$(\lambda+1)^2(\lambda-1)(\lambda-2)r^{\lambda-3}F+(\lambda-1)(\lambda-2)r^{\lambda-3}F''+$$
$$(\lambda+1)^2(\lambda-1)r^{\lambda-3}F+(\lambda-1)r^{\lambda-3}F''+(\lambda+1)^2 r^{\lambda-3}F''+r^{\lambda-3}F''''=0;\ r\neq 0$$

which can be simplified to get the following fourth order partial differential equation

$$F''''+2\left(\lambda^2+1\right)F''+\left(\lambda^2-1\right)^2F=0 \tag{3.44}$$

The general solution of this equation is

$$F(\theta)=C_1\sin(\lambda+1)\theta+C_2\cos(\lambda+1)\theta+C_3\sin(\lambda-1)\theta+C_4\cos(\lambda-1)\theta \tag{3.45}$$

provided that $\lambda\neq 0,\pm 1$. The solution for $\lambda=0$ is

$$F(\theta)=C_1\sin\theta+C_2\theta\sin\theta+C_3\cos\theta+C_4\theta\cos\theta \tag{3.46}$$

and for $\lambda=\pm 1$ is

$$F(\theta)=C_1+C_2\theta+C_3\sin 2\theta+C_4\cos 2\theta \tag{3.47}$$

From (3.37), (3.38), (3.39) and (3.42), the stress expressions are

$$\sigma_\theta = \frac{\partial^2 \Phi}{\partial r^2} = \frac{\partial^2}{\partial r^2}\left(r^{\lambda+1}F\right) = \frac{\partial}{\partial r}\left((\lambda+1)r^{\lambda}F\right)$$

$$\sigma_r = \nabla^2\Phi - \sigma_\theta = \left((\lambda+1)^2 r^{\lambda-1}F + r^{\lambda-1}F''\right) - (\lambda+1)\lambda r^{\lambda-1}F$$
$$\sigma_r = r^{\lambda-1}\left[F'' + \left((\lambda+1)^2 - (\lambda+1)\lambda\right)F\right]$$

$$\sigma_{r\theta} = \frac{1}{r^2}\frac{\partial \Phi}{\partial \theta} - \frac{1}{r}\frac{\partial^2 \Phi}{\partial r \partial \theta} = \frac{1}{r^2}r^{\lambda+1}F' - \frac{1}{r}\frac{\partial}{\partial r}\left(r^{\lambda+1}F'\right)$$
$$= \frac{1}{r^2}r^{\lambda+1}F' - \frac{1}{r}(\lambda+1)r^{\lambda}F' = r^{\lambda-1}F' - (\lambda+1)r^{\lambda-1}F'$$

or more concisely, they can be rewritten as

$$\sigma_r = r^{\lambda-1}\left[F'' + (\lambda+1)F\right] \tag{3.48}$$

$$\sigma_\theta = r^{\lambda-1}\left[\lambda(\lambda+1)F\right] \tag{3.49}$$

$$\sigma_{r\theta} = r^{\lambda-1}\left[-\lambda F'\right] \tag{3.50}$$

By applying the boundary conditions, the unknowns C_i and λ_i are determined, which can assume real or complex values. For traction-free boundary conditions, the following conditions are applied

$$\sigma_\theta(r, \pm\alpha) = 0 \tag{3.51}$$

$$\sigma_{r\theta}(r, \pm\alpha) = 0 \tag{3.52}$$

Substituting these conditions into equations (3.49) and (3.50) gives

$$F(\pm\alpha) = F'(\pm\alpha) = 0 \tag{3.53}$$

Applying these conditions to the general solution (3.45) of the differential equation (3.44), a linear system of four equations with four unknowns is obtained

$$C_1\sin(\lambda+1)\alpha + C_2\cos(\lambda+1)\alpha + C_3\sin(\lambda-1)\alpha + C_4\cos(\lambda-1)\alpha = 0$$
$$-C_1\sin(\lambda+1)\alpha + C_2\cos(\lambda+1)\alpha - C_3\sin(\lambda-1)\alpha + C_4\cos(\lambda-1)\alpha = 0$$

$$(\lambda+1)C_1\cos(\lambda+1)\alpha-(\lambda+1)C_2\sin(\lambda+1)\alpha+$$
$$(\lambda-1)C_3\cos(\lambda-1)\alpha-(\lambda-1)C_4\sin(\lambda-1)\alpha=0$$
$$(\lambda+1)C_1\cos(\lambda+1)\alpha+(\lambda+1)C_2\sin(\lambda+1)\alpha+$$
$$(\lambda-1)C_3\cos(\lambda-1)\alpha+(\lambda-1)C_4\sin(\lambda-1)\alpha=0$$

Using simple algebra, this system of four equations could be separated into two uncoupled systems. Each sub-system is with two unknowns of C_i.

$$\begin{bmatrix}\cos(\lambda+1)\alpha & \cos(\lambda-1)\alpha\\ (\lambda+1)\sin(\lambda+1)\alpha & (\lambda-1)\sin(\lambda-1)\alpha\end{bmatrix}\begin{Bmatrix}C_2\\ C_4\end{Bmatrix}=\begin{Bmatrix}0\\ 0\end{Bmatrix} \tag{3.54}$$

$$\begin{bmatrix}\sin(\lambda+1)\alpha & \sin(\lambda-1)\alpha\\ (\lambda+1)\cos(\lambda+1)\alpha & (\lambda-1)\cos(\lambda-1)\alpha\end{bmatrix}\begin{Bmatrix}C_1\\ C_3\end{Bmatrix}=\begin{Bmatrix}0\\ 0\end{Bmatrix} \tag{3.55}$$

The first sub-system, Eq. (3.54), leads to solutions that are symmetric (mode I) with respect to the x-axis because C_2 and C_4 are coefficients of cosine functions in Eq. (3.45). Similarly, the second sub-system, Eq. (3.55), leads to solutions that are anti-symmetric (mode II) with respect to the x-axis.

By equating the determinants of Eqs. (3.54) and (3.55) to zero in order for nontrivial solutions of C_1, C_2, C_3, C_4 to exist, the following characteristic equations are obtained

$$\lambda^I\sin 2\alpha+\sin 2\lambda^I\alpha=0 \tag{3.56}$$

and

$$\lambda^{II}\sin 2\alpha-\sin 2\lambda^{II}\alpha=0 \tag{3.57}$$

for mode I and II, respectively. The eigenvalues of mode I $\left(\lambda^I\right)$ and of mode II $\left(\lambda^{II}\right)$ are generally different from each other except for the special case of a crack problem, $\alpha=\pi\Rightarrow\sin 2\pi\lambda^I=\sin 2\pi\lambda^{II}=0$ which gives the following eigenvalues

$$\lambda^I=\lambda^{II}=\frac{n}{2} \tag{3.58}$$

The characteristic equations (3.56) and (3.57) can be solved numerically using Muller's iterative method (Press et al., 2007). The advantage of Muller's method is that the iteration can converge to a complex root, even if it has started with a real number. A flow chart of Muller's method is illustrated in Figure 3.5. In this figure, *inc*, *lim* and *er* refer to the step increment, the limit of iterations and the error. They are taken as $inc = 0.001$, *lim*=60 and $er = 10^{-5}$ for isotropic cases ($inc = 0.001 + i0.001$, *lim*=60 and $er = 10^{-10}$ for bi-material cases).

The dominant eigenvalues, which are the smallest eigenvalues greater than zero ($0 < \lambda < 1$), for different notch angles γ are plotted in Figure 3.6. This figure in conjunction with the stress expressions given by Eqs. (3.48) to (3.50) shows that the stresses are unbounded when the notch angle $\gamma < 180°$ for mode I, and $\gamma < 102.55°$ for mode II.

Eq. (3.45), from which the eigenvalues are derived, is not valid for $\lambda = 0, \pm 1$. $\lambda = -1$ is physically meaningless because it does not represent a physically possible displacement since Eqs. (3.100) and (3.101) show that when $\lambda = -1$ at the notch tip $u_r \to \pm\infty$ and $u_\theta \to \pm\infty$, i.e., the displacements, become unbounded. Therefore, $\lambda = -1$ is not an admissible root. Similarly, $\lambda = 0$ is not admissible because it represents a rigid body translation. $\lambda = 1$ is an eigenvalue for the notch angles $\gamma = 0°$ and $\gamma = 180°$ for mode I, and $\gamma = 102.55°$ for mode II.

From Eq. (3.54), C_4 can be written in terms of C_2 as

$$C_4 = -\frac{\cos\left(\lambda^I + 1\right)\alpha}{\cos\left(\lambda^I - 1\right)\alpha} C_2 = -\frac{\left(\lambda^I + 1\right)\sin\left(\lambda^I + 1\right)\alpha}{\left(\lambda^I - 1\right)\sin\left(\lambda^I - 1\right)\alpha} C_2 \tag{3.59}$$

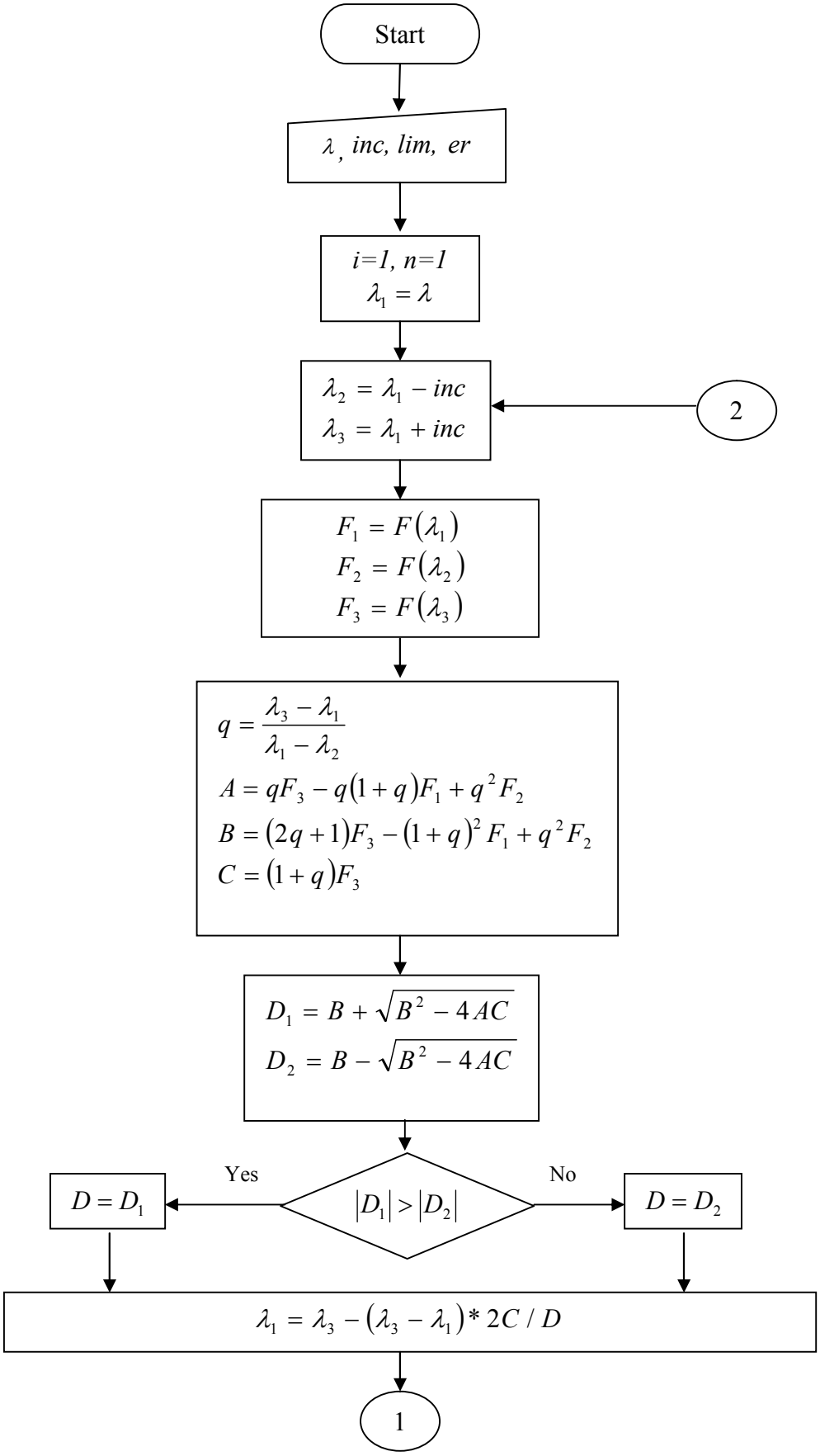

Figure 3.5. Muller's method flowchart.

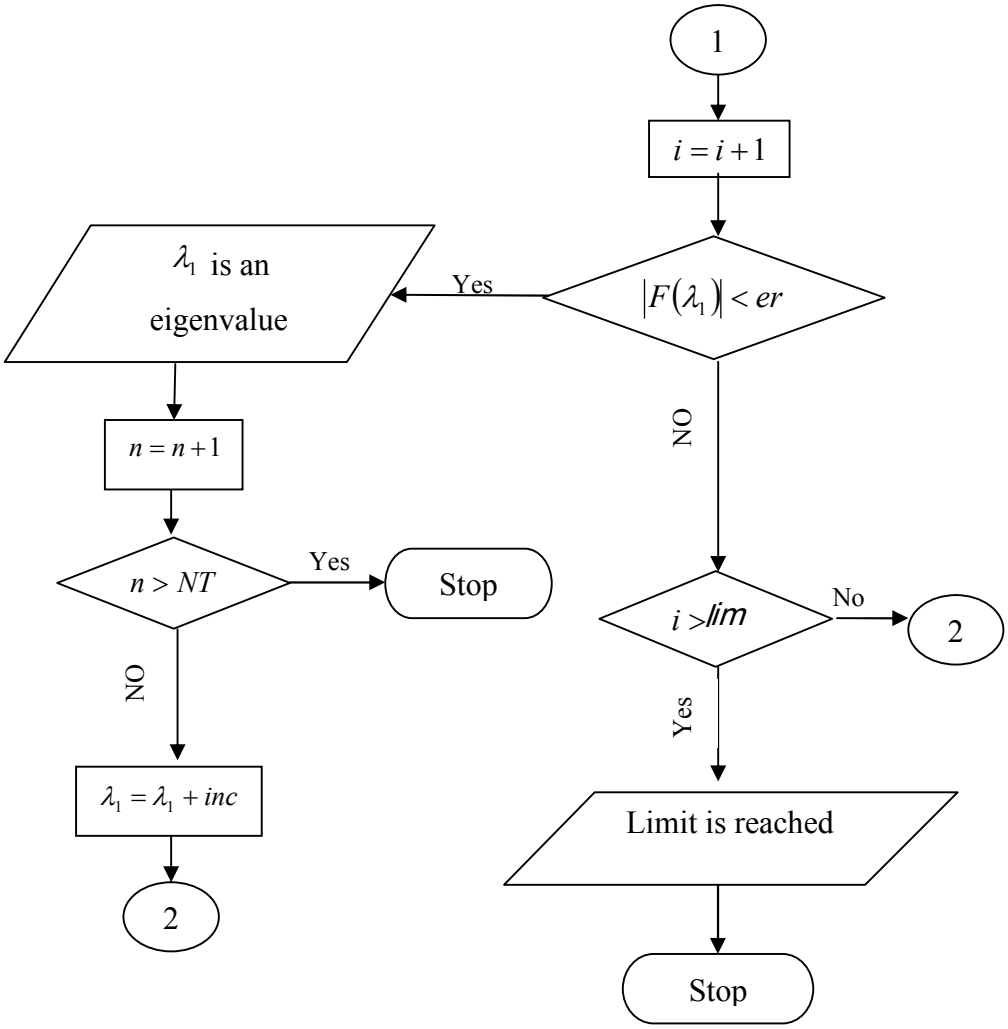

Figure 3.5. Continued.

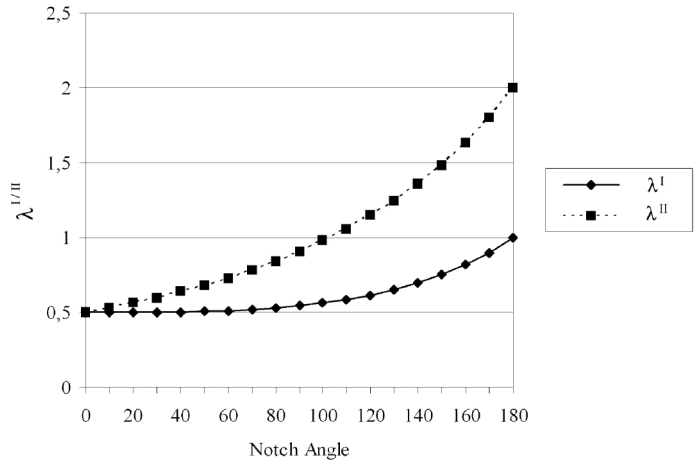

Figure 3.6. Notch angle vs. eigenvalues for mode I and mode II

Similarly, from Eq. (3.55), C_3 can be written in terms of C_1 as

$$C_3 = -\frac{\sin\left(\lambda^{II}+1\right)\alpha}{\sin\left(\lambda^{II}-1\right)\alpha}C_1 = -\frac{\left(\lambda^{II}+1\right)\cos\left(\lambda^{II}+1\right)\alpha}{\left(\lambda^{II}-1\right)\cos\left(\lambda^{II}-1\right)\alpha}C_1 \tag{3.60}$$

Therefore, $F(\theta)$ can be written as

$$\begin{aligned} F(\theta) = F^{I} + F^{II} = C_1\left[\sin\left(\lambda^{II}+1\right)\theta - \frac{\sin\left(\lambda^{II}+1\right)\alpha}{\sin\left(\lambda^{II}-1\right)\alpha}\sin\left(\lambda^{II}-1\right)\theta\right] + \\ C_2\left[\cos\left(\lambda^{I}+1\right)\theta - \frac{\cos\left(\lambda^{I}+1\right)\alpha}{\cos\left(\lambda^{I}-1\right)\alpha}\cos\left(\lambda^{I}-1\right)\theta\right] \end{aligned} \tag{3.61}$$

It would be helpful to mention that the part of $F(\theta)$ associated with the coefficient C_1 represents the mode II stress function. Similarly, the part of $F(\theta)$ associated with the coefficient C_2 represents the mode I stress function.

Now, Eq. (3.45) can be rewritten as

$$F(\theta) = F^{I} + F^{II} \tag{3.62}$$

where

$$F^{I} = C_2\cos\left(\lambda^{I}+1\right)\theta + C_4\cos\left(\lambda^{I}-1\right)\theta \tag{3.63}$$

$$F^{II} = C_1\sin\left(\lambda^{II}+1\right)\theta + C_3\sin\left(\lambda^{II}-1\right)\theta \tag{3.64}$$

and their derivatives as

$$\begin{aligned} F^{I'} &= -\left(\lambda^{I}+1\right)C_2\sin\left(\lambda^{I}+1\right)\theta - \left(\lambda^{I}-1\right)C_4\sin\left(\lambda^{I}-1\right)\theta \\ F^{I''} &= -\left(\lambda^{I}+1\right)^2 C_2\cos\left(\lambda^{I}+1\right)\theta - \left(\lambda^{I}-1\right)^2 C_4\cos\left(\lambda^{I}-1\right)\theta \end{aligned}$$

$$\begin{aligned} F^{II'} &= \left(\lambda^{II}+1\right)C_1\cos\left(\lambda^{II}+1\right)\theta + \left(\lambda^{II}-1\right)C_3\cos\left(\lambda^{II}-1\right)\theta \\ F^{II''} &= -\left(\lambda^{II}+1\right)^2 C_1\sin\left(\lambda^{II}+1\right)\theta - \left(\lambda^{II}-1\right)^2 C_3\sin\left(\lambda^{II}-1\right)\theta \end{aligned}$$

The stress expressions for mode I can be written according to (3.48), (3.49) and (3.50) as follows

$$\sigma_\theta^I = r^{\lambda^I-1}\left[\lambda^I\left(\lambda^I+1\right)F^I\right]$$

$$\sigma_\theta^I = \lambda^I\left(\lambda^I+1\right)r^{\lambda^I-1}\left[C_2\cos\left(\lambda^I+1\right)\theta + C_4\cos\left(\lambda^I-1\right)\theta\right] \tag{3.65}$$

$$\sigma_r^I = r^{\lambda^I-1}\left[F^{I\prime\prime} + \left(\lambda^I+1\right)F^I\right]$$

$$\sigma_r^I = r^{\lambda^I-1}[-\left(\lambda^I+1\right)^2 C_2\cos\left(\lambda^I+1\right)\theta - \left(\lambda^I-1\right)^2 C_4\cos\left(\lambda^I-1\right)\theta + \left(\lambda^I+1\right)\left(C_2\cos\left(\lambda^I+1\right)\theta + C_4\cos\left(\lambda^I-1\right)\theta\right)]$$

$$\sigma_r^I = r^{\lambda^I-1}[\left(-\lambda^{I2} - 2\lambda - 1 + \lambda + 1\right)C_2\cos\left(\lambda^I+1\right)\theta + \left(-\lambda^{I2} + 2\lambda - 1 + \lambda + 1\right)C_4\cos\left(\lambda^I-1\right)\theta]$$

$$\sigma_r^I = r^{\lambda^I-1}[\left(-\lambda^{I2} - \lambda^I\right)C_2\cos\left(\lambda^I+1\right)\theta + \left(-\lambda^{I2} + 3\lambda^I\right)C_4\cos\left(\lambda^I-1\right)\theta]$$
$$= r^{\lambda^I-1}[-\lambda^I\left(\lambda^I+1\right)C_2\cos\left(\lambda^I+1\right)\theta - \lambda^I\left(\lambda^I-3\right)C_4\cos\left(\lambda^I-1\right)\theta]$$

$$\sigma_r^I = -\lambda^I r^{\lambda^I-1}[\left(\lambda^I+1\right)C_2\cos\left(\lambda^I+1\right)\theta + \left(\lambda^I-3\right)C_4\cos\left(\lambda^I-1\right)\theta] \tag{3.66}$$

$$\sigma_{r\theta}^I = r^{\lambda^I-1}\left[-\lambda^I F^{I\prime}\right]$$
$$= -\lambda^I r^{\lambda^I-1}\left[-\left(\lambda^I+1\right)C_2\sin\left(\lambda^I+1\right)\theta - \left(\lambda^I-1\right)C_4\sin\left(\lambda^I-1\right)\theta\right]$$

$$\sigma_{r\theta}^I = \lambda^I r^{\lambda^I-1}\left[\left(\lambda^I+1\right)C_2\sin\left(\lambda^I+1\right)\theta + \left(\lambda^I-1\right)C_4\sin\left(\lambda^I-1\right)\theta\right] \tag{3.67}$$

Similarly, the stress expressions for mode II can be written according to (3.48), (3.49) and (3.50) as follows

$$\sigma_\theta^{II} = r^{\lambda^{II}-1}\left[\lambda^{II}\left(\lambda^{II}+1\right)F^{II}\right]$$

$$\sigma_\theta^{II} = \lambda^{II}\left(\lambda^{II}+1\right)r^{\lambda^{II}-1}\left[C_1\sin\left(\lambda^{II}+1\right)\theta + C_3\sin\left(\lambda^{II}-1\right)\theta\right] \tag{3.68}$$

$$\sigma_r^{II} = r^{\lambda^{II}-1}\left[F^{II\prime\prime} + \left(\lambda^{II}+1\right)F^{II}\right]$$

$$\sigma_r^{II} = r^{\lambda^{II}-1}[-(\lambda^I+1)^2 C_1 \sin(\lambda^{II}+1)\theta - (\lambda^{II}-1)^2 C_3 \sin(\lambda^{II}-1)\theta + (\lambda^{II}+1)(C_1 \sin(\lambda^{II}+1)\theta + C_3 \sin(\lambda^{II}-1)\theta)]$$

$$\sigma_r^{II} = r^{\lambda^{II}-1}[-\lambda^{II}(\lambda^{II}+1)C_1 \sin(\lambda^{II}+1)\theta - \lambda^{II}(\lambda^{II}-3)C_3 \sin(\lambda^{II}-1)\theta]$$

$$\sigma_r^{II} = -\lambda^{II} r^{\lambda^{II}-1}[(\lambda^{II}+1)C_1 \sin(\lambda^{II}+1)\theta + (\lambda^{II}-3)C_3 \sin(\lambda^{II}-1)\theta \tag{3.69}$$

$$\sigma_{r\theta}^{II} = r^{\lambda^{II}-1}\left[-\lambda^{II} F^{II\prime}\right]$$

$$\sigma_{r\theta}^{II} = -\lambda^{II} r^{\lambda^{II}-1}\left[(\lambda^{II}+1)C_1 \cos(\lambda^{II}+1)\theta + (\lambda^{II}-1)C_3 \cos(\lambda^{II}-1)\theta\right] \tag{3.70}$$

And finally, according to the principle of superposition, the stress expressions for mixed-mode cases are (it should be noted that these expressions are series expansions and that the $\sum$ symbols are dropped for simplicity. This has been adopted throughout the thesis)

$$\sigma_r = \sigma_r^I + \sigma_r^{II}$$
$$\sigma_r = -\lambda^I r^{\lambda^I-1}\left[(\lambda^I+1)C_2 \cos(\lambda^I+1)\theta + (\lambda^I-3)C_4 \cos(\lambda^I-1)\theta\right] - \lambda^{II} r^{\lambda^{II}-1}\left[(\lambda^{II}+1)C_1 \sin(\lambda^{II}+1)\theta + (\lambda^{II}-3)C_3 \sin(\lambda^{II}-1)\theta\right] \tag{3.71}$$

$$\sigma_\theta = \sigma_\theta^I + \sigma_\theta^{II}$$
$$\sigma_\theta = \lambda^I(\lambda^I+1) r^{\lambda^I-1}\left[C_2 \cos(\lambda^I+1)\theta + C_4 \cos(\lambda^I-1)\theta\right] + \lambda^{II}(\lambda^{II}+1) r^{\lambda^{II}-1}\left[C_1 \sin(\lambda^{II}+1)\theta + C_3 \sin(\lambda^{II}-1)\theta\right] \tag{3.72}$$

$$\sigma_{r\theta} = \sigma_{r\theta}^I + \sigma_{r\theta}^{II}$$
$$\sigma_{r\theta} = \lambda^I r^{\lambda^I-1}\left[(\lambda^I+1)C_2 \sin(\lambda^I+1)\theta + (\lambda^I-1)C_4 \sin(\lambda^I-1)\theta\right] - \lambda^{II} r^{\lambda^{II}-1}\left[(\lambda^{II}+1)C_1 \cos(\lambda^{II}+1)\theta + (\lambda^{II}-1)C_3 \cos(\lambda^{II}-1)\theta\right] \tag{3.73}$$

The stress expressions in the Cartesian co-ordinates can be derived by using the following transformation equations:

$$\sigma_x = \sigma_r \cos^2\theta + \sigma_\theta \sin^2\theta - 2\sigma_{r\theta} \sin\theta \cos\theta \tag{3.74}$$

$$\sigma_y = \sigma_r \sin^2\theta + \sigma_\theta \cos^2\theta + 2\sigma_{r\theta} \sin\theta\cos\theta \tag{3.75}$$

$$\sigma_{xy} = (\sigma_r - \sigma_\theta)\sin\theta\cos\theta + \sigma_{r\theta}(\cos^2\theta - \sin^2\theta) \tag{3.76}$$

Therefore, the mode I stress expressions in the Cartesian co-ordinates can be written as

$$\sigma_x^I = \lambda^I r^{\lambda^I - 1}\left\{\left[2C_4 - (\lambda^I + 1)C_2\right]\cos(\lambda^I - 1)\theta - (\lambda^I - 1)C_4 os(\lambda^I - 3)\theta\right\} \tag{3.77}$$

$$\sigma_y^I = \lambda^I r^{\lambda^I - 1}\left\{\left[2C_4 + (\lambda^I + 1)C_2\right]\cos(\lambda^I - 1)\theta + (\lambda^I - 1)C_4 \cos(\lambda^I - 3)\theta\right\} \tag{3.78}$$

$$\sigma_{xy}^I = \lambda^I r^{\lambda^I - 1}\left\{(\lambda^I + 1)C_2 \sin(\lambda^I - 1)\theta + (\lambda^I - 1)C_4 \sin(\lambda^I - 3)\theta\right\} \tag{3.79}$$

Similarly, the mode II stress expressions in the Cartesian co-ordinates can be written as

$$\sigma_x^{II} = \lambda^{II} r^{\lambda^{II} - 1}\left\{\left[2C_3 - (\lambda^{II} + 1)C_1\right]\sin(\lambda^{II} - 1)\theta - (\lambda^{II} - 1)C_3 \sin(\lambda^{II} - 3)\theta\right\} \tag{3.80}$$

$$\sigma_y^{II} = \lambda^{II} r^{\lambda^{II} - 1}\left\{\left[2C_3 + (\lambda^{II} + 1)C_1\right]\sin(\lambda^{II} - 1)\theta + (\lambda^{II} - 1)C_3 \sin(\lambda^{II} - 3)\theta\right\} \tag{3.81}$$

$$\sigma_{xy}^{II} = \lambda^{II} r^{\lambda^{II} - 1}\left\{-(\lambda^{II} + 1)C_1 \cos(\lambda^{II} - 1)\theta - (\lambda^{II} - 1)C_3 \cos(\lambda^{II} - 3)\theta\right\} \tag{3.82}$$

And finally, the stress expressions for mixed-mode cases are

$$\begin{aligned}\sigma_x &= \sigma_x^I + \sigma_x^{II} \\ \sigma_x &= \lambda^I r^{\lambda^I - 1}\left\{\left[2C_4 - (\lambda^I + 1)C_2\right]\cos(\lambda^I - 1)\theta - (\lambda^I - 1)C_4 os(\lambda^I - 3)\theta\right\} \\ &\quad + \lambda^{II} r^{\lambda^{II} - 1}\left\{\left[2C_3 - (\lambda^{II} + 1)C_1\right]\sin(\lambda^{II} - 1)\theta - (\lambda^{II} - 1)C_3 \sin(\lambda^{II} - 3)\theta\right\}\end{aligned} \tag{3.83}$$

$$\begin{aligned}\sigma_y &= \sigma_y^I + \sigma_y^{II} \\ \sigma_y &= \lambda^I r^{\lambda^I - 1}\left\{\left[2C_4 + (\lambda^I + 1)C_2\right]\cos(\lambda^I - 1)\theta + (\lambda^I - 1)C_4 \cos(\lambda^I - 3)\theta\right\} \\ &\quad + \lambda^{II} r^{\lambda^{II} - 1}\left\{\left[2C_3 + (\lambda^{II} + 1)C_1\right]\sin(\lambda^{II} - 1)\theta + (\lambda^{II} - 1)C_3 \sin(\lambda^{II} - 3)\theta\right\}\end{aligned} \tag{3.84}$$

$$\begin{aligned}\sigma_{xy} &= \sigma_{xy}^I + \sigma_{xy}^{II} \\ \sigma_{xy} &= \lambda^I r^{\lambda^I - 1}\left\{(\lambda^I + 1)C_2 \sin(\lambda^I - 1)\theta + (\lambda^I - 1)C_4 \sin(\lambda^I - 3)\theta\right\} \\ &\quad + \lambda^{II} r^{\lambda^{II} - 1}\left\{-(\lambda^{II} + 1)C_1 \cos(\lambda^{II} - 1)\theta - (\lambda^{II} - 1)C_3 \cos(\lambda^{II} - 3)\theta\right\}\end{aligned} \tag{3.85}$$

Displacement Expressions

The displacements can be expressed in a polar coordinate system as illustrated in Figure 3.4 as follows (Coker and Filon, 1931):

$$u_r = \frac{1}{2G}\left[-\frac{\partial \Phi}{\partial r} + (1-\eta) r \frac{\partial \psi}{\partial \theta}\right] \tag{3.86}$$

$$u_\theta = \frac{1}{2G}\left[-\frac{1}{r}\frac{\partial \Phi}{\partial \theta} + (1-\eta) r^2 \frac{\partial \psi}{\partial r}\right] \tag{3.87}$$

where G is the shear modulus, $\eta = \nu$ for plane strain, $\eta = \frac{\nu}{1+\nu}$ for plane stress and ν is the Poisson's ratio. The function ψ is related to the biharmonic function Φ as

$$\nabla^2 \Phi = \frac{\partial}{\partial r}\left(r \frac{\partial \psi}{\partial \theta}\right) \tag{3.88}$$

Also, ψ satisfies Laplace's equation (Coker and Filon, 1931), that is

$$\nabla^2 \psi = 0 \tag{3.89}$$

Solutions for ψ can be supposed to be

$$\psi(r,\theta) = r^m G(\theta) \tag{3.90}$$

Substituting Eq. (3.90) into Eq. (3.89) gives

$$m^2 G(\theta) + G''(\theta) = 0 \tag{3.91}$$

The general solution of this equation is

$$G(\theta) = A_1 \cos m\theta + A_2 \sin m\theta \tag{3.92}$$

Using Eqs. (3.42) and (3.90) in Eq. (3.88) provides a relation between $F(\theta)$ and $G(\theta)$. Equating the powers of r gives

$$m = \lambda - 1 \tag{3.93}$$

and equating the coefficients of similar trigonometric terms gives

$$A_1 = -\frac{4}{\lambda - 1} C_3 \tag{3.94}$$

$$A_2 = \frac{4}{\lambda - 1} C_4 \tag{3.95}$$

Therefore, $G(\theta)$ can be written as

$$G(\theta) = \frac{4}{\lambda - 1}\left[-C_3 \cos(\lambda - 1)\theta + C_4 \sin(\lambda - 1)\theta\right] \tag{3.96}$$

or by writing it in terms of C_1 and C_2 as

$$G(\theta) = \frac{4}{\lambda - 1}\left[C_1 \frac{\sin(\lambda + 1)\alpha}{\sin(\lambda - 1)\alpha} \cos(\lambda - 1)\theta - C_2 \frac{\cos(\lambda + 1)\alpha}{\cos(\lambda - 1)\alpha} \sin(\lambda - 1)\theta\right] \tag{3.97}$$

Equations (3.96) and (3.97), can be rewritten as follows (θ is omitted for convenience)

$$G = G^I + G^{II}$$

$$G^I = \frac{4}{\lambda^I - 1} C_4 \sin(\lambda^I - 1)\theta = -\frac{4}{\lambda^I - 1} C_2 \frac{\cos(\lambda^I + 1)\alpha}{\cos(\lambda^I - 1)\alpha} \sin(\lambda^I - 1)\theta \tag{3.98}$$

$$G^{II} = -\frac{4}{\lambda^{II} - 1} C_3 \cos(\lambda^{II} - 1)\theta = \frac{4}{\lambda^{II} - 1} C_1 \frac{\sin(\lambda^{II} + 1)\alpha}{\sin(\lambda^{II} - 1)\alpha} \cos(\lambda^{II} - 1)\theta \tag{3.99}$$

and their derivatives as

$$G^{I'} = 4C_4 \cos(\lambda^I - 1)\theta$$

$$G^{II'} = 4C_3 \sin(\lambda^{II} - 1)\theta$$

From (3.86) and (3.87), the displacement expressions in the radial and circumferential directions can be expressed as

$$u_r = \frac{1}{2G}\left[-(\lambda + 1) r^\lambda F(\theta) + (1 - \eta) r^\lambda G'(\theta)\right] \tag{3.100}$$

$$u_\theta = \frac{1}{2G}\left[-r^\lambda F'(\theta) + (1 - \eta)(\lambda - 1) r^\lambda G(\theta)\right] \tag{3.101}$$

From equations (3.45), (3.96), (3.100) and (3.101), the mode I displacement expressions in the radial direction can be written as follows

$$u_r^I = \frac{1}{2G}\left[-\left(\lambda^I+1\right)r^{\lambda^I}F^I(\theta)+(1-\eta)r^{\lambda^I}G^{I'}(\theta)\right]$$

$$u_r^I = \frac{r^{\lambda^I}}{2G}\left[-\left(\lambda^I+1\right)C_2\cos\left(\lambda^I+1\right)\theta + C_4\left(3-\lambda^I-4\eta\right)\cos\left(\lambda^I-1\right)\theta\right] \tag{3.102}$$

and in the circumferential direction as

$$u_\theta^I = \frac{1}{2G}\left[-r^{\lambda^I}F^{I'}(\theta)+(1-\eta)\left(\lambda^I-1\right)r^{\lambda^I}G^I(\theta)\right]$$

$$u_\theta^I = \frac{r^{\lambda^I}}{2G}\left[\left(\lambda^I+1\right)C_2\sin\left(\lambda^I+1\right)\theta + C_4\left(3+\lambda^I-4\eta\right)\sin\left(\lambda^I-1\right)\theta\right] \tag{3.103}$$

Similarly, the mode II displacement expressions in the radial direction can be written as follows

$$u_r^{II} = \frac{1}{2G}\left[-\left(\lambda^{II}+1\right)r^{\lambda^{II}}F^{II}(\theta)+(1-\eta)r^{\lambda^{II}}G^{II'}(\theta)\right]$$

$$u_r^{II} = \frac{r^{\lambda^{II}}}{2G}\left[-\left(\lambda^{II}+1\right)C_1\sin\left(\lambda^{II}+1\right)\theta + C_3\left(3-\lambda^{II}-4\eta\right)\sin\left(\lambda^{II}-1\right)\theta\right] \tag{3.104}$$

and in the circumferential direction as

$$u_\theta^{II} = \frac{1}{2G}\left[-r^{\lambda^{II}}F^{II'}(\theta)+(1-\eta)\left(\lambda^{II}-1\right)r^{\lambda^{II}}G^{II}(\theta)\right]$$

$$u_\theta^{II} = \frac{r^{\lambda^{II}}}{2G}\left[-\left(\lambda^{II}+1\right)C_1\cos\left(\lambda^{II}+1\right)\theta - \left(3+\lambda^{II}-4\eta\right)C_3\cos\left(\lambda^{II}-1\right)\theta\right] \tag{3.105}$$

According to the principle of superposition, the mixed-mode displacement field in the radial direction is

$$u_r = u_r^I + u_r^{II}$$

$$u_r = \frac{r^{\lambda^I}}{2G}\left[-\left(\lambda^I+1\right)C_2\cos\left(\lambda^I+1\right)\theta + C_4\left(3-\lambda^I-4\eta\right)\cos\left(\lambda^I-1\right)\theta\right]+ \\ \frac{r^{\lambda^{II}}}{2G}\left[-\left(\lambda^{II}+1\right)C_1\sin\left(\lambda^{II}+1\right)\theta + C_3\left(3-\lambda^{II}-4\eta\right)\sin\left(\lambda^{II}-1\right)\theta\right] \tag{3.106}$$

and in the circumferential direction

$$u_\theta = u_\theta^I + u_\theta^{II}$$

$$u_\theta = \frac{r^{\lambda^I}}{2G}\left[\left(\lambda^I+1\right)C_2\sin\left(\lambda^I+1\right)\theta + C_4\left(3+\lambda^I-4\eta\right)\sin\left(\lambda^I-1\right)\theta\right]+ \\ \frac{r^{\lambda^{II}}}{2G}\left[-\left(\lambda^{II}+1\right)C_1\cos\left(\lambda^{II}+1\right)\theta - C_3\left(3+\lambda^{II}-4\eta\right)\cos\left(\lambda^{II}-1\right)\theta\right] \tag{3.107}$$

In a Cartesian co-ordinate system, the displacement expressions can be written for mode I cases as

$$u^I = u_r^I\cos\theta - u_\theta^I\sin\theta$$

$$u^I = \frac{r^{\lambda^I}}{2G}\left[\left((3-4\eta)C_4 - \left(\lambda^I+1\right)C_2\right)\cos\lambda^I\theta - \lambda^I C_4\cos\left(\lambda^I-2\right)\theta\right] \tag{3.108}$$

$$v^I = u_r^I\sin\theta + u_\theta^I\cos\theta$$

$$v^I = \frac{r^{\lambda^I}}{2G}\left[\left((3-4\eta)C_4 + \left(\lambda^I+1\right)C_2\right)\sin\lambda^I\theta + \lambda^I C_4\sin\left(\lambda^I-2\right)\theta\right] \tag{3.109}$$

and for mode II cases as

$$u^{II} = u_r^{II}\cos\theta - u_\theta^{II}\sin\theta$$

$$u^{II} = \frac{r^{\lambda^{II}}}{2G}\left[\left((3-4\eta)C_3 - \left(\lambda^{II}+1\right)C_1\right)\sin\lambda^{II}\theta - \lambda^{II}C_3\sin\left(\lambda^{II}-2\right)\theta\right] \tag{3.110}$$

$$v^{II} = u_r^{II}\sin\theta + u_\theta^{II}\cos\theta$$

$$v^{II} = \frac{r^{\lambda^{II}}}{2G}\left[-\left((3-4\eta)C_3 + \left(\lambda^{II}+1\right)C_1\right)\cos\lambda^{II}\theta - \lambda^{II}C_3\cos\left(\lambda^{II}-2\right)\theta\right] \tag{3.111}$$

And finally, according to the principle of superposition, the displacement fields for mixed-mode cases in the Cartesian co-ordinates are

$$u = u^I + u^{II}$$

$$\begin{aligned} u = \frac{r^{\lambda^I}}{2G}\left[\left((3-4\eta)C_4 - \left(\lambda^I + 1\right)C_2\right)\cos\lambda^I\theta - \lambda^I C_4\cos\left(\lambda^I - 2\right)\theta\right] + \\ \frac{r^{\lambda^{II}}}{2G}\left[\left((3-4\eta)C_3 - \left(\lambda^{II} + 1\right)C_1\right)\sin\lambda^{II}\theta - \lambda^{II} C_3\sin\left(\lambda^{II} - 2\right)\theta\right] \end{aligned} \tag{3.112}$$

$$v = v^I + v^{II}$$

$$\begin{aligned} v = \frac{r^{\lambda^I}}{2G}\left[\left((3-4\eta)C_4 + \left(\lambda^I + 1\right)C_2\right)\sin\lambda^I\theta + \lambda^I C_4\sin\left(\lambda^I - 2\right)\theta\right] + \\ \frac{r^{\lambda^{II}}}{2G}\left[-\left((3-4\eta)C_3 + \left(\lambda^{II} + 1\right)C_1\right)\cos\lambda^{II}\theta - \lambda^{II} C_3\cos\left(\lambda^{II} - 2\right)\theta\right] \end{aligned} \tag{3.113}$$

3.5.2. Complex Variable Method

The stresses and displacements can be expressed in terms of complex potentials $\Omega(z)$ and $\omega(z)$ as follows (England, 1971)

$$2G\left(u_r + iu_\theta\right) = e^{-i\theta}\left\{(3-4\eta)\Omega(z) - z\,\overline{\Omega'(z)} - \overline{\omega(z)}\right\} \tag{3.114}$$

$$\sigma_r + i\sigma_{r\theta} = \Omega'(z) + \overline{\Omega'(z)} - \overline{z\Omega''(z)} - \frac{\bar{z}}{z}\overline{\omega'(z)} \tag{3.115}$$

$$\sigma_\theta - i\sigma_{r\theta} = \Omega'(z) + \overline{\Omega'(z)} + \overline{z\Omega''(z)} + \frac{\bar{z}}{z}\overline{\omega'(z)} \tag{3.116}$$

where z is a complex variable, $z = re^{i\theta}$, $\bar{z}$ is the conjugate of z, and $\Omega(z)$ and $\omega(z)$ are complex potentials that can be expressed as (Vasilopoulos, 1988)

$$\Omega(z) = A\,z^\lambda, \quad \omega(z) = B\,z^\lambda \tag{3.117}$$

where A, B are complex constants: $A = A_1 + iA_2$, $B = B_1 + iB_2$. Substituting Eq. (3.117) into Eqs. (3.114) to (116) gives

$$2G\left(u_r + iu_\theta\right) = r^\lambda \left\{(3-4\eta)A e^{i(\lambda-1)\theta} - \overline{A}\,\lambda e^{-i(\lambda-1)\theta} - \overline{B} e^{-i(\lambda+1)\theta}\right\} \tag{3.118}$$

$$\sigma_r + i\sigma_{r\theta} = r^{\lambda-1}\lambda\left\{A e^{i(\lambda-1)\theta} - \overline{A}(\lambda-2)e^{-i(\lambda-1)\theta} - \overline{B} e^{-i(\lambda+1)\theta}\right\} \tag{3.119}$$

$$\sigma_\theta - i\sigma_{r\theta} = r^{\lambda-1}\lambda\left\{A e^{i(\lambda-1)\theta} + \overline{A}\,\lambda e^{-i(\lambda-1)\theta} + \overline{B} e^{-i(\lambda+1)\theta}\right\} \tag{3.120}$$

From equation (3.120), applying traction-free boundary conditions at $\theta = \pm\alpha$ gives

$$Ae^{\pm 2i\lambda\alpha} + \overline{A}\,\lambda e^{\pm 2i\alpha} + \overline{B} = 0$$

The following system of equations is obtained by expanding this equation and equating the real and imaginary parts to zero

$$A_1\left(\cos 2\lambda\,\alpha + \lambda\,\cos 2\alpha\right) = -B_1 \tag{3.121a}$$

$$A_2\left(-\sin 2\lambda\,\alpha + \lambda\,\sin 2\alpha\right) = 0 \tag{3.121b}$$

$$A_1\left(\sin 2\lambda\,\alpha + \lambda\,\sin 2\alpha\right) = 0 \tag{3.121c}$$

$$A_2\left(\cos 2\lambda\,\alpha - \lambda\,\cos 2\alpha\right) = B_2 \tag{3.121d}$$

From these equations, for non-trivial solutions,

$$\left(\sin 2\lambda\,\alpha + \lambda\,\sin 2\alpha\right) = 0 \tag{3.121e}$$

$$\left(-\sin 2\lambda\,\alpha + \lambda\,\sin 2\alpha\right) = 0 \tag{3.121f}$$

which are called characteristic equations. On one hand, if the first characteristic equation $\left(\sin 2\lambda\,\alpha + \lambda\,\sin 2\alpha\right) = 0$, then $A_2 = B_2 = 0$ and $B_1 = -A_1\left(\cos 2\lambda\,\alpha + \lambda\,\cos 2\alpha\right)$. After substituting this back into Eq. (3.120), expanding and applying the definition of SIFs, A_1 is found to be related to K_I and consequently Eq. (3.121e) gives the mode I eigenvalues $\left(\lambda^I\right)$. Therefore, Eqs. (3.121a-d) can be written as

$$\left(\sin 2\lambda^I\alpha + \lambda^I \sin 2\alpha\right) = 0$$

$$B_1 = -A_1\left(\cos 2\lambda^I\alpha + \lambda^I \cos 2\alpha\right)$$

On the other hand, if the characteristic equation $\left(-\sin 2\lambda\,\alpha + \lambda\,\sin 2\alpha\right) = 0$, then $A_1 = B_1 = 0$ and $B_2 = A_2\left(\cos 2\lambda\,\alpha - \lambda\,\cos 2\alpha\right)$. Similarly, A_2 is found to be related to

K_{II} and consequently Eq. (3.121f) gives the mode II eigenvalues $\left(\lambda^{II}\right)$. Therefore, Eqs. (3.121a-d) can be written as

$$\left(-\sin 2\lambda^{II}\alpha + \lambda^{II}\sin 2\alpha\right) = 0$$

$$B_2 = A_2\left(\cos 2\lambda^{II}\alpha - \lambda^{II}\cos 2\alpha\right)$$

These characteristic equations are exactly the same as derived previously and, therefore, have the same fundamental roots as shown in Figure 3.6.

From Eqs. (3.118)-(3.120), the stress and displacement expressions can be written as

$$\begin{aligned} u_r = {} & \frac{r^{\lambda^I}}{2G} A_1\left[\left(3-4\eta-\lambda^I\right)\cos\left(\lambda^I-1\right)\theta + \left(\cos 2\lambda^I\alpha + \lambda^I\cos 2\alpha\right)\cos\left(\lambda^I+1\right)\theta\right] + \\ & \frac{r^{\lambda^{II}}}{2G} A_2\left[-\left(3-4\eta-\lambda^{II}\right)\sin\left(\lambda^{II}-1\right)\theta + \left(\cos 2\lambda^{II}\alpha - \lambda^{II}\cos 2\alpha\right)\sin\left(\lambda^{II}+1\right)\theta\right] \end{aligned} \tag{3.122}$$

$$\begin{aligned} u_\theta = {} & \frac{r^{\lambda^I}}{2G} A_1\left[\left(3-4\eta+\lambda^I\right)\sin\left(\lambda^I-1\right)\theta - \left(\cos 2\lambda^I\alpha + \lambda^I\cos 2\alpha\right)\sin\left(\lambda^I+1\right)\theta\right] + \\ & \frac{r^{\lambda^{II}}}{2G} A_2\left[\left(3-4\eta+\lambda^{II}\right)\cos\left(\lambda^{II}-1\right)\theta + \left(\cos 2\lambda^{II}\alpha - \lambda^{II}\cos 2\alpha\right)\cos\left(\lambda^{II}+1\right)\theta\right] \end{aligned} \tag{3.123}$$

$$\begin{aligned} \sigma_r = {} & r^{\lambda^I-1}\lambda^I A_1\left[-\left(\lambda^I-3\right)\cos\left(\lambda^I-1\right)\theta + \left(\cos 2\lambda^I\alpha + \lambda^I\cos 2\alpha\right)\cos\left(\lambda^I+1\right)\theta\right] + \\ & r^{\lambda^{II}-1}\lambda^{II} A_2\left[\left(\lambda^{II}-3\right)\sin\left(\lambda^{II}-1\right)\theta + \left(\cos 2\lambda^{II}\alpha - \lambda^{II}\cos 2\alpha\right)\sin\left(\lambda^{II}+1\right)\theta\right] \end{aligned} \tag{3.124}$$

$$\begin{aligned} \sigma_\theta = {} & r^{\lambda^I-1}\lambda^I A_1\left[\left(\lambda^I+1\right)\cos\left(\lambda^I-1\right)\theta - \left(\cos 2\lambda^I\alpha + \lambda^I\cos 2\alpha\right)\cos\left(\lambda^I+1\right)\theta\right] \\ & -r^{\lambda^{II}-1}\lambda^{II} A_2\left[\left(\lambda^{II}+1\right)\sin\left(\lambda^{II}-1\right)\theta + \left(\cos 2\lambda^{II}\alpha - \lambda^{II}\cos 2\alpha\right)\sin\left(\lambda^{II}+1\right)\theta\right] \end{aligned} \tag{3.125}$$

$$\begin{aligned} \sigma_{r\theta} = {} & r^{\lambda^I-1}\lambda^I A_1\left[\left(\lambda^I-1\right)\sin\left(\lambda^I-1\right)\theta - \left(\cos 2\lambda^I\alpha + \lambda^I\cos 2\alpha\right)\sin\left(\lambda^I+1\right)\theta\right] + \\ & r^{\lambda^{II}-1}\lambda^{II} A_2\left[\left(\lambda^{II}-1\right)\cos\left(\lambda^{II}-1\right)\theta + \left(\cos 2\lambda^{II}\alpha - \lambda^{II}\cos 2\alpha\right)\cos\left(\lambda^{II}+1\right)\theta\right] \end{aligned} \tag{3.126}$$

These expressions are equivalent to the ones derived using the eigenfunction expansion approach in the previous section.

For the case $\lambda = 1$, the complex potentials are given as

$$\Omega(z) = Az,\ \omega(z) = Bz \tag{3.127}$$

If $\gamma \neq 0^\circ, 180^\circ$, then $A_1 = B_1 = B_2 = 0$ and the displacements represent a rigid body movement and given as

$$u_r = 0,\ 2Gu_\theta = r\left(3 - 4\eta - 1\right) A_2$$

If $\gamma = 0^\circ, 180^\circ$, then $B_2 = 0,\ 2A_1 = -B_1 \cos 2\alpha$ and the displacement expressions are given as

$$2Gu_r = r\left[- B_1 \frac{3 - 4\eta}{2} \cos 2\alpha - B_1 \cos 2\theta \right] \tag{3.128}$$

$$2Gu_\theta = r\left[\left(3 - 4\eta + 1\right)A_2 + B_1 \sin 2\theta\right] \tag{3.129}$$

3.5.3. Mode I and II Stress Intensity Factors (SIFs)

The notch stress intensity factors are defined in a way similar to those of a crack as

$$K_I = \sqrt{2\pi} \lim_{r \to 0} r^{1-\lambda^I} \sigma_\theta (\theta = 0) \tag{3.130}$$

$$K_{II} = \sqrt{2\pi} \lim_{r \to 0} r^{1-\lambda^{II}} \sigma_{r\theta} (\theta = 0) \tag{3.131}$$

for mode I and mode II, respectively.

By substituting the stress expressions (3.72) and (3.73) into Eqs. (3.130) and (3.131), the relations between the SIFs and the generalised co-ordinates are obtained as

$$K_I = \sqrt{2\pi} \lambda^I \left(\lambda^I + 1\right)\left(1 - \frac{\cos\left(\lambda^I + 1\right)\alpha}{\cos\left(\lambda^I - 1\right)\alpha}\right) C_2 \tag{3.132}$$

$$K_{II} = -\sqrt{2\pi} \lambda^{II} \left[\left(\lambda^{II} + 1\right) - \left(\lambda^{II} - 1\right) \frac{\sin\left(\lambda^{II} + 1\right)\alpha}{\sin\left(\lambda^{II} - 1\right)\alpha} \right] C_1 \tag{3.133}$$

or by substituting equations (3.125) and (3.126) into (3.130) and (3.131) as

$$K_I = \sqrt{2\pi}\lambda^I\left(1+\lambda^I-\lambda^I\cos 2\alpha-\cos 2\lambda^I\alpha\right)A_1 \tag{3.134}$$

$$K_{II} = \sqrt{2\pi}\lambda^{II}\left(-1+\lambda^{II}-\lambda^{II}\cos 2\alpha+\cos 2\lambda^{II}\alpha\right)A_2 \tag{3.135}$$

Eqs. (3.132) to (3.135) show that the SIFs are directly related to the generalised coordinates. As the generalised coordinates are computed directly in the FFEM, no post-processing technique is necessary to extract the notch SIFs.

3.6. GIFs for Homogenous Isotropic Notch under Anti-plane Loading (Mode III)

3.6.1. Stress and Displacement Expressions

The stress and displacement expressions of a notch subject to anti-plane shear loading conditions can be derived by using a stress function approach. The only non-zero displacement component is in the z direction (w) and the non-zero stresses are τ_{rz} and $\tau_{\theta z}$ which can be derived by using a stress function (Φ) in a polar coordinate system centred at the tip of an infinite notch as illustrated in Figure 3.4. The equilibrium equations are satisfied if the stresses are derived as follows

$$\tau_{rz} = -\frac{1}{r}\frac{\partial\Phi}{\partial\theta} \tag{3.136}$$

$$\tau_{\theta z} = \frac{\partial\Phi}{\partial r} \tag{3.137}$$

The compatibility equations are reduced to

$$\nabla^2\Phi = 0 \tag{3.138}$$

where ∇^2 denotes the Laplacian operator. The stress function (Φ) can be taken as

$$\Phi = r^{\lambda^{III}} F(\theta) \tag{3.139}$$

where λ^{III} is an eigenvalue. For simplicity, the superscript is dropped for the rest of this section. After substituting Φ and its derivatives into the differential Eq. (3.138), the solution for Φ is

$$\Phi = r^{\lambda}\left(A\cos\lambda\theta + B\sin\lambda\theta\right) \tag{3.140}$$

Substituting Eq. (3.140) into Eqs. (3.136) and (3.137), the stress expressions are

$$\tau_{rz} = r^{\lambda-1}\lambda\left(A\sin\lambda\theta - B\cos\lambda\theta\right) \tag{3.141}$$

$$\tau_{\theta z} = r^{\lambda-1}\lambda\left(A\cos\lambda\theta + B\sin\lambda\theta\right) \tag{3.142}$$

The eigenvalues λ are obtained by imposing the following boundary conditions on the notch faces

$$\tau_{\theta z}\left(\pm\alpha\right) = 0 \tag{3.143}$$

Substituting Eq. (3.143) into Eq. (3.142) yields

$$r^{\lambda-1}\lambda\left(A\cos\lambda\alpha + B\sin\lambda\alpha\right) = 0 \tag{3.144}$$

$$r^{\lambda-1}\lambda\left(A\cos\lambda\alpha - B\sin\lambda\alpha\right) = 0 \tag{3.145}$$

For non-trivial solutions for A and B, the determinant of equations (3.144) and (3.145) must be zero. By solving the determinant, the eigenvalues are obtained as

$$\lambda = \frac{m\pi}{2\alpha};\ m = 1,2,3,... \tag{3.146}$$

When m is an odd number and assuming that $m = 2n-1$, then substituting that into Eq. (3.146) and (3.144) or (3.145) gives

$$\lambda_m = \left(n - \frac{1}{2}\right)\frac{\pi}{\alpha} \text{ and } B = 0$$

When m is an even number and assuming that $m = 2n$, it can be shown that substituting that into Eq. (3.146) and (3.144) or (3.145) gives

$$\lambda_m = \frac{n\pi}{\alpha} \text{ and } A = 0$$

The eigenfunction series expansions of the stresses can now be written as

$$\tau_{rz} = A\left(n - \frac{1}{2}\right)\frac{\pi}{\alpha} r^{\left(n-\frac{1}{2}\right)\frac{\pi}{\alpha}-1} \sin\left(\left(n - \frac{1}{2}\right)\frac{\pi}{\alpha}\theta\right) - B\frac{n\pi}{\alpha} r^{\frac{n\pi}{\alpha}-1} \cos\left(\frac{n\pi}{\alpha}\theta\right) \tag{3.147}$$

$$\tau_{\theta z} = A\left(n - \frac{1}{2}\right)\frac{\pi}{\alpha} r^{\left(n-\frac{1}{2}\right)\frac{\pi}{\alpha}-1} \cos\left(\left(n - \frac{1}{2}\right)\frac{\pi}{\alpha}\theta\right) + B\frac{n\pi}{\alpha} r^{\frac{n\pi}{\alpha}-1} \sin\left(\frac{n\pi}{\alpha}\theta\right) \tag{3.148}$$

The displacement function w can be derived using the following equations

$$\tau_{rz} = G\gamma_{rz} = G\frac{\partial w}{\partial r} \tag{3.149}$$

and

$$\tau_{\theta z} = G\gamma_{\theta z} = G\frac{\partial w}{r\partial \theta} \tag{3.150}$$

where G is the shear modulus. Integrating Eqs. (3.149) and (3.150) gives

$$Gw = Ar^{\left(n-\frac{1}{2}\right)\frac{\pi}{\alpha}} \sin\left(\left(n - \frac{1}{2}\right)\frac{\pi}{\alpha}\theta\right) - Br^{\frac{n\pi}{\alpha}} \cos\left(\frac{n\pi}{\alpha}\theta\right) \tag{3.151}$$

3.6.2. Mode III Stress Intensity Factors (SIFs)

The stress intensity factors of a notch are defined in a way similar to those of a crack as

$$K_{III} = \sqrt{2\pi} \lim_{r \to 0} r^{1-\lambda^{III}} \tau_{\theta z}(\theta = 0) \tag{3.152}$$

Substituting equations (3.148) into equations (3.152) gives

$$K_{III} = \sqrt{2\pi} \lambda^{III} A \tag{3.153}$$

Equation (3.153) demonstrates a direct and simple relationship between the SIFs and the generalised co-ordinates.

3.7. GIFs for Bi-material Notch under In-plane Loading (Modes I and II)

3.7.1. Stress and Displacement Expressions

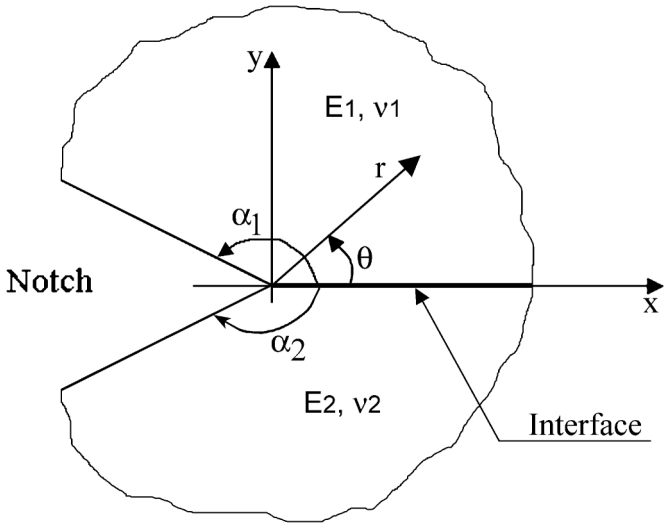

Figure 3.7. Bi-material notch geometry

The stress and displacement functions of a bi-material notch as shown in Figure 3.7 can be expressed using a complex variable approach as:

$$\sigma_{xx}^{j} + \sigma_{yy}^{j} = 4\,\mathrm{Re}\left(\phi^{j\prime}(z)\right) \tag{3.154}$$

$$\sigma_{yy}^{j} - i\tau_{xy}^{j} = \phi^{j\prime}(z) + (z - \bar{z})\overline{\phi^{j\prime\prime}(z)} + \overline{\omega^{j\prime}(z)} \tag{3.155}$$

$$-P_y^j + iP_x^j = \phi^j(z) + (z-\bar{z})\overline{\phi^{j\prime}(z)} + \overline{\omega^j(z)} \tag{3.156}$$

$$u_x^j + iu_y^j = \frac{1}{2G_j}\left[\kappa_j \phi^j(z) - (z-\bar{z})\overline{\phi^{j\prime}(z)} - \overline{\omega^j(z)}\right] \tag{3.157}$$

where j refers to material j, G_j is the shear modulus of material j, $\kappa_j = 3-4\nu_j$ for plane-strain or $\kappa_j = 3-4\nu_j/(1+\nu_j)$ for plane-stress and ν_j is the Poisson's ratio of material j. $\phi^j(z)$ and $\omega^j(z)$ are complex potentials and are assumed to be (Theocaris, 1974)

$$\begin{aligned}\phi^j(z) &= A_j z^{\lambda} + a_j z^{\bar{\lambda}} \\ \omega^j(z) &= B_j z^{\lambda} + b_j z^{\bar{\lambda}}\end{aligned} \tag{3.158}$$

Substituting Eq.(3.158) into Eqs. (3.155) to (3.157) gives

$$\begin{aligned}\sigma_{yy}^j - i\tau_{xy}^j = {} & \lambda r^{\lambda-1} e^{i\theta(1-\lambda)}[A_j e^{2i\theta(\lambda-1)} + \bar{a}_j\left(e^{2i\theta}-1\right)(\lambda-1) + \bar{b}_j] \\ & + \bar{\lambda} r^{\bar{\lambda}-1} e^{i\theta(1-\bar{\lambda})}[a_j e^{2i\theta(\bar{\lambda}-1)} + \bar{A}_j\left(e^{2i\theta}-1\right)(\bar{\lambda}-1) + \bar{B}_j]\end{aligned} \tag{3.159}$$

$$\begin{aligned}-P_y^j + iP_x^j = {} & r^{\lambda} e^{-i\theta\lambda}[A_j e^{2i\theta\lambda} + \bar{a}_j\lambda\left(e^{2i\theta}-1\right) + \bar{b}_j] \\ & + r^{\bar{\lambda}} e^{-i\theta\bar{\lambda}}[a_j e^{2i\theta\bar{\lambda}} + \bar{A}_j\bar{\lambda}\left(e^{2i\theta}-1\right) + \bar{B}_j]\end{aligned} \tag{3.160}$$

$$\begin{aligned}2G_j\left(u_x^j + iu_y^j\right) = {} & r^{\lambda} e^{-i\theta\lambda}[\kappa_j A_j e^{2i\theta\lambda} - \bar{a}_j\lambda\left(e^{2i\theta}-1\right) - \bar{b}_j] \\ & + r^{\bar{\lambda}} e^{-i\theta\bar{\lambda}}[\kappa_j a_j e^{2i\theta\bar{\lambda}} - \bar{A}_j\bar{\lambda}\left(e^{2i\theta}-1\right) - \bar{B}_j]\end{aligned} \tag{3.161}$$

3.7.1.1. Derivation of Eigenvalues

The complex potentials must satisfy the following continuity and boundary conditions

$$\begin{aligned}&-P_y^1 + iP_x^1\Big|_{\theta=0} = -P_y^2 + iP_x^2\Big|_{\theta=0} \\ &u_x^1 + iu_y^1\Big|_{\theta=0} = u_x^2 + iu_y^2\Big|_{\theta=0} \\ &-P_y^1 + iP_x^1\Big|_{\theta=\alpha_1} = 0 \\ &-P_y^2 + iP_x^2\Big|_{\theta=-\alpha_2} = 0\end{aligned} \tag{3.162}$$

Substituting Eqs. (3.160)-(3.161) into (3.162) gives, after simplification,

$$A_1 + \overline{b}_1 = A_2 + \overline{b}_2 \tag{3.163}$$

$$a_1 + \overline{B}_1 = a_2 + \overline{B}_2 \tag{3.164}$$

$$G_2\left(\kappa_1 A_1 - \overline{b}_1\right) = G_1\left(\kappa_2 A_2 - \overline{b}_2\right) \tag{3.165}$$

$$G_2\left(\kappa_1 a_1 - \overline{B}_1\right) = G_1\left(\kappa_2 a_2 - \overline{B}_2\right) \tag{3.166}$$

$$\overline{b}_1 = -A_1 e^{2i\lambda\alpha_1} - \left(e^{2i\alpha_1} - 1\right)\lambda\overline{a}_1 \tag{3.167}$$

$$\overline{B}_1 = -a_1 e^{2i\overline{\lambda}\alpha_1} - \left(e^{2i\alpha_1} - 1\right)\overline{\lambda A}_1 \tag{3.168}$$

$$\overline{b}_2 = -A_2 e^{-2i\lambda\alpha_2} - \left(e^{-2i\alpha_2} - 1\right)\lambda\overline{a}_2 \tag{3.169}$$

$$\overline{B}_2 = -a_2 e^{-2i\overline{\lambda}\alpha_2} - \left(e^{-2i\alpha_2} - 1\right)\overline{\lambda A}_2 \tag{3.170}$$

Substituting Eqs. (3.167) to (3.170) into Eqs. (3.163) to (3.166) gives

$$A_1\left(1 - e^{2i\lambda\alpha_1}\right) - \lambda\overline{a}_1\left(e^{2i\alpha_1} - 1\right) - A_2\left(1 - e^{-2i\lambda\alpha_2}\right) + \lambda\overline{a}_2\left(e^{-2i\alpha_2} - 1\right) = 0 \tag{3.171}$$

$$-\overline{\lambda A}_1\left(e^{2i\alpha_1} - 1\right) + a_1\left(1 - e^{2i\overline{\lambda}\alpha_1}\right) + \overline{\lambda A}_2\left(e^{-2i\alpha_2} - 1\right) - a_2\left(1 - e^{-2i\overline{\lambda}\alpha_2}\right) = 0 \tag{3.172}$$

$$\frac{G_2}{G_1}\left[A_1\left(\kappa_1 + e^{2i\lambda\alpha_1}\right) + \lambda\overline{a}_1\left(e^{2i\alpha_1} - 1\right)\right] - A_2\left(\kappa_2 + e^{-2i\lambda\alpha_2}\right) - \lambda\overline{a}_2\left(e^{-2i\alpha_2} - 1\right) = 0 \tag{3.173}$$

$$\frac{G_2}{G_1}\left[\overline{\lambda A}_1\left(e^{2i\alpha_1} - 1\right) + a_1\left(\kappa_1 + e^{2i\overline{\lambda}\alpha_1}\right)\right] - \overline{\lambda A}_2\left(e^{-2i\alpha_2} - 1\right) - a_2\left(\kappa_2 + e^{-2i\overline{\lambda}\alpha_2}\right) = 0 \tag{3.174}$$

The conjugates of Eqs (3.171) to (3.174) are

$$\overline{A}_1\left(1 - e^{-2i\overline{\lambda}\alpha_1}\right) - \overline{\lambda}a_1\left(e^{-2i\alpha_1} - 1\right) - \overline{A}_2\left(1 - e^{2i\overline{\lambda}\alpha_2}\right) + \overline{\lambda}a_2\left(e^{2i\alpha_2} - 1\right) = 0 \tag{3.175}$$

$$-\lambda A_1\left(e^{-2i\alpha_1} - 1\right) + \overline{a}_1\left(1 - e^{-2i\lambda\alpha_1}\right) + \lambda A_2\left(e^{2i\alpha_2} - 1\right) - \overline{a}_2\left(1 - e^{2i\lambda\alpha_2}\right) = 0 \tag{3.176}$$

$$\frac{G_2}{G_1}\left[\overline{A}_1\left(\kappa_1 + e^{-2i\overline{\lambda}\alpha_1}\right) + \overline{\lambda}a_1\left(e^{-2i\alpha_1} - 1\right)\right] - \overline{A}_2\left(\kappa_2 + e^{2i\overline{\lambda}\alpha_2}\right) - \overline{\lambda}\overline{a}_2\left(e^{2i\alpha_2} - 1\right) = 0 \tag{3.177}$$

$$\frac{G_2}{G_1}\left[\lambda A_1\left(e^{-2i\alpha_1} - 1\right) + \overline{a}_1\left(\kappa_1 + e^{-2i\lambda\alpha_1}\right)\right] - \lambda A_2\left(e^{2i\alpha_2} - 1\right) - \overline{a}_2\left(\kappa_2 + e^{2i\lambda\alpha_2}\right) = 0 \tag{3.178}$$

Eqs. (3.171), (3.173), (3.176) and (3.178) can be written in matrix form as

$$\begin{bmatrix} 1-e^{2i\lambda\alpha_1} & e^{-2i\lambda\alpha_2}-1 & \lambda\left(1-e^{2i\alpha_1}\right) & \lambda\left(e^{-2i\alpha_2}-1\right) \\ \frac{G_2}{G_1}\left(\kappa_1+e^{2i\lambda\alpha_1}\right) & -\kappa_2+e^{-2i\lambda\alpha_2} & \frac{G_2}{G_1}\lambda\left(e^{2i\alpha_1}-1\right) & \lambda\left(1-e^{-2i\alpha_2}\right) \\ \lambda\left(1-e^{-2i\alpha_1}\right) & \lambda\left(e^{2i\alpha_2}-1\right) & 1-e^{-2i\lambda\alpha_1} & e^{2i\lambda\alpha_2}-1 \\ \frac{G_2}{G_1}\lambda\left(e^{-2i\alpha_1}-1\right) & \lambda\left(1-e^{2i\alpha_2}\right) & \frac{G_2}{G_1}\left(\kappa_1+e^{-2i\lambda\alpha_1}\right) & -\left(\kappa_2+e^{2i\lambda\alpha_2}\right) \end{bmatrix} \begin{Bmatrix} A_1 \\ A_2 \\ \bar{a}_1 \\ \bar{a}_2 \end{Bmatrix} = \{0\} \tag{3.179}$$

Eq. (3.179) can be rewritten in a short form as

$$[\mathbf{D}][A_1 \quad A_2 \quad \bar{a}_1 \quad \bar{a}_2]^T = \{0\} \tag{3.180}$$

For non-trivial solutions the determinant of $[\mathbf{D}]$ should be zero, i.e.

$$\det[\mathbf{D}] = 0 \tag{3.181}$$

Solving Eq. (3.181) gives the values of λ, the eigenvalues, that make the determinant zero. The values of λ may be real or complex. A modified version of Muller's method is used to solve this equation. This is done because Muller's method might converge to a specific root within an interval leading to the missing of some of the eigenvalues. The algorithm of the technique used is demonstrated in Figure 3.8. The technique is very simple and is done to force Muller's method to move on to find the next eigenvalue using an incremental increase to the value of the root found in step i if it has the same value as the root found in step $i-1$.

3.7.1.2. Displacement Expressions for Complex Eigenvalues

For complex eigenvalues, Eq. (3.179) may be partitioned as follows

$$\begin{bmatrix} [\mathbf{D}_{11}] & \vdots & [\mathbf{D}_{12}] \\ \cdots & \cdots\cdots & \cdots \\ [\mathbf{D}_{21}] & \vdots & [\mathbf{D}_{22}] \end{bmatrix} \begin{Bmatrix} A_1 \\ \cdots \\ A_2 \\ \bar{a}_1 \\ \bar{a}_2 \end{Bmatrix} = \begin{Bmatrix} 0 \\ \cdots \\ 0 \\ 0 \\ 0 \end{Bmatrix} \tag{3.182}$$

From Eq. (3.182), $A_2, \bar{a}_1$ and $\bar{a}_2$ can be computed in term of A_1 as

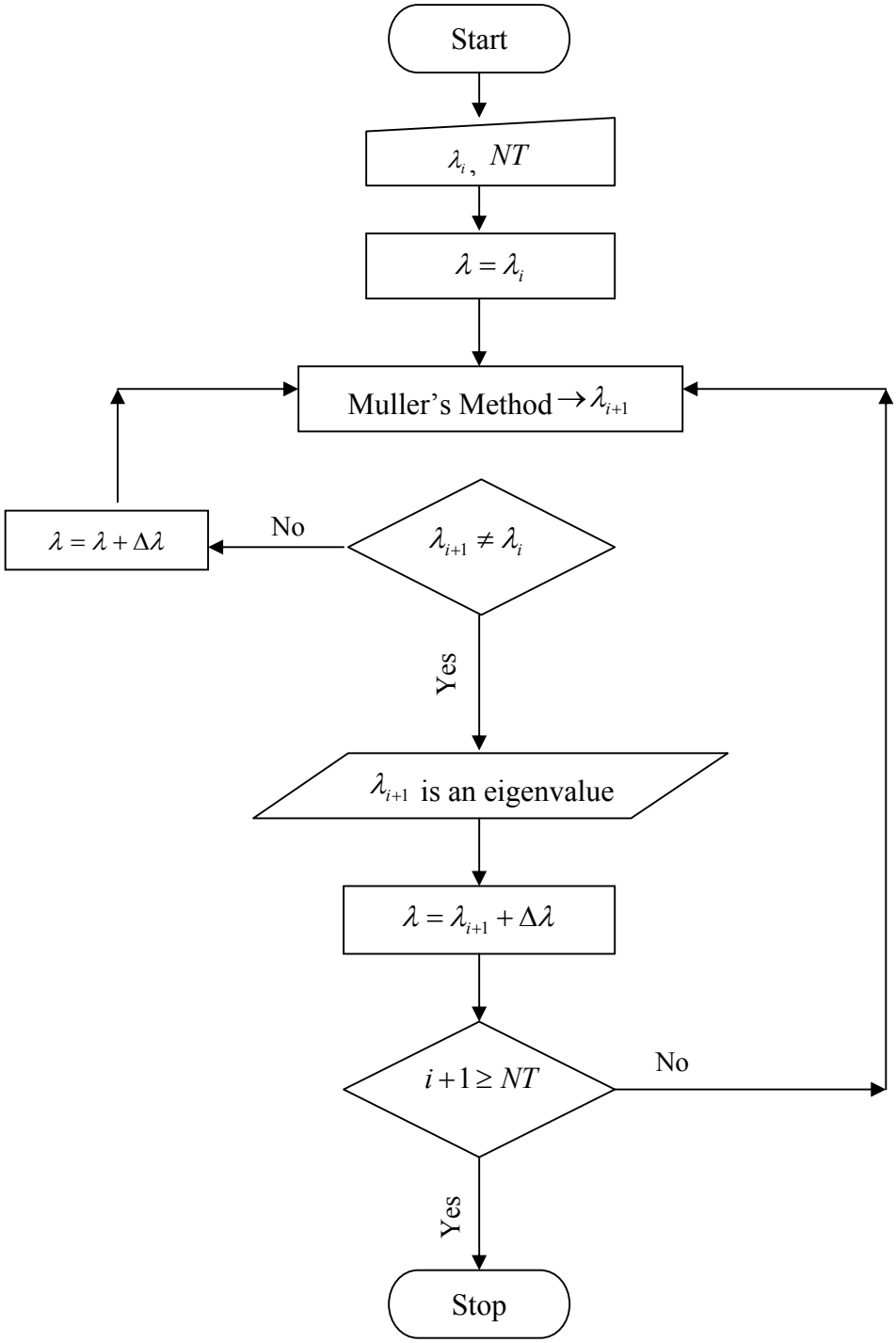

Figure 3.8. Numerical technique to compute the eigenvalues

$$\begin{Bmatrix} A_2 \\ \overline{a}_1 \\ \overline{a}_2 \end{Bmatrix} = -\left[\mathbf{D}_{22}\right]^{-1}\left[\mathbf{D}_{21}\right]A_1 = \{\mathbf{S}\}A_1 \tag{3.183}$$

Substituting the values of the coefficients A_2, $\overline{a}_1$ and $\overline{a}_2$ from Eq. (3.183) into Eqs. (3.167) to (3.170), all the coefficients of the complex potentials can be written in terms of A_1 and its conjugate $\overline{A}_1$ as

$$\begin{Bmatrix} A_1 \\ \overline{A}_1 \\ a_1 \\ \overline{a}_1 \\ B_1 \\ \overline{B}_1 \\ b_1 \\ \overline{b}_1 \end{Bmatrix} = \begin{bmatrix} 1 & 0 \\ 0 & 1 \\ 0 & \overline{\mathbf{S}(2)} \\ \mathbf{S}(2) & 0 \\ -\mathbf{S}(2)e^{-2i\lambda\alpha_1} - \lambda\left(e^{-2i\alpha_1} - 1\right) & 0 \\ 0 & -\overline{\mathbf{S}(2)}e^{2i\overline{\lambda}\alpha_1} - \overline{\lambda}\left(e^{2i\alpha_1} - 1\right) \\ 0 & -e^{-2i\overline{\lambda}\alpha_1} - \overline{\lambda}\,\overline{\mathbf{S}(2)}\left(e^{-2i\alpha_1} - 1\right) \\ -e^{2i\lambda\alpha_1} - \lambda\mathbf{S}(2)\left(e^{2i\alpha_1} - 1\right) & 0 \end{bmatrix} \begin{Bmatrix} A_1 \\ \overline{A}_1 \end{Bmatrix} = \left[\mathbf{H}_1\right] \begin{Bmatrix} A_1 \\ \overline{A}_1 \end{Bmatrix} \tag{3.184}$$

for material 1 and

$$\begin{Bmatrix} A_2 \\ \overline{A}_2 \\ a_2 \\ \overline{a}_2 \\ B_2 \\ \overline{B}_2 \\ b_2 \\ \overline{b}_2 \end{Bmatrix} = \begin{bmatrix} \mathbf{S}(1) & 0 \\ 0 & \overline{\mathbf{S}(1)} \\ 0 & \overline{\mathbf{S}(3)} \\ \mathbf{S}(3) & 0 \\ -\mathbf{S}(3)e^{2i\lambda\alpha_2} - \lambda\mathbf{S}(1)\left(e^{2i\alpha_2} - 1\right) & 0 \\ 0 & -\overline{\mathbf{S}(3)}e^{-2i\overline{\lambda}\alpha_2} - \overline{\lambda}\,\overline{\mathbf{S}(1)}\left(e^{-2i\alpha_2} - 1\right) \\ 0 & -\overline{\mathbf{S}(1)}e^{2i\overline{\lambda}\alpha_2} - \overline{\lambda}\,\overline{\mathbf{S}(3)}\left(e^{2i\alpha_2} - 1\right) \\ -\mathbf{S}(1)e^{-2i\lambda\alpha_2} - \lambda\mathbf{S}(3)\left(e^{-2i\alpha_2} - 1\right) & 0 \end{bmatrix} \begin{Bmatrix} A_1 \\ \overline{A}_1 \end{Bmatrix} = \left[\mathbf{H}_2\right] \begin{Bmatrix} A_1 \\ \overline{A}_1 \end{Bmatrix} \tag{3.185}$$

for material 2. A_1 and its conjugate $\overline{A}_1$ can be written in terms of the real and imaginary parts of A_1 as

$$\begin{Bmatrix} A_1 \\ \overline{A}_1 \end{Bmatrix} = \begin{bmatrix} 1 & i \\ 1 & -i \end{bmatrix} \begin{Bmatrix} \mathrm{Re}(A_1) \\ \mathrm{Im}(A_1) \end{Bmatrix} = \left[\mathbf{N}\right] \begin{Bmatrix} \mathrm{Re}(A_1) \\ \mathrm{Im}(A_1) \end{Bmatrix} \tag{3.186}$$

Assuming that

$$\left[\mathbf{L}_j\right]=\begin{bmatrix} r^{\lambda}\kappa_j e^{-i\lambda\theta}e^{2i\lambda\theta} \\ \overline{\lambda}r^{\overline{\lambda}}e^{-i\overline{\lambda}\theta}\left(1-e^{2i\theta}\right) \\ r^{\overline{\lambda}}\kappa_j e^{-i\overline{\lambda}\theta}e^{2i\overline{\lambda}\theta} \\ \lambda r^{\lambda}e^{-i\lambda\theta}\left(1-e^{2i\theta}\right) \\ 0 \\ -r^{\overline{\lambda}}e^{-i\overline{\lambda}\theta} \\ 0 \\ -r^{\lambda}e^{-i\lambda\theta} \end{bmatrix}^T \tag{3.187}$$

then Eq. (3.161), the displacement expression, can be rewritten as

$$2G_j\left(u_x^j+iu_y^j\right)=\left[\mathbf{L}_j\right]\left[\mathbf{H}_j\right]\left[\mathbf{N}\right]\begin{Bmatrix}\mathrm{Re}(A_1)\\ \mathrm{Im}(A_1)\end{Bmatrix}=\left[\mathbf{J}_j\right]\begin{Bmatrix}\mathrm{Re}(A_1)\\ \mathrm{Im}(A_1)\end{Bmatrix} \tag{3.188}$$

Equating the real and imaginary parts of both sides of Eq. (3.188) leads to

$$\begin{Bmatrix}u_x^j\\ u_y^j\end{Bmatrix}=\frac{1}{2G_j}\begin{bmatrix}\mathrm{Re}\left(\mathbf{J}_j(1,1)\right) & \mathrm{Re}\left(\mathbf{J}_j(1,2)\right)\\ \mathrm{Im}\left(\mathbf{J}_j(1,1)\right) & \mathrm{Im}\left(\mathbf{J}_j(1,2)\right)\end{bmatrix}\begin{Bmatrix}\mathrm{Re}(A_1)\\ \mathrm{Im}(A_1)\end{Bmatrix} \tag{3.189}$$

Eq. (3.189) shows that the displacement expressions for each complex eigenvalue can be written in terms of the real and imaginary parts of a complex coefficient. Therefore, each complex eigenvalue is associated with two elements of the generalised coordinates.

3.7.1. 3. Displacement Expressions for Real Eigenvalues

For real eigenvalues, the complex potentials $\phi^j(z)$ and $\omega^j(z)$ are reduced to

$$\begin{aligned}\phi^j(z)&=A_j z^{\lambda}\\ \omega^j(z)&=B_j z^{\lambda}\end{aligned} \tag{3.190}$$

Substituting Eq. (3.190) into Eqs. (3.155) to (3.157) gives

$$\sigma_{yy}^j-i\tau_{xy}^j=\lambda r^{\lambda-1}e^{i\theta(1-\lambda)}[A_j e^{2i\theta(\lambda-1)}+\overline{A}_j\left(e^{2i\theta}-1\right)(\lambda-1)+\overline{B}_j] \tag{3.191}$$

$$-P_y^j+iP_x^j=r^{\lambda}e^{-i\theta\lambda}[A_j e^{2i\theta\lambda}+\overline{A}_j\lambda\left(e^{2i\theta}-1\right)+\overline{B}_j] \tag{3.192}$$

$$2G_j\left(u_x^j + iu_y^j\right) = r^{\lambda}e^{-i\theta\lambda}[\kappa_j A_j e^{2i\theta\lambda} - \overline{A}_j\lambda\left(e^{2i\theta} - 1\right) - \overline{B}_j] \tag{3.193}$$

Substituting Eqs. (3.191) to (3.193) into Eqs. (3.162) gives

$$G_2\left[\kappa_1 A_1 - \overline{B}_1\right] = G_1\left[\kappa_2 A_2 - \overline{B}_2\right] \tag{3.194}$$

$$A_1 + \overline{B}_1 = A_2 + \overline{B}_2 \tag{3.195}$$

$$\overline{B}_1 = -A_1 e^{2i\lambda\alpha_1} - \left(e^{2i\alpha_1} - 1\right)\lambda\overline{A}_1 \tag{3.196}$$

$$\overline{B}_2 = -A_2 e^{-2i\lambda\alpha_2} - \left(e^{-2i\alpha_2} - 1\right)\lambda\overline{A}_2 \tag{3.197}$$

Substituting Eqs. (3.196) and (3.197) into Eqs. (3.194) and (3.195) gives

$$A_1 d_1 + \overline{A}_1 d_2 + A_2 d_3 + \overline{A}_2 d_4 = 0 \tag{3.198}$$

$$A_1 d_5 + \overline{A}_1 d_6 + A_2 d_7 + \overline{A}_2 d_8 = 0 \tag{3.199}$$

where $d_1 = G_2\left(\kappa_1 + e^{2i\lambda\alpha_1}\right)$, $d_2 = G_2\lambda\left(e^{2i\alpha_1} - 1\right)$, $d_3 = -G_1\left(\kappa_2 + e^{-2i\lambda\alpha_2}\right)$, $d_4 = -G_1\lambda\left(e^{-2i\alpha_2} - 1\right)$, $d_5 = 1 - e^{2i\lambda\alpha_1}$, $d_6 = -\lambda\left(e^{2i\alpha_1} - 1\right)$, $d_7 = e^{-2i\lambda\alpha_2} - 1$, and $d_8 = \lambda\left(e^{-2i\alpha_2} - 1\right)$. Eqs. (3.198) and (3.199) can be written in matrix form as

$$\begin{bmatrix} d_1 & d_2 \\ d_5 & d_6 \end{bmatrix}\begin{Bmatrix} A_1 \\ \overline{A}_1 \end{Bmatrix} + \begin{bmatrix} d_3 & d_4 \\ d_7 & d_8 \end{bmatrix}\begin{Bmatrix} A_2 \\ \overline{A}_2 \end{Bmatrix} = \{0\} \tag{3.200}$$

Solving Eqs. (3.200) for A_2 and its conjugate $\overline{A}_2$ gives

$$A_2 = s_1 A_1 + s_2\overline{A}_1 \tag{3.201}$$

$$\overline{A}_2 = s_3 A_1 + s_4\overline{A}_1 \tag{3.202}$$

where $s_1 = \dfrac{d_4 d_5 - d_1 d_8}{d_3 d_8 - d_7 d_4}$, $s_2 = \dfrac{d_6 d_4 - d_2 d_8}{d_3 d_8 - d_7 d_4}$, $s_3 = \dfrac{d_5 d_3 - d_1 d_7}{d_4 d_7 - d_8 d_3}$, and $s_4 = \dfrac{d_6 d_3 - d_2 d_7}{d_4 d_7 - d_8 d_3}$.

Subtracting Eq. (3.202) from the conjugate of Eq. (3.201) gives

$$t_1 A_1 + t_2\overline{A}_1 = 0 \tag{3.203}$$

where $t_1 = \bar{s}_2 - s_3$ and $t_2 = \bar{s}_1 - s_4$. Eq. (3.203) could be written in terms of the real and imaginary parts of the A_1 as

$$\begin{bmatrix} q_{11} & q_{12} \\ q_{21} & q_{22} \end{bmatrix} \begin{Bmatrix} \mathrm{Re}(A_1) \\ \mathrm{Im}(A_1) \end{Bmatrix} = \{0\} \tag{3.204}$$

where $q_{11} = \mathrm{Re}(t_1) + \mathrm{Re}(t_2)$, $q_{12} = \mathrm{Im}(t_2) - \mathrm{Im}(t_1)$, $q_{21} = \mathrm{Im}(t_1) + \mathrm{Im}(t_2)$, and $q_{22} = \mathrm{Re}(t_1) - \mathrm{Re}(t_2)$.

Eq. (3.204) shows that $\mathrm{Im}(A_1)$ can be determined in terms of $\mathrm{Re}(A_1)$ or vice versa, i.e.,

$$\begin{Bmatrix} \mathrm{Re}(A_1) \\ \mathrm{Im}(A_1) \end{Bmatrix} = \begin{Bmatrix} p_1 \\ p_2 \end{Bmatrix} c = [\mathbf{P}]c \tag{3.205}$$

where c is either $\mathrm{Re}(A_1)$ or $\mathrm{Im}(A_1)$. To avoid division by zero, p_1 and p_2 may be computed from Table 3.1 depending on the largest absolute value of q_{ij}.

Table 3.1. Values of p_1 and p_2

Largest $\lvert q_{ij} \rvert$	p_1	p_2
q_{11}	$-q_{12}/q_{11}$	1
q_{12}	1	$-q_{11}/q_{12}$
q_{21}	$-q_{22}/q_{21}$	1
q_{22}	1	$-q_{21}/q_{22}$

From Eq. (3.186) and (3.205), A_1 and its conjugate $\overline{A}_1$ can be written in terms of c as

$$\begin{Bmatrix} A_1 \\ \overline{A}_1 \end{Bmatrix} = \begin{bmatrix} 1 & i \\ 1 & -i \end{bmatrix} \begin{Bmatrix} \mathrm{Re}(A_1) \\ \mathrm{Im}(A_1) \end{Bmatrix} = [\mathbf{N}] \begin{Bmatrix} \mathrm{Re}(A_1) \\ \mathrm{Im}(A_1) \end{Bmatrix} = [\mathbf{N}][\mathbf{P}]c \tag{3.206}$$

and A_2 and its conjugate $\overline{A}_2$ can be written in terms of A_1 and $\overline{A}_1$ and therefore in terms of c as

$$\begin{Bmatrix} A_2 \\ \overline{A}_2 \end{Bmatrix} = \begin{bmatrix} s_1 & s_2 \\ s_3 & s_4 \end{bmatrix} \begin{Bmatrix} A_1 \\ \overline{A}_1 \end{Bmatrix} = [\mathbf{S}] \begin{Bmatrix} A_1 \\ \overline{A}_1 \end{Bmatrix} = [\mathbf{S}][\mathbf{N}][\mathbf{P}]c \tag{3.207}$$

Using Eqs. (3.196), (3.197), (3.206) and (3.207), the coefficients of the complex potentials in Eqs. (3.191) to (3.193) can be written as

$$\begin{Bmatrix} A_1 \\ \overline{A}_1 \\ \overline{B}_1 \end{Bmatrix} = \begin{bmatrix} 1 & 0 \\ 0 & 1 \\ -e^{2i\lambda\alpha_1} & -\lambda\left(e^{2i\alpha_1}-1\right) \end{bmatrix} \begin{Bmatrix} A_1 \\ \overline{A}_1 \end{Bmatrix} = [\mathbf{H}_1][\mathbf{N}][\mathbf{P}]c = [\mathbf{R}_1]c \tag{3.208}$$

for material 1 and

$$\begin{Bmatrix} A_2 \\ \overline{A}_2 \\ \overline{B}_2 \end{Bmatrix} = \begin{bmatrix} 1 & 0 \\ 0 & 1 \\ -e^{-2i\lambda\alpha_2} & -\lambda\left(e^{-2i\alpha_2}-1\right) \end{bmatrix} \begin{Bmatrix} A_2 \\ \overline{A}_2 \end{Bmatrix} = [\mathbf{H}_2][\mathbf{S}][\mathbf{N}][\mathbf{P}]c = [\mathbf{R}_2]c \tag{3.209}$$

for material 2.

Assuming that

$$[\mathbf{L}_j] = r^{\lambda} e^{-i\lambda\theta} \left[\kappa_j e^{2i\lambda\theta} \quad -\lambda\left(e^{2i\theta}-1\right) \quad -1\right] \tag{3.210}$$

then Eq. (3.193),the displacement expression for real eigenvalues, could be rewritten as

$$2G_j\left(u_x^j + iu_y^j\right) = [\mathbf{L}_j][\mathbf{R}_j]c = [\mathbf{J}_j]c \tag{3.211}$$

Equating the real and imaginary parts of both sides of Eq. (3.211) leads to

$$\begin{Bmatrix} u_x^j \\ u_y^j \end{Bmatrix} = \frac{1}{2G_j} \begin{bmatrix} \mathrm{Re}\left(\mathbf{J}_j(1,1)\right) \\ \mathrm{Im}\left(\mathbf{J}_j(1,1)\right) \end{bmatrix} c \tag{3.212}$$

Eq. (3.212) shows that the displacement expressions for each real eigenvalue can be written in terms of a real variable. Therefore, each real eigenvalue is associated with a single element of the generalised coordinates.

3.7.1.4. Generalised Coordinates

The displacement expressions around a notch tip are the sum of terms of Eqs. (3.189) and (3.212) repeated for as many eigenvalues considered. The coefficients c in Eq. (3.212) and the real and imaginary parts of the coefficients A_1 in Eq. (3.189) are called generalised coordinates and will be computed directly in the FFEM. The ones associated with the singular eigenvalues ($\mathrm{Re}(\lambda)<1$) are related directly to the SIFs of a general notch. The rest are the constants of the higher order terms.

3.7.2. Stress Intensity Factors

The eigenvalues computed using Eq. (3.181) could be real or complex. For a general bi-material notch, the singular eigenvalues ($\mathrm{Re}(\lambda)<1$) are either two real singular eigenvalues associated with mode I and mode II $(\lambda_I, \lambda_{II})$ or a single complex singular eigenvalue with real and imaginary parts. A complex singular eigenvalue is associated with a complex SIF that can be computed using one of the following equations

$$K_c = \sqrt{2\pi}\lim_{r\to 0} r^{1-\lambda}\left(\sigma_{yy} + i\sigma_{xy}\right)\Big|_{\theta=0} \tag{3.213}$$

or

$$K_c = \sqrt{2\pi}\lim_{r\to 0} r^{1-\bar{\lambda}}\left(\sigma_{yy} + i\sigma_{xy}\right)\Big|_{\theta=0} \tag{3.214}$$

Substituting Eq. (3.159) into Eqs. (3.213) and (3.214) gives

$$K_c = \sqrt{2\pi}\lambda A_1\left(\mathbf{S}(2)\left(1-e^{-2i\lambda\alpha_1}\right)-\lambda\left(e^{-2i\alpha_1}-1\right)\right) \tag{3.215}$$

$$K_c = \sqrt{2\pi}\overline{\lambda A_1}\left(1-e^{-2i\bar{\lambda}\alpha_1}-\bar{\lambda}\,\overline{\mathbf{S}(2)}\left(e^{-2i\alpha_1}-1\right)\right) \tag{3.216}$$

The real and imaginary parts of K_c represent the mode I and II SIFs, respectively.

For the case of two real singular eigenvalues, where one eigenvalue is associated with mode I while the other is associated with mode II, the SIFs expressions are computed using

$$K_I = \sqrt{2\pi} \lim_{r\to 0} r^{1-\lambda^I} \sigma_{yy}(\theta = 0) \tag{3.217}$$

$$K_{II} = \sqrt{2\pi} \lim_{r\to 0} r^{1-\lambda^{II}} \sigma_{xy}(\theta = 0) \tag{3.218}$$

Substituting the stress expression, Eq. (3.191), into Eqs. (3.217) and (3.218) gives

$$\begin{aligned} K_I = \sqrt{2\pi}\,\frac{\lambda_I c_I}{2}[&(p_{I1} + ip_{I2})\left(1 + \lambda_I\left(1 - e^{-2i\alpha_1}\right) - e^{2i\lambda_I\alpha_1}\right) \\ &+ (p_{I1} - ip_{I2})\left(1 + \lambda_I\left(1 - e^{2i\alpha_1}\right) - e^{-2i\lambda_I\alpha_1}\right)] \end{aligned} \tag{3.219}$$

for mode I, and

$$\begin{aligned} K_{II} = \sqrt{2\pi}\,\frac{\lambda_{II} c_{II}}{2i}[&(p_{II1} + ip_{II2})\left(\lambda_{II}\left(1 - e^{-2i\alpha_1}\right) + e^{2i\lambda_{II}\alpha_1} - 1\right) \\ &+ (p_{II1} - ip_{II2})\left(\lambda_{II}\left(e^{2i\alpha_1} - 1\right) - e^{-2i\lambda_I\alpha_1} + 1\right)] \end{aligned} \tag{3.220}$$

for mode II.

3.8. GIFs for Bi-material Notch under Anti-plane Loading (Mode III)

3.8.1. Stress and Displacement Expressions

Let (r,θ) be a polar co-ordinate system centred at the tip of a bi-material notch as shown in Figure 3.7. In the state of anti-plane, the only non-zero stress components are τ_{rz} and $\tau_{\theta z}$, and the only non-zero displacement component is in the z direction (w). The stress components can be expressed in terms of w as

$$\tau_{rz}^{(j)} = G_j \frac{\partial w^{(j)}}{\partial r} \tag{3.221}$$

$$\tau_{\theta z}^{(j)} = G_j \frac{1}{r} \frac{\partial w^{(j)}}{\partial \theta} \tag{3.222}$$

where G_j is the shear modulus of material j; $j = 1,2$. The equilibrium equation can be written in terms of the stress components as

$$\frac{\partial \tau_{\theta z}^{(j)}}{\partial \theta} + r \frac{\partial \tau_{rz}^{(j)}}{\partial r} + \tau_{rz}^{(j)} = 0 \tag{3.223}$$

Substituting Eqs. (3.221) and (3.222) into Eq. (3.223), the equilibrium equation can be expressed in terms of the displacement component w as

$$\frac{1}{r} \frac{\partial^2 w^{(j)}}{\partial \theta^2} + r \frac{\partial^2 w^{(j)}}{\partial r^2} + \frac{\partial w^{(j)}}{\partial r} = 0 \tag{3.224}$$

The displacement function $w^{(j)}$ can be assumed as

$$w^{(j)} = r^{\lambda} F_j(\theta) \tag{3.225}$$

where λ is an eigenvalue. Substituting $w^{(j)}$ and its derivatives into the differential Eq. (3.224) gives

$$F_j''(\theta) + \lambda^2 F_j(\theta) = 0 \tag{3.226}$$

Substituting the general solution of the differential Eq. (3.226) into Eq. (3.225) gives

$$w^{(j)} = r^{\lambda} \left(A_j \cos \lambda\theta + B_j \sin \lambda\theta \right) \tag{3.227}$$

where A_j and B_j are the generalised co-ordinates (or the coefficients of the higher terms of the mode III notch asymptotic field). On substituting Eq. (3.227) into Eqs. (3.221) and (3.222), the stress expressions are

$$\tau_{rz}^{(j)} = G_j \lambda r^{\lambda - 1} \left(A_j \cos \lambda\theta + B_j \sin \lambda\theta \right) \tag{3.228}$$

$$\tau_{\theta z}^{(j)} = G_j \lambda r^{\lambda - 1} \left(- A_j \sin \lambda\theta + B_j \cos \lambda\theta \right) \tag{3.229}$$

The eigenvalues λ are obtained by imposing the following boundary and continuity conditions:

$$\tau_{\theta z}^{(1)}\left(r,\theta=+\alpha_1\right)=0 \tag{3.230}$$

$$\tau_{\theta z}^{(2)}\left(r,\theta=-\alpha_2\right)=0 \tag{3.231}$$

$$w^{(1)}\left(r,\theta=0\right)=w^{(2)}\left(r,\theta=0\right) \tag{3.232}$$

$$\tau_{\theta z}^{(1)}\left(r,\theta=0\right)=\tau_{\theta z}^{(2)}\left(r,\theta=0\right) \tag{3.233}$$

Substituting Eqs. (3.227) and (3.229) into Eqs. (3.230) to (3.233) yields

$$B_1=A_1\frac{\sin\lambda\alpha_1}{\cos\lambda\alpha_1} \tag{3.234}$$

$$B_2=-A_2\frac{\sin\lambda\alpha_2}{\cos\lambda\alpha_2} \tag{3.235}$$

$$A_2=A_1 \tag{3.236}$$

$$B_2=\frac{G_1}{G_2}B_1 \tag{3.237}$$

Eqs. (3.234) to (3.237) can be written in matrix form as

$$\begin{bmatrix} -\sin\lambda\alpha_1 & \cos\lambda\alpha_1 & 0 & 0 \\ 0 & 0 & \sin\lambda\alpha_2 & \cos\lambda\alpha_2 \\ 1 & 0 & -1 & 0 \\ 0 & G_1 & 0 & -G_2 \end{bmatrix}\begin{Bmatrix} A_1 \\ B_1 \\ A_2 \\ B_2 \end{Bmatrix}=\{0\} \tag{3.238}$$

which can be rewritten in a short form as

$$\left[\mathbf{D}\right]\begin{bmatrix} A_1 & B_1 & A_2 & B_2 \end{bmatrix}^T=\{0\} \tag{3.239}$$

For non-trivial solutions the determinant of $\left[\mathbf{D}\right]$ must vanish, i.e.

$$\det\left[\mathbf{D}\right]=0 \tag{3.240}$$

After some algebraic manipulations, Eq. (3.240) can be written as

$$G_1\sin\lambda\alpha_1\cos\lambda\alpha_2+G_2\cos\lambda\alpha_1\sin\lambda\alpha_2=0 \tag{3.241}$$

Eq. (3.241) can be simplified further as

$$\left(\frac{G_1}{G_2}+1\right)\sin\lambda(\alpha_1+\alpha_2)+\left(\frac{G_1}{G_2}-1\right)\sin\lambda(\alpha_1-\alpha_2)=0 \tag{3.242}$$

By solving Eq. (3.242), the eigenvalues are obtained. Eq. (3.242) can be solved using Muller's iterative method. The solution of Eq. (3.242) is always real. For the special case when $G_1 = G_2$ and $\alpha_1 = \alpha_2 = \alpha$, Eq. (3.242) is reduced to

$$\lambda = \frac{n\pi}{2\alpha} \tag{3.243}$$

which is the same relationship as the one derived for a symmetric homogeneous notch (Eq. (3.146)).

Using Eqs. (3.227) to (3.229), the displacement and stress expressions in materials 1 and 2 can be written as

$$w^{(1)} = r^{\lambda}\left(A_1\cos\lambda\theta + B_1\sin\lambda\theta\right) \tag{3.244}$$

$$w^{(2)} = r^{\lambda}\left(A_1\cos\lambda\theta + \frac{G_1}{G_2}B_1\sin\lambda\theta\right) \tag{3.245}$$

$$\tau_{rz}^{(1)} = G_1\lambda r^{\lambda-1}\left(A_1\cos\lambda\theta + B_1\sin\lambda\theta\right) \tag{3.246}$$

$$\tau_{\theta z}^{(1)} = G_1\lambda r^{\lambda-1}\left(-A_1\sin\lambda\theta + B_1\cos\lambda\theta\right) \tag{3.247}$$

$$\tau_{rz}^{(2)} = G_2\lambda r^{\lambda-1}\left(A_1\cos\lambda\theta + \frac{G_1}{G_2}B_1\sin\lambda\theta\right) \tag{3.248}$$

$$\tau_{\theta z}^{(2)} = G_2\lambda r^{\lambda-1}\left(-A_1\sin\lambda\theta + \frac{G_1}{G_2}B_1\cos\lambda\theta\right) \tag{3.249}$$

3.8.2. Stress Intensity Factors

The mode III SIF of an anti-plane bi-material notch is defined as

$$K_{III}^{(j)} = \sqrt{2\pi} \lim_{r \to 0} r^{1-\lambda} \tau_{\theta z}^{(j)} (\theta = 0) \tag{3.250}$$

Substituting Eq. (3.247) or (3.249) into Eq. (3.250) gives

$$K_{III}^{(j)} = \sqrt{2\pi} G_j \lambda B_j = \sqrt{2\pi} G_1 \lambda B_1 \tag{3.251}$$

3.9. Implementation of the FFEM

Based on the theory presented in the previous sections, the structure of the FFEM program implemented is shown in Figure 3.9. The code is programmed in FORTRAN90. The next sub-sections explain the steps in more details.

3.9.1. Discretisation and Mesh Generation

For the purpose of mesh generation, the ABAQUS software is used to generate the nodal and element definitions. Basically, a plate is drawn, partitioned and meshed. Then, an input file is generated that contains only a list of the nodes' labels and coordinates and the elements labels and nodes. This file is then used in the FFEM Input File Generation sub-routine explained next.

3.9.2. Input File for FFEM

The data required for an FFEM input file are similar to the data of a conventional FEM input file. The only difference is defining the singular and regular nodes and elements. Therefore, a sub-routine was developed and used to convert an FEM input file containing basic data, i.e. the node labels and coordinates and the element labels and nodal topology, to an FFEM input file. The sub-routine was written in FORTRAN 90. The sub-routine is

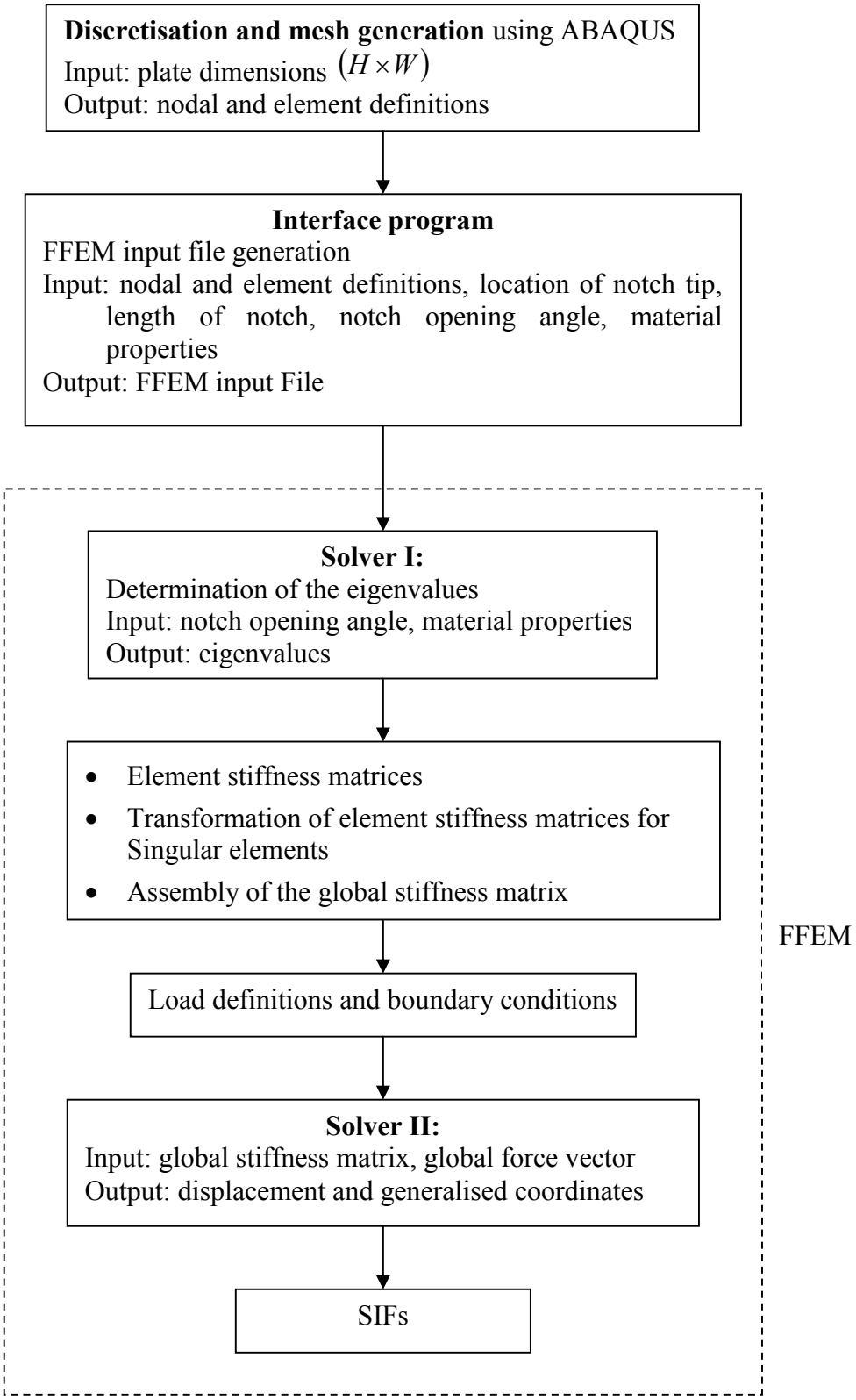

Figure 3.9. Flowchart of FFEM program

simple as it only contains conditions to recognise the singular and regular nodes and, therefore, singular and regular elements by using simple comparison criteria of the nodes coordinates. Any commercial FE package could be used to mesh a model and create a mesh file. In this study, The ABAQUS software is used for this purpose (to draw and mesh the geometry of a notched plate) as mentioned in the previous section. The subroutine reads the file, defines all the parameters needed (singular and regular nodes and elements, notch angle and material properties) and then writes a new input file suitable for the FFEM code.

3.9.3. Eigenvalue Solver

The eigenvalues are determined using a sub-routine based on Muller's iterative method (Press et al., 2007). The sub-routine was written in FORTRAN 90 and was incorporated in the FFEM code. It is based on the flowcharts presented in Figures (3.5) and (3.8). The characteristic equations of the eigenvalues are solved using this sub-routine.

3.9.4. Assembly of Global Stiffness Matrix and Force Vector

Six-node triangular elements are used to mesh the plates. Seven point integration scheme is employed to compute the element stiffness matrices. It should be noted that any conventional finite elements can be used for modelling both the regular and singular regions. The element stiffness matrices are computed. If an element is within the singular region then its local stiffness matrix is transformed using the GIFs. This is carried out at this level (element level), so the orders of matrices involved are very small and, therefore,

reducing the computational cost and time. As the element stiffness matrices are built and transformed, they are also assembled into the global stiffness matrix.

3.9.5. Simultaneous Linear Equations Solver

After applying the boundary conditions and building the global force vector, the equilibrium equation, which is now in matrix form, is solved numerically to obtain the nodal displacements and the generalised coordinates. This is done by triangulating (decomposing) the global stiffness matrix and then obtaining the unknowns by direct substitution. The SIFs are subsequently computed using the generalised coordinates corresponding to the singular eigenvalues of mode I, II, or III. All the computations are carried out using a code written in Fortran 90.

3.10. Strain Energy Approach (SEA)

The strain energy of a finite volume is

$$E^{(e)} = \int_V W^{(e)} dV \tag{3.252}$$

where $W^{(e)}$ is the strain energy density and can be computed as follows

$$W^{(e)} = \int \boldsymbol{\sigma} : \partial \boldsymbol{\varepsilon} \tag{3.253}$$

where $\boldsymbol{\sigma}$ and $\boldsymbol{\varepsilon}$ are stress and strain tensors, respectively. For an isotropic material, the strain energy density $W^{(e)}$ for a generalised state of stress can be written as

$$W^{(e)} = \frac{1}{2}\left[\sigma_{xx}\varepsilon_{xx} + \sigma_{yy}\varepsilon_{yy} + \sigma_{zz}\varepsilon_{zz} + \tau_{xy}\gamma_{xy} + \tau_{xz}\gamma_{xz} + \tau_{yz}\gamma_{yz}\right] \tag{3.253}$$

The strains can be written in terms of the stresses by using Hooke's law

$$\varepsilon_{xx} = \frac{1}{E}\left[\sigma_{xx} - \nu\left(\sigma_{yy} + \sigma_{zz}\right)\right] \tag{3.254}$$

$$\varepsilon_{yy} = \frac{1}{E}\left[\sigma_{yy} - \nu\left(\sigma_{xx} + \sigma_{zz}\right)\right] \tag{3.255}$$

$$\varepsilon_{zz} = \frac{1}{E}\left[\sigma_{zz} - \nu\left(\sigma_{xx} + \sigma_{yy}\right)\right] \tag{3.256}$$

$$\gamma_{xy} = \frac{1}{G}\tau_{xy} \tag{3.257}$$

$$\gamma_{yz} = \frac{1}{G}\tau_{yz} \tag{3.258}$$

$$\gamma_{xz} = \frac{1}{G}\tau_{xz} \tag{3.259}$$

where E is the Young's modulus, ν is the Poisson's ratio and $G = \frac{E}{2(1+\nu)}$ is the shear modulus. It was shown in the previous sections that the stresses could be written in terms of the generalised coordinates. It was also shown that the generalised coordinates are related to the SIFs. Therefore, the singular stresses at the notch tip can be expressed in terms of the SIFs. For simplicity, assuming that the stresses could be written in terms of the mode I, II and III SIFs in the near field region as

$$\sigma_{ij} = f\left(K_I, K_{II}, K_{III}, r, \theta\right) \tag{3.260}$$

The higher order terms in this equation are ignored because of the dominance of the leading order terms in the singular region. By substituting the stress expressions into Eq. (3.252) and carrying out the integration over a finite volume around the notch tip, Eq. (3.252) becomes a representation of a direct relation between the strain energy for a finite volume and the SIFs and could be written as

$$E^{(e)} = F\left(K_I, K_{II}, K_{III}\right) \tag{3.261}$$

The strain energy could be easily computed using a commercial finite element package. Most FE packages are not, to our knowledge, capable of computing the SIFs for general notches. Therefore, this approach is quite useful to extract SIFs for general notches by using current commercial FE packages. In this study, the ABAQUS software is used to compute the strain energy. Eq. (3.252) can be partitioned to deal with bi-material and mixed mode cases where two equations are needed to compute mode I and mode II SIFs as follows

$$\begin{aligned} E_1^{(e)} &= F_1\left(K_I, K_{II}\right) \\ E_2^{(e)} &= F_2\left(K_I, K_{II}\right) \end{aligned} \tag{3.262}$$

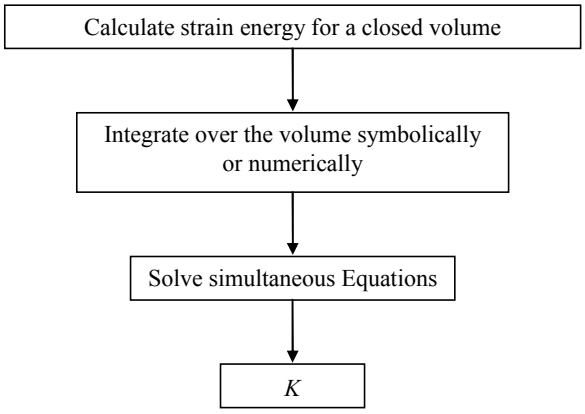

Figure 3.10. Essential steps of the SEA

The integration of Eq. (3.252) can be carried out symbolically for simple pure mode cases resulting in closed form formulae as presented in Chapter 10. For more complex cases such as mixed mode cases, the integration can be carried out numerically using for example the MATLAB software. In this study, a sub-routine based on the Composite Simpson's Method is developed and used to carry out the integration. Then, the simultaneous Eqs. (3.262) are solved using the MATLAB software. Figure 3.10 shows the essential steps of the SEA.

3.11. Conclusion

In this chapter the background theory of the FFEM and derivations of the stress and displacement expressions around a notch tip that are used in the subsequent chapters were presented. In addition, the numerical techniques and computational steps of the FFEM and the SEA that were developed and used were also described. This was done because of the brief nature of the published work presented in the rest of this thesis.

Chapter 4

Research Overview

4. Research Overview

4.1. Introduction

This thesis is presented in an Alternative Format, in which research, techniques and findings are presented in the form of scientific papers that have been published in externally refereed contexts. The papers included are linked to each other, and together make up a coherent and continuous research work. In total, seven papers are included of which four have already been published. The other three papers are currently under review. In this chapter, an overview of the research, a short description of each paper and a statement of the authors' contributions are presented.

4.2. Research Overview

The main aim of this research as detailed in Chapter 1 is to extend the FFEM to compute the mode I, II and III SIFs for general notches in isotropic homogeneous and bi-material plates. The exact analytical solutions of the displacement field around a notch tip in an isotropic material subjected to in-plane loading are derived and used as GIFs in the FFEM. The mode I and II SIFs values predicted by the FFEM for notched plates subjected to tension, shear, and bending loading conditions are of good accuracy compared to available published data (Treifi et al., 2008, 2009a, 2009b). The method at this stage has proved promising. As superposition of the results for mode I, II and III is sufficient to describe the most general case of loading on a specimen with a notch, the method is extended to compute mode III SIFs. Therefore, the exact analytical solution of the displacement field around a notch tip in an isotropic notch subjected to out-of-plane

shear loading conditions is derived and employed in the FFEM to compute the mode III SIFs for general notches in isotropic notched plates (Treifi et al., 2009c).

In many engineering applications, materials are increasingly joined together and quite frequently they are joined together with a corner/notch created between the two materials. The presence of corners/notches is known to cause stress intensity at the tip of such corner/notch. Therefore, the development of the FFEM to compute the SIFs for bi-material notches is the next logical step.

Firstly, the FFEM is extended to compute mode III SIFs for bi-material notches. This is done by deriving the exact analytical solution of the displacement field around a bi-material notch tip subjected to out-of-plane shear loading conditions and employing the solution in the FFEM (Treifi and Oyadiji, 2013a). Secondly, the exact analytical solutions of the displacement field around a bi-material notch tip subjected to in-plane loading conditions are derived and employed as GIFs to extend the FFEM to compute mode I and II SIFs for bi-material plates (Treifi and Oyadiji, 2013b).

Most of the results produced by the FFEM for the notch cases, especially for bi-material notch cases, are new. To prove the accuracy of the FFEM, the results are compared to available published results and numerical solutions obtained using commercial FE packages such as the ABAQUS software. However, the published results are generally only for crack cases or isotropic notch cases, and the commercial FE packages are not capable of computing the SIFs for general notches. Therefore, a new approach based on the strain energy of a finite volume around a notch tip is developed to compute the SIF values for isotropic homogeneous and bi-material notches (Treifi and Oyadiji, 2013c).

The good agreement between the results obtained using the FFEM and the corresponding results computed using the SEA increases the confidence in the FFEM results especially for the bi-material notch problems. Indeed, both methods seem promising, one as a stand alone method (FFEM) and the other as a subroutine that could be used to compute the SIFs for general notches using commercial FE packages.

4.3. Outline of Included Published Papers

As this thesis is presented in an Alternative Format, the papers published that are mentioned in the previous Section are included as separate chapters following the Alternative Format guidelines. In total seven papers are included. Four of them are co-authored by me and my supervisor, Dr S O Oyadiji. As the leading author, I contributed the major ideas and contents of these papers, and I solely carried out the work in these papers under the supervision of Dr. Oyadiji. The other three are co-authored by three researchers: I, Dr S O Oyadiji, and Dr D K L Tsang. As the leading author, I contributed the major ideas and contents of these papers, and I solely carried out the work in these papers under the supervision of Dr. Oyadiji and Dr Tsang. It should be mentioned that the SIF values presented in those papers are non-dimensionalised. Also, the stress and displacement expressions around the notch tip are series expansions and that the $\sum$ symbol is dropped for simplicity. Brief descriptions of the seven papers are presented next in the order they appear in the subsequent chapters. Table 4.1 gives an illustrative overview of them.

Table 4.1. Overview of included published papers

Ch. No.	Paper Details	Mode	Material	Illustration
5.	Computation of the SIFs of Sharp Notched Plates by the FFEM. *Int J Numer Meth Engng 2009*	I and II	Isotropic	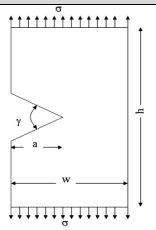
6.	Computations of Modes I and II SIFs of Sharp Notched Plates under In-plane Shear and Bending Loading by the FFEM. *Int J Solids Struct 2008*	I and II	Isotropic	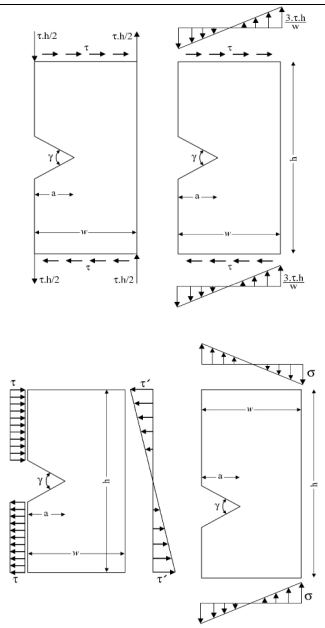
7.	Computations of SIFs for Non-symmetric V-notched Plates by the FFEM. *Proceedings of the ASME IDETC/CIE 2009*	I and II	Isotropic	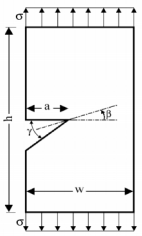
8.	Computations of the SIFs of Double-edge and Centre V-notched Plates under Tension and Anti-Plane Shear by the FFEM. *Engng Fract Mech 2009*	I, II and III	Isotropic	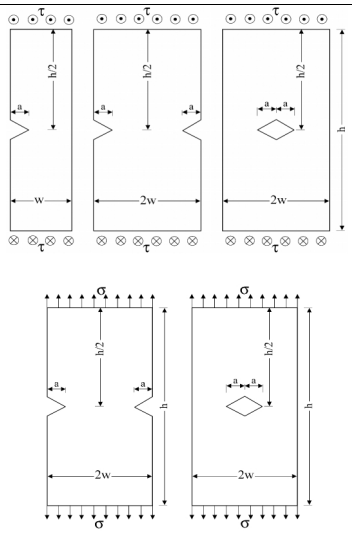

Table 4.1. Continued

9.	Evaluation of Mode III SIFs for Bi-material Notched Bodies Using the FFEM. *Comput Struct 2013*	III	Bi-material	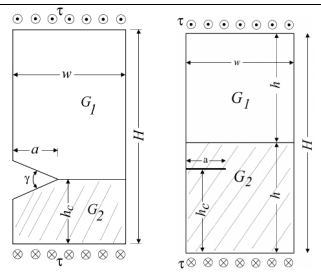
10.	SEA to Compute SIFs for Isotropic Homogeneous and Bi-material V-notches. *Int J Solids Struct 2013*	I, II and III	Isotropic and bi-material	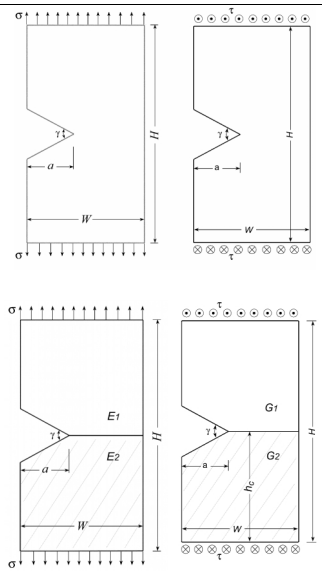
11.	Bi-material V-notch SIFs by the FFEM. *Engng Fract Mech 2013*	I and II	Bi-material	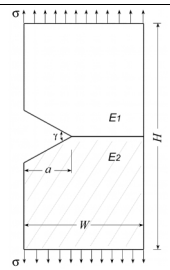

4.3.1. Computation of the Stress Intensity Factors of Sharp Notched Plates by the Fractal-like Finite Element Method

Authors: Muhammad Treifi, S. Olutunde Oyadiji and Derek K. L. Tsang

Published in: International Journal for Numerical Methods in Engineering 2009; 77:558–580.

In this paper, The FFEM is extended to analyse the singularity problems of sharp notched plates subject to tension loading conditions. The exact stress and displacement fields of a

general notch are derived for plane-stress/strain conditions. The exact analytical expressions of the displacements, which are eigenfunction expansion series, are used to perform the global transformation and to determine the SIFs. A convergence study of a notched plate subject to pure mode I loading conditions is carried out to determine the optimal similarity ratio, number of layers and number of terms of the GIFs. Different numerical examples are also presented of V-notched plates for different notch opening angles and different notch locations under tension loading conditions. To demonstrate the accuracy and efficiency of the FFEM to compute the notch SIFs, the results are compared to available published results and numerical solutions predicted using the ABAQUS software. The ABAQUS software is used only for crack cases, because ABAQUS is not capable of computing SIFs for general notches. The accuracy of Mode I SIFs computed using the FFEM is shown to be very good. New results are also presented.

4.3.2. Computations of Modes I and II Stress Intensity Factors of Sharp Notched Plates under In-plane Shear and Bending Loading by the Fractal-like Finite Element Method

Authors: Muhammad Treifi, S. Olutunde Oyadiji and Derek K. L. Tsang

Published in: International Journal of Solids and Structures 2008; 45:6468–6484.

The FFEM is used to compute the SIFs for different configurations of cracked/notched plates subjected to in-plane shear and bending loading conditions. A convergence study of a V-notched plate subject to pure mode II loading conditions is carried out to determine the optimal similarity ratio, number of layers and number of terms of the GIFs. Different numerical examples of various configurations of cracked/notched plates under different types of shear and bending loading conditions are presented. The results of the FFEM for

mode II SIFs are validated via published data for crack and notch cases or numerical solutions predicted using the ABAQUS software for crack cases. Very good accuracy is achieved. New results are also presented.

4.3.3. Computations of SIFs for Non-symmetric V-notched Plates by the FFEM

Authors: Muhammad Treifi and S. Olutunde Oyadiji

Published in: Proceedings of ASME Conference IDETC/CIE2009; 3:711–717.

This paper further develops The FFEM to compute the SIFs for non-symmetrical configurations of sharp V-notched plates. This is when the bisector of a notch opening angle does not lie on or is not parallel to the x-axis of the global coordinate system. The same exact analytical expressions of the displacements around a notch tip derived for a symmetrical notch case can be used as GIFs when the notch is non-symmetrical by introducing an appropriate local coordinate transformation to obtain the correct global stiffness matrix. To demonstrate the accuracy of the FFEM to compute the mode I and II SIFs for a non-symmetrical notch, various numerical examples are presented and results are validated via available published data. The accuracy of the FFEM results compared to the corresponding published data is shown to be very good.

4.3.4. Computations of the Stress Intensity Factors of Double-edge and Centre V-notched Plates under Tension and Anti-plane Shear by the Fractal-like Finite Element Method

Authors: Muhammad Treifi, S. Olutunde Oyadiji and Derek K. L. Tsang

Published in: Engineering Fracture Mechanics 2009; 76:2091–2108.

In this paper, the FFEM is extended to compute the SIFs of double-edge-/centre-notched plates subjected to out-of-plane shear or tension loading conditions. The exact stress and displacement fields of a general notch under pure mode III loading conditions are derived. The exact analytical expressions of the displacements, which are eigenfunction expansion series, are used to perform the global transformation and to determine the SIFs. A convergence study of a notched plate subject to pure mode III loading conditions is carried out to determine the optimal similarity ratio, number of layers and number of terms of the GIFs. The GIFs derived in the previous papers are used for in-plane (mode I and II) problems, and the GIFs derived in this paper are used for out-of-plane (mode III) problems. Many numerical examples of double-edge-/centre-notched plates are presented, and the results are validated via existing published data or numerical solutions obtained by using the ABAQUS software (for crack cases only). Also, an example on the ability of the FFEM to compute the coefficients of the higher order terms is presented. The FFEM results for mode III are shown to be of very good accuracy. New results of notched plate problems are also introduced.

4.3.5. Evaluation of Mode III Stress Intensity Factors for Bi-material Notched Bodies Using the Fractal-like Finite Element Method

Authors: Muhammad Treifi and S. Olutunde Oyadiji

Published (early view) in: Computers and Structures 2013; http://dx.doi.org/10.1016/j.compstruc.2013.02.015.

In this paper, the FFEM is extended to compute the SIFs for bi-material notched bodies subjected to anti-plane shear (mode III) loading conditions. The notched bodies are formed by bonding two materials together (isotropic-isotropic/isotropic-orthotropic). The

exact stress and displacement fields of a general bi-material notch under pure mode III loading conditions are derived and employed as GIFs in the FFEM. Also, a strain energy-based approach (SEA) is developed and used to extract the mode III SIFs for a bi-material notch using standard finite element (FE) commercial packages for comparison with corresponding data produced using the FFEM. This is done because there are no available published results to compare the mode III notch SIFs to. Various numerical results for bi-material cracked/notched bodies under anti-plane shear, many of which are new, are presented. The results are compared to published results or numerical solutions and shown to be of very good accuracy. Some interesting results of a crack parallel to an interface for different crack locations and different material property ratios are also presented.

4.3.6. Strain Energy Approach to Compute Stress Intensity Factors for Isotropic Homogeneous and Bi-material V-notches

Authors: Muhammad Treifi and S. Olutunde Oyadiji

Published (early view) in: International Journal of Solids and Structures 2013; 50: 2196-2212. http://dx.doi.org/10.1016/j.ijsolstr.2013.03.011.

In this paper, a strain energy approach (SEA) is developed to compute the general stress intensity factors (SIFs) for isotropic homogeneous and bi-material plates containing cracks and notches subjected to modes I, II and III loading conditions. The approach is based on the strain energy of a control volume around the notch tip, which may be computed using commercial finite element packages. Therefore, this approach enables analysts to compute the notch SIFs using current commercial FE packages, despite the fact that these packages are only capable of computing SIFs for crack problems. The

relations between the strain energy of a control volume around the crack/notch tip are derived for the in-plane (mode I and II) and out-of-plane (mode III) cases for isotropic homogeneous and bi-material notches. Convergence studies are carried out to determine the control volume size for each case. Various numerical examples of isotropic homogeneous and bi-material notched plates are presented and results are compared to corresponding published results or results that are computed using different numerical methods. The accuracy of the SIF values predicted by the SEA is shown to be very good. Many of the presented results are new, especially for the cases of bi-material notches where the problem is quite complicated.

4.3.7. Bi-material V-notch Stress Intensity Factors by the Fractal-like Finite Element Method

Authors: Muhammad Treifi and S. Olutunde Oyadiji

Published (early view) in: Engineering Fracture Mechanics 2013; http://dx.doi.org/10.1016/j.engfracmech.2013.04.006.

In this paper, The FFEM is developed to compute SIF values for bi-material notches under mode I and II loading conditions. The displacement fields around a bi-material notch tip are derived and employed as GIFs in the FFEM to transform the large number of nodal displacements in the singular region to a small set of generalized coordinates leading to direct computation of the SIFs and the constants of the higher order terms. Various numerical examples for bi-material crack and notch cases are presented. It is demonstrated, via convergence studies, that the size of the singular region has an effect on the results. Recommendations are made on the choice of the size of the singular region. Compared to available published results and numerical solutions obtained by using

different numerical methods, the FFEM is shown to produce results with very good accuracy. Also, new results for bi-material notches are introduced.

4.4. Conclusion

In this chapter, an overview of the research undertaken was presented along with short descriptions of the published scientific papers included in this thesis. A statement on the contributions of the co-authors to those papers was also stated. The author of this thesis was the major contributor to those papers; he carried out the analytical derivations and the computations and wrote the papers as lead author. The role of the co-authors was mainly supervisory. The papers included make up the subsequent chapters of this thesis as it is submitted in an Alternative Format.

Chapter 5

Computation of the Stress Intensity Factors of Sharp Notched Plates by the Fractal-like Finite Element Method

International Journal for Numerical Methods in Engineering 2009; 77:558–580

INTERNATIONAL JOURNAL FOR NUMERICAL METHODS IN ENGINEERING
Int. J. Numer. Meth. Engng 2009; **77**:558–580
Published online 22 July 2008 in Wiley InterScience (www.interscience.wiley.com). DOI: 10.1002/nme.2425

Computation of the stress intensity factors of sharp notched plates by the fractal-like finite element method

Muhammad Treifi, S. Olutunde Oyadiji*, † and Derek K. L. Tsang

Dynamics and Aeroelasticity Research Group, School of Mechanical, Aerospace and Civil Engineering, University of Manchester, Manchester M60 1QD, U.K.

SUMMARY

The fractal-like finite element method (FFEM) is an accurate and efficient method to compute the stress intensity factors (SIFs) of different crack configurations. In the FFEM, the cracked/notched body is divided into singular and regular regions; both regions are modelled using conventional finite elements. A self-similar fractal mesh of an 'infinite' number of conventional finite elements is used to model the singular region. The corresponding large number of local variables in the singular region around the crack tip is transformed to a small set of global co-ordinates after performing a global transformation by using global interpolation functions. In this paper, we extend this method to analyse the singularity problems of sharp notched plates. The exact stress and displacement fields of a plate with a notch of general angle are derived for plane-stress/strain conditions. These exact analytical solutions which are eigenfunction expansion series are used to perform the global transformation and to determine the SIFs. The use of the global interpolation functions reduces the computational cost significantly and neither post-processing technique to extract SIFs nor special singular elements to model the singular region are needed. The numerical examples demonstrate the accuracy and efficiency of the FFEM for sharp notched problems.

Received 4 October 2007; Revised 27 March 2008; Accepted 9 June 2008

KEY WORDS: edge-cracked plate; stress intensity factors; edge-notched plate; notch; finite element method; fracture mechanics

1. INTRODUCTION

The computation of stress fields inside elastic bodies with corners is a common problem in mechanical and civil engineering. Therefore, much research has been devoted to the analysis of sharp notches where stresses diverge and oscillate. The task of computing the so-called notch stress intensity factors (SIFs) is important and has relevance for strength calculations. Experiments

*Correspondence to: S. Olutunde Oyadiji, Dynamics and Aeroelasticity Research Group, School of Mechanical, Aerospace and Civil Engineering, University of Manchester, Manchester M60 1QD, U.K.
†E-mail: s.o.oyadiji@manchester.ac.uk

show that simple failure criteria based on critical values of such factors exist, at least for brittle fracture [1].

Gross and Mendelson [2] used a boundary collocation procedure of the stress functions derived by Williams [3] to calculate the SIFs. Tong and Pian [4] pointed out that the interpolation functions must include terms that can account for the analytical form of the singularity in order to improve the rate of convergence. In addition, these interpolation functions should be used for elements within a finite region, and not only for those around the singular point. Sinclair *et al.* [5, 6] discussed the idea of a generalised stress intensity at sharp corners and outlined an approach to obtain it based on the calculation of a contour integral, which was an extension of the work of Stern *et al.* [7, 8]. Carpenter [9–12] independently also applied the contour integral of Stern *et al.* [7, 8] to compute fracture mechanics parameters and introduced a collocation approach to calculate stress intensities.

Lin and Tong [13] developed a special hybrid finite element. Their results were limited to mode I cases. Portela and Aliabadi [14] developed the boundary element singularity subtraction. As the method's name suggests, they used a technique to subtract the singularity. They published results for symmetric and non-symmetric notch configurations. However, this method requires extra boundary conditions that they referred to as 'singularity conditions of the regularisation procedure.' Babuška *et al.* [15–17] developed finite element techniques to extract SIFs for mixed modes. They discussed two broad types of methods: one involves an 'influence' function and the other is related to the energy principle of fracture mechanics. These techniques are post-processing procedures and known as extraction techniques.

The fractal-like finite element method (FFEM) is a semi-analytical method. Its idea goes back to the work of Leung and Cheung [18]. Originally they proposed a two-level finite element technique of constructing a frame super-element to reduce the computational cost for solving dynamic problems of a large-scale frame. The idea was based on the concept of global–local interpolation functions introduced by Mote [19]. The concept was that while local interpolation functions (shape functions) reduce the infinite number of degrees of freedom of a continuum to a finite number of degrees of freedom related to the nodes of the continuous element, the global finite element interpolation functions can be used to reduce the number of nodal unknowns to a small number of unknowns, called generalised co-ordinates.

The study was extended to model two-dimensional plates subject to concentrated static and harmonic loads by Leung and Wong [20, 21] and two-dimensional crack problems by Leung and Wong [22]. Leung and Su extended the method further to include many two-dimensional crack problems [23–29]. They applied the method to mode I [23], mixed mode [24], and body force crack problems [25] in 1994, 1995, 1996, respectively, as well as to cracked Kirchhoff's plates [26], cracked Reissner's plates [27] and further to axisymmetric cracks and penny-shaped and circumferential cracks [28, 29]. Leung and Tsang [30] studied mode III crack problems. It has been shown that the fractal-like finite element method gives very accurate results for many different crack problems.

In this paper, we extend the fractal-like finite element method to model the singularity resulting at the notch tip. Williams' eigenfunction series expansion will be used as global interpolation functions to perform the fractal transformation. No special singular finite elements are necessary to model the singular region—any conventional finite elements can be used to model the singular region. Also, no post-processing is necessary to extract the SIFs, because some of the unknown coefficients of the exact analytical solutions employed as the global interpolation functions are related to the SIFs. Various numerical results concerning different notch configuration problems

DOI: 10.1002/nme

subjected to mode I load conditions are presented to demonstrate the accuracy and efficiency of the FFEM to calculate SIFs of sharp notched plates.

2. FORMULATION OF THE FRACTAL-LIKE FINITE ELEMENT METHOD (FFEM)

Following the work of Leung and Su [23–29], in the FFEM, the cracked body is divided into singular regions (near fields) and regular regions (far fields) delineated by curves Γ_0^1 and Γ_0^2 as illustrated in Figure 1. Conventional finite elements are used to model both near-field and far-field regions. However, a very fine mesh of conventional finite elements is used within the singular regions. This mesh is generated layer by layer in a self-similar fractal process. The nodal displacements are the unknowns in the regular region. The nodal displacements in the singular region are transformed into a small set of generalised co-ordinates, which are the unknowns in the singular region. Two of the generalised co-ordinates are related to the SIFs for modes I and II; and therefore no post-processing is necessary to extract the SIFs. Williams' analytical solutions for the displacements near the crack tip are used for performing the transformation.

By using ρ as the similarity ratio and the crack tip as the centre of similarity, a set of curves $\{\Gamma_1, \Gamma_2, \Gamma_3, \ldots\}$, similar to Γ_0, is generated within the singular region. The layer between the curves Γ_{n-1} and Γ_n is called the nth layer. All nodes on Γ_0 are considered master nodes, while the nodes inside Γ_0 are considered slave nodes as shown in Figure 2.

In the conventional finite element method, the displacements can be expressed as follows:

$$\mathbf{u} = \mathbf{N}\mathbf{d} \tag{1}$$

where $\mathbf{u}$ is the displacement field, $\mathbf{d}$ is the nodal displacement vector, and $\mathbf{N}$ is the shape functions matrix. The strain can be obtained by

$$\boldsymbol{\varepsilon} = \mathbf{B}\mathbf{d} \tag{2}$$

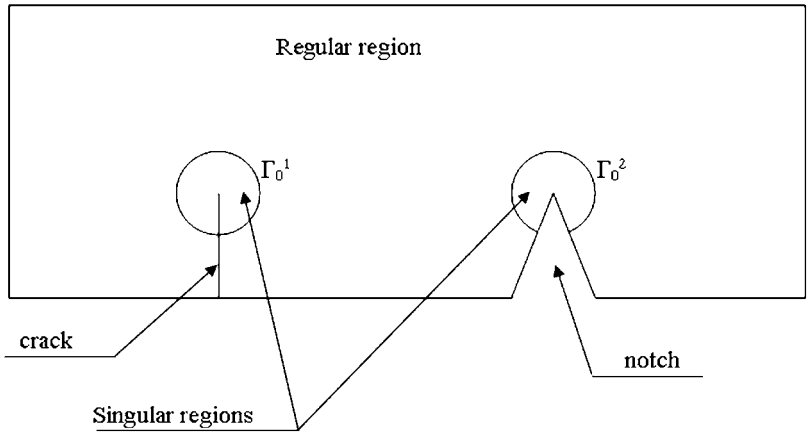

Figure 1. Singular and regular regions of cracked and notched plates.

DOI: 10.1002/nme

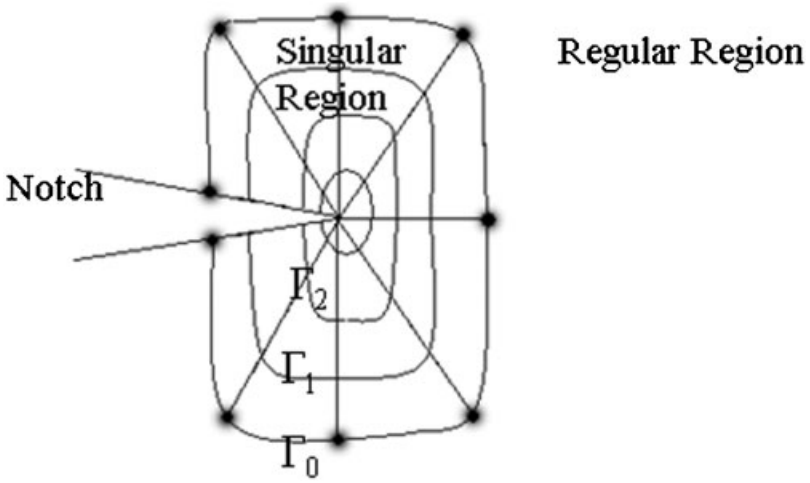

Figure 2. Detailed sketch of the near-field region (master nodes are highlighted).

where $\boldsymbol{\varepsilon}$ is the strain vector and $\mathbf{B}$ is the strain-displacement operator. The stress vector is related to the strain vector as

$$\boldsymbol{\sigma} = \mathbf{D}\boldsymbol{\varepsilon} \tag{3}$$

where $\boldsymbol{\sigma}$ is the stress vector and $\mathbf{D}$ is the material properties matrix.

The equilibrium equation is

$$\mathbf{K}\mathbf{d} = \mathbf{f} \tag{4}$$

where $\mathbf{K}$ is the stiffness matrix and $\mathbf{f}$ is the nodal force vector:

$$\mathbf{K} = \int_V \mathbf{B}^{\mathrm{T}}\mathbf{D}\mathbf{B}\,\mathrm{d}V \tag{5}$$

where V is the volume of an element. For the regular region, the equilibrium equation can be written as

$$\begin{bmatrix} \mathbf{K}_{rr} & \mathbf{K}_{rm} \\ \mathbf{K}_{mr} & \mathbf{K}_{mm} \end{bmatrix} \begin{Bmatrix} \mathbf{d}_r \\ \mathbf{d}_m \end{Bmatrix} = \begin{Bmatrix} \mathbf{f}_r \\ \mathbf{f}_m \end{Bmatrix} \tag{6}$$

where $\mathbf{d}_r$ are the displacements of the nodes in the regular region, and $\mathbf{d}_m$ are the displacements of the master nodes. Similarly, for the first layer in the singular region, the equilibrium equation can be written as

$$\begin{bmatrix} \mathbf{K}_{mm}^{1\mathrm{st}} & \mathbf{K}_{ms}^{1\mathrm{st}} \\ \mathbf{K}_{sm}^{1\mathrm{st}} & \mathbf{K}_{ss}^{1\mathrm{st}} \end{bmatrix} \begin{Bmatrix} \mathbf{d}_m \\ \mathbf{d}_s^{1\mathrm{st}} \end{Bmatrix} = \begin{Bmatrix} \mathbf{f}_m^{1\mathrm{st}} \\ \mathbf{f}_s^{1\mathrm{st}} \end{Bmatrix} \tag{7}$$

where $\mathbf{d}_s^{1\mathrm{st}}$ are the displacements of the slave nodes in the first layer which can be expressed in terms of the generalised co-ordinates $\mathbf{c}^{\mathrm{T}} = \{C_1^{\mathrm{I}}, C_1^{\mathrm{II}}, C_2^{\mathrm{I}}, C_2^{\mathrm{II}}, C_3^{\mathrm{I}}, \ldots\}$ as follows:

$$\mathbf{d}_s^{1\mathrm{st}} = \mathbf{T}_s^{1\mathrm{st}}\mathbf{c} \tag{8}$$

DOI: 10.1002/nme

$\mathbf{T}_s^{1st}$ is the transformation matrix in terms of polar co-ordinates (r, θ) for the slave nodes in the first layer. Therefore, Equation (7) can be written as

$$\begin{bmatrix} \mathbf{I} & 0 \\ 0 & \mathbf{T}_s^{1st} \end{bmatrix}^T \begin{bmatrix} \mathbf{K}_{mm}^{1st} & \mathbf{K}_{ms}^{1st} \\ \mathbf{K}_{sm}^{1st} & \mathbf{K}_{ss}^{1st} \end{bmatrix} \begin{bmatrix} \mathbf{I} & 0 \\ 0 & \mathbf{T}_s^{1st} \end{bmatrix} \begin{Bmatrix} \mathbf{d}_m \\ \mathbf{c} \end{Bmatrix} = \begin{bmatrix} \mathbf{I} & 0 \\ 0 & \mathbf{T}_s^{1st} \end{bmatrix}^T \begin{Bmatrix} \mathbf{f}_m^{1st} \\ \mathbf{f}_s^{1st} \end{Bmatrix} \tag{9}$$

or

$$\begin{bmatrix} \mathbf{K}_{mm}^{1st} & \mathbf{K}_{ms}^{1st}\mathbf{T}_s^{1st} \\ \mathbf{T}_s^{1st^T}\mathbf{K}_{sm}^{1st} & \mathbf{T}_s^{1st^T}\mathbf{K}_{ss}^{1st}\mathbf{T}_s^{1st} \end{bmatrix} \begin{Bmatrix} \mathbf{d}_m \\ \mathbf{c} \end{Bmatrix} = \begin{Bmatrix} \mathbf{f}_m^{1st} \\ \mathbf{T}_s^{1st^T}\mathbf{f}_s^{1st} \end{Bmatrix} \tag{10}$$

In order to provide the continuity between the singular and the regular region, $\mathbf{d}_m$ are not transformed.

Now, for the nth layer in the singular region; $n>1$

$$\mathbf{K}_s^n \mathbf{d}_s^n = \mathbf{f}_s^n \tag{11}$$

Applying the transformation gives

$$\mathbf{T}_s^{n^T}\mathbf{K}_s^n\mathbf{T}_s^n\mathbf{c} = \mathbf{T}_s^{n^T}\mathbf{f}_s^n \tag{12}$$

where

$$\mathbf{K}_s^n = \begin{bmatrix} \mathbf{K}_{s,ii}^n & \mathbf{K}_{s,ij}^n \\ \mathbf{K}_{s,ji}^n & \mathbf{K}_{s,jj}^n \end{bmatrix}$$

Since $\mathbf{d}_m$ are not transformed, the size of $\mathbf{T}_s^{1st}$ is smaller than that of $\mathbf{T}_s^n$.

The global stiffness matrix equation is

$$\begin{bmatrix} \mathbf{K}_{rr} & \mathbf{K}_{rm} & & & & & \\ \mathbf{K}_{mr} & \mathbf{K}_{mm}+\mathbf{K}_{mm}^{1st} & \mathbf{K}_{ms}^{1st} & & & & \\ & \mathbf{K}_{sm}^{1st} & \mathbf{K}_{ss}^{1st}+\mathbf{K}_{s,ii}^{2nd} & \mathbf{K}_{s,ij}^{2nd} & & & \\ & & \mathbf{K}_{s,ji}^{2nd} & \mathbf{K}_{s,jj}^{2nd}+\mathbf{K}_{s,ii}^{3rd} & \mathbf{K}_{s,ij}^{3rd} & & \\ & & & \ddots & \ddots & \ddots & \\ & & & & \mathbf{K}_{s,ji}^{nl} & \mathbf{K}_{s,jj}^{nl} \end{bmatrix} \begin{Bmatrix} \mathbf{d}_r \\ \mathbf{d}_m \\ \mathbf{d}_s^{1st} \\ \mathbf{d}_s^{2nd} \\ \vdots \\ \mathbf{d}_s^{nl} \end{Bmatrix} = \begin{Bmatrix} \mathbf{f}_r \\ \mathbf{f}_m \\ \mathbf{f}_s^{1st} \\ \mathbf{f}_s^{2nd} \\ \vdots \\ \mathbf{f}_s^{nl} \end{Bmatrix} \tag{13}$$

where nl is the number of layers in the singular region. We can rewrite Equation (13) by applying the transformation as follows:

$$\begin{bmatrix} \mathbf{K}_{rr} & \mathbf{K}_{rm} & 0 \\ \mathbf{K}_{mr} & \mathbf{K}_{mm}+\mathbf{K}_{mm}^{1st} & \mathbf{K}_{ms}^{1st}\mathbf{T}_s^{1st} \\ 0 & \mathbf{T}_s^{1st^T}\mathbf{K}_{sm}^{1st} & \mathbf{T}_s^{1st^T}\mathbf{K}_{ss}^{1st}\mathbf{T}_s^{1st}+\sum_{n=2}^{nl}\mathbf{T}_s^{n^T}\mathbf{K}_s^n\mathbf{T}_s^n \end{bmatrix} \begin{Bmatrix} \mathbf{d}_r \\ \mathbf{d}_m \\ \mathbf{c} \end{Bmatrix} = \begin{Bmatrix} \mathbf{f}_r \\ \mathbf{f}_m+\mathbf{f}_m^{1st} \\ \mathbf{T}_s^{1st^T}\mathbf{f}_s^{1st}+\sum_{n=2}^{nl}\mathbf{T}_s^{n^T}\mathbf{f}_s^n \end{Bmatrix} \tag{14}$$

DOI: 10.1002/nme

or

$$\begin{bmatrix} \mathbf{K}_{rr} & \mathbf{K}_{rm} & 0 \\ \mathbf{K}_{mr} & \mathbf{K}_{mm}+\mathbf{K}_{mm}^{1st} & \bar{\mathbf{K}}_{ms}^{1st} \\ 0 & \bar{\mathbf{K}}_{sm}^{1st} & \bar{\mathbf{K}}_{ss}^{1st}+\sum_{n=2}^{nl}\bar{\mathbf{K}}_{s}^{n} \end{bmatrix} \begin{Bmatrix} \mathbf{d}_r \\ \mathbf{d}_m \\ \mathbf{c} \end{Bmatrix} = \begin{Bmatrix} \mathbf{f}_r \\ \mathbf{f}_m+\mathbf{f}_m^{1st} \\ \bar{\mathbf{f}}_s^{1st}+\sum_{n=2}^{nl}\bar{\mathbf{f}}_s^{n} \end{Bmatrix} \tag{15}$$

where $\bar{\mathbf{K}}_{ms}^{1st}=\mathbf{K}_{ms}^{1st}\mathbf{T}_s^{1st}$, $\bar{\mathbf{K}}_s^n=\mathbf{T}_s^{n^T}\mathbf{K}_s^n\mathbf{T}_s^n$, $\bar{\mathbf{f}}_s^n=\mathbf{T}_s^{n^T}\mathbf{f}_s^n$, etc.

The unknowns now are the displacements $\mathbf{d}_r$ and $\mathbf{d}_m$ in the regular region and the generalised co-ordinates $\mathbf{c}$. If we consider $\mathbf{d}_s$ as the vector of displacements in the singular region except for those on Γ_0, the size of the vector $\mathbf{d}_s$ is much bigger than the vector of the generalised co-ordinates $\mathbf{c}$. Therefore, solving the system of Equation (15) is much more efficient than solving the system of Equation (13).

3. GLOBAL INTERPOLATION FUNCTIONS FOR A NOTCH PROBLEM

The global interpolation functions, which are used for the fractal transformation, have an essential role in the FFEM; therefore, exact analytical solutions are employed as the global interpolation functions. An eigenfunction expansion approach or a complex variable approach can be used to derive analytical solutions of the stress and displacement fields around a notch tip [31, 32]. For the sake of completeness, the following is a short description of those approaches.

3.1. Eigenfunction expansion method

The airy stress function approach can be used to derive the displacement and stress series expansions around a notch tip in the manner of Williams [3]. He investigated the analytical form of the most critical singularity cases of notches. Williams' eigenfunctions were proved to be complete for the annular sector [33, 34]. According to this method, the stress and displacement expressions in a

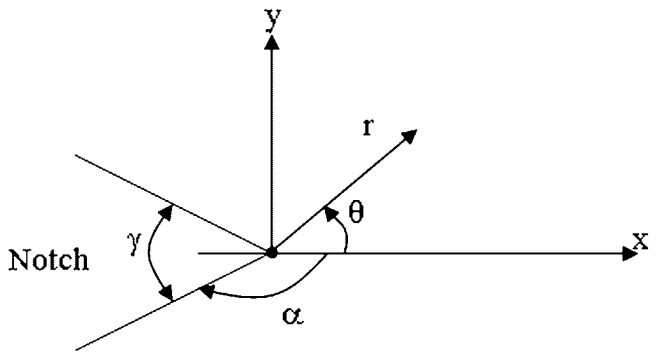

Figure 3. Notch geometry and the co-ordinate systems.

DOI: 10.1002/nme

polar co-ordinate system centred at the tip of an infinite notch as illustrated in Figure 3 (the $\theta=0$ axis and the Cartesian x-axis coincide with the bisector of the notch angle) can be written as

$$\sigma_r = -\lambda^{\mathrm{I}} r^{\lambda^{\mathrm{I}}-1}[(\lambda^{\mathrm{I}}+1)C_2\cos(\lambda^{\mathrm{I}}+1)\theta+(\lambda^{\mathrm{I}}-3)C_4\cos(\lambda^{\mathrm{I}}-1)\theta]$$
$$-\lambda^{\mathrm{II}} r^{\lambda^{\mathrm{II}}-1}[(\lambda^{\mathrm{II}}+1)C_1\sin(\lambda^{\mathrm{II}}+1)\theta+(\lambda^{\mathrm{II}}-3)C_3\sin(\lambda^{\mathrm{II}}-1)\theta] \quad (16)$$

$$\sigma_\theta = \lambda^{\mathrm{I}}(\lambda^{\mathrm{I}}+1) r^{\lambda^{\mathrm{I}}-1}[C_2\cos(\lambda^{\mathrm{I}}+1)\theta+C_4\cos(\lambda^{\mathrm{I}}-1)\theta]$$
$$+\lambda^{\mathrm{II}}(\lambda^{\mathrm{II}}+1) r^{\lambda^{\mathrm{II}}-1}[C_1\sin(\lambda^{\mathrm{II}}+1)\theta+C_3\sin(\lambda^{\mathrm{II}}-1)\theta] \quad (17)$$

$$\sigma_{r\theta} = \lambda^{\mathrm{I}} r^{\lambda^{\mathrm{I}}-1}[(\lambda^{\mathrm{I}}+1)C_2\sin(\lambda^{\mathrm{I}}+1)\theta+(\lambda^{\mathrm{I}}-1)C_4\sin(\lambda^{\mathrm{I}}-1)\theta]$$
$$-\lambda^{\mathrm{II}} r^{\lambda^{\mathrm{II}}-1}[(\lambda^{\mathrm{II}}+1)C_1\cos(\lambda^{\mathrm{II}}+1)\theta+(\lambda^{\mathrm{II}}-1)C_3\cos(\lambda^{\mathrm{II}}-1)\theta] \quad (18)$$

$$u_r = \frac{r^{\lambda^{\mathrm{I}}}}{2G}[-(\lambda^{\mathrm{I}}+1)C_2\cos(\lambda^{\mathrm{I}}+1)\theta+C_4(3-\lambda^{\mathrm{I}}-4\eta)\cos(\lambda^{\mathrm{I}}-1)\theta]$$
$$+\frac{r^{\lambda^{\mathrm{II}}}}{2G}[-(\lambda^{\mathrm{II}}+1)C_1\sin(\lambda^{\mathrm{II}}+1)\theta+C_3(3-\lambda^{\mathrm{II}}-4\eta)\sin(\lambda^{\mathrm{II}}-1)\theta] \quad (19)$$

$$u_\theta = \frac{r^{\lambda^{\mathrm{I}}}}{2G}[(\lambda^{\mathrm{I}}+1)C_2\sin(\lambda^{\mathrm{I}}+1)\theta+C_4(3+\lambda^{\mathrm{I}}-4\eta)\sin(\lambda^{\mathrm{I}}-1)\theta]$$
$$+\frac{r^{\lambda^{\mathrm{II}}}}{2G}[-(\lambda^{\mathrm{II}}+1)C_1\cos(\lambda^{\mathrm{II}}+1)\theta-C_3(3+\lambda^{\mathrm{II}}-4\eta)\cos(\lambda^{\mathrm{II}}-1)\theta] \quad (20)$$

where G is the shear modulus, $\eta=\nu$ for plane strain, $\eta=\nu/(1+\nu)$ for plane stress, and ν is Poisson ratio. λ^{I} and λ^{II} are eigenvalues for modes I and II, respectively, and are calculated from the characteristic equations:

$$\lambda^{\mathrm{I}}\sin 2\alpha+\sin 2\lambda^{\mathrm{I}}\alpha=0 \quad (21)$$

$$\lambda^{\mathrm{II}}\sin 2\alpha-\sin 2\lambda^{\mathrm{II}}\alpha=0 \quad (22)$$

C_1, C_2, C_3, C_4 are the generalised co-ordinates. C_3 and C_4 can be calculated in terms of C_1 and C_2

$$C_4 = -\frac{\cos(\lambda^{\mathrm{I}}+1)\alpha}{\cos(\lambda^{\mathrm{I}}-1)\alpha}C_2 = -\frac{(\lambda^{\mathrm{I}}+1)\sin(\lambda^{\mathrm{I}}+1)\alpha}{(\lambda^{\mathrm{I}}-1)\sin(\lambda^{\mathrm{I}}-1)\alpha}C_2 \quad (23)$$

$$C_3 = -\frac{\sin(\lambda^{\mathrm{II}}+1)\alpha}{\sin(\lambda^{\mathrm{II}}-1)\alpha}C_1 = -\frac{(\lambda^{\mathrm{II}}+1)\cos(\lambda^{\mathrm{II}}+1)\alpha}{(\lambda^{\mathrm{II}}-1)\cos(\lambda^{\mathrm{II}}-1)\alpha}C_1 \quad (24)$$

The characteristic equations (21) and (22) can be solved numerically using Muller's iteration method [14]. Muller's method can converge to a complex root, even if the iteration has started with a real number. A comprehensive discussion of the behaviour of the roots of Equations (21) and (22) is given in References [31, 35].

The dominant eigenvalues, which are the smallest eigenvalues greater than zero, for different notch angles γ are plotted in Figure 4. From Figure 4 and Equations (16)–(18), it can be inferred

DOI: 10.1002/nme

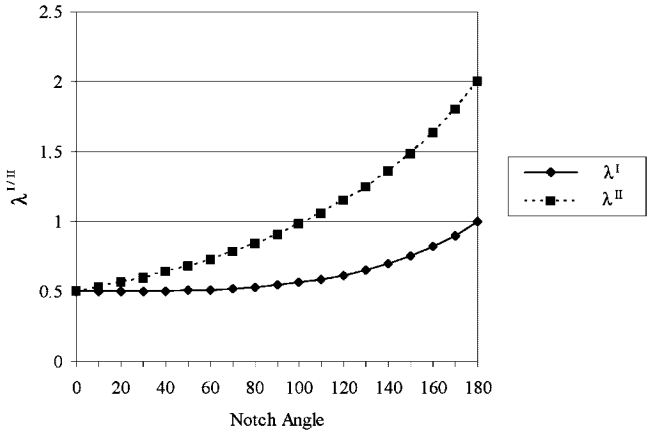

Figure 4. Notch angle vs. dominant eigenvalues for modes I and II.

that the stresses are unbounded at the notch tip when the notch angle $\gamma<180°$ for mode I, and $\gamma<102.55°$ for mode II.

3.2. Complex variable approach

According to the complex variable approach [36], the displacement and stress expressions can be written as

$$u_r = \frac{r^{\lambda^{\mathrm{I}}}}{2G}A_1[(3-4\eta-\lambda^{\mathrm{I}})\cos(\lambda^{\mathrm{I}}-1)\theta+(\cos 2\lambda^{\mathrm{I}}\alpha+\lambda^{\mathrm{I}}\cos 2\alpha)\cos(\lambda^{\mathrm{I}}+1)\theta] + \frac{r^{\lambda^{\mathrm{II}}}}{2G}A_2[-(3-4\eta-\lambda^{\mathrm{II}})\sin(\lambda^{\mathrm{II}}-1)\theta+(\cos 2\lambda^{\mathrm{II}}\alpha-\lambda^{\mathrm{II}}\cos 2\alpha)\sin(\lambda^{\mathrm{II}}+1)\theta] \quad (25)$$

$$u_\theta = \frac{r^{\lambda^{\mathrm{I}}}}{2G}A_1[(3-4\eta+\lambda^{\mathrm{I}})\sin(\lambda^{\mathrm{I}}-1)\theta-(\cos 2\lambda^{\mathrm{I}}\alpha+\lambda^{\mathrm{I}}\cos 2\alpha)\sin(\lambda^{\mathrm{I}}+1)\theta] + \frac{r^{\lambda^{\mathrm{II}}}}{2G}A_2[(3-4\eta+\lambda^{\mathrm{II}})\cos(\lambda^{\mathrm{II}}-1)\theta+(\cos 2\lambda^{\mathrm{II}}\alpha-\lambda^{\mathrm{II}}\cos 2\alpha)\cos(\lambda^{\mathrm{II}}+1)\theta] \quad (26)$$

$$\sigma_r = r^{\lambda^{\mathrm{I}}-1}\lambda^{\mathrm{I}}A_1[-(\lambda^{\mathrm{I}}-3)\cos(\lambda^{\mathrm{I}}-1)\theta+(\cos 2\lambda^{\mathrm{I}}\alpha+\lambda^{\mathrm{I}}\cos 2\alpha)\cos(\lambda^{\mathrm{I}}+1)\theta] + r^{\lambda^{\mathrm{II}}-1}\lambda^{\mathrm{II}}A_2[(\lambda^{\mathrm{II}}-3)\sin(\lambda^{\mathrm{II}}-1)\theta+(\cos 2\lambda^{\mathrm{II}}\alpha-\lambda^{\mathrm{II}}\cos 2\alpha)\sin(\lambda^{\mathrm{II}}+1)\theta] \quad (27)$$

$$\sigma_\theta = r^{\lambda^{\mathrm{I}}-1}\lambda^{\mathrm{I}}A_1[(\lambda^{\mathrm{I}}+1)\cos(\lambda^{\mathrm{I}}-1)\theta-(\cos 2\lambda^{\mathrm{I}}\alpha+\lambda^{\mathrm{I}}\cos 2\alpha)\cos(\lambda^{\mathrm{I}}+1)\theta] - r^{\lambda^{\mathrm{II}}-1}\lambda^{\mathrm{II}}A_2[(\lambda^{\mathrm{II}}+1)\sin(\lambda^{\mathrm{II}}-1)\theta+(\cos 2\lambda^{\mathrm{II}}\alpha-\lambda^{\mathrm{II}}\cos 2\alpha)\sin(\lambda^{\mathrm{II}}+1)\theta] \quad (28)$$

$$\sigma_{r\theta} = r^{\lambda^{\mathrm{I}}-1}\lambda^{\mathrm{I}}A_1[(\lambda^{\mathrm{I}}-1)\sin(\lambda^{\mathrm{I}}-1)\theta-(\cos 2\lambda^{\mathrm{I}}\alpha+\lambda^{\mathrm{I}}\cos 2\alpha)\sin(\lambda^{\mathrm{I}}+1)\theta] + r^{\lambda^{\mathrm{II}}-1}\lambda^{\mathrm{II}}A_2[(\lambda^{\mathrm{II}}-1)\cos(\lambda^{\mathrm{II}}-1)\theta+(\cos 2\lambda^{\mathrm{II}}\alpha-\lambda^{\mathrm{II}}\cos 2\alpha)\cos(\lambda^{\mathrm{II}}+1)\theta] \quad (29)$$

where A_1 and A_2 are the generalised co-ordinates.

DOI: 10.1002/nme

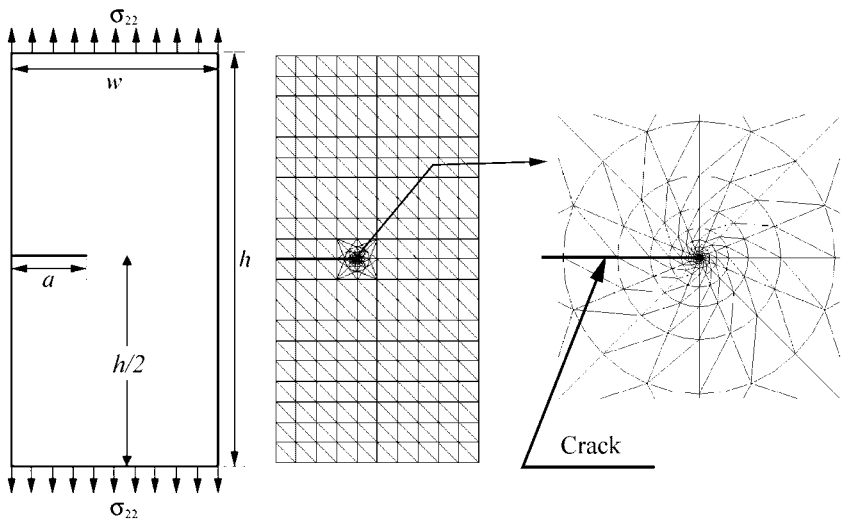

Figure 5. Single edge-cracked plate and the mesh used for the analysis.

Expressions (25)–(29) are equivalent to the ones derived using the eigenfunction expansion approach and, therefore, produce similar results. It should be noted that both forms of expressions have been presented to emphasise the fact that while they are different symbolically, they produce similar results.

3.3. The stress intensity factors (SIFs)

The SIFs are defined in a way similar to those of a crack by some authors [2] as

$$K_{\mathrm{I}} = \sqrt{2\pi} \lim_{r\to 0} r^{1-\lambda^{\mathrm{I}}} \sigma_\theta(\theta=0) \tag{30}$$

$$K_{\mathrm{II}} = \sqrt{2\pi} \lim_{r\to 0} r^{1-\lambda^{\mathrm{II}}} \sigma_{r\theta}(\theta=0) \tag{31}$$

for modes I and II, respectively.

The relationships between the SIFs and the generalised co-ordinates are obtained by substituting the stress expressions (17) and (18) into Equations (30) and (31):

$$K_{\mathrm{I}} = \sqrt{2\pi}\lambda^{\mathrm{I}}(\lambda^{\mathrm{I}}+1)\left(1-\frac{\cos(\lambda^{\mathrm{I}}+1)\alpha}{\cos(\lambda^{\mathrm{I}}-1)\alpha}\right)C_2 \tag{32}$$

$$K_{\mathrm{II}} = -\sqrt{2\pi}\lambda^{\mathrm{II}}\left[(\lambda^{\mathrm{II}}+1)-(\lambda^{\mathrm{II}}-1)\frac{\sin(\lambda^{\mathrm{II}}+1)\alpha}{\sin(\lambda^{\mathrm{II}}-1)\alpha}\right]C_1 \tag{33}$$

DOI: 10.1002/nme

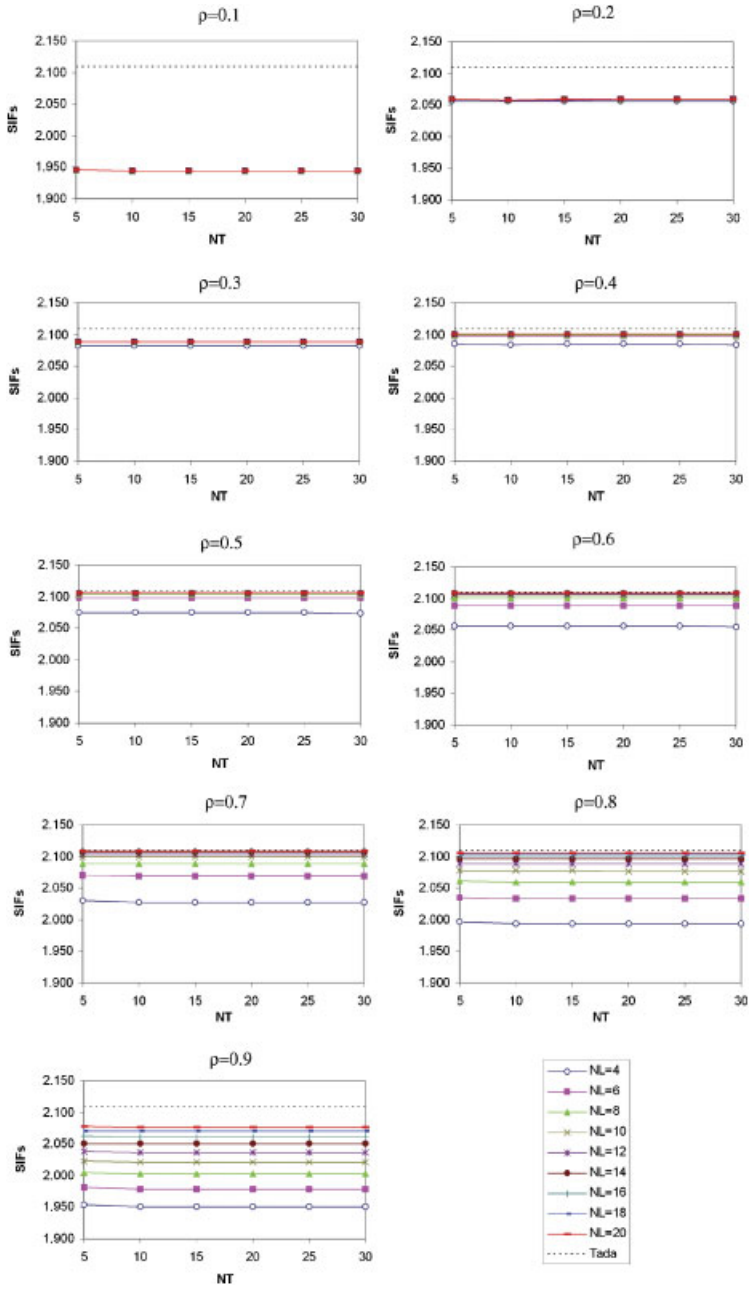

Figure 6. Variations of SIFs with number of terms (NT) and for different numbers of layers (NL) and similarity ratios ρ compared with those of Tada [37].

DOI: 10.1002/nme

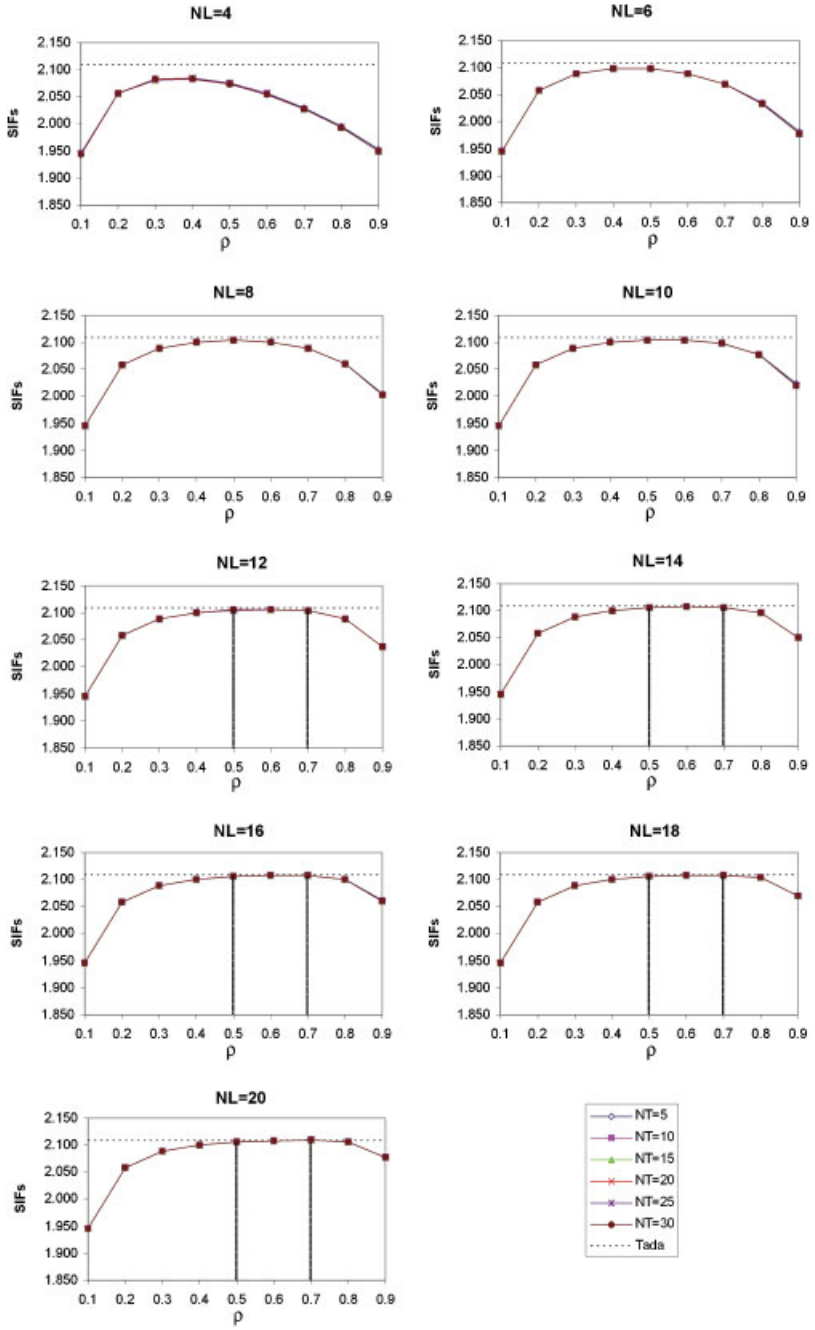

Figure 7. Variations of SIFs with similarity ratio and for different numbers of terms and numbers of layers compared with those of Tada [37].

DOI: 10.1002/nme

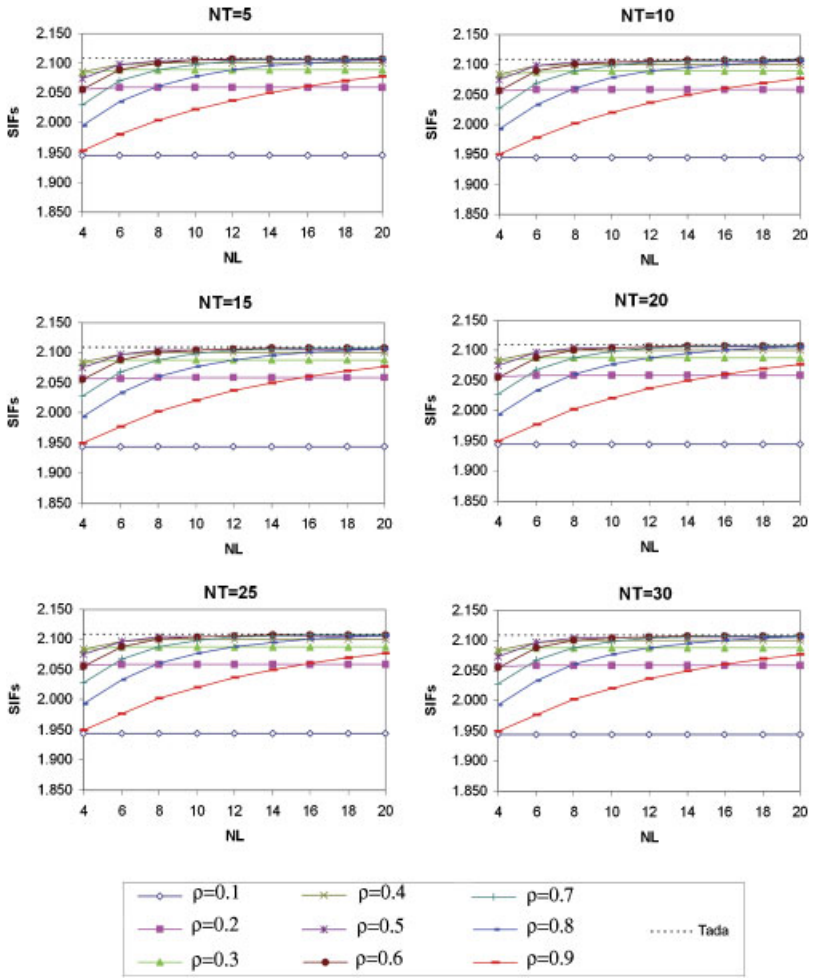

Figure 8. Variations of SIFs with number of layers and for different similarity ratios and numbers of terms compared with those of Tada [37].

or by substituting Equations (28) and (29) into (30) and (31):

$$K_{\mathrm{I}} = \sqrt{2\pi}\lambda^{\mathrm{I}}(1+\lambda^{\mathrm{I}}-\lambda^{\mathrm{I}}\cos 2\alpha-\cos 2\lambda^{\mathrm{I}}\alpha)A_1 \tag{34}$$

$$K_{\mathrm{II}} = \sqrt{2\pi}\lambda^{\mathrm{II}}(-1+\lambda^{\mathrm{II}}-\lambda^{\mathrm{II}}\cos 2\alpha+\cos 2\lambda^{\mathrm{II}}\alpha)A_2 \tag{35}$$

Relationships (32)–(35) show that no post-processing technique is necessary to extract the SIFs.

DOI: 10.1002/nme

4. NUMERICAL EXAMPLES

4.1. Convergence study for a crack case

A convergence study will be performed to demonstrate the accuracy and stability of the FFEM. The effects of the similarity ratio (for a range of 0.1–0.9), the number of layers in the singular region (for a range of 4–20), and the number of terms of the eigenfunction expansion series used as global interpolation functions (for a range of 5–30) on the SIFs will be considered.

Two-dimensional mode I plane-stress crack problem of a single edge-cracked plate as shown in Figure 5 will be analysed. The aspect ratio and the ratio of the crack length to the plate width are $h/w=2$ and $a/w=0.4$, respectively. Six-node triangle elements are used to model the plate. Also, the singular region volume is held constant with increasing numbers of layers.

The results compared to those of Tada [37] are presented in Figures 6–8. Figures 6 and 7 show that the number of transformation terms (NT) does not have a significant effect on the results when NT$\geqslant$5.

Table I. SIFs for an edge-cracked plate for different crack lengths.

	$K_I/\sigma\sqrt{\pi}a^{1-\lambda_1^I}$						
				FFEM			
a/w	Gross [37]	Tada [37]	Yang [38]	5 layers	10 layers	15 layers	20 layers
0.1	1.186	1.196	1.204	1.165	1.185	1.186	1.186
0.2	1.373	1.367	1.380	1.342	1.363	1.365	1.365
0.3	1.662	1.655	1.676	1.629	1.655	1.657	1.658
0.4	2.106	2.108	2.134	2.071	2.105	2.108	2.108
0.5	2.829	2.827	2.858	2.767	2.814	2.818	2.818
0.6	4.030	4.043	4.090	3.946	4.015	4.020	4.021
0.7	—	6.376	6.471	6.203	6.318	6.328	6.328
0.8	—	11.993	—	11.610	11.850	11.869	11.871
0.9	—	34.719	—	33.176	34.068	34.139	34.145

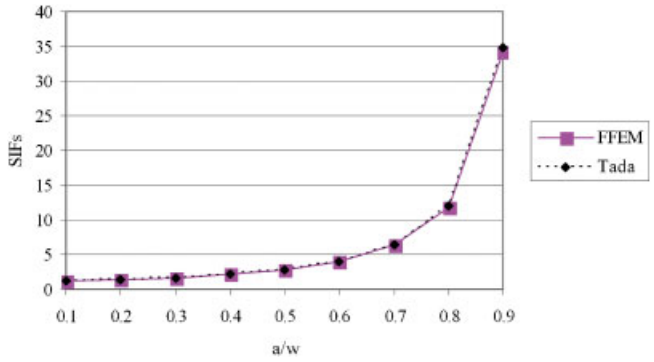

Figure 9. Variations of SIFs with crack length (using 20 layers) compared with that of Tada [37].

DOI: 10.1002/nme

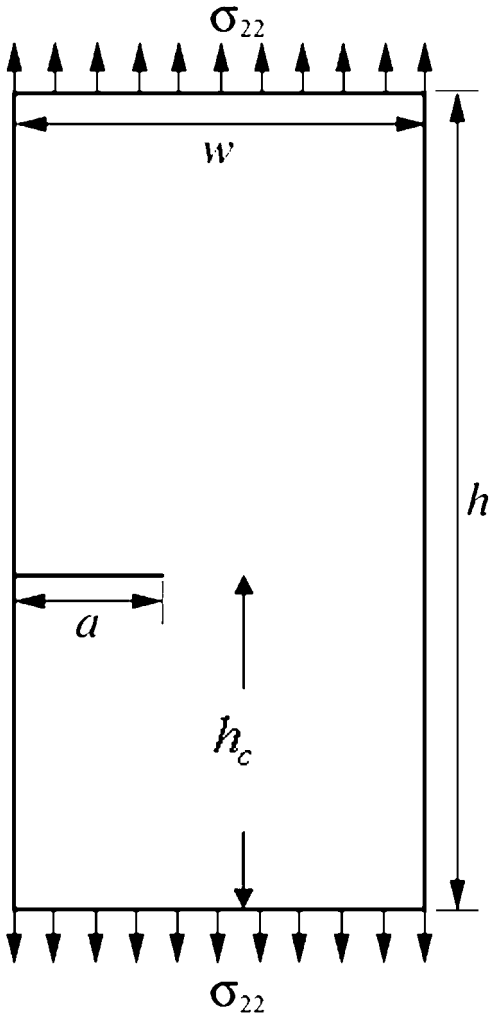

Figure 10. Single off-centre edge-cracked plate subjected to mode I load condition.

From Figure 7, good results can be obtained by using values of similarity ratios between 0.5 and 0.7 for the range of numbers of layers used in this study. Also, Figure 8 illustrates that the results converge asymptotically with increasing numbers of layers used to model the singular region when $\rho>0.3$. Good results can be obtained by using 10 layers or more.

4.2. Examples of single edge-cracked plates subjected to mode I load conditions

Two-dimensional mode I plane-stress crack problems of a single edge-cracked plate will be analysed for different crack lengths. The problem is shown in Figure 5. Based on the convergence study, 10 terms of the eigenfunction series are used for the fractal transformation. The aspect ratio and the similarity ratio are $h/w=2$ and $\rho=0.6$, respectively. Six-node triangle elements are used.

DOI: 10.1002/nme

Table II. SIFs for an off-centre edge-cracked plate for different crack positions.

	$K_{\mathrm{I}}/\sigma\sqrt{\pi a}(K_{\mathrm{II}}/\sigma\sqrt{\pi a})$	
h_c/h	FFEM	ABAQUS
0.1	3.488 (1.037)	3.488 (1.039)
0.2	2.343 (0.230)	2.343 (0.232)
0.3	2.150 (0.053)	2.150 (0.054)
0.4	2.113 (0.009)	2.113 (0.010)
0.5	2.108 (0.000)	2.108 (0.000)

Different numbers of layers are used to model the singular region whose volume is held constant with increasing numbers of layers.

The comparisons of the computed SIFs and corresponding published data [37, 38] are shown in Table I for different ratios of crack length to plate width. Also, the SIFs computed using 20 layers to model the singular region by the FFEM compared to those of Tada [37] are plotted in Figure 9.

Table I as well as Figure 8 show that the SIF values increase asymptotically with increasing numbers of layers. In addition, the SIF values increase with increasing ratios of crack length to plate width (a/w) as shown in Table I and Figure 9. It is also seen from Table I and Figure 9 that there is a sharp increase in the SIF value when the crack length to plate width ratio (a/w) exceeds 0.8. Furthermore, the FFEM results for the SIFs of single edge-cracked plates show very good agreement with the published results. The results in Table I prove that the eigenfunction expansion series derived for notch problems yield accurate results for crack problems (when the notch opening angle $\gamma=0°$).

4.3. Examples of single off-centre edge-cracked plates under tension

A single off-centre edge-cracked plate as illustrated in Figure 10 is considered in this section. The ratio of the crack length to the width of the plate is taken as $a/w=0.4$. Sixteen layers in the singular region, 10 terms of the eigenfunctions, an aspect ratio of $h/w=2$, a similarity ratio of $\rho=0.6$, and six-node triangle elements are used.

Using the parameters stated above, the FFEM is used to compute the modes I and II SIF values. The results obtained are tabulated in Table II. But it should be noted that these are new results and that there are no published data with which to compare them. Therefore, in order to validate the results, the ABAQUS 6.5-4 finite element analysis (FEA) package is used to model the cracked plates. A similar mesh to that shown in Figure 5 is used. In addition, the elements around the crack tip are modelled using quarter-point crack tip elements [39].

The values of the SIFs for modes I and II predicted by the ABAQUS FEA package are also tabulated in Table II. It should be mentioned that mode II occurs in this example because of the geometrical asymmetry of the plate configuration. It can be seen from Table II that the SIF values increase as the crack gets closer to the top or bottom boundaries of the plate, and the minimum values occur when the crack is central. In order to show clearly the sharp drop in the SIF values as the crack location moves from the edge to the centre of the plate, the K_{I} and K_{II} values are plotted in Figure 11. From this figure, it can be inferred that cracks located within 20% of the ends of the plate are more critical as they give the highest SIFs. Also, the FFEM and ABAQUS results are in very good agreement.

DOI: 10.1002/nme

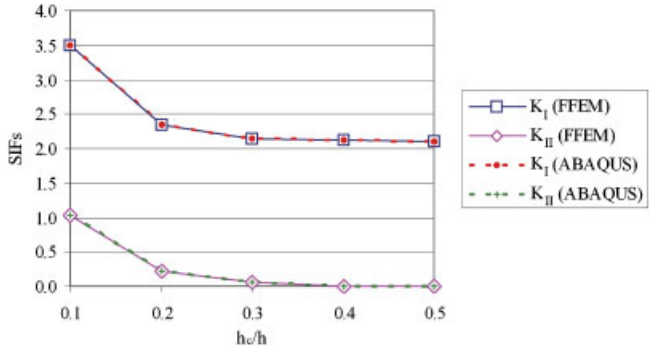

Figure 11. Variations of SIFs of an off-centre edge-cracked plate compared with those calculated using ABAQUS FEA package.

4.4. Numerical examples of single edge-notched plates subjected to mode I load conditions

Two-dimensional mode I plane-stress notch problems of a single edge-notched plate is analysed for different notch angles. The problem is shown in Figures 12 and 13. Ten terms of the eigenfunction series are used for the fractal transformation. The aspect ratio, the similarity ratio, and the ratio of the notch length to the plate width are $h/w=2$, $\rho=0.6$, and $a/w=0.4$, respectively. Six-node triangle elements are used to model the plate. The volume of the singular region is held constant with increasing numbers of layers.

The SIFs calculated by the FFEM for different numbers of layers and different notch angles compared to numerical published data are shown in Table III. In addition, the SIFs computed using 16 layers to model the singular region by the FFEM are compared to those of Gross [2] in Figure 14.

The results in Table III increase asymptotically with increasing numbers of layers. The SIF values increase monotonically as the notch opening angle increases as shown in Table III and Figure 14. It can be observed that the difference between a crack SIF and a notch SIF when the notch angle is less than 30° is less than 1% for mode I. This could be of high importance from an experimental point of view, as making notches is relatively much easier than developing cracks in test specimens.

The FFEM results in Table III for single edge-notched plates ascertain that the use of the eigenfunction series derived in Section 3 as the global interpolation functions of the FFEM gives results in very good agreement with the published results.

4.5. Numerical examples of single off-centre edge-notched plates

Figure 15 illustrates a single off-centre edge-notched plate under tension. The number of layers in the singular region, the number of terms of the eigenfunction series, the aspect ratio, and the similarity ratio are nl = 16, nt = 20, $h/w=2$, $\rho=0.6$, respectively. Six-node triangle elements are used to model the notched plates as shown in Figure 16. A circumferentially denser mesh is used to model the singular region, as it was necessary to obtain non-oscillatory SIFs for mode II when the notch opening angle is rather large.

The modes I and II SIFs for different notch positions are tabulated for a ratio of the notch length to the plate width $a/w=0.4$ and different notch opening angles in Table IV and for a notch

DOI: 10.1002/nme

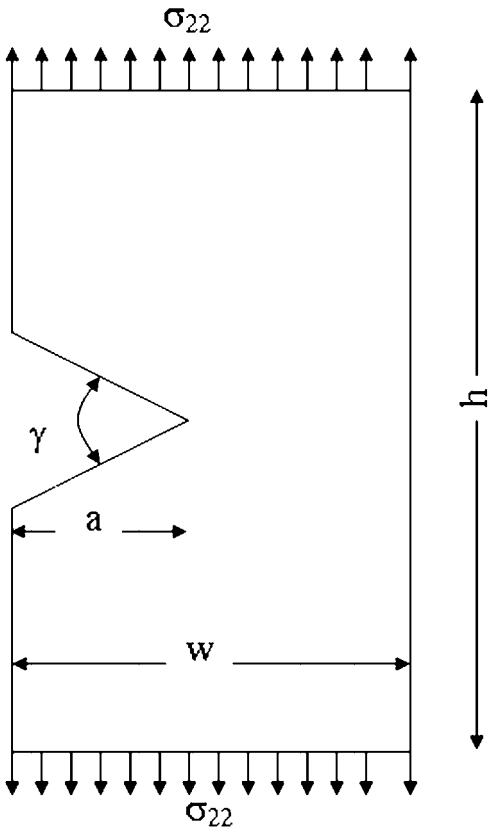

Figure 12. Single edge-notched plate subjected to mode I load conditions.

opening angle $\gamma = 50°$ and various ratios of the notch length to the plate width in Table V. In addition, in order to show clearly how SIF values change, they are plotted in Figures 17 and 18, respectively. Published SIF values appear to be unavailable for most of the cases analysed in this section.

The missing values in Tables IV and V are because the geometry of the plate is no more rectangular (the top and bottom boundaries are no more equal). The results in Tables IV and V converged well as the density of the mesh in the singular region was increased in the circumferential direction. Compared to the cases studied in previous sections for which published data existed, the values of the SIFs in Tables IV and V that correspond to these cases are, respectively, similar. Consequently, the SIF values in Tables IV and V are valid.

It can be seen from Table IV and Figure 17 that the SIFs monotonically increase as the notch opening angle increases. Also, the values of the SIFs increase as the notch gets closer to the top or bottom boundaries of the plate. The minimum values of the SIFs occur when the notch is central and the notch opening angle is 0°. It is worth mentioning that the difference between the crack SIFs and the notch SIFs when the notch angle is 30° or less is around 1.5% or less for mode I, but is up to 39% for mode II.

DOI: 10.1002/nme

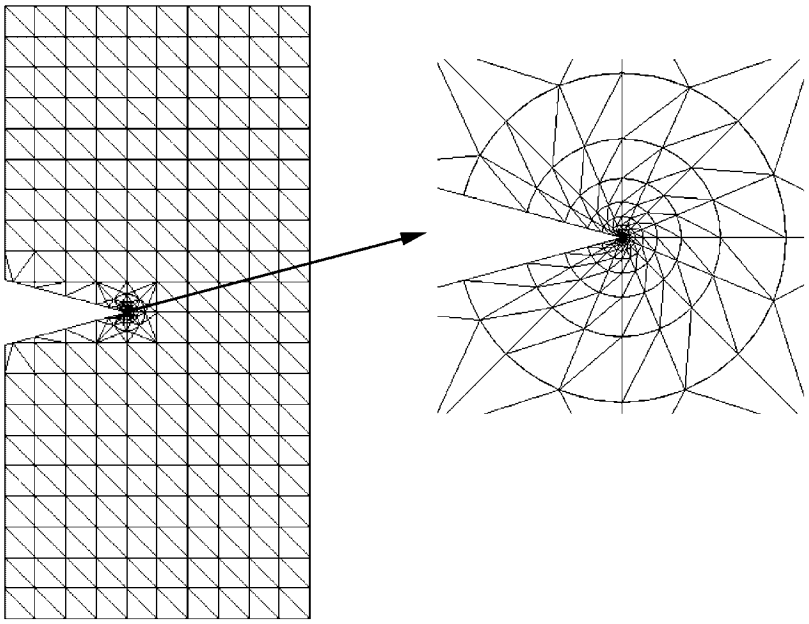

Figure 13. FE mesh of the geometry of a single edge-notched plate.

Table III. Mode I SIFs for various notch angles compared with published results.

	$K_{\mathrm{I}}/\sigma\sqrt{\pi}a^{1-\lambda_1^{\mathrm{I}}}$					
				FFEM		
γ (deg)	λ_1^{I}	Gross [2]	Aliabadi [14]	10 layers	16 layers	20 layers
0	0.500000	2.113	2.113	2.105	2.108	2.108
30	0.501453	2.128	2.129	2.122	2.124	2.125
60	0.512221	2.223	2.222	2.218	2.220	2.220
90	0.544484	2.473	2.471	2.466	2.467	2.467
120	0.615731	3.021	—	3.016	3.016	3.016

Table V and Figure 18 show that the SIF values of a notched plate whose notch opening angle is $\gamma = 50^\circ$ increase as the notch length increases and as the notch gets closer to the top or bottom boundaries of the plate. Also, from Figures 17 and 18, the curves of the mode II SIFs are steeper when the notch is closer to the top or bottom boundaries of the plate.

5. CONCLUSIONS

In this paper, the fractal-like finite element method (FFEM) has been extended to model notch problems. The FFEM divides the cracked or notched body into singular and regular regions.

DOI: 10.1002/nme

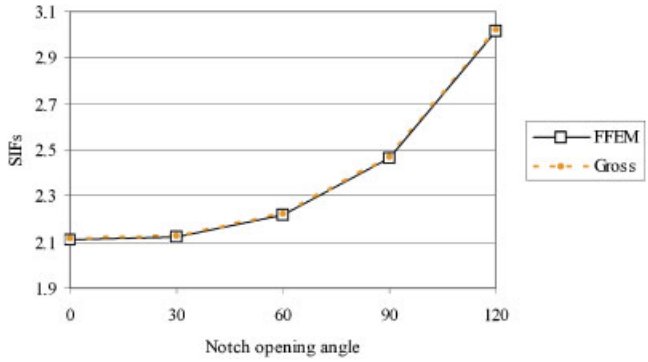

Figure 14. Variations of SIFs with notch opening angle (using 16 layers) compared with those of Gross [2].

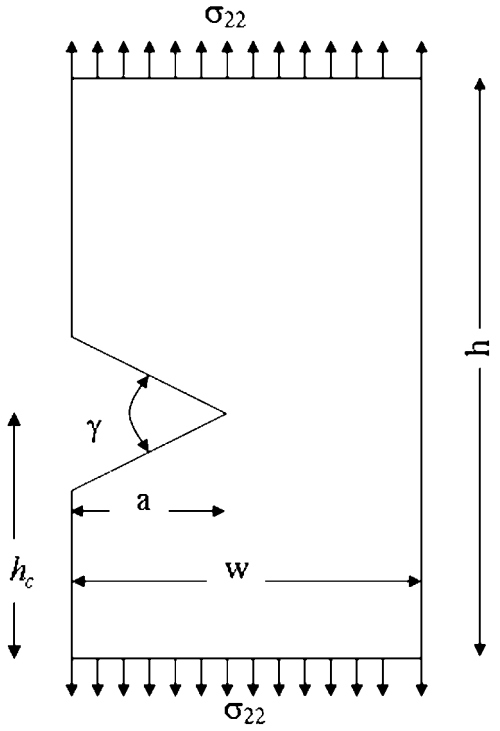

Figure 15. Single off-centre edge-notched plate under tension.

Conventional finite elements are used to model all regions. The singular region is modelled using a large number of elements generated layer by layer in a self-similar manner. The FFEM utilises the fractal transformation concept to reduce the large number of degrees of freedom around a singular point, such as a crack or notch tip, to a small set of generalised co-ordinates by using global interpolation functions.

DOI: 10.1002/nme

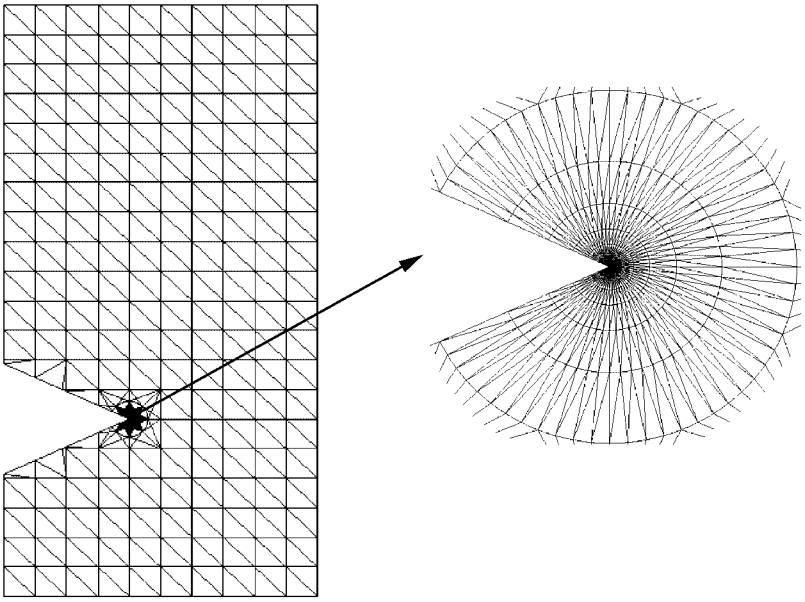

Figure 16. FE mesh of the geometry of a single off-centre edge-notched plate.

Table IV. Normalised SIFs of a single off-centre edge-notched plate for various notch positions and opening angles for $a/w=0.4$.

	(h_c/h)									
	0.1		0.2		0.3		0.4		0.5	
γ (deg)	K_{I}	K_{II}	K_{I}	K_{II}	K_{I}	K_{II}	K_{I}	K_{II}	K_{I}	K_{II}
0	3.490	1.040	2.344	0.232	2.151	0.054	2.114	0.011	2.109	0.001
10	3.503	1.153	2.346	0.253	2.152	0.059	2.115	0.011	2.110	0.001
20	3.517	1.287	2.350	0.278	2.156	0.064	2.119	0.012	2.114	0.001
30	3.544	1.448	2.361	0.307	2.167	0.070	2.131	0.014	2.125	0.001
40	3.580	1.596	2.381	0.335	2.186	0.076	2.150	0.015	2.145	0.002
50	3.741	1.758	2.427	0.368	2.218	0.083	2.180	0.016	2.174	0.002
60	—	—	2.472	0.404	2.263	0.090	2.226	0.018	2.221	0.003
70	—	—	2.534	0.448	2.325	0.099	2.289	0.020	2.284	0.003
80	—	—	2.615	0.507	2.407	0.110	2.372	0.022	2.367	0.004
90	—	—	—	—	2.511	0.127	2.477	0.026	2.473	0.005

The global interpolation functions used to perform the fractal transformation were exact analytical solutions of the stress and displacement fields around a notch tip and were derived analytically by using an eigenfunction expansion technique and a complex variable approach. Those functions were found to be eigenfunction expansion series, and some of their coefficients are related directly to the SIFs, and therefore no post-processing technique is necessary to extract the SIFs.

DOI: 10.1002/nme

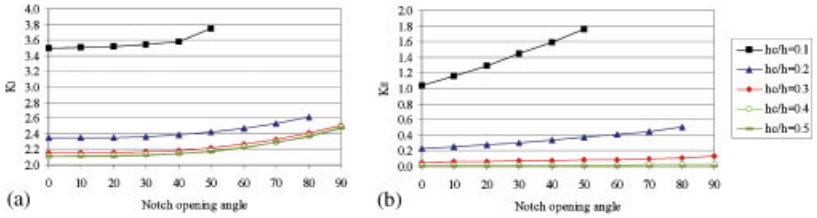

Figure 17. Normalised mode I (a) and mode II (b) SIFs of a single off-centre edge-notched plate for various notch positions and opening angles.

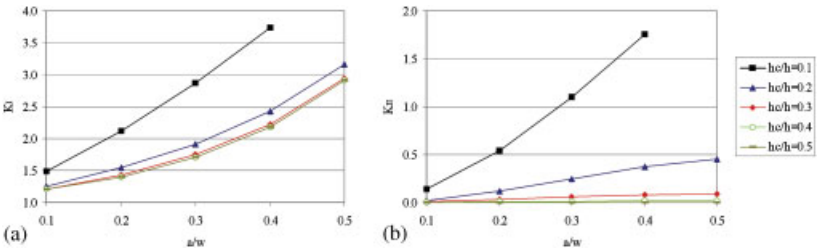

Figure 18. Normalised mode I (a) and mode II (b) SIFs of a single off-centre edge-notched plate for various notch positions and notch lengths for notch opening angle $\gamma = 50°$.

Table V. Normalised SIFs of a single off-centre edge-notched plate for various notch positions and notch lengths for notch opening angle $\gamma = 50°$.

	(h_c/h)									
	0.1		0.2		0.3		0.4		0.5	
a/w	K_I	K_{II}	K_I	K_{II}	K_I	K_{II}	K_I	K_{II}	K_I	K_{II}
0.1	1.481	0.139	1.252	0.024	1.212	0.005	1.205	0.001	1.204	0.001
0.2	2.117	0.539	1.537	0.115	1.425	0.026	1.402	0.005	1.399	0.001
0.3	2.869	1.097	1.918	0.243	1.746	0.057	1.711	0.011	1.706	0.001
0.4	3.741	1.758	2.427	0.368	2.218	0.083	2.180	0.016	2.174	0.002
0.5	—	—	3.159	0.450	2.948	0.090	2.917	0.017	2.913	0.003

The robustness and the accuracy of the FFEM in modelling and analysing notch problems were tested via many numerical examples of cracked and notched plates. The numerical results of two-dimensional single symmetric/off-centre edge-cracked/edge-notched plates under tension conditions that the study generated are in very good agreement with existing published data or numerical solutions. However, the results for single off-centre edge-notched plates appear to be new results.

DOI: 10.1002/nme

REFERENCES

1. Seweryn A. Brittle fracture criterion for structures with sharp notches. *Engineering Fracture Mechanics* 1994; **47**:673–681.
2. Gross B, Mendelson A. Plane elastostatic analysis of V-notched plates. *International Journal of Fracture* 1972; **8**:267–276.
3. Williams ML. Stress singularities resulting from various boundary conditions in angular corners of plates in extension. *ASME Journal of Applied Mechanics* 1952; **19**:526–528.
4. Tong P, Pian THH. On the convergence of the FEM for problems with singularity. *International Journal of Solids and Structures* 1973; **9**:313–321.
5. Sinclair GB, Kondo M. On the stress concentration at sharp re-entrant corners in plates. *International Journal of Mechanical Sciences* 1984; **26**:477–487.
6. Sinclair GB, Okajima M, Griffin JH. Path independent integrals for computing stress intensity factors at sharp notches in elastic plates. *International Journal for Numerical Methods in Engineering* 1984; **20**:999–1008.
7. Stern M, Soni ML. On the computation of stress intensities at fixed-free corners. *International Journal of Solids and Structures* 1976; **12**:331–337.
8. Stern M, Becker EB, Dunham RS. A contour integral computation of mixed-mode stress intensity factors. *International Journal of Fracture* 1976; **12**:359–368.
9. Carpenter WC. Calculation of fracture parameters for a general corner. *International Journal of Fracture* 1984; **24**:45–58.
10. Carpenter WC. A collocation procedure for determining fracture mechanics parameters at a corner. *International Journal of Fracture* 1984; **24**:255–266.
11. Carpenter WC. Mode I and mode II stress intensities for plates with cracks of finite opening. *International Journal of Fracture* 1984; **26**:201–214.
12. Carpenter WC. The eigenvector solution for a general comer or finite opening crack with further studies on the collocation procedure. *International Journal of Fracture* 1985; **27**:63–74.
13. Lin KY, Tong P. Singular finite elements for the fracture analysis of V-notched plates. *International Journal for Numerical Methods in Engineering* 1980; **15**:1343–1354.
14. Portela A, Aliabadi MH, Rooke DP. Efficient boundary element analysis of sharp notched plates. *International Journal for Numerical Methods in Engineering* 1991; **32**:445–470.
15. Babuška I, Miller A. The post-processing approach in the finite element method—Part 1: calculation of displacements stresses and other higher derivatives of displacements. *International Journal for Numerical Methods in Engineering* 1984; **20**:1085–1109.
16. Babuška I, Miller A. The post-processing approach in the finite element method—Part 2: calculation of the stress intensity factors. *International Journal for Numerical Methods in Engineering* 1984; **20**:1111–1129.
17. Szabo A, Babuška I. Computation of the amplitude of stress singular terms for cracks and re-entrant corners. *Fracture Mechanics*, *Proceedings of the Nineteenth National Symposium*, San Antonio, TX, U.S.A., 30 June–2 July 1986. 1988; 101–124.
18. Leung AYT, Cheung YK. Dynamic analysis of frames by a two-level finite element method. *Journal of Sound and Vibration* 1981; **74**:1–9.
19. Mote CD. Global–local finite element. *International Journal for Numerical Methods in Engineering* 1971; **3**:565–574.
20. Leung AYT, Wong SC. Two-level finite element method for plates subjected to concentrated loads. *Microcomputer in Civil Engineering* 1988; **3**:126–127.
21. Leung AYT, Wong SC. Two-level finite element method for thin plate vibration subject to concentrated harmonic loads. *Journal of Sound and Vibration* 1992; **152**(1):95–105.
22. Leung AYT, Wong SC. Two-level finite element method for plane cracks. *Microcomputer Communications in Applied Numerical Methods* 1989; **5**:263–274.
23. Leung AYT, Su RKL. Mode I crack problems by fractal two level finite element method. *Engineering Fracture Mechanics* 1994; **48**(6):847–856.
24. Leung AYT, Su RKL. Mixed-mode two-dimensional crack problem by fractal two level finite element method. *Engineering Fracture Mechanics* 1995; **51**(6):889–895.
25. Leung AYT, Su RKL. Body-force linear elastic stress intensity factor calculation using fractal two level finite element method. *Engineering Fracture Mechanics* 1995; **51**(6):879–888.
26. Leung AYT, Su RKL. Fractal two-level finite element method for cracked Kirchhoff's plates using DKT elements. *Engineering Fracture Mechanics* 1996; **54**(5):703–711.

DOI: 10.1002/nme

27. Leung AYT, Su RKL. Fractal two-level finite element analysis of cracked Reissner's plate. *Thin-Walled Structures* 1996; **24**:315–334.
28. Leung AYT, Su RKL. Two-level finite element study of axisymmetric cracks. *International Journal of Fracture* 1998; **89**:193–203.
29. Leung AYT, Su RKL. Eigenfunction expansion for penny-shaped and circumferential cracks. *International Journal of Fracture* 1998; **89**:205–222.
30. Leung AYT, Tsang KL. Mode III two-dimensional crack problem by two-level finite element method. *International Journal of Fracture* 2000; **102**:245–258.
31. Vasilopoulos D. On the determination of higher order terms of singular elastic stress fields near corners. *Numerische Mathematik* 1988; **53**:51–95.
32. Aliabadi MH, Rooke DP. *Numerical Fracture Mechanics*. Kluwer Academic Publishers: Dordrecht, 1991.
33. Gregory RD. Green's functions, bi-linear forms, and completeness of the eigenfunctions for the elastostatic strip and wedge. *Journal of Elasticity* 1979; **9**:283–309.
34. Gray LJ, Paulino GH. Crack tip interpolation, revisited. *SIAM Journal on Applied Mathematics* 1998; **58**(2): 428–455.
35. Rösel R. On the wedge/notch eigenvalues. *International Journal of Fracture* 1987; **33**:61–71.
36. England AH. *Complex Variable Methods in Elasticity*. Wiley: New York, 1971.
37. Tada H, Paris PC, Irwin GR. *The Stress Analysis of Cracks Handbook* (3rd edn). ASME: New York, 2000.
38. Yang B, Ravi-Chandar K. Evaluation of elastic t-stress by the stress different method. *Engineering Fracture Mechanics* 1999; **64**:589–605.
39. ABAQUS, *ABAQUS Documentation*: *Version 6.5*. ABAQUS, Inc.: 2004.

DOI: 10.1002/nme

Chapter 6

Computations of Modes I and II Stress Intensity Factors of Sharp Notched Plates under In-plane Shear and Bending Loading by the Fractal-like Finite Element Method

International Journal of Solids and Structures 2008; 45:6468–6484

International Journal of Solids and Structures 45 (2008) 6468–6484

Contents lists available at ScienceDirect

International Journal of Solids and Structures

journal homepage: www.elsevier.com/locate/ijsolstr

Computations of modes I and II stress intensity factors of sharp notched plates under in-plane shear and bending loading by the fractal-like finite element method

Muhammad Treifi, S. Olutunde Oyadiji *, Derek K.L. Tsang

Dynamics and Aeroelasticity Research Group, School of Mechanical, Aerospace and Civil Engineering, University of Manchester, Sackville Street, Manchester M60 1QD, UK

ARTICLE INFO

Article history:
Received 27 February 2008
Received in revised form 14 July 2008
Available online 22 August 2008

Keywords:
Mode I and mode II stress intensity factors
Edge-cracked plate
Edge-notched plate
Notch
Finite element method
Fracture mechanics
Global interpolation functions

ABSTRACT

The fractal-like finite element method (FFEM) is used to compute the stress intensity factors (SIFs) for different configurations of cracked/notched plates subject to in-plane shear and bending loading conditions. In the FFEM, the large number of unknown variables in the singular region around a notch tip is reduced to a small set of generalised co-ordinates by performing a fractal transformation using global interpolation functions. The use of exact analytical solutions of the displacement field around a notch tip as the global interpolation functions reduces the computational cost significantly and neither post-processing technique to extract SIFs nor special singular elements to model the singular region are required. The results of numerical examples of various configurations of cracked/notched plates are presented and validated via published data. Also, new results for cracked/notched plate problems are presented. These results demonstrate the accuracy and efficiency of the FFEM to compute the SIFs for notch problems under in-plane shear and bending loading conditions.

1. Introduction

There are many cases in engineering design where it is necessary to compute the stress fields inside notched elastic bodies. The presence of notches affects the capacity of structural members to withstand loading and may result in crack initiation. Therefore, much research has been devoted to the analysis of sharp notches where stresses diverge and oscillate. However, most published data is about mode I (tension) cases. There are only few results concerning pure mode II and in-plane bending cases of notch problems.

The task of computing the so-called notch stress intensity factors (SIFs) is important and has relevance for strength calculations. Experimental findings have indicated that simple failure criteria based on critical notch SIFs exist, at least for brittle fracture (Seweryn, 1994). By means of a boundary collocation procedure which is based on the stress functions derived by Williams (1952), Gross and Mendelson (1972) computed the stress intensity factors for notch problems. They presented many cases of mode I and limited cases of mode II. Tong and Pian (1973) concluded that the interpolation functions of a finite element formulation must include terms that can account for the analytical form of a singularity in order to improve the convergence rate of finite element solutions of problems with singularities. In addition, these interpolation functions should be used for elements within a finite region, and not only for those around the singular point. Sinclair and Kondo (1984) and

* Corresponding author. Tel.: +44 161 2754348.
E-mail addresses: Muhammad.Treifi@postgrad.manchester.ac.uk (M. Treifi), s.o.oyadiji@manchester.ac.uk (S.O. Oyadiji), kwong-lai.tsang@manchester.ac.uk (D.K.L. Tsang).

0020-7683/$ - see front matter © 2008 Elsevier Ltd. All rights reserved.
doi:10.1016/j.ijsolstr.2008.08.013

Sinclair et al. (1984) proposed a generalised stress intensity concept at sharp corners and outlined an approach to obtain it based on the calculation of a contour integral. Their work was an extension of the work of Stern and Soni (1976) and Stern et al. (1976). Independently, Carpenter (1984a,b,c, 1985) also applied the contour integral of Stern and Soni (1976) and Stern et al. (1976) to compute fracture mechanics parameters and introduced a collocation approach to calculate stress intensity factors of notch problems.

The use of a special hybrid finite element was proposed by Lin and Tong (1980). Their results were limited to mode I cases. Similarly, a boundary element singularity subtraction technique was proposed by Portela et al. (1991). They used a technique to subtract the singularity and published results for mode I and mode II cases of symmetric and non-symmetric notch configurations. But their method requires extra boundary conditions that they referred to as "singularity conditions of the regularisation procedure." Babuška and Miller (1984a,b) and Szabo and Babuška (1988) also developed finite element techniques to extract stress intensity factors for mixed mode problems. They presented two approaches, namely: one approach which involves an "influence" function and another approach which is related to the energy principle of fracture mechanics. These techniques, which are post-processing procedures, are known as extraction techniques. Zhao and Hahn (1992) developed a method to determine the stress intensity factors of a notch problem from the stress intensity factors of a crack problem. They reported results for mode I and mode II cases.

The focus of this paper is on the use of the fractal-like finite element (FFEM) method for analysing notch problems involving mode II loading and in-plane bending. The method is a semi-analytical method, whose idea goes back to the work of Leung and Cheung (1981). Initially, they employed a two-level finite element technique for constructing a frame super-element in order to reduce the computational cost for solving dynamic problems of a large-scale frame. The idea was based on the concept of global–local interpolation functions introduced by Mote (1971). The concept was that while local interpolation functions (shape functions) of a finite element formulation reduce the infinite number of degrees of freedom of a continuum to a finite number of degrees of freedom related to the nodes of the continuous element, the global finite element interpolation functions can be used to reduce the number of nodal unknowns to a small number of unknowns, called generalised coordinates.

Leung and co-workers applied the method to model two-dimensional crack problems, thin plate vibration subject to concentrated harmonic loads (Leung and Wong, 1989, 1992), mode I crack problems (Leung and Su, 1994), mixed mode (Leung and Su, 1995a), body force crack problems (Leung and Su, 1995b), cracked Kirchhoff's plates (Leung and Su, 1996a), cracked Reissner's plates (Leung and Su, 1996b), axisymmetric cracks (Leung and Su, 1998a), penny-shaped and circumferential cracks (Leung and Su, 1998b), and mode III crack problems (Leung and Tsang, 2000). Xie et al. (2003) carried out a parametric study on the fractal finite element method for crack problems. It has been proven that the fractal-like finite element method gives very accurate results for many different crack problems. Recently Treifi et al. (2007, 2008) have extended the FFEM to

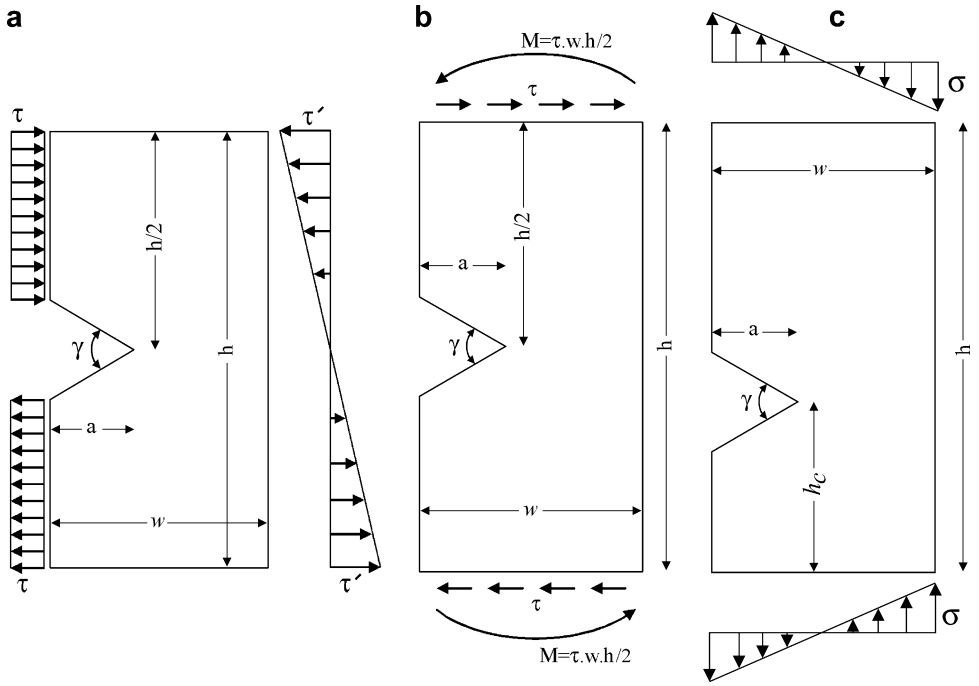

Fig. 1. Notched plates subject to mode II (a, b) and bending (c) load conditions.

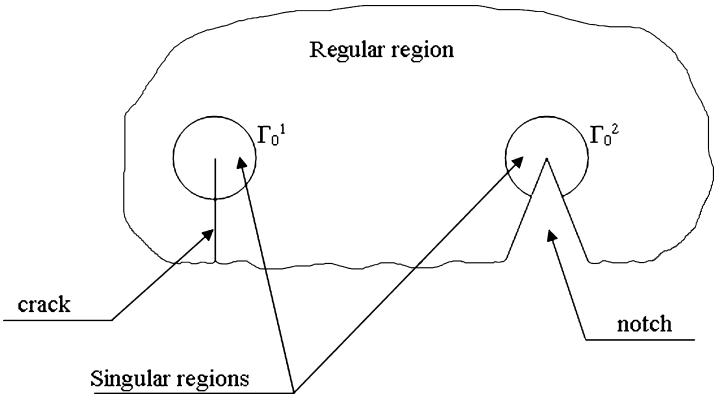

Fig. 2. Singular and regular regions of cracked/notched body.

model the singularity resulting at a notch tip. They presented results of symmetric and non-symmetric notched plates subjected to mode I loading conditions.

In this paper, we investigate the cases of edge-notched plates subjected to mode II loading conditions shown in Figs. 1(a) and (b) and in-plane bending shown in Fig. 1(c) by using the fractal-like finite element method. The singular stress field around the notch tip is represented by the Williams' eigenfunction series which is used as global interpolation functions to perform the fractal transformation. No special singular finite elements are required to model the stress singularity at the notch tip – any conventional finite elements can be used to model the singularity. Also, no post-processing is required to extract the stress intensity factors, because some of the unknown coefficients of the exact analytical solutions employed as the global interpolation functions are related to the SIFs. Various numerical examples concerning different notch configuration problems are presented to demonstrate the accuracy and efficiency of the FFEM to calculate mode I and mode II stress intensity factors of sharp notched plates.

2. Formulation of the fractal-Like finite element method (FFEM)

In the FFEM, a body containing singular points such as crack/notch tips is divided into singular and regular regions delineated by curves Γ_0^1 and Γ_0^2 as illustrated in Fig. 2. For the discretisation of the singular and regular regions, any conventional finite elements can be used. However, a very fine mesh is used within the singular regions. This mesh is generated layer by layer in a self-similar manner. The nodal displacements in the singular region are transformed into a small set of generalised co-ordinates, which are the unknowns in the singular region, by using global interpolation functions. In the regular region, the unknowns are the nodal displacements. The stress intensity factors for modes I and II are related to two coefficients of the generalised co-ordinate set; and therefore no post-processing is needed to extract them. Analytical solutions of the displacement field around a notch tip are used for performing the transformation.

The singular region is meshed as shown in Fig. 3. By assuming that ρ is a similarity ratio and using the notch tip as a centre of similarity, a set of curves $\{\Gamma_1,\Gamma_2,\Gamma_3,\ldots\}$, similar to the curve Γ_0, that separates the singular and regular regions, is generated within the singular region. The layer between the curves Γ_{n-1} and Γ_n is called the nth layer. All nodes on Γ_0 are considered master nodes, while the nodes inside Γ_0 are considered slave nodes as shown in Fig. 3.

In the conventional finite element method, the static equilibrium equation can be written as

$$\mathbf{K}\mathbf{d} = \mathbf{f} \tag{1}$$

where $\mathbf{K}$ is the stiffness matrix, $\mathbf{d}$ is the nodal displacement vector and $\mathbf{f}$ is the nodal force vector.

The equilibrium equation of the regular region can be written as

$$\begin{bmatrix} \mathbf{K}_{rr} & \mathbf{K}_{rm} \\ \mathbf{K}_{mr} & \mathbf{K}_{mm} \end{bmatrix} \begin{Bmatrix} \mathbf{d}_r \\ \mathbf{d}_m \end{Bmatrix} = \begin{Bmatrix} \mathbf{f}_r \\ \mathbf{f}_m \end{Bmatrix} \tag{2}$$

where $\mathbf{d}_r$ are the displacements of the nodes in the regular region, and $\mathbf{d}_m$ are the displacements of the master nodes. Similarly, the equilibrium equation of the first layer in the singular region can be written as

$$\begin{bmatrix} \mathbf{K}_{mm}^{1st} & \mathbf{K}_{ms}^{1st} \\ \mathbf{K}_{sm}^{1st} & \mathbf{K}_{ss}^{1st} \end{bmatrix} \begin{Bmatrix} \mathbf{d}_m \\ \mathbf{d}_s^{1st} \end{Bmatrix} = \begin{Bmatrix} \mathbf{f}_m^{1st} \\ \mathbf{f}_s^{1st} \end{Bmatrix} \tag{3}$$

where $\mathbf{d}_s^{1st}$ are the displacements of the slave nodes in the first layer which can be expressed in terms of the vector of the generalised co-ordinates $\mathbf{a}^T = \{A_1^I, A_1^{II}, A_2^I, A_2^{II}, A_3^I, \ldots\}$ as

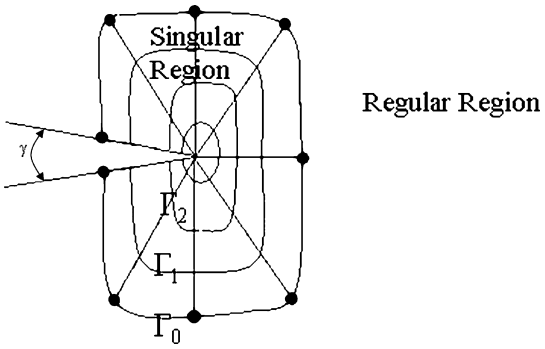

Fig. 3. Illustration of a singular region (master nodes are highlighted.)

$$\mathbf{d}_s^{1st} = \mathbf{T}_s^{1st}\mathbf{a} \tag{4}$$

where $\mathbf{T}_s^{1st}$ is the transformation matrix in terms of polar co-ordinates (r,θ) for transforming the nodal displacements of the slave nodes in the first layer into the generalised co-ordinates. Therefore, Eq. (3) can be rewritten as

$$\begin{bmatrix} \mathbf{K}_{mm}^{1st} & \mathbf{K}_{ms}^{1st}\mathbf{T}_s^{1st} \\ \mathbf{T}_s^{1st^T}\mathbf{K}_{sm}^{1st} & \mathbf{T}_s^{1st^T}\mathbf{K}_{ss}^{1st}\mathbf{T}_s^{1st} \end{bmatrix} \begin{Bmatrix} \mathbf{d}_m \\ \mathbf{a} \end{Bmatrix} = \begin{Bmatrix} \mathbf{f}_m^{1st} \\ \mathbf{T}_s^{1st^T}\mathbf{f}_s^{1st} \end{Bmatrix} \tag{5}$$

The displacements of the master nodes $\mathbf{d}_m$ are not transformed in order to provide continuity between the singular and the regular regions.

Now, for the nth layer in the singular region; $n > 1$

$$\mathbf{K}_s^n\mathbf{d}_s^n = \mathbf{f}_s^n \tag{6}$$

Applying the transformation, Eq. (6) can be rewritten as

$$\mathbf{T}_s^{n^T}\mathbf{K}_s^n\mathbf{T}_s^n\mathbf{a} = \mathbf{T}_s^{n^T}\mathbf{f}_s^n \tag{7}$$

The size of $\mathbf{T}_s^{1st}$ is smaller than that of $\mathbf{T}_s^n$, because $\mathbf{d}_m$ are not transformed.

Finally, the global stiffness equation can be written as

$$\begin{bmatrix} \mathbf{K}_{rr} & \mathbf{K}_{rm} & 0 \\ \mathbf{K}_{mr} & \mathbf{K}_{mm} + \mathbf{K}_{mm}^{1st} & \overline{\mathbf{K}}_{ms}^{1st} \\ 0 & \overline{\mathbf{K}}_{sm}^{1st} & \overline{\mathbf{K}}_{ss}^{1st} + \overline{\mathbf{K}}_s^{inn} \end{bmatrix} \begin{Bmatrix} \mathbf{d}_r \\ \mathbf{d}_m \\ \mathbf{a} \end{Bmatrix} = \begin{Bmatrix} \mathbf{f}_r \\ \mathbf{f}_m + \mathbf{f}_m^{1st} \\ \bar{\mathbf{f}}_s^{1st} + \bar{\mathbf{f}}_s^{inn} \end{Bmatrix} \tag{8}$$

where nl is the number of layers in the singular region, $\overline{\mathbf{K}}_{ms}^{1st} = \mathbf{K}_{ms}^{1st}\mathbf{T}_s^{1st}$, $\overline{\mathbf{K}}_s^{inn} = \sum_{n=2}^{nl}\overline{\mathbf{K}}_s^n$, $\overline{\mathbf{K}}_s^n = \mathbf{T}_s^{n^T}\mathbf{K}_s^n\mathbf{T}_s^n$, $\bar{\mathbf{f}}_s^{1st} = \mathbf{T}_s^{1st^T}\mathbf{f}_s^{1st}$, $\bar{\mathbf{f}}_s^{inn} = \sum_{n=2}^{nl}\bar{\mathbf{f}}_s^n$, and $\bar{\mathbf{f}}_s^n = \mathbf{T}_s^{n^T}\mathbf{f}_s^n$. $\overline{\mathbf{K}}_s^{inn}$ is the generalised stiffness matrix of the inner layers ($n \geqslant 2$) in the singular region:

$$\overline{\mathbf{K}}_s^{inn} = \sum_{n=2}^{nl}\overline{\mathbf{K}}_s^n = \sum_{n=2}^{nl}\mathbf{T}_s^{n^T}\mathbf{K}_s^n\mathbf{T}_s^n \tag{9}$$

The stiffness matrix of every layer in the singular region is the same because the stiffness matrices of the two-dimensional isoparametric finite elements of similar shapes are the same (Leung and Su, 1994). Therefore,

$$\mathbf{K}_s^n = \mathbf{K}_s^{1st} \tag{10}$$

The transformation matrix of the nth layer can be written in terms of that of the first layer as

$$\mathbf{T}_s^n = \mathbf{T}_s^f[\delta] \tag{11}$$

where $\mathbf{T}_s^f$ is the transformation matrix of the nodal displacements of all the nodes (slave and master) in the first layer and it is different from the aforementioned $\mathbf{T}_s^{1st}$, and $[\delta]$ is a diagonal matrix where

$$\delta_{ii} = \rho^{(n-1)\lambda_i}; \quad \lambda_i = \lambda_1^{\mathrm{I}}, \lambda_1^{\mathrm{II}}, \lambda_2^{\mathrm{I}}, \lambda_2^{\mathrm{II}}, \ldots \tag{12}$$

Substituting Eqs. (10)–(12) into Eq. (9) gives

$$\overline{\mathbf{K}}_s^{inn} = \sum_{n=2}^{nl}[\delta]^T\mathbf{T}_s^{f^T}\mathbf{K}_s^{1st}\mathbf{T}_s^f[\delta] = [\bar{\delta}_{ij}\bar{k}_{ij}] \tag{13}$$

where

$$[\bar{k}_{ij}] = \mathbf{T}_s^{f^{\mathrm{T}}} \mathbf{K}_s^{1\mathrm{st}} \mathbf{T}_s^f \tag{14}$$

and

$$\bar{\delta}_{ij} = \sum_{n=2}^{nl} \rho^{(n-1)\lambda_i} \rho^{(n-1)\lambda_j} = \sum_{n=2}^{nl} \rho^{(n-1)(\lambda_i+\lambda_j)} = \rho^{(\lambda_i+\lambda_j)} + \rho^{2(\lambda_i+\lambda_j)} + \cdots + \rho^{(nl-1)(\lambda_i+\lambda_j)} \tag{15}$$

This sum is a geometric series. For a finite number of layers, $\bar{\delta}_{ij}$ can be written as

$$\bar{\delta}_{ij} = \frac{\rho^{(\lambda_i+\lambda_j)}(1-\rho^{(nl-1)(\lambda_i+\lambda_j)})}{1-\rho^{(\lambda_i+\lambda_j)}} \tag{16}$$

and for an infinite number of layers ($nl \to \infty$) as

$$\bar{\delta}_{ij} = \frac{\rho^{(\lambda_i+\lambda_j)}}{1-\rho^{(\lambda_i+\lambda_j)}} \tag{17}$$

For a crack problem ($\gamma = 0$), Eq. (17) yields the same equation derived by Leung and Su (1995) for a crack problem. A similar procedure can be followed to compute the generalised force vector of the inner layers in the singular region $\bar{\mathbf{f}}_s^{\mathrm{inn}}$.

The unknowns of the problem now are the displacements $\mathbf{d}_r$ and $\mathbf{d}_m$ in the regular region and the generalised co-ordinates $\mathbf{a}$ instead of the nodal displacements of the nodes in the singular region. If we consider $\mathbf{d}_s$ as the vector of the nodal displacements of the nodes in the singular region except for those on Γ_0, the size of the vector $\mathbf{d}_s$ is much bigger than that of the vector of the generalised co-ordinates $\mathbf{a}$. Therefore, solving the system of Eqs. (8) reduces the computational cost considerably. For more details about the formulation of the FFEM, see Treifi et al. (2008) and Leung and Su (1994–1998).

3. Global interpolation functions for a notch problem

The global interpolation functions are very important in the FFEM, because they are employed to perform the fractal transformation. Therefore, exact analytical solutions of the displacement field around a notch tip are used as the global interpolation functions. Those analytical solutions can be derived by using an eigenfunction expansion approach (Williams, 1952) or a complex variable approach (England, 1971).

According to the Complex Variable Method, the stress and displacement expressions in a polar co-ordinate system centred at the tip of an infinite notch as illustrated in Fig. 4 can be written as

$$\begin{aligned} u_r = {} & \tfrac{r^{\lambda^{\mathrm{I}}}}{2G} A_1[(3-4\eta-\lambda^{\mathrm{I}})\cos(\lambda^{\mathrm{I}}-1)\theta + (\cos 2\lambda^{\mathrm{I}}\alpha + \lambda^{\mathrm{I}}\cos 2\alpha)\cos(\lambda^{\mathrm{I}}+1)\theta] \\ & + \tfrac{r^{\lambda^{\mathrm{II}}}}{2G} A_2[-(3-4\eta-\lambda^{\mathrm{II}})\sin(\lambda^{\mathrm{II}}-1)\theta + (\cos 2\lambda^{\mathrm{II}}\alpha - \lambda^{\mathrm{II}}\cos 2\alpha)\sin(\lambda^{\mathrm{II}}+1)\theta] \end{aligned} \tag{18}$$

$$\begin{aligned} u_\theta = {} & \tfrac{r^{\lambda^{\mathrm{I}}}}{2G} A_1[(3-4\eta+\lambda^{\mathrm{I}})\sin(\lambda^{\mathrm{I}}-1)\theta - (\cos 2\lambda^{\mathrm{I}}\alpha + \lambda^{\mathrm{I}}\cos 2\alpha)\sin(\lambda^{\mathrm{I}}+1)\theta] \\ & + \tfrac{r^{\lambda^{\mathrm{II}}}}{2G} A_2[(3-4\eta+\lambda^{\mathrm{II}})\cos(\lambda^{\mathrm{II}}-1)\theta + (\cos 2\lambda^{\mathrm{II}}\alpha - \lambda^{\mathrm{II}}\cos 2\alpha)\cos(\lambda^{\mathrm{II}}+1)\theta] \end{aligned} \tag{19}$$

$$\begin{aligned} \sigma_r = {} & r^{\lambda^{\mathrm{I}}-1}\lambda^{\mathrm{I}} A_1[-(\lambda^{\mathrm{I}}-3)\cos(\lambda^{\mathrm{I}}-1)\theta + (\cos 2\lambda^{\mathrm{I}}\alpha + \lambda^{\mathrm{I}}\cos 2\alpha)\cos(\lambda^{\mathrm{I}}+1)\theta] \\ & + r^{\lambda^{\mathrm{II}}-1}\lambda^{\mathrm{II}} A_2[(\lambda^{\mathrm{II}}-3)\sin(\lambda^{\mathrm{II}}-1)\theta + (\cos 2\lambda^{\mathrm{II}}\alpha - \lambda^{\mathrm{II}}\cos 2\alpha)\sin(\lambda^{\mathrm{II}}+1)\theta] \end{aligned} \tag{20}$$

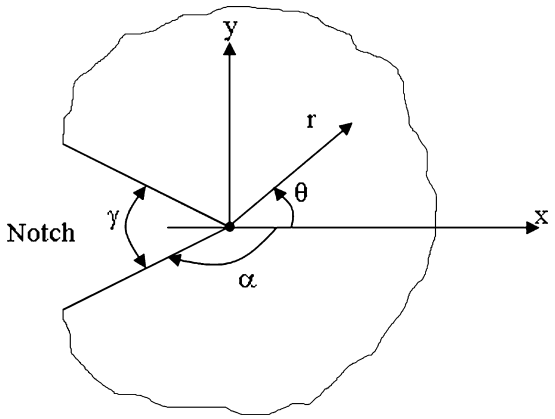

Fig. 4. Notch geometry and the co-ordinate systems.

Table 1
Dominant eigenvalues of different notch angles

γ (°)	λ_1^{I}	λ_1^{II}
0	0.5000000	0.5000000
10	0.5000530	0.5293547
20	0.5004264	0.5620065
30	0.5014530	0.5981919
40	0.5034904	0.6381825
50	0.5069329	0.6822948
60	0.5122214	0.7309008
70	0.5198543	0.7844406
80	0.5303957	0.8434395
90	0.5444837	0.9085292

$$\sigma_\theta = r^{\lambda^{\mathrm{I}}-1}\lambda^{\mathrm{I}}A_1[(\lambda^{\mathrm{I}}+1)\cos(\lambda^{\mathrm{I}}-1)\theta - (\cos 2\lambda^{\mathrm{I}}\alpha + \lambda^{\mathrm{I}}\cos 2\alpha)\cos(\lambda^{\mathrm{I}}+1)\theta] - r^{\lambda^{\mathrm{II}}-1}\lambda^{\mathrm{II}}A_2[(\lambda^{\mathrm{II}}+1)\sin(\lambda^{\mathrm{II}}-1)\theta + (\cos 2\lambda^{\mathrm{II}}\alpha - \lambda^{\mathrm{II}}\cos 2\alpha)\sin(\lambda^{\mathrm{II}}+1)\theta] \tag{21}$$

$$\sigma_{r\theta} = r^{\lambda^{\mathrm{I}}-1}\lambda^{\mathrm{I}}A_1[(\lambda^{\mathrm{I}}-1)\sin(\lambda^{\mathrm{I}}-1)\theta - (\cos 2\lambda^{\mathrm{I}}\alpha + \lambda^{\mathrm{I}}\cos 2\alpha)\sin(\lambda^{\mathrm{I}}+1)\theta] + r^{\lambda^{\mathrm{II}}-1}\lambda^{\mathrm{II}}A_2[(\lambda^{\mathrm{II}}-1)\cos(\lambda^{\mathrm{II}}-1)\theta + (\cos 2\lambda^{\mathrm{II}}\alpha - \lambda^{\mathrm{II}}\cos 2\alpha)\cos(\lambda^{\mathrm{II}}+1)\theta] \tag{22}$$

where G is the shear modulus, $\eta = \nu$ for plane strain, $\eta = \frac{\nu}{1+\nu}$ for plane stress, and ν is the Poisson's ratio. λ^{I} and λ^{II} are eigenvalues for mode I and mode II, respectively, and are calculated from the following characteristic equations:

$$\lambda^{\mathrm{I}}\sin 2\alpha + \sin 2\lambda^{\mathrm{I}}\alpha = 0 \tag{23}$$

$$\lambda^{\mathrm{II}}\sin 2\alpha - \sin 2\lambda^{\mathrm{II}}\alpha = 0 \tag{24}$$

The eigenvalues of mode I (λ^{I}) and mode II (λ^{II}) for a notch problem are different from each other except for the special case of a crack problem. Detailed derivations of the stress and displacement expressions around a notch tip can be found in references such as Vasilopoulos (1988).

Muller's iteration method can be used to find the roots of the characteristic equations (23) and (24) (Portela et al., 1991). Muller's method can converge to a complex root, even if the iteration has started with a real number. The dominant eigenvalues, which are the eigenvalues that satisfy the condition $0 < \mathrm{Re}(\lambda_1) < 1$, for different opening notch angles are tabulated in Table 1.

The stress intensity factors of a notch are defined in a way similar to those of a crack as

$$K_{\mathrm{I}} = \sqrt{2\pi}\lim_{r\to 0} r^{1-\lambda^{\mathrm{I}}}\sigma_\theta(\theta = 0) \tag{25}$$

$$K_{\mathrm{II}} = \sqrt{2\pi}\lim_{r\to 0} r^{1-\lambda^{\mathrm{II}}}\sigma_{r\theta}(\theta = 0) \tag{26}$$

for mode I and mode II, respectively (Gross and Mendelson, 1972).

Substituting Eqs. (21) and (22) into Eqs. (25) and (26) gives

$$K_{\mathrm{I}} = \sqrt{2\pi}\lambda^{\mathrm{I}}(1 + \lambda^{\mathrm{I}} - \lambda^{\mathrm{I}}\cos 2\alpha - \cos 2\lambda^{\mathrm{I}}\alpha)A_1 \tag{27}$$

$$K_{\mathrm{II}} = \sqrt{2\pi}\lambda^{\mathrm{II}}(-1 + \lambda^{\mathrm{II}} - \lambda^{\mathrm{II}}\cos 2\alpha + \cos 2\lambda^{\mathrm{II}}\alpha)A_2 \tag{28}$$

Eqs. (27) and (28) demonstrate direct relationships between the SIFs and the generalised co-ordinates. Therefore, no post-processing technique is required to extract the SIFs.

4. Numerical examples

4.1. Convergence study of mode II for a crack case

A convergence study is carried out to demonstrate the accuracy and stability of the FFEM to compute mode II SIFs. The effects of the number of layers in the singular region (for a range of 4–20 and when $nl = \infty$), the similarity ratio (for a range of 0.1–0.9), and the number of terms of the eigenfunction expansion series used as global interpolation functions (for a range of 5–30) on the mode II SIFs will be investigated.

A two-dimensional mode II plane-stress problem of a single edge-cracked plate as shown in Fig. 5(a) is analysed. The moments applied at the top and the bottom boundaries are to counter the moment caused by the shear stresses applied at the top and the bottom boundaries of the plate. These counter-moments can be modelled using one of the two cases shown in Figs. 5(b) and (c). The loading system shown in Fig. 5(b) is used in this convergence study. The aspect ratio and the ratio of the crack length to the plate width are $h/w = 2$ and $a/w = 0.4$, respectively. Six-node triangle elements (seven-point integration scheme) are used to mesh the plate as shown in Fig. 6. Also, the singular region volume is held constant with increasing numbers of layers.

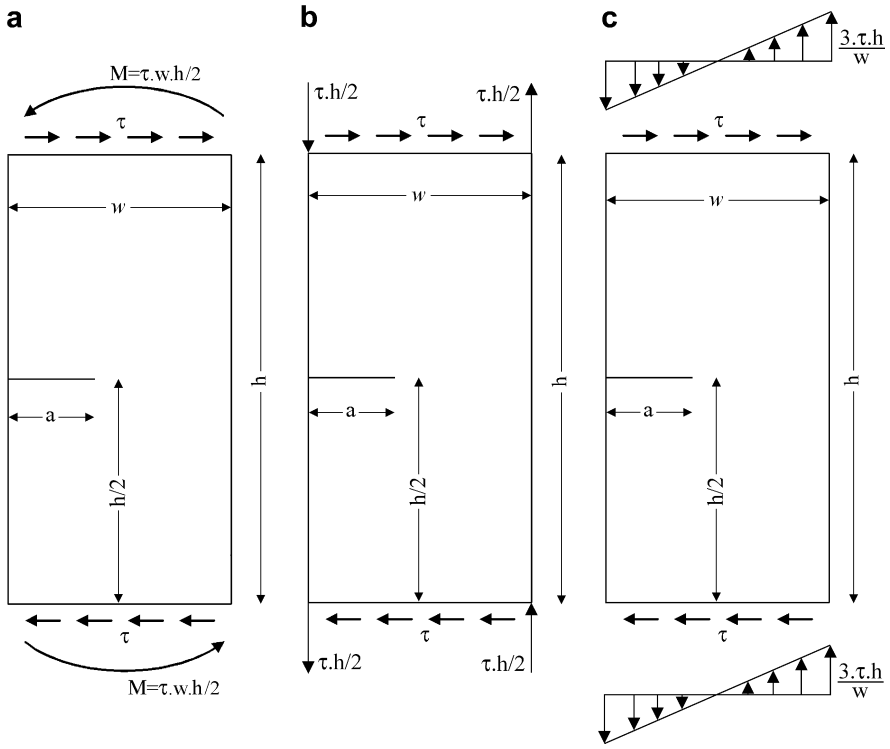

Fig. 5. Edge-cracked plate subject to mode II loading conditions.

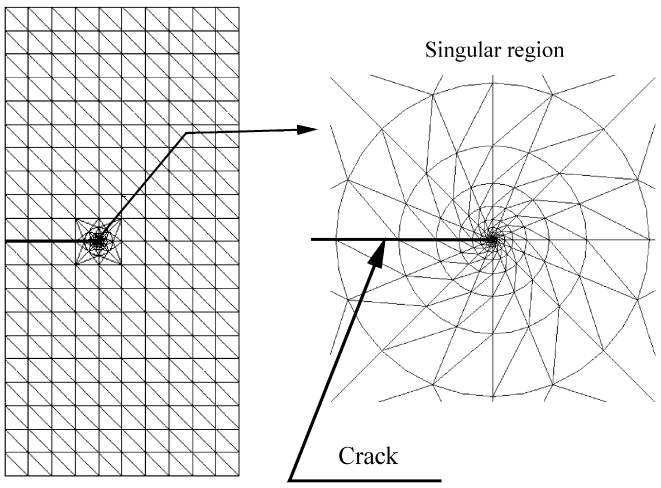

Fig. 6. FE mesh of the geometry of a single edge-cracked plate.

The results compared to those obtained by using the ABAQUS 6.5-4 finite element analysis (FEA) package are presented in Figs. 7–9. A similar mesh to that shown in Fig. 6 is used to model and analyse the cracked plate in ABAQUS. In addition, the elements around the crack tip are modelled using quarter-point crack tip elements (ABAQUS, 2004). Figs. 7 and 8 show that the number of transformation terms (NT) does not have a significant effect on the results when NT $\geqslant$ 5 for the ranges of variables (numbers of layers (NL), similarity ratios (ρ) and NT) used in this study.

Fig. 8 demonstrates that good results can be obtained by using values of similarity ratios larger than 0.5 for the ranges of variables used in this study. Also, it can be seen that when $nl \to \infty$, larger similarity ratios (finer meshes of the singular re-

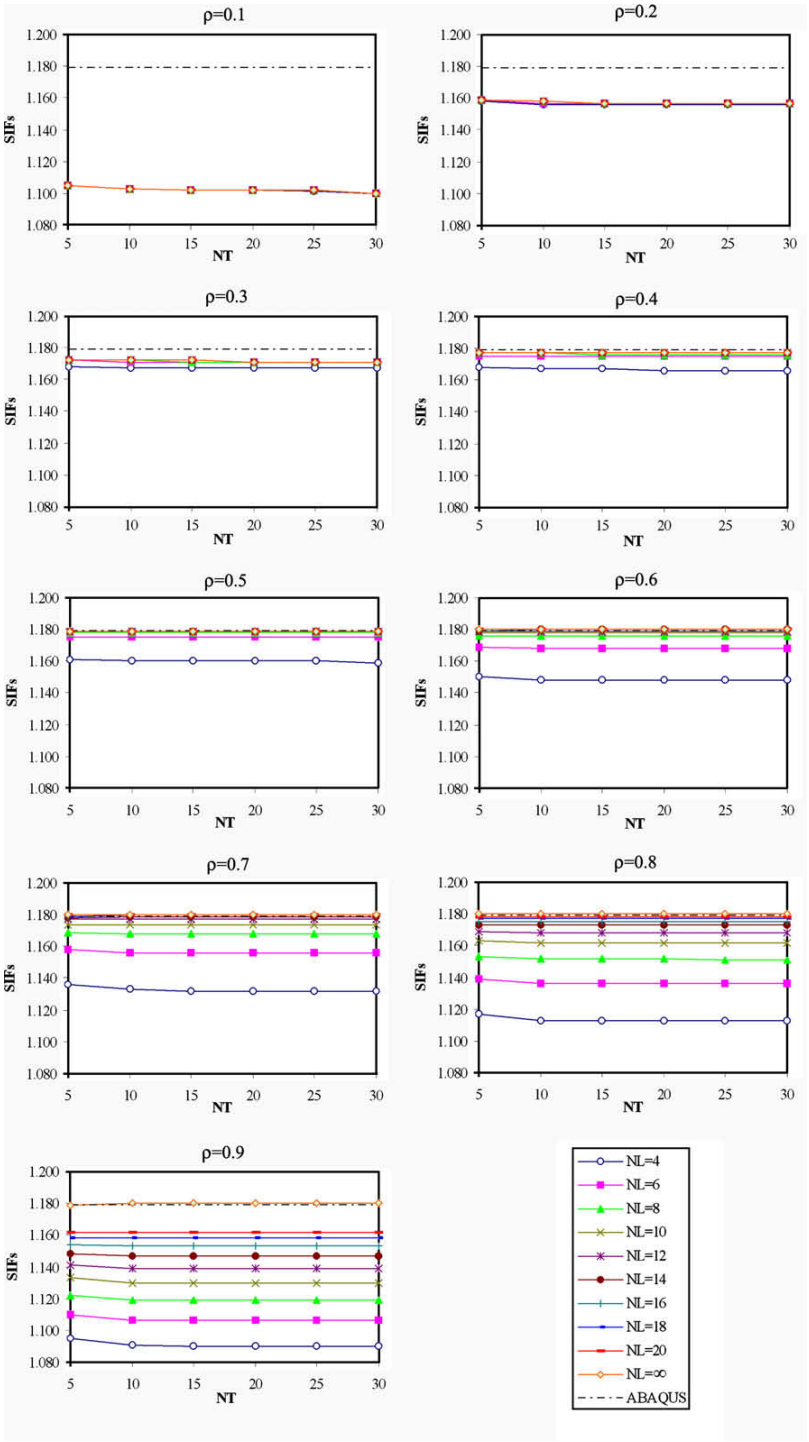

Fig. 7. Variations of SIFs with number of terms (NT) for different number of layers (NL) and similarity ratios ρ compared to those obtained by using ABAQUS.

gion) are needed to provide good results. Fig. 9 illustrates that the results converge asymptotically with increasing numbers of layers used to model the singular region when $\rho > 0.3$. Good results can be obtained by using ten layers or more. A similar behaviour was observed for the cases of mode I loading conditions (Treifi et al., 2008).

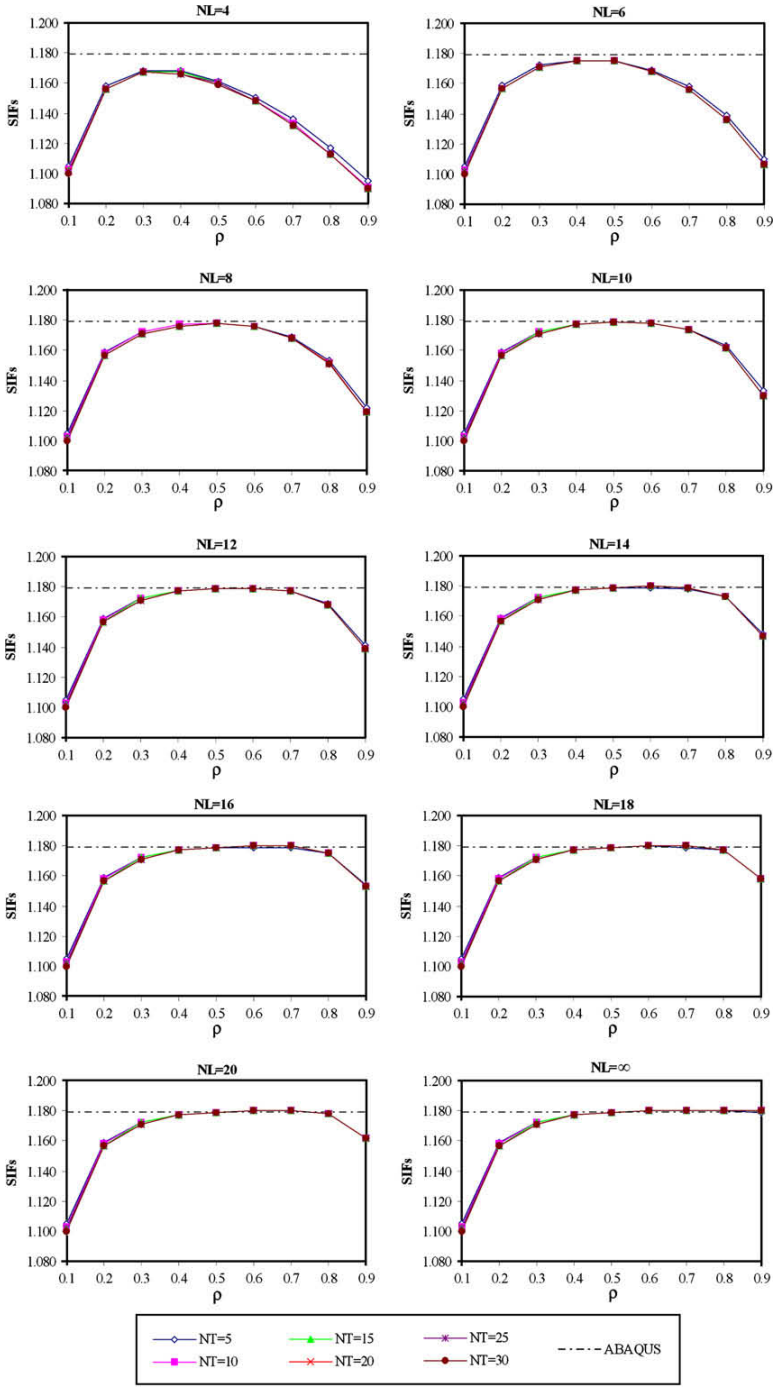

Fig. 8. Variations of SIFs with similarity ratio for different number of terms and numbers of layers compared to those obtained by using ABAQUS.

4.2. Examples of single edge-cracked plates subjected to mode II load conditions

Two-dimensional mode II plane-stress problems of a single edge-cracked plate are analysed for different crack lengths. The problem is shown in Fig. 5. Based on the convergence study, 16 layers are used to model the singular region and 10 terms of the eigenfunction series are used for the fractal transformation. The similarity ratio and the aspect ratio are $\rho = 0.6$, and $h/$

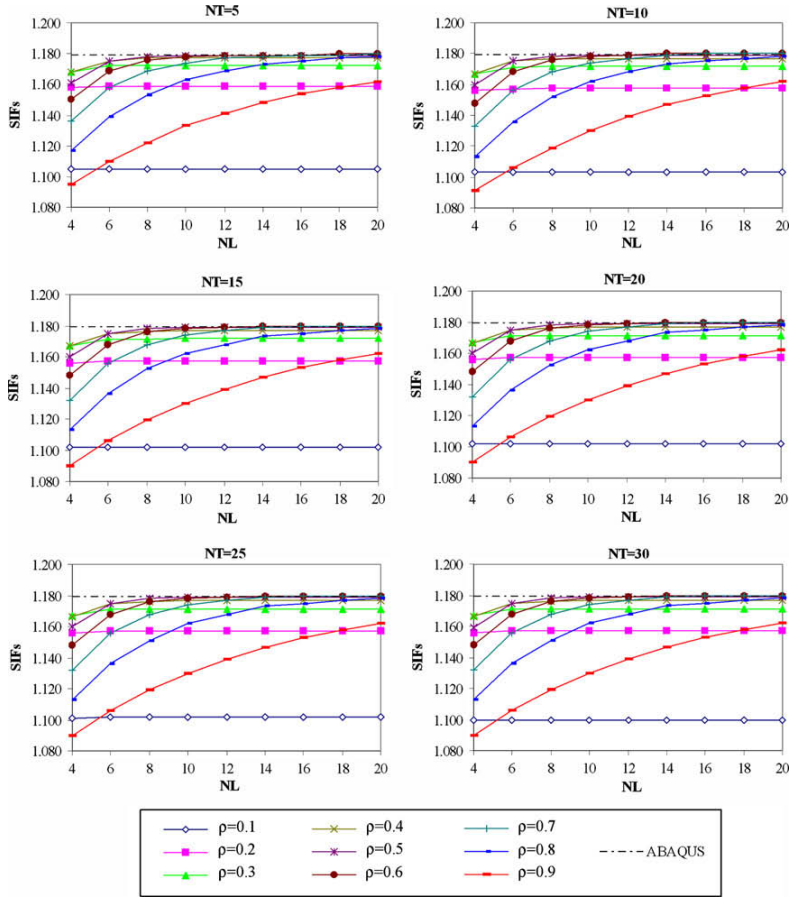

Fig. 9. Variations of SIFs with Number of layers for different similarity ratios and numbers of terms compared to those obtained by using ABAQUS.

$w = 2$, respectively. Six-node triangle elements (seven-point integration scheme) are used to mesh the geometry of the plate as shown in Fig. 6.

The stress intensity factors computed for the mode II problems illustrated in Figs. 5(b) and (c) by the FFEM compared to corresponding published data (Zhao and Hahn, 1991, 1992) and those computed by using ABAQUS (the counter-moments were modelled as in Fig. 5(b) and the mesh is similar to that shown in Fig. 6) are tabulated in Table 2 for different ratios of crack length to plate width.

Table 2
Mode II SIFs of an edge-cracked plate for different crack lengths

$\frac{a}{w}$	$K_{II}/\tau\sqrt{\pi}a^{1-\lambda_1^{II}}$				
	Zhao and Hahn (1991)	Zhao and Hahn (1992)	ABAQUS (Counter-moments modelled as in Fig. 5(b))	FFEM	
				Counter-moments modelled as in Fig. 5(b)	Counter-moments modelled as in Fig. 5(c)
0.1	–	–	0.376	0.376	0.376
0.2	–	0.441	0.695	0.696	0.694
0.3	–	0.830	0.960	0.960	0.958
0.4	1.166	1.150	1.179	1.180	1.179
0.5	–	1.394	1.369	1.370	1.371
0.6	–	1.581	1.549	1.550	1.552
0.7	–	1.771	1.752	1.753	1.754
0.8	–	–	2.053	2.054	2.054
0.9	–	–	2.738	2.740	2.739

Table 2 shows that the mode II SIF values increase with increasing ratios of crack length to plate width (a/w). More importantly, Table 2 illustrates that the SIF values computed by the FFEM are in very good agreement with those predicted by the ABAQUS FEA package and their accuracy is better than those calculated by Zhao and Hahn (1991, 1992). Therefore, the results in Table 2 prove that the eigenfunction expansion series presented in Section 3 which were derived for notch problems produce accurate results for mode II crack problems (when the notch opening angle $\gamma = 0°$).

4.3. Examples of single off-centre edge-cracked plates under mode II loading conditions

A single off-centre edge-cracked plate as illustrated in Fig. 10 is analysed in this section. The ratio of the crack length to the width of the plate is taken as $a/w = 0.4$. Ten terms of the eigenfunctions, 16 layers in the singular region, an aspect ratio $h/w = 2$, and a similarity ratio $\rho = 0.6$ are used. Six-node triangle elements (seven-point integration scheme) are used to mesh the geometries of the plates in a similar manner of that shown in Fig. 6.

The FFEM is used to compute the mode I and mode II SIF values using the parameters stated above for both cases of applying the counter-moments at the top and the bottom boundaries of the plate illustrated in Figs. 5(b) and (c). The results obtained are tabulated in Table 3. But it should be noted that these are new results and that there are no published data with which to compare them. Therefore, in order to validate the results, the ABAQUS 6.5-4 FEA package is used to model the cracked plates. A similar mesh to that shown in Fig. 6 is used. Moreover, the elements around the crack tip are modelled using quarter-point crack tip elements, and the counter-moments applied on the top and the bottom boundaries of the plate are modelled as in Fig. 5(b). It should be noted that although similar meshes (and therefore similar numbers of nodes) are used in the FFEM and ABAQUS, the number of equations that need to be solved in the FFEM is much smaller than that in ABAQUS, because of the transformation process described in Section 3.

The values of the stress intensity factors for mode I and mode II predicted by the ABAQUS FEA package are also tabulated in Table 3. Mode I occurs in this example because of the geometrical asymmetry of the plate configuration. It can be seen from Table 3 that the SIF values increase as the crack gets closer to the bottom boundary of the plate, and the minimum values occur when the crack is on the centre line. Also, the FFEM and the ABAQUS results are in very good agreement. It is however worth noting that the differences between the FFEM results are due to the differences in the methods of application of the counter-moments which produce different influences of the concentrated and linearly varying loads applied at the top and the bottom boundaries of the plates shown in Figs. 5(b) and (c).

4.4. Examples of single edge-notched plates subjected to mode II load conditions

Two-dimensional mode II plane-stress problems of single edge-notched plates shown in Figs. 1(a) and (b) are analysed for different notch angles. Sixteen layers are used to model the singular region, and 10 terms of the eigenfunction series are used

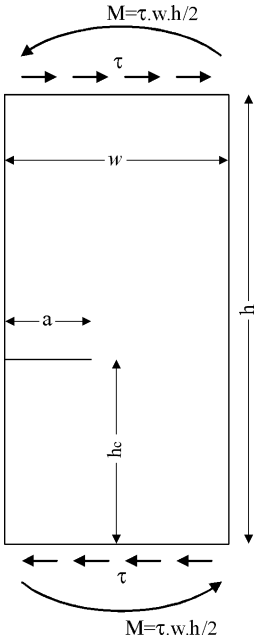

Fig. 10. Single off-centre edge-cracked plate subjected to mode II load conditions.

Table 3
Normalised SIFs for an off-centre edge-cracked plate for different crack positions

h_c/h	ABAQUS (Counter-moments modelled as in Fig. 5(b))		FFEM			
			Counter-moments modelled as in Fig. 5(b)		Counter-moments modelled as in Fig. 5(c)	
	K_I	K_{II}	K_I	K_{II}	K_I	K_{II}
0.1	10.459	5.563	10.458	5.565	11.021	5.033
0.2	4.978	1.924	4.978	1.925	5.238	1.853
0.3	3.062	1.305	3.062	1.305	3.121	1.292
0.4	1.512	1.193	1.512	1.194	1.520	1.191
0.5	0.001	1.179	0.000	1.180	0.000	1.179

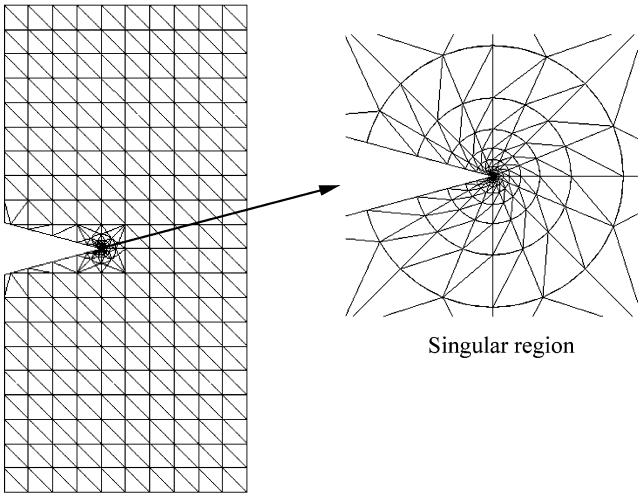

Fig. 11. FE mesh of the geometry of a single edge-notched plate.

Table 4
Mode II SIFs of a plate as shown in Fig. 1(a) for various notch angles compared with published results

γ (°)	$K_{II}/\tau\sqrt{\pi}a^{1-\lambda_1^{II}}$		
	Gross and Mendelson (1972)	Portela et al. (1991)[1]	FFEM
0	0.282	0.282	0.282
10	0.206	0.205	0.206
20	0.129	0.129	0.129
30	0.051	0.051	0.051

for the fractal transformation. The similarity ratio and the ratio of the notch length to the plate width are $\rho = 0.6$ and $a/w = 0.4$, respectively. Six-node triangle elements (seven-point integration scheme) are used to model the plate as shown in Fig. 11.

Firstly, a plate under mode II loading conditions as illustrated in Fig. 1(a) is considered. The SIFs computed by the FFEM for different notch angles and an aspect ratio $h/w = 0.8$ compared to published data (Gross and Mendelson, 1972; Portela et al., 1991[1]) are tabulated in Table 4.

Now a plate under mode II loading conditions as shown in Fig. 1(b) is analysed. The SIF values calculated by the FFEM for different notch angles and an aspect ratio $h/w = 2$ compared to the published results of Zhao and Hahn (1991, 1992) are presented in Table 5. Also, both ways of modelling the counter-moments as shown in Figs. 12(a) and (b) are investigated.

The results in Table 4 show that the SIF values computed by the FFEM are in very good agreement with those predicted by Gross and Mendelson (1972) and Portela et al. (1991). This again proves the accuracy of the FFEM for computing mode II SIFs. Table 5 demonstrates that there is a discrepancy of about 1% between the FFEM results and those reported by Zhao and Hahn

[1] It seems that there is a typographical error in Portela et al., 1991; in Table 3: $\frac{K_{II}}{t\sqrt{\pi}a^{1-\lambda_1}}$ should be $\frac{K_{II}}{ta^{1-\lambda_1}}$.

Table 5
Mode II SIFs of a plate as shown in Fig. 1(b) for various notch angles compared with published results

γ (°)	$K_{II}/\tau\sqrt{\pi}a^{1-\lambda_1^{II}}$			
	Zhao and Hahn (1992)	Zhao and Hahn (1991)	FFEM	
			Counter-moments modelled as couples (Fig. 12(a))	Counter-moments modelled as linearly varying loads (Fig. 12(b))
0	1.150	1.166	1.180	1.179
30	1.863	1.625	1.634	1.634
60	2.355	2.292	2.314	2.317
90	3.126	3.215	3.190	3.198

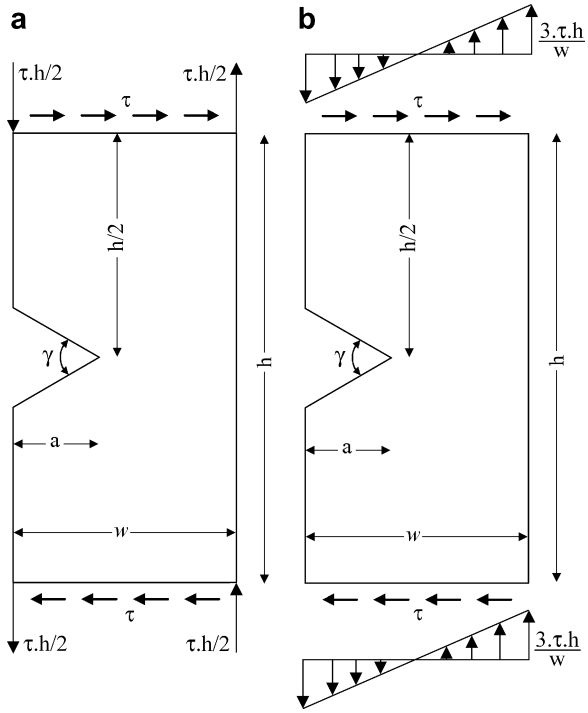

Fig. 12. Two ways of modelling the counter-moments of an edge-notched plate subject to mode II loading conditions.

(1991), but it is up to 14% compared to the results of Zhao and Hahn (1992). However, it was shown in a previous example on cracked plates that the accuracy of the FFEM results is better than that of the results of Zhao and Hahn (1991, 1992).

The results in Tables 4 and 5 for single edge-notched plates subject to mode II loading conditions ascertain that the use of the eigenfunction series presented in Section 3 as the global interpolation functions of the FFEM gives results which are in very good agreement with published data.

4.5. Examples of single off-centre edge-notched plates subjected to mode II load conditions

Fig. 13 illustrates a single off-centre edge-notched plate under mode II loading conditions. The number of terms of the eigenfunction series, the number of layers in the singular region, the similarity ratio, and the aspect ratio are $nt = 20$, $nl = 16$, $\rho = 0.6$, and $h/w = 2$, respectively. Six-node triangle elements (seven-point integration scheme) are used to model the notched plates as shown in Fig. 14. In order to obtain non-oscillatory SIFs when the notch opening angle is rather large, a circumferentially denser mesh is used to model the singular region.

The mode I and mode II SIFs for different notch positions are tabulated for different notch opening angles and for a ratio of the notch length to the plate width $a/w = 0.4$ in Tables 6(a) and 6(b) and for a notch opening angle $\gamma = 50°$ and for various ratios of the notch length to the plate width in Tables 7(a) and 7(b). In these tables, (a) and (b) indicate that the counter-moments are applied in the same ways shown in Figs. 12(a) and (b), respectively. Published SIF values appear to be unavailable for most of the cases analysed in this section.

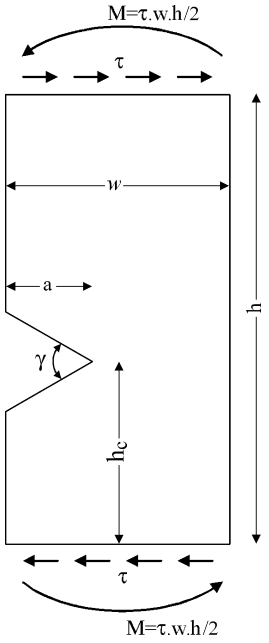

Fig. 13. Single off-centre edge-notched plate under mode II loading conditions.

The results in Tables 6(a), 6(b), 7(a) and 7(b) converged well as the density of the mesh in the singular region was increased in the circumferential direction. The SIF values in those tables that correspond to cases which were studied in previous sections and for which published data exist are respectively similar. Therefore, the results in Tables 6(a), 6(b), 7(a) and 7(b) are valid. The missing values in those tables are due to the fact that the geometry of the plate is no more rectangular (the top and bottom boundaries are no more equal).

Tables 6(a) and 6(b) show that the SIFs monotonically increase as the notch opening angle increases. Also, the values of the SIFs increase as the notch gets closer to the bottom boundary of the plate. The minimum values of the SIFs occur when the notch is on the centre line and the notch opening angle is 0°. From Tables 7(a) and 7(b), it can be seen that the SIFs for an edge-notched plate with a notch opening angle $\gamma = 50°$ increase as the notch length increases.

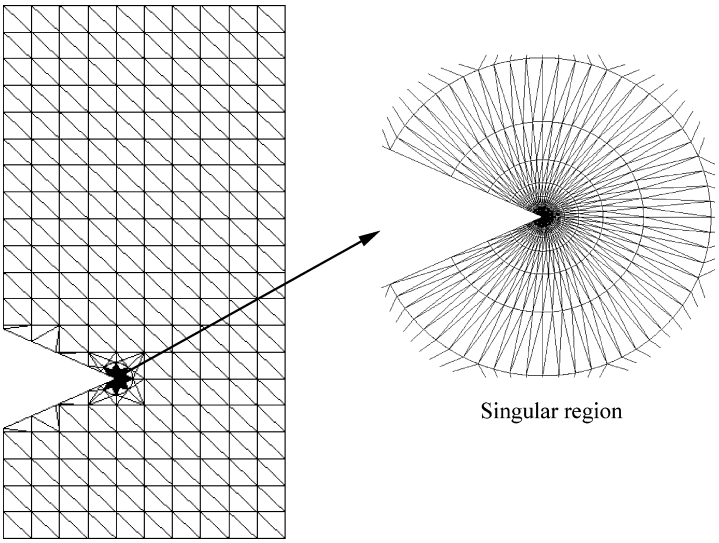

Fig. 14. FE mesh of the geometry of a single off-centre edge-notched plate.

Table 6(a)
Normalised SIFs of a single off-centre edge-notched plate subject to mode II load conditions (similar to that in Fig. 12(a)) for various notch positions and opening angles for $a/w = 0.4$

γ (°)	h_c/h									
	0.1		0.2		0.3		0.4		0.5	
	K_I	K_{II}	K_I	K_{II}	K_I	K_{II}	K_I	K_{II}	K_I	K_{II}
0	10.465	5.568	4.981	1.926	3.064	1.306	1.513	1.194	0.000	1.180
10	10.543	6.165	4.990	2.116	3.064	1.445	1.513	1.327	0.000	1.312
20	10.613	6.871	5.000	2.334	3.068	1.605	1.515	1.478	0.000	1.463
30	10.732	7.716	5.020	2.582	3.077	1.787	1.519	1.651	0.000	1.635
40	10.855	8.474	5.053	2.843	3.096	1.993	1.529	1.854	0.000	1.837
50	11.548	9.284	5.204	3.130	3.163	2.221	1.560	2.078	0.000	2.061
60	–	–	5.268	3.448	3.207	2.468	1.584	2.323	0.000	2.307
70	–	–	5.364	3.819	3.270	2.737	1.617	2.585	0.000	2.568
80	–	–	5.482	4.283	3.352	3.039	1.660	2.873	0.000	2.855
90	–	–	–	–	3.462	3.389	1.716	3.195	0.000	3.175

Table 6(b)
Normalised SIFs of a single off-centre edge-notched plate subject to mode II load conditions (similar to that in Fig. 12(b)) for various notch positions and opening angles for $a/w = 0.4$

γ (°)	h_c/h									
	0.1		0.2		0.3		0.4		0.5	
	K_I	K_{II}	K_I	K_{II}	K_I	K_{II}	K_I	K_{II}	K_I	K_{II}
0	11.029	5.035	5.241	1.854	3.123	1.293	1.521	1.192	0.000	1.180
10	11.085	5.603	5.247	2.056	3.123	1.436	1.521	1.325	0.000	1.311
20	11.143	6.275	5.256	2.289	3.127	1.602	1.523	1.478	0.000	1.462
30	11.242	7.076	5.277	2.558	3.138	1.791	1.528	1.652	0.000	1.635
40	11.364	7.860	5.315	2.862	3.159	2.012	1.538	1.857	0.000	1.837
50	12.000	8.715	5.468	3.203	3.229	2.258	1.570	2.085	0.000	2.063
60	–	–	5.547	3.584	3.278	2.529	1.595	2.335	0.000	2.309
70	–	–	5.660	4.015	3.348	2.823	1.629	2.602	0.000	2.572
80	–	–	5.799	4.534	3.437	3.155	1.673	2.897	0.000	2.860
90	–	–	–	–	3.552	3.540	1.731	3.229	0.000	3.183

Table 7(a)
Normalised SIFs of a single off-centre edge-notched plate subject to mode II load conditions (similar to that in Fig. 12(a)) for various notch positions and notch lengths for a notch opening angle $\gamma = 50°$

a/w	h_c/h									
	0.1		0.2		0.3		0.4		0.5	
	K_I	K_{II}	K_I	K_{II}	K_I	K_{II}	K_I	K_{II}	K_I	K_{II}
0.1	10.010	4.534	4.630	1.419	2.674	0.844	1.289	0.735	0.000	0.720
0.2	10.147	6.463	4.644	2.283	2.714	1.449	1.313	1.282	0.000	1.258
0.3	10.730	7.982	4.795	2.794	2.857	1.892	1.396	1.721	0.000	1.698
0.4	11.548	9.284	5.204	3.130	3.163	2.221	1.560	2.078	0.000	2.061
0.5	–	–	5.981	3.373	3.729	2.501	1.852	2.397	0.000	2.388

Table 7(b)
Normalised SIFs of a single off-centre edge-notched plate subject to mode II load conditions (similar to that in Fig. 12(b)) for various notch positions and notch lengths for a notch opening angle $\gamma = 50°$

a/w	h_c/h									
	0.1		0.2		0.3		0.4		0.5	
	K_I	K_{II}	K_I	K_{II}	K_I	K_{II}	K_I	K_{II}	K_I	K_{II}
0.1	6.012	1.153	3.906	0.722	2.556	0.712	1.276	0.718	0.000	0.719
0.2	8.062	3.405	4.310	1.554	2.651	1.292	1.304	1.257	0.000	1.255
0.3	10.099	6.060	4.840	2.432	2.873	1.815	1.397	1.707	0.000	1.695
0.4	12.000	8.715	5.468	3.203	3.229	2.258	1.570	2.085	0.000	2.063
0.5	–	–	6.302	3.760	3.801	2.617	1.863	2.419	0.000	2.392

Table 8
Normalised SIFs of a single off-centre edge-notched plate subject to bending load conditions for various notch positions and opening angles for $a/w = 0.4$

γ (°)	h_c/h									
	0.1		0.2		0.3		0.4		0.5	
	K_I	K_{II}	K_I	K_{II}	K_I	K_{II}	K_I	K_{II}	K_I	K_{II}
0	2.244	0.761	1.429	0.169	1.290	0.039	1.263	0.008	1.260	0.001
10	2.253	0.844	1.429	0.185	1.290	0.043	1.263	0.008	1.260	0.000
20	2.263	0.943	1.431	0.203	1.291	0.047	1.265	0.009	1.261	0.001
30	2.280	1.062	1.435	0.225	1.295	0.051	1.269	0.010	1.265	0.001
40	2.301	1.170	1.444	0.246	1.303	0.056	1.277	0.011	1.273	0.001
50	2.422	1.287	1.482	0.270	1.331	0.061	1.303	0.012	1.299	0.001
60	–	–	1.502	0.297	1.350	0.067	1.323	0.013	1.319	0.002
70	–	–	1.530	0.331	1.378	0.073	1.351	0.015	1.347	0.002
80	–	–	1.565	0.377	1.414	0.083	1.388	0.017	1.384	0.002
90	–	–	–	–	1.460	0.097	1.435	0.020	1.432	0.004

Table 9
Normalised SIFs of a single off-centre edge-notched plate subject to bending load conditions for various notch positions and notch lengths for a notch opening angle $\gamma = 50°$

a/w	h_c/h									
	0.1		0.2		0.3		0.4		0.5	
	K_I	K_{II}	K_I	K_{II}	K_I	K_{II}	K_I	K_{II}	K_I	K_{II}
0.1	1.321	0.128	1.111	0.022	1.074	0.005	1.067	0.001	1.066	0.000
0.2	1.696	0.463	1.201	0.098	1.106	0.022	1.087	0.005	1.084	0.001
0.3	2.070	0.874	1.325	0.192	1.189	0.045	1.162	0.009	1.158	0.001
0.4	2.422	1.287	1.482	0.270	1.331	0.061	1.303	0.012	1.299	0.001
0.5	–	–	1.708	0.306	1.568	0.063	1.547	0.012	1.544	0.002

Table 10
SIFs of a single edge-notched plate subject to bending load conditions for various notch angles compared with published results ($a/w = 0.4$, $h/w = 2$)

γ (°)	$K_I/\sigma\sqrt{\pi}a^{1-\lambda_1}$			
	Zhao and Hahn (1992)	Gross and Mendelson (1972)	Chen (1995)	FFEM
0	1.258	1.261	–	1.260
10	–	1.261	–	1.260
20	–	1.263	–	1.261
30	1.262	1.267	1.266	1.265
60	1.327	1.309	1.309	1.319
90	1.484	1.437	1.433	1.432

4.6. Examples of single edge-notched plates subjected to bending load conditions

A single edge-notched plate under bending loading conditions as illustrated in Fig. 1(c) is analysed for different opening notch angles and different notch positions. The parameters used in this examples are $nt = 20$, $nl = 16$, $\rho = 0.6$, and $h/w = 2$. Six-node triangle elements (seven-point integration scheme) are used to model the notched plates as shown in Fig. 14.

The mode I and mode II SIFs for different notch positions are tabulated for different notch opening angles and for a ratio of the notch length to the plate width $a/w = 0.4$ in Table 8 and for a notch opening angle $\gamma = 50°$ and for various ratios of the notch length to the plate width in Table 9. Most of the cases studied in this section appear to be new. However, there are few published results that correspond to cases in Tables 8 and 9. Those cases are tabulated in Table 10 for comparison. The FFEM results in Table 10 are in very good agreement with the published data. Therefore, the results tabulated in Tables 8 and 9 are valid.

The SIFs in Tables 8 and 9 increase monotonically with increasing notch opening angles and increasing notch lengths. Also, the SIF values increase as the notch gets closer to the top or bottom boundaries of the plate.

5. Conclusions

In this paper, the fractal-like finite element method was used to model and analyse notched plates subject to in-plane shear and bending loading conditions. The FFEM utilises the fractal transformation concept to reduce significantly the large

number of unknowns in the singular region. The transformation is performed by using global interpolation functions. Neither post-processing technique to extract the stress intensity factors nor special singular finite elements to model the singular the region are required.

The SIFs of many examples of edge-notched plates under in-plane shear and bending loading conditions were computed by using the FFEM. The results were in very good agreement with published data, and their accuracy was better than some of those reported results. Moreover, the results for single off-centre edge-notched plates appear to be new results.

References

ABAQUS, 2004. ABAQUS Documentation: Version 6.5, ABAQUS, Inc.

Babuška, I., Miller, A., 1984a. The post-processing approach in the finite element method-Part 1: Calculation of displacements stresses and other higher derivatives of displacements. International Journal for Numerical Methods in Engineering 20, 1085–1109.

Babuška, I., Miller, A., 1984b. The post-processing approach in the finite element method-Part 2 Calculation of the stress intensity factors. International Journal for Numerical Methods in Engineering 20, 1111–1129.

Carpenter, W.C., 1984a. Calculation of fracture parameters for a general corner. International journal of Fracture 24, 45–58.

Carpenter, W.C., 1984b. A collocation procedure for determining fracture mechanics parameters at a corner. International Journal of Fracture 24, 255–266.

Carpenter, W.C., 1984c. Mode I and mode II stress intensities for plates with cracks of finite opening. International Journal of Fracture 26, 201–214.

Carpenter, W.C., 1985. The eigenvector solution for a general comer or finite opening crack with further studies on the collocation procedure. International Journal of Fracture 27, 63–74.

Chen, D-H., 1995. Stress intensity factors for V-notched strip under tension or in-plane bending. International Journal of Fracture 70, 81–97.

England, A.H., 1971. Complex Variable Methods in Elasticity. John Wiley & Sons Ltd..

Gross, B., Mendelson, A., 1972. Plane elastostatic analysis of V-notched plates. International Journal of Fracture 8, 267–276.

Leung, A.Y.T., Su, R.K.L., 1994. Mode I crack problems by fractal two level finite element method. Engineering Fracture Mechanics 48 (6), 847–856.

Leung, A.Y.T., Su, R.K.L., 1995a. Mixed-mode two-dimensional crack problem by fractal two level finite element method. Engineering Fracture Mechanics 51 (6), 889–895.

Leung, A.Y.T., Su, R.K.L., 1995b. Body-force linear elastic stress intensity factor calculation using fractal two level finite element method. Engineering Fracture Mechanics 51 (6), 879–888.

Leung, A.Y.T., Su, R.K.L., 1996a. Fractal two-level finite element method for cracked Kirchhoff's plates using DKT elements. Engineering Fracture Mechanics 54 (5), 703–711.

Leung, A.Y.T., Su, R.K.L., 1996b. Fractal two-level finite element analysis of cracked Reissner's plate. Thin-Walled Structures 24, 315–334.

Leung, A.Y.T., Su, R.K.L., 1998a. Two-level finite element study of axisymmetric cracks. International Journal of Fracture 89, 193–203.

Leung, A.Y.T., Su, R.K.L., 1998b. Eigenfunction expansion for penny-shaped and circumferential cracks. International Journal of Fracture 89, 205–222.

Leung, A.Y.T., Tsang, K.L., 2000. Mode III two-dimensional crack problem by two-level finite element method. International Journal of Fracture 102, 245–258.

Leung, A.Y.T., Cheung, Y.K., 1981. Dynamic analysis of frames by a two-level finite element method. Journal of Sound and Vibration 74, 1–9.

Leung, A.Y.T., Wong, S.C., 1989. Two-level finite element method for plane cracks. Microcomputer Communications in Applied Numerical Methods 5, 263–274.

Leung, A.Y.T., Wong, S.C., 1992. Two-level finite element method for thin plate vibration subject to concentrated harmonic loads. Journal of Sound and Vibration 152 (1), 95–105.

Lin, K.Y., Tong, P., 1980. Singular finite elements for the fracture analysis of V-notched plates. International Journal for Numerical Methods in Engineering 15, 1343–1354.

Mote, C.D., 1971. Global–local finite element. International Journal for Numerical Methods in Engineering 3, 565–574.

Portela, A., Aliabadi, M.H., Rooke, D.P., 1991. Efficient boundary element analysis of sharp notched plates. International Journal for Numerical Methods in Engineering 32, 445–470.

Seweryn, A., 1994. Brittle fracture criterion for structures with sharp notches. Engineering Fracture Mechanics 47, 673–681.

Sinclair, G.B., Kondo, M., 1984. On the stress concentration at sharp re-entrant corners in plates. International Journal of Mechanical Sciences 26, 477–487.

Sinclair, G.B., Okajima, M., Griffin, J.H., 1984. Path independent integrals for computing stress intensity factors at sharp notches in elastic plates. International Journal for Numerical Methods in Engineering 20, 999–1008.

Stern, M., Soni, M.L., 1976. On the computation of stress intensities at fixed-free corners. International Journal of Solids and Structures 12, 331–337.

Stern, M., Becker, E.B., Dunham, R.S., 1976. A contour integral computation of mixed-mode stress intensity factors. International Journal of Fracture 12, 359–368.

Szabo, A., Babuška, I., 1988. Computation of the amplitude of stress singular terms for cracks and re-entrant corners, Fracture mechanics. In: Proceedings of the Nineteenth National Symposium, 30 June-2 July 1986, San Antonio, TX, United States, pp. 101–124.

Tong, P., Pian, T.H.H., 1973. On the convergence of the FEM for problems with singularity. International Journal of Solids and Structures 9, 313–321.

Treifi, M., Oyadiji, S.O., Tsang, D.K.L., 2008. Computation of the stress intensity factors of sharp notched plates by the fractal-like finite element method. International Journal for Numerical Methods in Engineering. doi:10.1002/nme.2425.

Treifi, M., Tsang, D.K.L., Oyadiji, S.O., 2007. Applications of the fractal-like finite element method to sharp notched plates. In: Proceedings of the ASME 2007 International Design Engineering Technical Conferences & Computers and Information in Engineering Conference IDETC/CIE 2007. Las Vegas, Nevada, USA.

Vasilopoulos, D., 1988. On the determination of higher order terms of singular elastic stress fields near corners. Numerische Mathematik 53, 51–95.

Williams, M.L., 1952. Stress singularities resulting from various boundary conditions in angular corners of plates in extension. ASME Journal of Applied Mechanics 19, 526–528.

Xie, J.F., Fok, S.L., Leung, A.Y.T., 2003. A parametric study on the fractal finite element method for two-dimensional crack problems. International Journal for Numerical Methods in Engineering 58, 631–642.

Zhao, Z., Hahn, H.G., 1991. A path independent integral for computing stress intensities of V-notched cracks and mixed-mode problems. International Conference on Mixed-Mode Fracture and Fatigue. Vienna, Austria.

Zhao, Z., Hahn, H.G., 1992. Determining the SIF of a v-notch from the results of a mixed-mode crack. Engineering Fracture Mechanics 43 (4), 511–518.

Chapter 7

Computations of SIFs for Non-symmetric V-notched Plates by the FFEM

Proceedings of the ASME 2009 International Design Engineering Technical Conferences & Computers and Information in Engineering Conference IDETC/CIE 2009 August 30 - September 2, 2009, San Diego, CA, USA; 3:711–717

Proceedings of the ASME 2009 International Design Engineering Technical Conferences & Computers and Information in Engineering Conference
IDETC/CIE 2009
August 30 - September 2, 2009, San Diego, CA, USA

DETC2009-86585

COMPUTATIONS OF SIFS FOR NON-SYMMETRIC V-NOTCHED PLATES BY THE FFEM

Muhammad Treifi **S Olutunde Oyadiji**

Dynamics and Aeroelasticity Research Group, School of Mechanical, Aerospace and Civil Engineering, University of Manchester, Manchester M60 1QD, U.K.

ABSTRACT

The present paper further develops The Fractal-like Finite Element Method (FFEM) to compute the stress intensity factors (SIFs) for non-symmetrical configurations of sharp V-notched plates. The use of global interpolation functions (GIFs) in the FFEM significantly reduces the number of unknown variables (nodal displacements) in a singular region surrounding a singular point to a small set of generalised coordinates. The same exact analytical solutions of the notch tip asymptotic field derived for a symmetrical notch case can be used as GIFs when the notch is non-symmetrical. However, appropriate local coordinate transformation in the singular region is required to obtain the correct global stiffness matrix. Neither post-processing technique to extract SIFs nor special singular elements to model the singular region are required. Any conventional finite elements can be used to model the singular region. The SIFs are directly computed because of the use of exact analytical solutions as GIFs whose coefficients (generalised coordinates) are the unknowns in the singular region. To demonstrate the accuracy and efficiency of the FFEM to compute the SIFs and model the singularity at a notch tip of non-symmetrical configurations of notched plates, various numerical examples are presented and results are validated via available published data.

KEYWORDS:

notch, stress intensity factors, fracture mechanics, finite element method, fractal-like finite element method.

1 INTRODUCTION

In two-dimensional elasticity, stresses near sharp notches or corners exhibit singular behaviour. Sharp notches/corners are stress raisers of major interest. Their presence in engineering components significantly influences the capacity of those components and may result in a crack initiation leading to a catastrophic failure or to a shortening of the service life. Therefore, much research has been devoted to investigate notch problems. Failure criteria for notch problems based on notch stress intensity factors exist, at least for brittle fracture [1]. Similar to crack problems, the failure occurs when the notch stress intensity factors reach critical values.

Many procedures have been developed to calculate the notch SIFs and to model the singularity resulting at a notch tip. Gross and Mendelson [2] used a Boundary Collocation Approach based on the stress functions derived by Williams [3] to compute mode I and mode II SIFs of many notch cases. It has been well recognised that the Finite Element Method has slow convergence rate when dealing with problems involving stress singularities. Tong and Pian [4] concluded that in order to improve the convergence of a finite element solution of a problem with a singularity, the finite element interpolation functions must include terms that can account for the analytical form of the singularity. These functions should also be used for elements within a finite region around the singular point. Special hybrid finite elements were developed by Lin and Tong [5] to account for the notch tip singularities. Carpenter [6,7] introduced a collocation procedure based on the contour integral of Stern [8] to compute the notch stress

intensity factors. A boundary element singularity subtraction technique to compute the SIFs for notch problems was proposed by Portela et al. [9]. Chen [10] computed the notch SIFs of notched plates under tension or in-plane bending by means of the body force method.

The Fractal-like Finite Element Method is semi-analytical. It brings together the agility of the Finite Element Method and the accuracy of the analytical solutions. The method is based on the global-local interpolation functions introduced by Mote [11]. The FFEM was applied to compute the SIFs for crack problems by Leung and co-workers [12-14]. Treifi et al. [15,16] further extended the method to compute the SIFs for symmetrical notch problems. In general, notches are not always symmetrical. Therefore, extending the method to compute the SIFs for non-symmetrical notch problems is in order.

In this paper, the FFEM is extended to compute the SIFs for non-symmetrical notch problems. The exact solutions of the singular displacement field around a notch tip used as global interpolation functions for a symmetrical notch can be used for a non-symmetrical notch. Only simple local coordinate transformation is needed in the singular region, so that the local x-axis lies on the bisector of the notch opening angle. Various numerical examples of non-symmetrically notched plates are presented, and results are validated via comparison with available published results to demonstrate the accuracy and efficiency of the FFEM.

2 GLOBAL INTERPOLATION FUNCTIONS

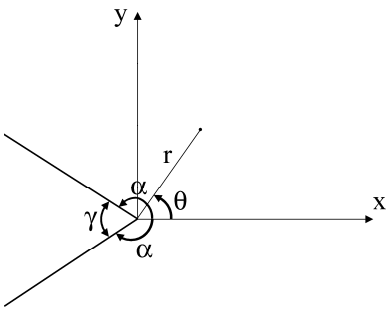

Figure 1. Coordinate systems centred at the notch tip

The exact analytical solutions of the displacement field around a notch tip are used as global interpolation functions to perform the transformation of the local variable (nodal displacements) in the singular region into a small set of generalised coordinates. Those generalised coordinates are the coefficients of the notch tip asymptotic field, which represent the SIFs, the T-stress, and the higher order coefficients. The generalised coordinates are computed directly in the FFEM. Therefore, no post-processing technique is necessary to extract the SIFs. The stress and displacement expressions around a notch tip can be derived by using a stress function approach or a complex variable method. Both approaches lead to equivalent expressions. For the sake of completeness, only a short description of the analytical solutions of the stress and displacement fields around a notch tip is presented here. Detailed derivations may be found in references such as Vasilopoulos [17] and Treifi et al. [15].

By using a complex variable method, the notch-tip stress and displacement expressions in a local polar coordinate system, centred at the notch tip and that the $\theta = 0$ axis is the bisector of the notch opening angle γ coincides with the local Cartesian x axis, derived for a semi-infinite notch as illustrated in Figure 1 can be written as

$$u_r = \frac{r^{\lambda^I}}{2G} A_1 \begin{bmatrix} \left(3-4\eta-\lambda^I\right)\cos\left(\lambda^I-1\right)\theta + \\ \left(\cos 2\lambda^I\alpha + \lambda^I\cos 2\alpha\right)\cos\left(\lambda^I+1\right)\theta \end{bmatrix} + \frac{r^{\lambda^{II}}}{2G} A_2 \begin{bmatrix} -\left(3-4\eta-\lambda^{II}\right)\sin\left(\lambda^{II}-1\right)\theta + \\ \left(\cos 2\lambda^{II}\alpha - \lambda^{II}\cos 2\alpha\right)\sin\left(\lambda^{II}+1\right)\theta \end{bmatrix} \quad (1)$$

$$u_\theta = \frac{r^{\lambda^I}}{2G} A_1 \begin{bmatrix} \left(3-4\eta+\lambda^I\right)\sin\left(\lambda^I-1\right)\theta - \\ \left(\cos 2\lambda^I\alpha + \lambda^I\cos 2\alpha\right)\sin\left(\lambda^I+1\right)\theta \end{bmatrix} + \frac{r^{\lambda^{II}}}{2G} A_2 \begin{bmatrix} \left(3-4\eta+\lambda^{II}\right)\cos\left(\lambda^{II}-1\right)\theta + \\ \left(\cos 2\lambda^{II}\alpha - \lambda^{II}\cos 2\alpha\right)\cos\left(\lambda^{II}+1\right)\theta \end{bmatrix} \quad (2)$$

$$\sigma_r = r^{\lambda^I-1}\lambda^I A_1 \begin{bmatrix} -\left(\lambda^I-3\right)\cos\left(\lambda^I-1\right)\theta + \\ \left(\cos 2\lambda^I\alpha + \lambda^I\cos 2\alpha\right)\cos\left(\lambda^I+1\right)\theta \end{bmatrix} + r^{\lambda^{II}-1}\lambda^{II} A_2 \begin{bmatrix} \left(\lambda^{II}-3\right)\sin\left(\lambda^{II}-1\right)\theta + \\ \left(\cos 2\lambda^{II}\alpha - \lambda^{II}\cos 2\alpha\right)\sin\left(\lambda^{II}+1\right)\theta \end{bmatrix} \quad (3)$$

$$\sigma_\theta = r^{\lambda^I-1}\lambda^I A_1 \begin{bmatrix} \left(\lambda^I+1\right)\cos\left(\lambda^I-1\right)\theta - \\ \left(\cos 2\lambda^I\alpha + \lambda^I\cos 2\alpha\right)\cos\left(\lambda^I+1\right)\theta \end{bmatrix} - r^{\lambda^{II}-1}\lambda^{II} A_2 \begin{bmatrix} \left(\lambda^{II}+1\right)\sin\left(\lambda^{II}-1\right)\theta + \\ \left(\cos 2\lambda^{II}\alpha - \lambda^{II}\cos 2\alpha\right)\sin\left(\lambda^{II}+1\right)\theta \end{bmatrix} \quad (4)$$

$$\sigma_{r\theta} = r^{\lambda^I-1}\lambda^I A_1 \begin{bmatrix} \left(\lambda^I-1\right)\sin\left(\lambda^I-1\right)\theta - \\ \left(\cos 2\lambda^I\alpha + \lambda^I\cos 2\alpha\right)\sin\left(\lambda^I+1\right)\theta \end{bmatrix} + r^{\lambda^{II}-1}\lambda^{II} A_2 \begin{bmatrix} \left(\lambda^{II}-1\right)\cos\left(\lambda^{II}-1\right)\theta + \\ \left(\cos 2\lambda^{II}\alpha - \lambda^{II}\cos 2\alpha\right)\cos\left(\lambda^{II}+1\right)\theta \end{bmatrix} \quad (5)$$

where A_1 and A_2 are complex constants (the generalised coordinates), G is the shear modulus, $\eta = \nu$ for plane strain, $\eta = \frac{\nu}{1+\nu}$ for plane stress, and ν is the Poisson's ratio. λ^I and λ^{II} are eigenvalues for mode I and mode II, respectively, and are calculated from the following characteristic equations

$$\lambda^I \sin 2\alpha + \sin 2\lambda^I\alpha = 0 \quad (6)$$

$$\lambda^{II} \sin 2\alpha - \sin 2\lambda^{II}\alpha = 0 \quad (7)$$

λ^I and λ^{II} are generally complex numbers and different from each other, except for the special case of a crack (when the notch opening angle $\gamma = 0^\circ$). Equations (6) and (7) can be solved by using Muller's Method.

The stress intensity factors of a notch are defined as

$$K_I = \sqrt{2\pi} \lim_{r\to 0} r^{1-\lambda^I} \sigma_\theta(\theta = 0) \tag{8}$$

$$K_{II} = \sqrt{2\pi} \lim_{r\to 0} r^{1-\lambda^{II}} \sigma_{r\theta}(\theta = 0) \tag{9}$$

for mode I and mode II, respectively [2].

Substituting equations (4) and (5) into equations (8) and (9) gives

$$K_I = \sqrt{2\pi}\,\lambda^I \left(1 + \lambda^I - \lambda^I \cos 2\alpha - \cos 2\lambda^I \alpha\right) A_1 \tag{10}$$

$$K_{II} = \sqrt{2\pi}\,\lambda^{II} \left(-1 + \lambda^{II} - \lambda^{II} \cos 2\alpha + \cos 2\lambda^{II} \alpha\right) A_2 \tag{11}$$

From Equations (10) and (11) it can be seen that no post-processing technique is required to extract the SIFs, because these equations demonstrate direct relations between the SIFs and the generalised coordinates.

3 FORMULATION OF THE FFEM

A short description of the FFEM is presented in this section with a focus on the coordinate transformation required for modelling the singular region of a non-symmetrical notch. In the FFEM, a body with a singularity is divided into singular and regular regions as shown in Figure 2. Both regions are modelled using conventional finite elements. No special singular finite elements are needed to model the singular region in order to account for the analytical form of the singularity. A very fine mesh generated layer by layer in a self-similar manner (by assuming a similarity ratio ρ and the notch tip is used as a centre of similarity) is used in the singular region as illustrated in Figure 3. The large number of the nodal displacements (of slave nodes) in the singular region is then transformed into a small set of generalised coordinates by using global interpolation functions. This process reduces the computational cost significantly, because the number of unknowns is greatly reduced. The exact analytical displacement expressions presented in the previous section are used as global interpolation functions in the FFEM. Because the layers of finite elements in the singular region are self-similar, only the first layer is needed to generate the global stiffness matrix by using a fractal transformation [12,16].

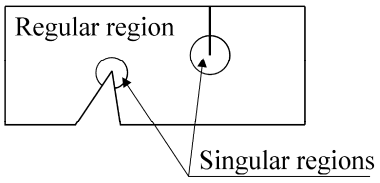

Figure 2. Singular and regular regions of a plate with singularities.

In the conventional finite element method the equilibrium equation can be written as

$$\mathbf{Kd} = \mathbf{f} \tag{12}$$

where $\mathbf{K}$ is the stiffness matrix, $\mathbf{d}$ is the nodal displacement vector, and $\mathbf{f}$ is the nodal force vector.

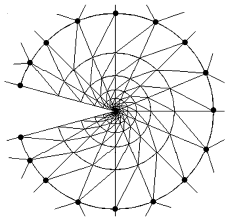

Figure 3. A singular region mesh (master nodes highlighted).

In the FFEM, equation (12) is partitioned into regular, master and singular parts as

$$\begin{bmatrix} \mathbf{K}_{rr} & \mathbf{K}_{rm} & 0 \\ \mathbf{K}_{mr} & \mathbf{K}_{mm} + \mathbf{K}_{mm}^{1st} & \overline{\mathbf{K}}_{ms}^{1st} \\ 0 & \overline{\mathbf{K}}_{sm}^{1st} & \overline{\mathbf{K}}_{ss}^{1st} + \overline{\mathbf{K}}_{s}^{inn} \end{bmatrix} \begin{Bmatrix} \mathbf{d}_r \\ \mathbf{d}_m \\ \mathbf{a} \end{Bmatrix} = \begin{Bmatrix} \mathbf{f}_r \\ \mathbf{f}_m + \mathbf{f}_m^{1st} \\ \overline{\mathbf{f}}_s^{1st} + \overline{\mathbf{f}}_s^{inn} \end{Bmatrix} \tag{13}$$

where r, m and s refer to regular region, master nodes and singular region, $\mathbf{a}$ is the vector of the generalised coordinates $\mathbf{a}^T = \left\{A_1^I, A_1^{II}, A_2^I, A_2^{II}, A_3^I, \ldots\right\}$, $\overline{\mathbf{K}}_{ms}^{1st} = \mathbf{K}_{ms}^{1st}\mathbf{T}_s^{1st}$, $\overline{\mathbf{K}}_s^{inn} = \sum_{n=2}^{nl} \overline{\mathbf{K}}_s^n$, $\overline{\mathbf{K}}_s^n = \mathbf{T}_s^{n\,T} \mathbf{K}_s^n \mathbf{T}_s^n$, $\overline{\mathbf{f}}_s^{1st} = \mathbf{T}_s^{1st\,T} \mathbf{f}_s^{1st}$, $\overline{\mathbf{f}}_s^{inn} = \sum_{n=2}^{nl} \overline{\mathbf{f}}_s^n$, $\overline{\mathbf{f}}_s^n = \mathbf{T}_s^{n\,T} \mathbf{f}_s^n$, and nl is the number of layers in the singular region. $\mathbf{T}_s^n$ is the transformation matrix of the n^{th} layer in the singular region.

In Equation (13), the nodal displacements of the slave nodes are replaced by the generalised coordinates by using the transformation matrices of the layers in the singular region $\mathbf{T}_s^n$ as follows

$$\mathbf{d}_s^n = \mathbf{T}_s^n \mathbf{a} \tag{14}$$

where n refers to the n^{th} layer in the singular region. $\mathbf{T}_s^n$ is computed using the global interpolation functions presented in the previous section. $\overline{\mathbf{K}}_s^{inn}$, which is the generalised stiffness matrix of the inner layers $(n \geq 2)$ in the singular region, can be generated from the stiffness matrix of the first layer only by utilising the property of the self-similar two-dimensional isoparametric finite elements as reported by Treifi et al. [16] as

$$\begin{aligned} \overline{\mathbf{K}}_s^{inn} &= \sum_{n=2}^{nl} \overline{\mathbf{K}}_s^n = \sum_{n=2}^{nl} \mathbf{T}_s^{n\,T} \mathbf{K}_s^n \mathbf{T}_s^n \\ &= \sum_{n=2}^{nl} [\delta]^T \mathbf{T}_s^{f\,T} \mathbf{K}_s^{1st} \mathbf{T}_s^f [\delta] = \left[\overline{\delta}_{ij}\, \overline{k}_{ij}\right] \end{aligned} \tag{15}$$

where $[\delta]$ is a diagonal matrix ($\delta_{ii} = \rho^{(n-1)\lambda_i}$, $\lambda_i = \lambda_1^I, \lambda_1^{II}, \lambda_2^I, \lambda_2^{II}, \ldots$), $\left[\overline{k}_{ij}\right] = \mathbf{T}_s^{f\,T} \mathbf{K}_s^{1st} \mathbf{T}_s^f$, and

$\bar{\delta}_{ij} = \rho^{(\lambda_i+\lambda_j)} + \rho^{2(\lambda_i+\lambda_j)} + ... + \rho^{(nl-1)(\lambda_i+\lambda_j)}$. Equation (15) represents a sum of a geometric series. Therefore, $\bar{\delta}_{ij}$ can be written as

$$\bar{\delta}_{ij} = \frac{\rho^{(\lambda_i+\lambda_j)}\left(1-\rho^{(nl-1)(\lambda_i+\lambda_j)}\right)}{1-\rho^{(\lambda_i+\lambda_j)}} \quad (16)$$

and for the case of an infinite number of layers $(nl \to \infty)$ as

$$\bar{\delta}_{ij} = \frac{\rho^{(\lambda_i+\lambda_j)}}{1-\rho^{(\lambda_i+\lambda_j)}} \quad (17)$$

A similar procedure can be followed to compute the generalised force vector of the inner layers in the singular region $\bar{\mathbf{f}}_s^{inn}$.

The unknowns of the problem are the displacements $\mathbf{d}_r$ and $\mathbf{d}_m$ and the generalised co-ordinates $\mathbf{a}$. If we consider $\mathbf{d}_s$ as the vector of the nodal displacements of the slave nodes in the singular region, the size of the vector $\mathbf{d}_s$ is much greater than that of the vector of the generalised co-ordinates $\mathbf{a}$. Therefore, solving the system of equations (13) reduces the computational cost considerably. For more details about the formulation of the FFEM, see Treifi et al. [16] and Leung and Su [12-14].

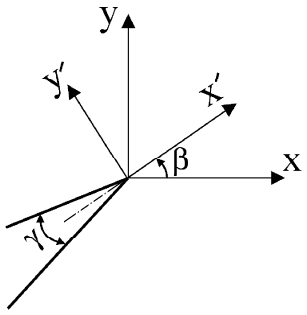

Figure 4. A non-symmetrical notch.

Now for the case of a non-symmetrical notch case shown in Figure 4 when the bisector of the notch opening angle does not coincide with the x-axis, suitable coordinate transformation is needed to obtain the generalised stiffness matrix of the singular region. The stress and displacement expressions presented in Section 2 were derived in a local coordinate system (x', y'). Therefore, a coordinate transformation is needed to obtain correct values in a global coordinate system. Let $\mathbf{d}_G$ and $\mathbf{d}_L$ be the nodal displacement vectors of the n^{th} layer in the singular region in global (x, y) and local (x', y') Cartesian coordinate systems, respectively. The local Cartesian coordinate system is assumed to be centred at the notch tip and that its x'-axis coincides with the bisector of the notch opening angle. The relation between the nodal displacement components in the two coordinate systems shown in Figure 4 is:

$$\mathbf{d}_G = \mathbf{T}_c \mathbf{d}_L \quad (18)$$

where $\mathbf{T}_c$ is the matrix of direction cosines. Substituting Equation (14) (s and n are omitted for simplicity) into Equation (18) yields

$$\mathbf{d}_G = \mathbf{T}_c \mathbf{T} \mathbf{a} = \mathbf{T}' \mathbf{a} \quad (19)$$

The transformation matrix $\mathbf{T}$ can be replaced by $\mathbf{T}'$ in the formulation of the FFEM to solve both symmetrical and non-symmetrical notch problems.

4 NUMERICAL EXAMPLES AND VALIDATION

A few examples of various non-symmetrical configurations of single-edge-notched rectangular plates are presented in this section. Consider a rectangular plate which contains a non-symmetrical notch whose bisector is inclined an angle β over the plate horizontal axis of symmetry as shown in Figures 5 and 6. Published results for these cases exist and are compared with to demonstrate the accuracy of the approach proposed in the previous section.

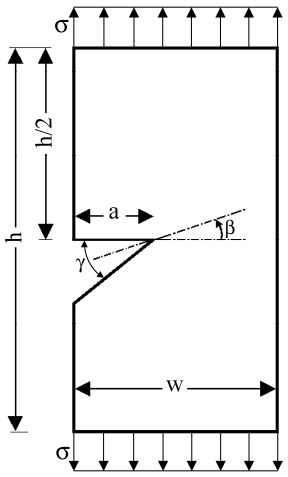

Figure 5. A non-symmetrically notched plate (h/w = 2 and $\beta = \gamma/2$).

First, consider a rectangular plate under tension loading conditions as shown in Figure 5 with an aspect ratio h/w = 2 and a ratio of the notch length to the plate width a/w = 0.4. The results are obtained by using twenty terms of the eigenfunction series, a similarity ratio $\rho = 0.9$, and an 'infinite' number of layers in the singular region. The geometry of the plate is meshed in a similar way to that shown in Figure 7 using six-node triangle elements (seven-point integration scheme). The inclined angle β is taken to be half of the notch opening angle γ, that is $\beta = \gamma/2$. The SIFs computed by the FFEM for different notch opening angles compared to corresponding published results obtained by Portela et al [9] are plotted in Figure 8.

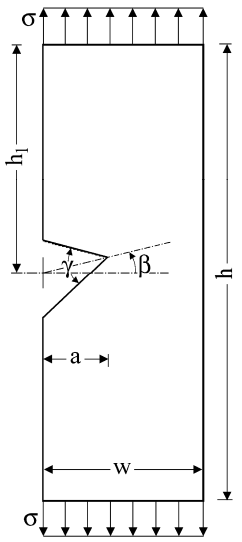

Figure 6. A non-symmetrically notched plate (h/w = 3).

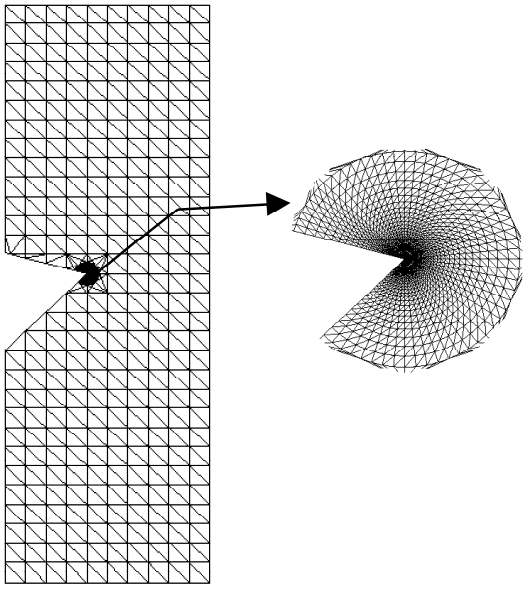

Figure 7. FE mesh of the notched plate.

Now, consider a rectangular plate under tension loading conditions as shown in Figure 6 with an aspect ratio $h/w = 3$ and $h_1/h = 0.5$. Similar parameters to those of the previous example are used to obtain the FFEM results. The geometry of the plate is meshed in a way similar to that shown in Figure 7. The FFEM results for different notch opening angles, different inclined angles and different notch lengths are plotted in Figures 9, 10 and 11. Corresponding published results reported by Chen [10] are also plotted in those figures for comparison.

From Figures 8 to 11, it can be seen that the mode I and mode II SIFs vary in opposite directions as the inclined angle β increases; the mode I SIFs decrease while the mode II SIFs increase. it can also be seen from those figures that the SIFs predicted by the FFEM are in very good agreement with the published results. The discrepancies between the FFEM results and those predicted by Portela et al [9] are less than 1% for mode I and mode II SIFs. The discrepancies between the FFEM results and those predicted by Chen [10] are about 1% for mode I SIFs and less than 5% for mode II SIFs.

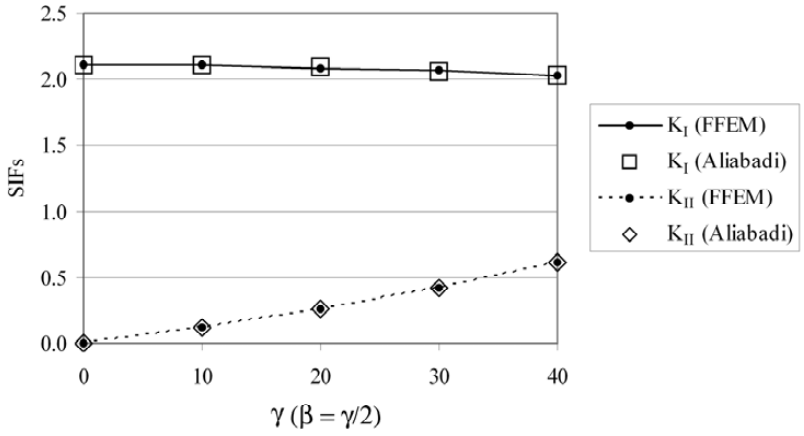

Figure 8. SIFs of non-symmetrically notched plates for different notch angles ($h/w = 2$, $a/w = 0.4$, $\beta = \gamma/2$)compared to those of reference [9].

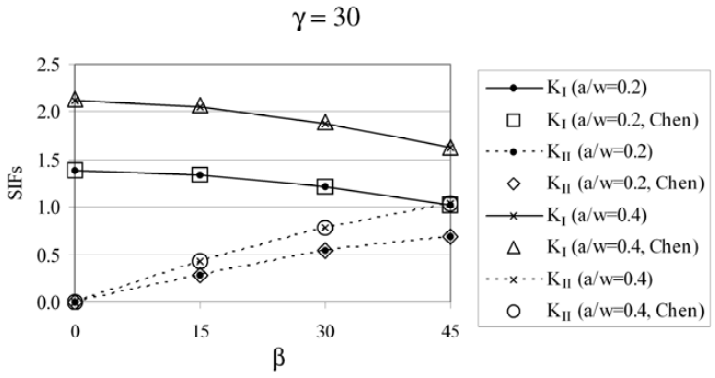

Figure 9. SIFs of non-symmetrically notched plates for different inclined angles ($h/w = 3$, $h_1/h = 0.5$, $\gamma = 30^\circ$) compared to those of reference [10].

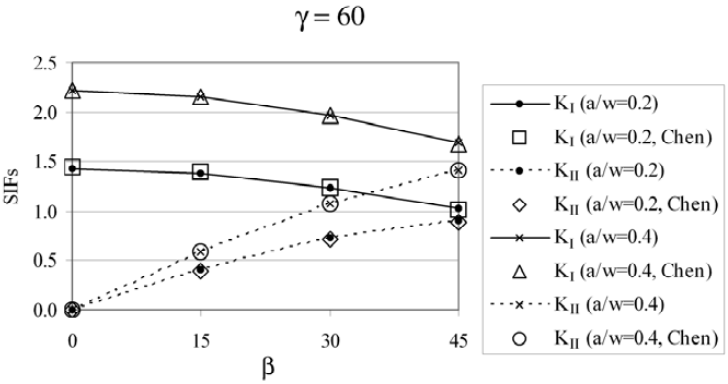

Figure 10. SIFs of non-symmetrically notched plates for different inclined angles ($h/w = 3$, $h_1/h = 0.5$, $\gamma = 60^\circ$) compared to those of reference [10].

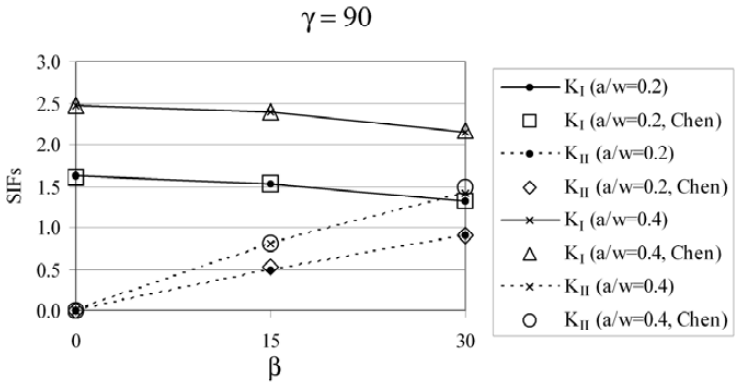

Figure 11. SIFs of non-symmetrically notched plates for different inclined angles ($h/w = 3$, $h_1/h = 0.5$, $\gamma = 90^\circ$) compared to those of reference [10].

5 CONCLUSIONS

In this paper, the FFEM was extended to model and analyse non-symmetrical notch problems. A simple coordinate transformation is needed to evaluate the SIFs of a non-symmetrical notch based on the global interpolation functions derived for a symmetrical notch case. In the FFEM, no complicated mathematics is involved; only simple matrix multiplication. Post-processing techniques to extract the SIFs or special singular finite elements are not needed. The SIFs are computed directly because of the use of exact analytical solutions as global interpolation functions. Also, the FFEM reduces the number of unknowns significantly and therefore the computational cost. It can practically be applied when the agile and widely used Finite Element Method has convergence difficulties as in the case of the presence of singular points and when there is a need to reduce the computational cost associated with a large number of unknown variables of a problem without the need of using other methods.

Various numerical examples of non-symmetrically notched plates under tension loading conditions were presented, and results were validated via comparison with corresponding published results. The good agreement achieved between the FFEM results and published results proved the validity of the use of the simple local coordinate transformation in the FFEM when dealing with non-symmetrical notch cases.

6 REFERENCES

[1] Seweryn, A., 1994, "Brittle fracture criterion for structures with sharp notches", *Engineering Fracture Mechanics*, Vol. 47, pp. 673–681.

[2] Gross, B. and Mendelson, A., 1972, "Plane elastostatic analysis of V-notched plates", *International Journal of Fracture*, Vol. 8, pp. 267–276.

[3] Williams, M. L., 1952, "Stress singularities resulting from various boundary conditions in angular corners of plates in extension", *ASME Journal of Applied Mechanics*, Vol. 19, pp. 526–528.

[4] Tong, P. and Pian, T. H. H., 1973, "On the convergence of the FEM for problems with singularity", *International Journal of Solids and Structures*, Vol. 9, pp. 313–321.

[5] Lin, K. Y. and Tong, P., 1980, "Singular finite elements for the fracture analysis of V-notched plates", *International Journal for Numerical Methods in Engineering*, Vol. 15, pp. 1343–1354.

[6] Carpenter, W. C., 1984, "A collocation procedure for determining fracture mechanics parameters at a corner", *International Journal of Fracture*, Vol. 24, pp. 255–266.

[7] Carpenter, W. C., 1985, "The eigenvector solution for a general comer or finite opening crack with further studies on the collocation procedure", *International Journal of Fracture*, Vol. 27, pp. 63–74.

[8] Stern, M., Becker, E. B. and Dunham R. S., 1976, "A contour integral computation of mixed-mode stress intensity factors", *International Journal of Fracture*, Vol. 12, pp. 359–368.

[9] Portela, A., Aliabadi, M. H. and Rooke, D. P., 1991, "Efficient boundary element analysis of sharp notched plates", *International Journal for Numerical Methods in Engineering*, Vol. 32, pp. 445–470.

[10] Chen, D-H., 1995, "Stress intensity factors for V-notched strip under tension or in-plane bending", *International Journal of Fracture*, Vol. 70, pp. 81-97.

[11] Mote, C. D., 1971, "Global-local finite element", *International Journal for Numerical Methods in Engineering*, Vol. 3, pp. 565–574.

[12] Leung, A. Y. T. and Su, R. K. L., 1994, "Mode I crack problems by fractal two level finite element method", *Engineering Fracture Mechanics*, Vol. 48(6), pp. 847–856.

[13] Leung, A. Y. T. and Su, R. K. L., 1995, "Mixed-mode two-dimensional crack problem by fractal two level finite element method", *Engineering Fracture Mechanics*, Vol. 51(6), pp. 889–895.

[14] Leung, A. Y. T. And Su, R. K. L., 1998, "Two-level finite element study of axisymmetric cracks", *International Journal of Fracture*, Vol. 89, pp.193–203.

[15] Treifi, M., Oyadiji, S. O. and Tsang, D. K. L., 2009, "Computation of the stress intensity factors of sharp notched plates by the fractal-like finite element method", *International Journal for Numerical Methods in Engineering*, Vol. 77, pp. 558–580.

[16] Treifi, M., Oyadiji, S. O. and Tsang, D. K. L., 2008, "Computations of modes I and II stress intensity factors of sharp notched plates under in-plane shear and bending loading by the fractal-like finite element method". *International Journal of Solids and Structures*, Vol. 45, pp. 6468–6484.

[17] Vasilopoulos, D., 1988, "On the determination of higher order terms of singular elastic stress fields near corners", *Numerische Mathematik*, Vol. 53, pp. 51–95.

Chapter 8

Computations of the Stress Intensity Factors of Double-edge and Centre V-notched Plates under Tension and Anti-Plane Shear by the Fractal-like Finite Element Method

Engineering Fracture Mechanics 2009; 76:2091–2108

Engineering Fracture Mechanics 76 (2009) 2091–2108

Contents lists available at ScienceDirect

Engineering Fracture Mechanics

journal homepage: www.elsevier.com/locate/engfracmech

Computations of the stress intensity factors of double-edge and centre V-notched plates under tension and anti-plane shear by the fractal-like finite element method

Muhammad Treifi, S. Olutunde Oyadiji *, Derek K.L. Tsang

School of Mechanical, Aerospace and Civil Engineering, University of Manchester, Manchester M60 1QD, UK

ARTICLE INFO

Article history:
Received 17 October 2008
Received in revised form 14 January 2009
Accepted 28 May 2009
Available online 3 June 2009

Keywords:
Stress intensity factors
Single-edge-notched plate
Double-edge-notched plate
Centre-notched plate
Finite element method

ABSTRACT

The fractal-like finite element method (FFEM) is extended to compute the stress intensity factors (SIFs) of double-edge-/centre-notched plates subject to out-of-plane shear or tension loading conditions. In the FFEM, the use of global interpolation functions reduces the large number of unknowns in a singular region to a small set of generalised co-ordinates. Therefore, the computational cost is reduced significantly. Also, neither post-processing techniques to extract the SIFs nor special singular elements are needed. Many numerical examples of double-edge-/centre-notched plates are presented, and results are validated via existing published data. New results of notched plate problems are also introduced.

1. Introduction

Structural components with corners/notches are common occurrences in engineering design. The presence of notches affects the loading resistance capacity of those components and may result in a crack initiation leading to a structural failure or to a shortening of the service life. Therefore, much research has been devoted to the analysis of sharp notch problems. However, most of the cases reported in the literature are about mode I cases. There are only few results concerning pure modes II and III cases of notch problems.

In linear elastic fracture mechanics, the stress intensity factors provide a means to assess the stability of cracks. Similarly, for notch problems experimental results have demonstrated that simple failure criteria based on the so-called notch/generalised stress intensity factors exist, at least for brittle fracture [1]. The failure occurs when the notch stress intensity factors reach critical values. The limiting cases of the notch opening angle $\gamma = 0^\circ$ and $\gamma = 180^\circ$ correspond to a cracked solid and a solid with no notch, respectively. For tension loading conditions, if a failure is presumed to occur at a critical value of the generalised stress intensity factor for both of those cases, then in the case of a crack the critical value is the fracture toughness while in the case of a solid without a notch it is the tensile strength [2]. The case of a notch when $0^\circ < \gamma < 180^\circ$ is between those two limiting cases. Therefore, many researchers have tried to develop a criterion to calculate or measure the critical values of notch stress intensity factors while others have tried to compute the notch stress intensity factors by using numerical, analytical or empirical methods. Just to mention a few of those who have tried to establish a failure criterion for a notch, Seweryn [1] introduced a brittle fracture criterion for structures with sharp notches that states that a crack will

* Corresponding author. Tel.: +44 161 2754348.
E-mail addresses: Muhammad.Treifi@postgrad.manchester.ac.uk (M. Treifi), s.o.oyadiji@manchester.ac.uk (S.O. Oyadiji), kwong-lai.tsang@manchester.ac.uk (D.K.L. Tsang).

0013-7944/$ - see front matter © 2009 Elsevier Ltd. All rights reserved.
doi:10.1016/j.engfracmech.2009.05.018

Nomenclature

a	crack/notch length
$\mathbf{a}$	vector of generalised co-ordinates
A, B	generalised co-ordinates
$\mathbf{d}$	nodal displacement vector
$\mathbf{d}_r$, $\mathbf{d}_m$, and $\mathbf{d}_s$	nodal displacement vectors of nodes in regular region, master nodes, and in singular region
$\mathbf{d}_s^{1st,\,2nd,\,\ldots}$	nodal displacements of the nodes in the first layer, second layer, ... in the singular region
$\mathbf{f}$	nodal force vector
$\mathbf{f}_r$, $\mathbf{f}_m$, and $\mathbf{f}_s$	nodal force vectors of nodes in regular region, master nodes, and in singular region
$\bar{\mathbf{f}}_s^{1st,\,inn}$	transformed nodal force vectors of the first layer and the inner layers in the singular region
G	shear modulus
h	plate height
h_c	distance between crack/notch tip and bottom boundary of plate
$\mathbf{K}$	stiffness matrix
$\mathbf{K}_{rr}$, $\mathbf{K}_{mr}$, $\mathbf{K}_{mm}$, $\mathbf{K}_{ss}$, ...	partitioned stiffness matrices (r refers to regular region, m to master nodes, and s to slave nodes)
$\mathbf{K}_s^n$	partitioned stiffness matrix of the nth layer in the singular region
$\bar{\mathbf{K}}_s^{1st}$, $\bar{\mathbf{K}}_s^{inn}$	transformed partitioned stiffness matrices of the first layer and the inner layers in the singular region
K_{I}, K_{II}, K_{III}	stress intensity factors of modes I, II, and III
m, n	integer variables
NL, nl	number of layers in the singular region
NT, nt	number of terms of eigenfunction series expansion
r,θ	polar co-ordinates
$\mathbf{T}_s^n$	transformation matrix of the nodal displacements of the nth layer in the singular region
$\mathbf{T}_s^{1st}$	transformation matrix of the nodal displacements of the first layer in the singular region
$\mathbf{T}_s^T$	transformation matrix of the nodal displacements of all the nodes (slave and master) in the first layer in the singular region
W	width of single-edge-notched plate or half width of double-edge-/centre-notched plate
w	displacement in z direction
x, y, z	Cartesian co-ordinates
α	angle between notch face and x-axis
δ	scaling variable
γ	notch opening angle
Γ	boundary curve
Φ	stress function
λ	eigenvalue
ρ	similarity ratio
σ	tensile stress
τ	shear stress
∇^2	the Laplacian operator

propagate from a tip of a notch when the actual value of the notch stress intensity factor reaches a critical value, Knésl [3] extended the stability criterion of a crack to the general case of a notch, Gómez and Elices [4] showed the advantages of the cohesive crack model for predicting fracture of notched components, and recently Carpinteri et al. [5] presented an expression for the generalised fracture toughness which is a function of material tensile strength, fracture toughness and notch opening angle.

Many procedures have been developed to compute the generalised stress intensity factors of sharp notched components. Gross and Mendelson [6] computed the SIFs of many cases of modes I and II notch problems by means of a Boundary Collocation Method (BCM) based on the stress functions derived by Williams [7]. It was concluded by Tong and Pian [8] that in order to improve the convergence rate of finite element solutions of problems with a singularity, the interpolation functions of a finite element formulation must include terms that can account for the analytical form of the singularity. In addition, these interpolation functions should be used for elements within a finite region, and not only for those around the singular point. Lin and Tong [9] developed special hybrid finite elements to account for the notch tip singularities. A generalised stress intensity concept at sharp corners was proposed by Sinclair et al. [10]. They outlined an approach based on the calculation of a contour integral that was an extension of the work of Stern et al. [11,12]. Independently, Carpenter [13,14] introduced a collocation approach to calculate stress intensity factors of notch problems based on the contour integral of Stern et al. [11,12]. Babuška et al. [15,16] developed post-processing approaches to extract the SIFs for mixed mode problems from a finite element solution. Portela et al. [17] proposed a boundary element singularity subtraction technique to compute the SIFs of notch problems. Their method requires extra boundary conditions that they referred to as "singularity conditions of the regularisation procedure". Zhao and Hahn [18] developed a method to determine the SIFs of a notch problem from

the SIFs of a crack problem. All the aforementioned methods were mainly used to predict the SIFs of mode I, mode II, or mixed modes (I and II) cases of single-edge-notched plates. Chen [19] computed the SIF of single-edge- and double-edge-notched plates subject to tension or in-plane bending loading conditions by means of the Body Force Method.

Results of mode III SIFs of cracked plates were reported by some authors such as Zhang [20] who presented results for off-centre single-edge-cracked plates with the aid of the basic theorem of the Fourier transform and Fourier series. Leung and Tsang [21] extended the two-level finite element method to analyse mode III crack problems. Noda and Takase [22] calculated the generalised SIFs for a V-shaped notched round bar under tension, bending, and torsion using the singular integral equation of the body force method.

The fractal-like finite element method, which is based on the concept of global-local interpolation functions introduced by Mote [23], is semi-analytical. Leung and co-workers [24–27] applied the FFEM to compute the stress intensity factors of many two-dimensional crack problems only. It has been proven that the FFEM produces very accurate results [24–25]. Recently Treifi et al. [28–30] have extended the FFEM to analyse the singularity resulting at a notch tip. They presented many results of various configurations of notched plates subjected to mode I or mode II loading conditions of single-edge-notched plates.

In general, superposition of the results of modes I, II and III can be used to describe the most general case of loading on a V-notched specimen. Therefore, the extension of the FFEM to analyse mode III notch problems is in order. The mode III case might appear to be simpler than the mode I and mode II cases, because of the fact that it reduces to a one-dimensional problem. However, entirely different global interpolation functions that account for the analytical form of the mode III singularity around a notch tip are needed to be used in the FFEM. As a result, the mode III problem is completely different from the modes I and II cases with regard to handling and final results. Only the general outlines of those cases are similar. Furthermore, providing mode III results of different notch problems with different notch opening angles will give further insight into the behaviour of fracture parameters of notched components.

The FFEM can be used to calculate directly not only the stress intensity factors but also the coefficients of the higher order terms of the crack/notch tip asymptotic field. Only few methods such as the Boundary Collocation Method (BCM), Hybrid Crack Element (HCE) and the Scaled Boundary Finite Element Method (SBFEM) are available in the literature which can be used to evaluate the crack tip higher order terms. The BCM is a method that satisfies the boundary conditions at selected locations or points; it is powerful for use for structures with simple geometries and simple loading conditions.

The HCE was developed by Karihaloo and Xiao [31] based on the Hybrid Element Approach introduced by Tong et al. [32]. A simplified variational principle using truncated asymptotic crack tip displacement and stress series expansions was used to formulate the HCE [31]. Despite the good accuracy of the numerical results obtained by the HCE, the element was incompatible with the surrounding finite elements because of the exclusion of coefficients of the Williams series expansion that do not contribute to the stresses and strains in the formulation of the HCE [33]. To minimise the incompatibility, Xiao and Karihaloo [34] recovered these coefficients by an indirect method that involves the application of a least-squares method. The SBFEM, developed by Wolf [35], is a numerical finite element-based procedure in the circumferential directions and an analytical procedure in the radial direction. In the SBFEM, the governing partial differential equations are transformed to a scaled boundary co-ordinate system. By introducing shape functions in the circumferential directions, these equations are reduced to a set of second-order ordinary differential equations. These ordinary differential equations are solved analytically in the radial direction after determining their coefficients by a finite element approximation in the circumferential directions. However, the mathematics of the SBFEM compared to the finite element method is rather complicated [36].

The FFEM combines the accuracy of analytical solutions and the agility of the finite element method. No complicated mathematics is involved; only simple matrix multiplication is needed. The exact solutions of the singular displacement field around a notch tip are used as global interpolation functions to perform a transformation of the nodal displacements in the singular region into a set of generalised co-ordinates. The transformation reduces the number of unknowns significantly and consequently the computational cost too. Because of the employment of exact analytical solutions as global interpolation functions, the stress intensity factors and the coefficients of the higher order terms of the notch tip asymptotic field become primary unknowns of the problem. Therefore, no post-processing is required to extract them. In addition, special singular finite elements are not needed to model the stress singularity at the notch tip—any conventional finite elements can be used to model the singular region. Hence, some practical applications of the FFEM are when the standard Finite Element Method has convergence difficulties as in the case of the presence of a singular point and when there is a need to reduce the computational cost associated with the large number of unknowns of a problem. The limitation to the use of the FFEM is the availability of "good" global interpolation functions, whether they be exact analytical or not.

In this paper, the FFEM is extended to model and analyse many cases of double-edge- and centre-notched plates subjected to anti-plane shear (mode III) or tension (mode I) loading conditions. The accuracy and efficiency of the FFEM to compute modes I, II and III SIFs is demonstrated by comparison with many numerical examples concerning different configurations of cracked/notched plates subject to anti-plane shear or tension loading conditions of which published results exist. Also, many new results of notch problems are presented.

2. Formulation of the fractal-like finite element method (FFEM)

A short description of the FFEM formulation is presented in this section. For detailed description, one may refer to Refs. [24–27,29]. In the FFEM, a body containing singular points is divided into singular and regular regions delineated by curves such as Γ_0^1 and Γ_0^2 as shown in Fig. 1a. Any conventional finite elements can be used to model all regions. In the singular

regions, however, a very fine mesh generated layer by layer in a self-similar manner is used. The nodal displacements in the singular region are transformed into a small set of generalised co-ordinates by using global interpolation functions. This transformation process reduces the number of unknowns significantly. Now, the unknowns of the problem are the nodal displacements of the regular region and the generalised co-ordinates of the singular region. The stress intensity factors are related to some of the coefficients of the generalised co-ordinate set, as is shown in the next section; and therefore no post-processing is needed to extract them.

The singular region is discretised as shown in Fig. 1b. By using the notch tip as a centre of similarity and assuming that ρ is a similarity ratio, a set of curves $\{\Gamma_1, \Gamma_2, \Gamma_3, \ldots\}$ similar to the curve that separates the singular and regular regions Γ_0 is generated within the singular region. All nodes within Γ_0 are considered slave nodes, while the nodes on Γ_0 are considered master nodes as illustrated in Fig. 1b.

In the conventional finite element method, the static equilibrium equation can be written as

$$\mathbf{K}\mathbf{d} = \mathbf{f} \tag{1}$$

where $\mathbf{K}$ is the stiffness matrix, $\mathbf{d}$ is the nodal displacement vector, and $\mathbf{f}$ is the nodal force vector.

By dividing the matrix equation into regular and singular parts, the global stiffness matrix equation can be rewritten as

$$\begin{bmatrix} \mathbf{K}_{rr} & \mathbf{K}_{rm} & & & & & \\ \mathbf{K}_{mr} & \mathbf{K}_{mm}+\mathbf{K}_{mm}^{1st} & \mathbf{K}_{ms}^{1st} & & & & \\ & \mathbf{K}_{sm}^{1st} & \mathbf{K}_{ss}^{1st}+\mathbf{K}_{s,ii}^{2nd} & \mathbf{K}_{s,ij}^{2nd} & & & \\ & & \mathbf{K}_{s,ji}^{2nd} & \mathbf{K}_{s,jj}^{2nd}+\mathbf{K}_{s,ii}^{3rd} & \mathbf{K}_{s,ij}^{3rd} & & \\ & & & \ddots & \ddots & \ddots & \\ & & & & \mathbf{K}_{s,ji}^{nl} & \mathbf{K}_{s,jj}^{nl} \end{bmatrix} \begin{Bmatrix} \mathbf{d}_r \\ \mathbf{d}_m \\ \mathbf{d}_s^{1st} \\ \mathbf{d}_s^{2nd} \\ \vdots \\ \mathbf{d}_s^{nl} \end{Bmatrix} = \begin{Bmatrix} \mathbf{f}_r \\ \mathbf{f}_m \\ \mathbf{f}_s^{1st} \\ \mathbf{f}_s^{2nd} \\ \vdots \\ \mathbf{f}_s^{nl} \end{Bmatrix} \tag{2}$$

where $\mathbf{d}_r$ are the displacements of the nodes in the regular region, $\mathbf{d}_m$ are the displacements of the master nodes, $\mathbf{d}_s^{1st,2nd,\ldots}$ are the displacements of the nodes in the first layer, second layer, ... in the singular region, and nl is the number of layers in the singular region. The same notation applies to $\mathbf{K}$ and $\mathbf{f}$.

The nodal displacements of the nodes in the nth layer in the singular region can be expressed in terms of a vector of generalised co-ordinates $\mathbf{a}$ as

$$\mathbf{d}_s^n = \mathbf{T}_s^n \mathbf{a} \tag{3}$$

where $\mathbf{T}_s^n$ is the transformation matrix of the nth layer in the singular region.

After applying the transformation, the global stiffness equation becomes

$$\begin{bmatrix} \mathbf{K}_{rr} & \mathbf{K}_{rm} & 0 \\ \mathbf{K}_{mr} & \mathbf{K}_{mm}+\mathbf{K}_{mm}^{1st} & \bar{\mathbf{K}}_{ms}^{1st} \\ 0 & \bar{\mathbf{K}}_{sm}^{1st} & \bar{\mathbf{K}}_{ss}^{1st}+\bar{\mathbf{K}}_{s}^{innn} \end{bmatrix} \begin{Bmatrix} \mathbf{d}_r \\ \mathbf{d}_m \\ \mathbf{a} \end{Bmatrix} = \begin{Bmatrix} \mathbf{f}_r \\ \mathbf{f}_m+\mathbf{f}_m^{1st} \\ \bar{\mathbf{f}}_s^{1st}+\bar{\mathbf{f}}_s^{innn} \end{Bmatrix} \tag{4}$$

where

$$\bar{\mathbf{K}}_{ms}^{1st} = \mathbf{K}_{ms}^{1st}\mathbf{T}_s^{1st}, \quad \bar{\mathbf{K}}_s^{innn} = \sum_{n=2}^{nl} \bar{\mathbf{K}}_s^n, \quad \bar{\mathbf{K}}_s^n = \mathbf{T}_s^{n^T}\mathbf{K}_s^n\mathbf{T}_s^n, \quad \bar{\mathbf{f}}_s^{1st} = \mathbf{T}_s^{1st^T}\mathbf{f}_s^{1st}, \quad \bar{\mathbf{f}}_s^{innn} = \sum_{n=2}^{nl} \bar{\mathbf{f}}_s^n, \quad \text{and} \quad \bar{\mathbf{f}}_s^n = \mathbf{T}_s^{n^T}\mathbf{f}_s^n$$

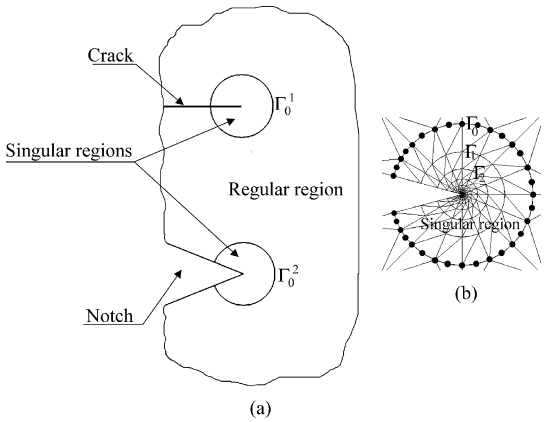

Fig. 1. (a) Singular and regular regions of a cracked/notched body and (b) an illustration of a singular region (master nodes are highlighted).

The vector of the generalised co-ordinates **a** is much smaller than the vector of the nodal displacements in the singular region $\mathbf{d}_s$. Therefore, solving the system of Eq. (4) reduces the computational cost considerably compared to solving the system of Eq. (2).

Now, the generalised stiffness matrix of the inner layers ($n \geqslant 2$) in the singular region, $\bar{\mathbf{K}}_s^{inn}$, can be simplified by utilising the properties of the self-similar two-dimensional isoparametric finite elements. The stiffness matrices of the layers in the singular region are the same because the stiffness matrices of two-dimensional isoparametric finite elements of similar shapes are the same [24]. Therefore,

$$\mathbf{K}_s^n = \mathbf{K}_s^{1st} \tag{5}$$

and the transformation matrix of the nth layer can be written in terms of that of the first layer as

$$\mathbf{T}_s^n = \mathbf{T}_s^f[\delta] \tag{6}$$

where $\mathbf{T}_s^f$ is the transformation matrix of the nodal displacements of all the nodes (slave and master) in the first layer and it is different from the aforementioned $\mathbf{T}_s^{1st}$, which is the transformation matrix of the nodal displacements of the slave nodes only in the first layer, and $[\delta]$ is a diagonal matrix where

$$\delta_{ii} = \rho^{(n-1)\lambda_i}; \quad \lambda_i = \lambda_1, \lambda_2, \lambda_3, \ldots \tag{7}$$

From Eqs. (5)–(7), $\bar{\mathbf{K}}_s^{inn}$ can be rewritten as

$$\bar{\mathbf{K}}_s^{inn} = \sum_{n=2}^{nl} \bar{\mathbf{K}}_s^n = \sum_{n=2}^{nl} \mathbf{T}_s^{n^T} \mathbf{K}_s^n \mathbf{T}_s^n = \sum_{n=2}^{nl} [\delta]^T \mathbf{T}_s^{f^T} \mathbf{K}_s^{1st} \mathbf{T}_s^f [\delta] = [\bar{\delta}_{ij} \bar{k}_{ij}] \tag{8}$$

where

$$[\bar{k}_{ij}] = \mathbf{T}_s^{f^T} \mathbf{K}_s^{1st} \mathbf{T}_s^f \tag{9}$$

and

$$\begin{aligned} \bar{\delta}_{ij} &= \sum_{n=2}^{nl} \rho^{(n-1)\lambda_i} \rho^{(n-1)\lambda_j} = \sum_{n=2}^{nl} \rho^{(n-1)(\lambda_i+\lambda_j)} \\ &= \rho^{(\lambda_i+\lambda_j)} + \rho^{2(\lambda_i+\lambda_j)} + \cdots + \rho^{(nl-1)(\lambda_i+\lambda_j)} \end{aligned} \tag{10}$$

This sum is a geometric series. For a finite number of layers, $\bar{\delta}_{ij}$ can be written as

$$\bar{\delta}_{ij} = \frac{\rho^{(\lambda_i+\lambda_j)}\left(1 - \rho^{(nl-1)(\lambda_i+\lambda_j)}\right)}{1 - \rho^{(\lambda_i+\lambda_j)}} \tag{11}$$

and for an infinite number of layers ($nl \to \infty$) as

$$\bar{\delta}_{ij} = \frac{\rho^{(\lambda_i+\lambda_j)}}{1 - \rho^{(\lambda_i+\lambda_j)}} \tag{12}$$

A similar procedure can be followed to compute the generalised force vector of the inner layers in the singular region $\bar{\mathbf{f}}_s^{inn}$.

3. Global interpolation functions

Exact analytical solutions of the displacement field around a notch tip are employed as global interpolation functions. The stress and displacement expressions can be derived by using a stress function approach or a complex variable method. A description of the derivation of the global interpolation functions for a two-dimensional plane stress/strain case (modes I and II) of a notch may be found in Refs. [7,29,37]. A short description of the derivation of the global interpolation functions for a mode III notch problem is presented next.

3.1. Global interpolation functions for a mode III notch problem

The stress and displacement expressions of a notch subject to out-of-plane shear loading conditions can be derived by using a stress function approach. This approach follows the general framework presented by Williams [7] for the in-plane notch case. The only non-zero displacement component is in the z direction (w) and the non-zero stresses are τ_{rz} and $\tau_{\theta z}$, which can be derived by using a stress function (Φ) in a polar co-ordinate system centred at the tip of an infinite notch as illustrated in Fig. 2. The equilibrium equations are satisfied if the stresses are derived as follows:

$$\tau_{rz} = -\frac{1}{r}\frac{\partial \Phi}{\partial \theta} \tag{13}$$

$$\tau_{\theta z} = \frac{\partial \Phi}{\partial r} \tag{14}$$

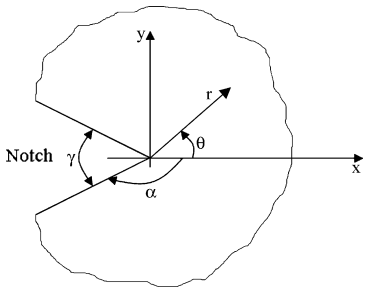

Fig. 2. Notch geometry and co-ordinate systems.

The compatibility equations are reduced to

$$\nabla^2 \Phi = 0 \tag{15}$$

where ∇^2 denotes the Laplacian operator. The stress function (Φ) can be taken as

$$\Phi = r^{\lambda} F(\theta) \tag{16}$$

After substituting Φ and its derivatives into the differential Eq. (15), the general solution of the resulting equation is

$$\Phi = r^{\lambda}(A\cos\lambda\theta + B\sin\lambda\theta) \tag{17}$$

where A and B are the generalised co-ordinates (or the coefficients of the terms of the mode III notch asymptotic field). On substituting Eq. (17) into Eqs. (13) and (14), the stress expressions are

$$\tau_{rz} = r^{\lambda-1}\lambda(A\sin\lambda\theta - B\cos\lambda\theta) \tag{18}$$

$$\tau_{\theta z} = r^{\lambda-1}\lambda(A\cos\lambda\theta + B\sin\lambda\theta) \tag{19}$$

The eigenvalues λ are obtained by imposing the following boundary conditions on the notch faces:

$$\tau_{\theta z}(\pm\alpha) = 0 \tag{20}$$

Substituting Eq. (20) into Eq. (19) yields

$$r^{\lambda-1}\lambda(A\cos\lambda\alpha + B\sin\lambda\alpha) = 0 \tag{21}$$

$$r^{\lambda-1}\lambda(A\cos\lambda\alpha - B\sin\lambda\alpha) = 0 \tag{22}$$

For non-trivial solutions of A and B, the determinant of Eqs. (21) and (22) should be zero. By solving the determinant, the eigenvalues are obtained as

$$\lambda = \frac{m\pi}{2\alpha}; \quad m = 1, 2, 3, \ldots \tag{23}$$

When m is an odd number and by assuming $m = 2n - 1$, it can be shown that $\lambda_m = \left(n - \frac{1}{2}\right)\frac{\pi}{\alpha}$ and $B = 0$. When m is an even number and by assuming $m = 2n$, it can be shown that $\lambda_m = \frac{n\pi}{\alpha}$ and $A = 0$.

The eigenfunction series expansions of the stresses can now be written as

$$\tau_{rz} = A\left(n - \frac{1}{2}\right)\frac{\pi}{\alpha} r^{(n-\frac{1}{2})\frac{\pi}{\alpha}-1} \sin\left(\left(n - \frac{1}{2}\right)\frac{\pi}{\alpha}\theta\right) - B\frac{n\pi}{\alpha} r^{\frac{n\pi}{\alpha}-1} \cos\left(\frac{n\pi}{\alpha}\theta\right) \tag{24}$$

$$\tau_{\theta z} = A\left(n - \frac{1}{2}\right)\frac{\pi}{\alpha} r^{(n-\frac{1}{2})\frac{\pi}{\alpha}-1} \cos\left(\left(n - \frac{1}{2}\right)\frac{\pi}{\alpha}\theta\right) + B\frac{n\pi}{\alpha} r^{\frac{n\pi}{\alpha}-1} \sin\left(\frac{n\pi}{\alpha}\theta\right) \tag{25}$$

and of the displacement as

$$Gw = Ar^{(n-\frac{1}{2})\frac{\pi}{\alpha}} \sin\left(\left(n - \frac{1}{2}\right)\frac{\pi}{\alpha}\theta\right) - Br^{\frac{n\pi}{\alpha}} \cos\left(\frac{n\pi}{\alpha}\theta\right) \tag{26}$$

where G is the shear modulus.

The mode III stress intensity factor of a notch is defined in a way similar to that of a crack as

$$K_{\mathrm{III}} = \sqrt{2\pi} \lim_{r\to 0} r^{1-\lambda} \tau_{\theta z}(\theta = 0) \tag{27}$$

Substituting Eqs. (25) into Eqs. (27) gives

$$K_{III} = \sqrt{2\pi}\lambda A \tag{28}$$

Eq. (28) demonstrates a direct relationship between the SIFs and the generalised co-ordinates which are calculated directly in the FFEM. Therefore, no post-processing technique is required to extract the SIFs.

4. Numerical examples and verification

The use of the global interpolation functions derived in Section 3 for a mode III notch problem is verified via many examples of crack problems for which published data exist. This is done because of the lack of existing results concerning notched plate problems under mode III loading conditions. For the plane stress/strain case, the global interpolation functions used in the FFEM were tested and verified in Refs. [29,30]. Crack problems are special cases of notch problems (the notch opening angle $\gamma = 0°$). First, a numerical verification for crack problems is presented that includes a convergence study to demonstrate the accuracy and stability of the method to compute mode III SIFs, many examples of central and off-central single- and double-edge-cracked plates and centre- and off-centre-cracked plates under mode III loading conditions, and an example about computing the coefficients of the higher order terms of the asymptotic field for a centre crack problem under tension. Published results for these examples exist and are compared with to validate the FFEM results and demonstrate the accuracy and the stability of the method. Then many examples of central and off-central double-edge notch problems and centre- and off-centre-notch problems under out-of-plane shear or tension loading conditions are presented. Most of the results of the notch examples presented in this study are new.

Because of the nature of mode III problems, the SIF values for the cases of single-edge-notched, double-edge-notched and centre-notched plates shown in Fig. 3 are equal. Therefore, for the case of mode III, we will not differentiate between those cases and we will only use "single-edge notch" to refer to those three cases. This is not the case for plane stress/strain problems. For the cases of a double-edge-notched plate shown in Fig. 4a and a centre-notched plate shown in Fig. 4c, half of the plate can be modelled with applying proper boundary conditions along the symmetry line as shown in Fig. 4b and d, respectively. The case of a single-edge-notched plate subject to tension loading conditions was presented in Ref. [29].

4.1. Numerical verification for crack problems

4.1.1. Convergence study of mode III for a crack case

The accuracy and stability of the FFEM to compute mode III SIFs is demonstrated by carrying out a convergence study. The effects of the number of layers in the singular region (for a range of 4–20 and when $NL = \infty$), the similarity ratio (for a range of 0.1–0.9), and the number of terms of the eigenfunction series expansion used as global interpolation functions (for a range of 5–30) on the mode III SIF values of a cracked plate are investigated.

A mode III problem of a single-edge-cracked plate as shown in Fig. 5a is analysed. The aspect ratio and the ratio of the crack length to the plate width are $h/w = 3$ and $a/w = 0.4$, respectively. Six-node triangle elements (seven-point integration scheme is used for all the examples in this paper) are used to mesh the plate as shown in Fig. 5b. Also, the singular region

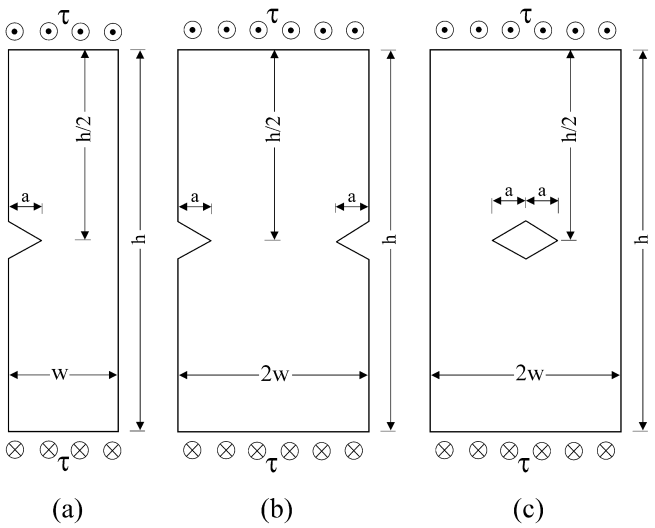

Fig. 3. (a) Central single-edge-notched, (b) central double-edge-notched, and (c) centre-notched plate subject to out-of-plane shear loading conditions.

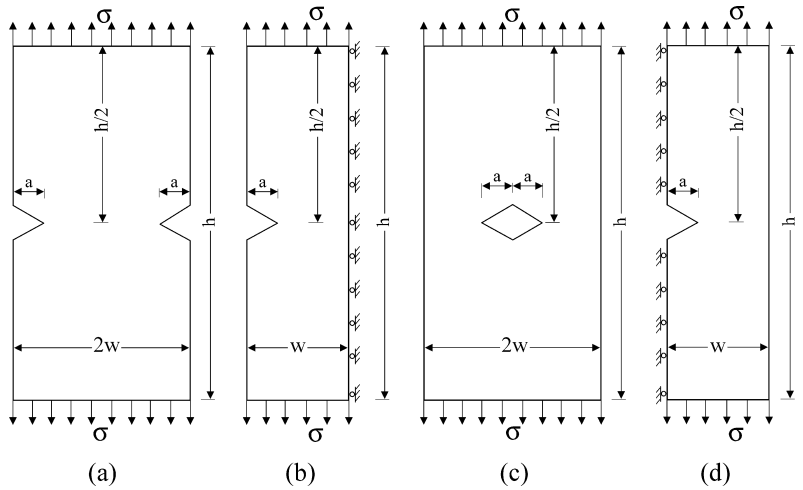

Fig. 4. (a) and (b): Central double-edge-notched plate under tension. (c) and (d): centre-notched plate under tension.

volume is held constant with increasing numbers of layers. The analytical solution of this problem exists for infinite height. The normalised SIF value is $K_{III} = 1.075$ [38].

The results are presented in Figs. 6–8. Figs. 6 and 7 show that the number of transformation terms (*NT*) does not have a significant effect on the results when $NT \geqslant 5$ for the ranges of variables (numbers of layers (*NL*), similarity ratios (ρ) and *NT*) used in this study. Also, Fig. 7 demonstrates that accurate results can be obtained by using values of similarity ratios larger than 0.5 for the ranges of variables used in this study. Moreover, it can be seen that when $NL = \infty$, larger similarity ratios (finer meshes of the singular region) are needed to obtain accurate results. Fig. 8 illustrates that the results converge asymptotically with increasing numbers of layers used to model the singular region when $\rho > 0.3$. Good results can be obtained by using ten layers or more. A similar behaviour was observed for the cases of mode I/II loading conditions [29,30].

4.1.2. Examples of single-edge-cracked plates subjected to mode III load conditions

Mode III problems of a single-edge-cracked plate are analysed for different crack lengths and different numbers of layers. The cracked plate is shown in Fig. 5a. Based on the convergence study, 10 terms of the eigenfunction series are used for the fractal transformation. The similarity ratio and the aspect ratio are $\rho = 0.6$, and $h/w = 3$, respectively. Six-node triangle elements are used to mesh the geometry of the plate as shown in Fig. 5b. The singular region volume is held constant with increasing numbers of layers.

The stress intensity factors computed for the mode III problems by the FFEM compared to corresponding published data of infinite plate height [38] are tabulated in Table 1 for different ratios of crack length to plate width and different numbers of

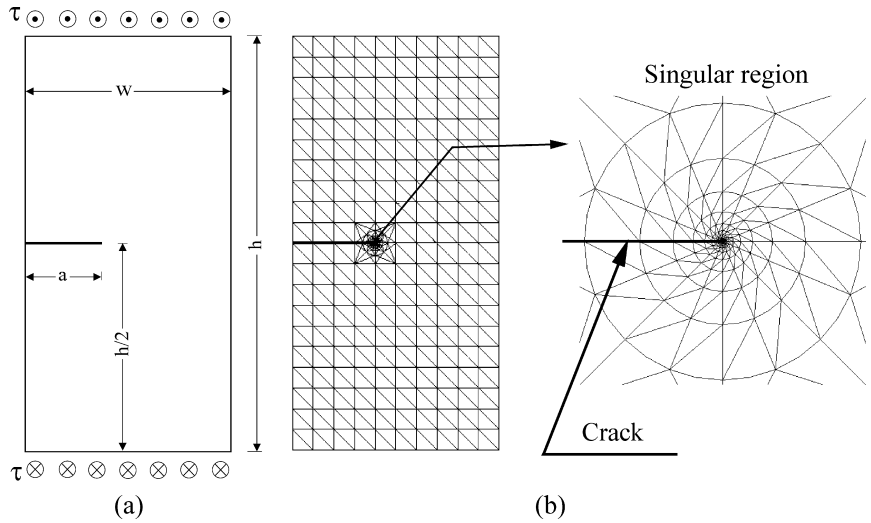

Fig. 5. (a) Central single-edge-cracked plate subject to mode III loading conditions and (b) the FE mesh used for the analyses.

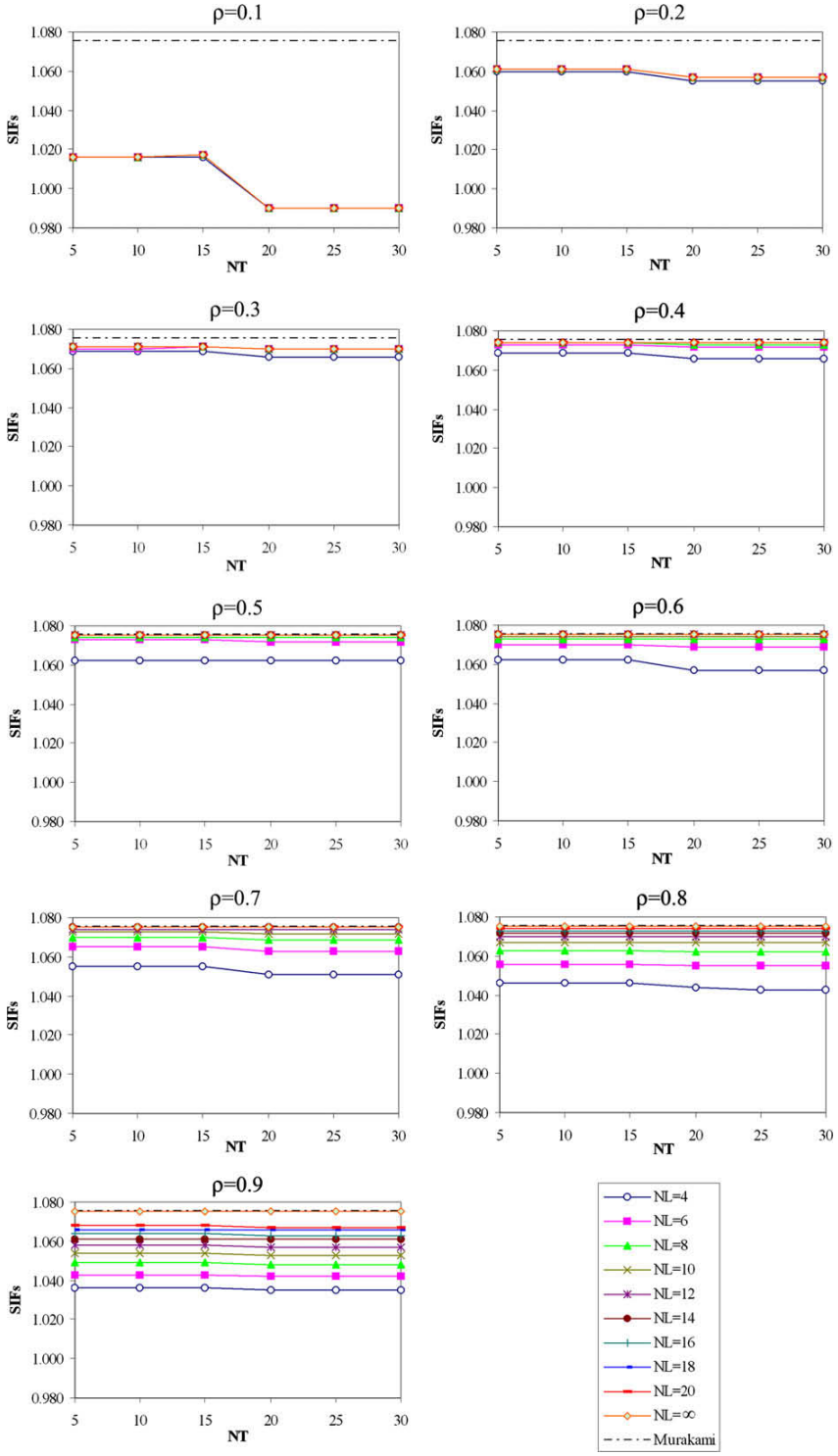

Fig. 6. Variations of SIFs with number of terms (NT) for different number of layers (NL) and similarity ratios ρ compared to corresponding published results (Murakami [38]).

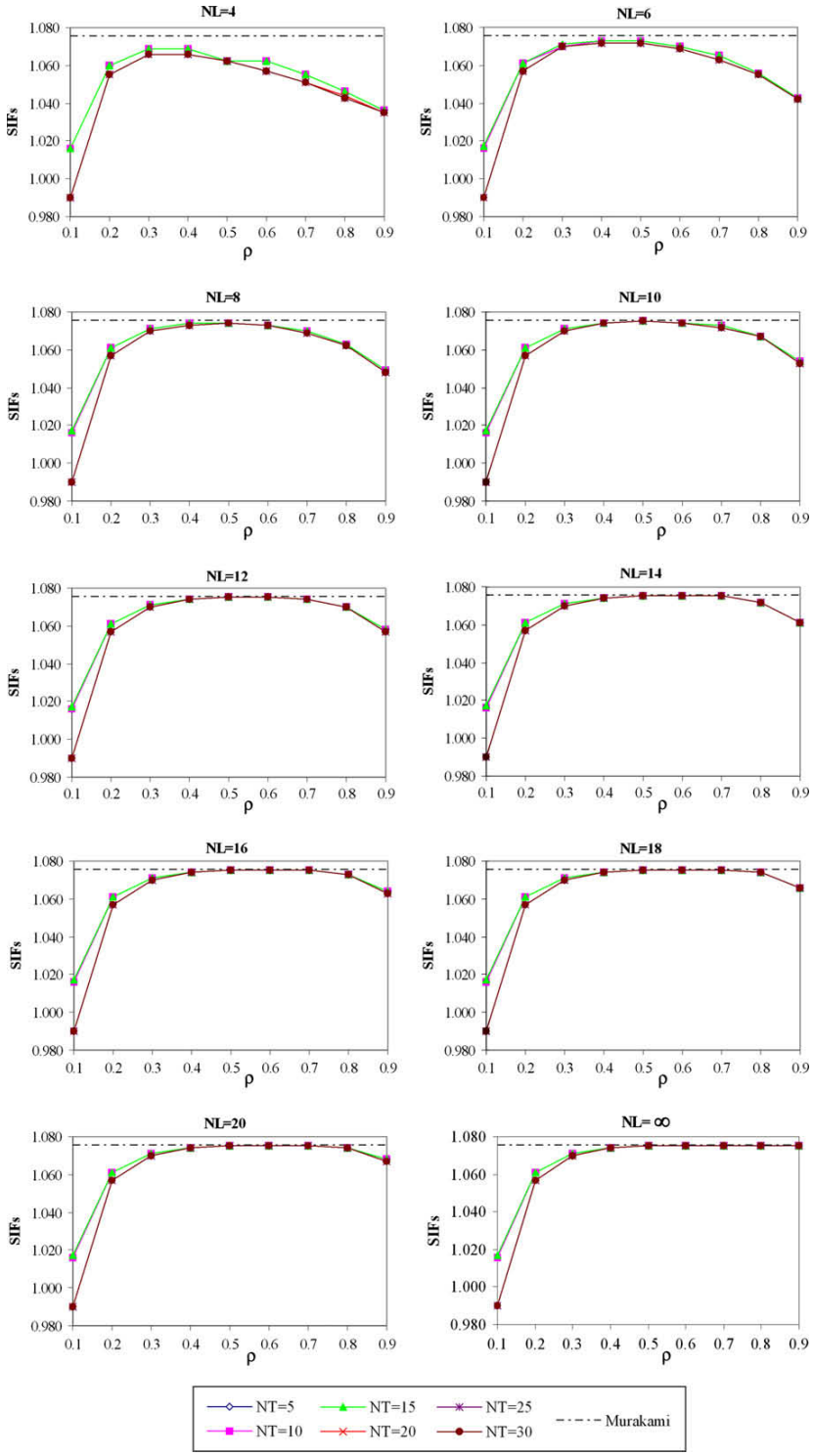

Fig. 7. Variations of SIFs with similarity ratio for different number of terms and numbers of layers compared to corresponding published results (Murakami [38]).

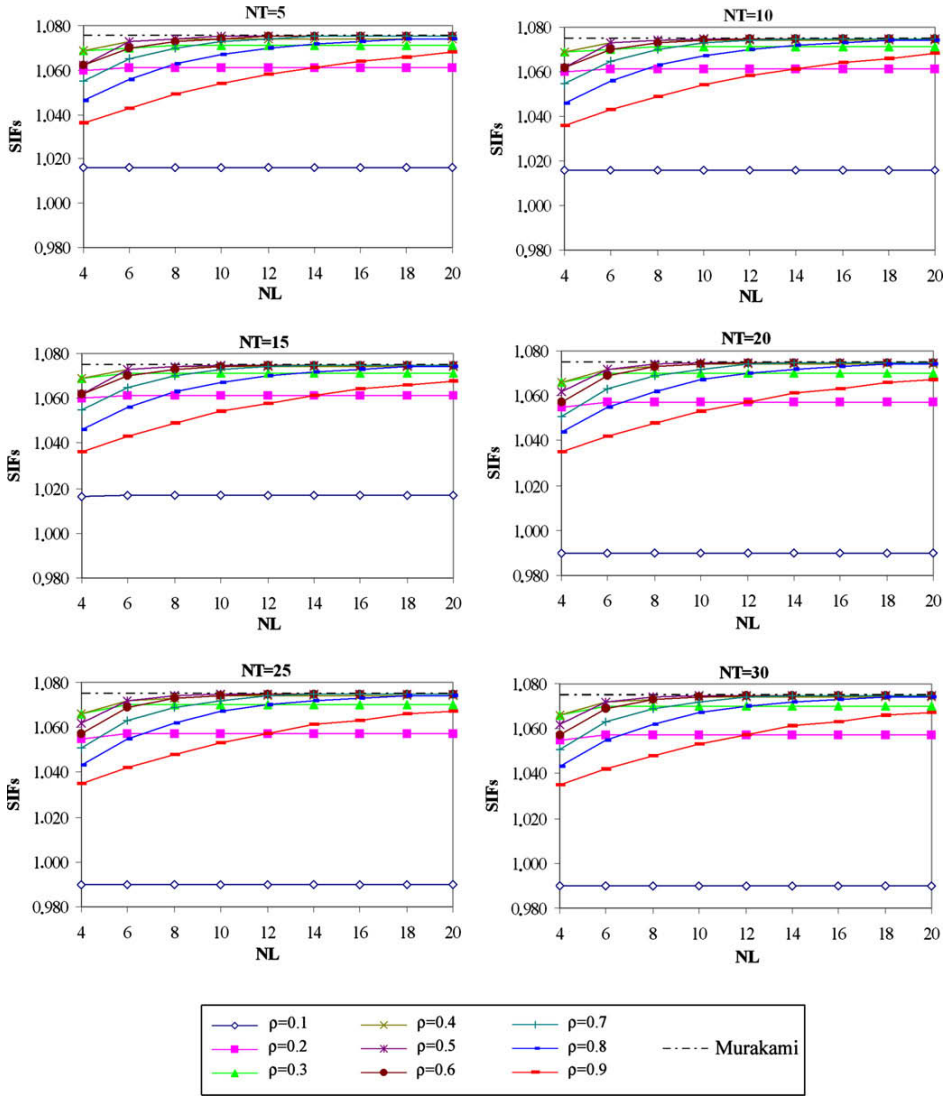

Fig. 8. Variations of SIFs with number of layers for different similarity ratios and numbers of terms compared to corresponding published results (Murakami [38]).

layers. Table 1 shows that the mode III SIF values increase with increasing ratios of crack length to plate width (a/w). The results converge asymptotically with increasing numbers of layers used to model the singular region. More importantly, Table 1 illustrates that the SIF values computed by the FFEM are in very good agreement with the published data. Therefore, the results in Table 1 prove that the eigenfunction series expansions presented in Section 3 which were derived for notch problems produce accurate results for mode III crack problems (when the notch opening angle $\gamma = 0°$).

4.1.3. Examples of off-central single-edge-cracked plates under mode III loading conditions

Many configurations of an off-central single-edge-cracked plate under mode III loading conditions as illustrated in Fig. 9 are analysed in this section. Ten terms of the eigenfunction series, 16 layers in the singular region and a similarity ratio $\rho = 0.6$ are used. Six-node triangle elements are used to mesh the geometries of the plates in a similar manner to that shown in Fig. 5b.

The values of the SIFs for mode III for many asymmetric (off-central) single-edge-cracked plates computed by the FFEM are compared to those predicted by Zhang [20] in Table 2. It can be seen from Table 2 that the FFEM results and those of Zhang [20] are in very good agreement. This again proves that the FFEM results using the eigenfunction series expansions presented in Section 3 as global interpolation functions which were derived for notch problems produce accurate results

Table 1
Mode III SIFs of a central single-edge-cracked plate for different crack lengths.

a/w	$K_{III}/\tau\sqrt{\pi}a^{1-\lambda^{III}}$				
	Murakami [38]	FFEM			
		5 layers	10 layers	15 layers	20 layers
0.1	1.004	0.996	1.003	1.004	1.004
0.2	1.017	1.009	1.016	1.017	1.017
0.3	1.040	1.032	1.039	1.040	1.040
0.4	1.075	1.067	1.074	1.075	1.075
0.5	1.128	1.120	1.127	1.128	1.128
0.6	1.208	1.199	1.207	1.208	1.208
0.7	1.336	1.325	1.335	1.336	1.336
0.8	1.565	1.552	1.563	1.564	1.564
0.9	2.113	2.094	2.111	2.112	2.112

for mode III crack problems (when the notch opening angle $\gamma = 0°$). Therefore, they can be used with confidence to produce results for notch problems as done in Section 4.2.

4.1.4. Coefficients of the higher order terms of a centre-cracked plate

The five leading coefficients of the higher order terms of the crack tip asymptotic field are obtained for a centre-cracked plate under tension. The geometrical parameters of the cracked plate are: $h/2 = w = 4$, $a = 1$. Twenty terms of the eigenfunction series, an "infinite" number of layers in the singular region, a similarity ratio $\rho = 0.9$, and six-node triangle elements are used. Only half of the plate is modelled in a similar way to that shown in Fig. 4d, and a coarse mesh is used in the regular region (four and eight elements are used along the horizontal and vertical boundaries of the plate, respectively) similar to that shown in Fig. 5b, but the singular region is meshed more finely in the circumferential direction than that of Fig. 5b.

The coefficients are tabulated in Table 3. Karihaloo and Xiao [33] provided solutions for this example by using the Hybrid Crack Element (HCE) and the Boundary Collocation Method (BCM). They also compared their results with interpolated results from Fett's solutions [39]. These published results are also tabulated in Table 3 for comparison. The current values of the coefficients are in good agreement with the published results. The biggest discrepancy occurred for the fourth coefficient computed by the HCE. However, Karihaloo and Xiao [33] computed these values by using a half-polygonal HCE to exploit the symmetry. Only mode I expansion was used in the formulation of this element. They stated that the half-polygonal HCE predicts accurate coefficients for the first three terms if only mode I expansion is used in the formulation. They found that the results deteriorated when they used both modes I and II expansions in the formulation of the half-polygonal HCE. However, they proved in the same work that using a polygonal HCE without exploiting the symmetry in the formulation gives results with good accuracy.

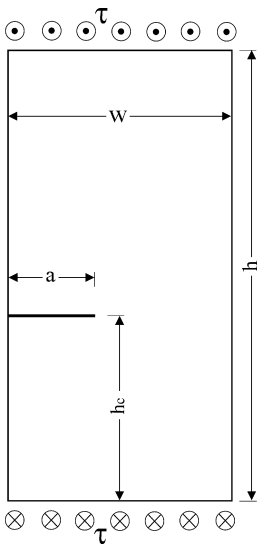

Fig. 9. Off-central single-edge-cracked plate subjected to mode III load conditions.

Table 2
Mode III SIFs ($K_{III}/\tau\sqrt{\pi}a^{1-\lambda^{III}}$) of an off-central single-edge-cracked plate.

h_c:w:h		a:w:h					
		1:w:h	2:w:h	3:w:h	4:w:h	5:w:h	6:w:h
14:12:24	FFEM	1.002	1.012	1.028	1.052	1.085	1.131
	Zhang [20]	1.003	1.013	1.030	1.053	1.085	1.125
14:10:24	FFEM	1.004	1.017	1.040	1.076	1.129	1.209
	Zhang [20]	1.004	1.018	1.041	1.076	1.124	1.189
14:8:24	FFEM	1.006	1.027	1.065	1.128	1.234	1.431
	Zhang [20]	1.006	1.027	1.065	1.123	1.209	1.331

Table 3
Coefficients for centre-cracked plate ($h/2 = w = 4$, $a = 1$) under tension.

	A_1/σ	A_2/σ	A_3/σ	A_4/σ	A_5/σ
FFEM	0.7666	−0.2794	0.1914	0.0037	−0.0293
Karihaloo and Xiao (HCE) [33]	0.7665	−0.2779	0.1915	−0.0018	−0.0235
Karihaloo and Xiao (BCM) [33]	0.768	−0.2777	0.1866	0.003	−0.0279
Fett (BCM) [39] (interpolated)	0.767	−0.276	0.188	0.0033	−0.032

4.2. Numerical examples for notch problems

4.2.1. Examples of central single-edge-notched plates subjected to mode III load conditions

Mode III problems of a central single-edge-notched plate shown in Fig. 10a are analysed for different notch angles. Different numbers of layers are used to model the singular region whose volume is held constant with increasing numbers of layers. Ten terms of the eigenfunction series are used for the fractal transformation. The aspect ratio, the ratio of the notch length to the plate width, and the similarity ratio are $h/w = 2$, $a/w = 0.4$, and $\rho = 0.6$, respectively. Six-node triangle elements are used to model the plate as shown in Fig. 10b.

The SIFs predicted by the FFEM for different notch opening angles and different numbers of layers are tabulated in Table 4. This table shows that the SIF values increase monotonically as the notch opening angle increases. Also, the results converge asymptotically with increasing numbers of layers used to model the singular region. Similar convergence was observed for the case of crack problems presented in Section 4.1. It should be noted that these results appear to be new and that there are no published data with which to compare them. However, it was shown in the previous numerical examples in Section 4.1 that using the eigenfunction series expansions presented in Section 3 as global interpolation functions which were

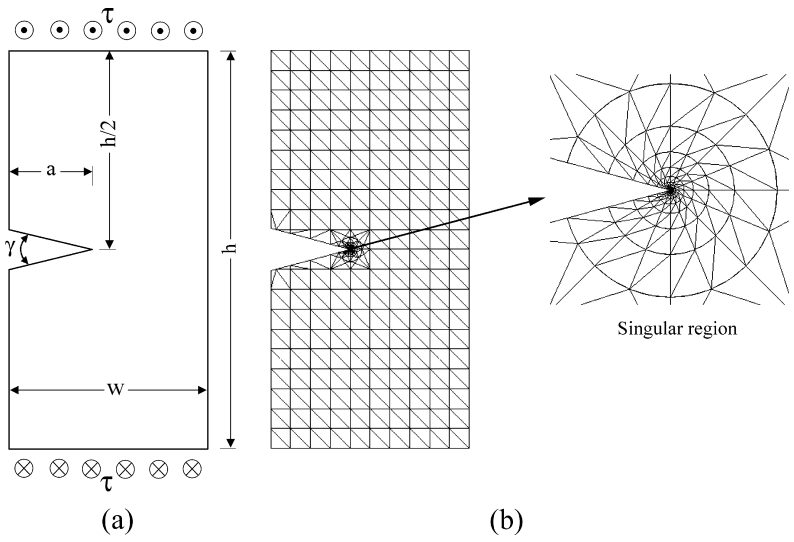

Fig. 10. (a) Central single-edge-notched plate subject to mode III loading conditions and (b) the FE mesh used for the analyses.

Table 4
Mode III SIFs ($K_{III}/\tau\sqrt{\pi}a^{1-\lambda^{III}}$) of a central single-edge-notched plate for various notch angles and different numbers of layers ($h/w = 2$, $a/w = 0.4$).

γ (°)	*NL*		
	10 layers	16 layers	20 layers
0	1.076	1.077	1.077
30	1.233	1.233	1.233
60	1.417	1.417	1.417
90	1.628	1.628	1.628
120	1.859	1.859	1.859

derived for notch problems produced accurate results for mode III crack problems (when the notch angle $\gamma = 0°$). Therefore, it can be assumed that the results in Table 4 are valid.

4.2.2. Examples of off-central single-edge-notched plates subject to mode III load conditions

Many problems of an off-central single-edge-notched plate under mode III loading conditions as illustrated in Fig. 11a are investigated. The number of terms of the eigenfunction series, the number of layers in the singular region, the similarity ratio, and the aspect ratio are $nt = 20$, $nl = 16$, $\rho = 0.6$, and $h/w = 2$, respectively. Six-node triangle elements are used to model the notched plates as shown in Fig. 11b.

The mode III SIFs for different notch positions are tabulated for different notch opening angles and for a ratio of the notch length to the plate width $a/w = 0.4$ in Table 5, and for a notch opening angle $\gamma = 50°$ and for various ratios of the notch length

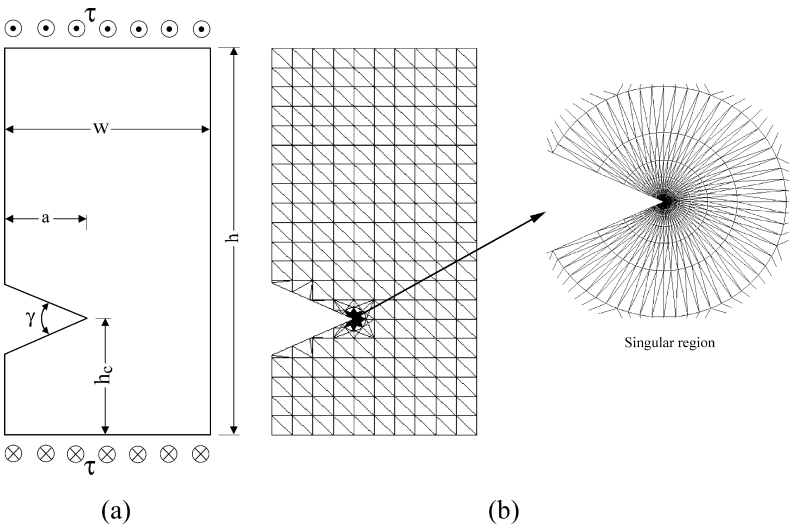

Fig. 11. (a) Off-central single-edge-notched plate under mode III loading conditions and (b) the FE mesh used for the analyses.

Table 5
Mode III SIFs ($K_{III}/\tau\sqrt{\pi}a^{1-\lambda^{III}}$) of off-central single-edge-notched plate for various notch angles and notch positions ($h/w = 2$, $a/w = 0.4$).

γ (°)	h_c/h				
	0.1	0.2	0.3	0.4	0.5
0	1.243	1.116	1.086	1.079	1.077
10	1.303	1.168	1.136	1.128	1.126
20	1.368	1.223	1.189	1.180	1.178
30	1.437	1.281	1.245	1.235	1.233
40	1.511	1.343	1.304	1.293	1.291
50	1.590	1.408	1.366	1.355	1.352
60	–	1.477	1.431	1.419	1.417
70	–	1.550	1.500	1.487	1.484
80	–	1.627	1.572	1.558	1.555
90	–	–	1.647	1.631	1.628

Table 6
Mode III SIFs ($K_{III}/\tau\sqrt{\pi}a^{1-\lambda^{III}}$) of off-central single-edge-notched plate for various notch positions and notch lengths ($h/w = 2$, $\gamma = 50°$).

a/w	h_c/h				
	0.1	0.2	0.3	0.4	0.5
0.1	1.282	1.253	1.248	1.247	1.247
0.2	1.373	1.288	1.271	1.267	1.266
0.3	1.479	1.340	1.310	1.302	1.300
0.4	1.590	1.408	1.366	1.355	1.352
0.5	–	1.495	1.447	1.434	1.431

to the plate width in Table 6. The missing values in those tables are due to the fact that the geometry of the plate is no more rectangular (the top and bottom boundaries are no more equal and the notch faces have unequal lengths).

Table 5 shows that the SIFs monotonically increase as the notch opening angle increases. Also, the values of the SIFs increase as the notch gets closer to the bottom boundary of the plate. The minimum values of the SIFs occur when the notch is on the centre line and the notch opening angle is 0°. In Table 6, it can be seen that the SIFs for a single-edge-notched plate with a notch opening angle $\gamma = 50°$ increase as the notch length increases and as the notch gets closer to the bottom boundary of the plate.

It should be noted that most of the results in this section appear to be new and that there are no published SIF values available with which to compare them. To assess the accuracy of the results, two meshes of the singular region as shown in Figs. 10b and 11b were investigated. The differences in the results were much less than 1%. Also, it was shown in the previous examples that using the eigenfunction series expansions presented in Section 3 as global interpolation functions which were derived for notch problems produced accurate results for mode III crack problems (when the notch angle $\gamma = 0°$). Consequently, it can be assumed that the results in Tables 5 and 6 are valid. The results reported in these tables are obtained by using the denser mesh of the singular region illustrated in Fig. 11b.

4.2.3. Examples of central double-edge-notched and centre-notched plates subject to tension load conditions

A central double-edge-notched plate shown in Fig. 4a and a centre-notched plate shown in Fig. 4c are investigated for different notch lengths and different notch opening angles. Only half of the plate is analysed after applying the appropriate boundary conditions along the symmetry line as shown in Fig. 4b and d. The number of terms of the eigenfunction series, the number of layers in the singular region, the similarity ratio, and the aspect ratio are $nt = 20$, $nl = 16$, $\rho = 0.6$, and $h/2w = 2$, respectively. Six-node triangle elements are used to model the notched plates as shown in Fig. 12.

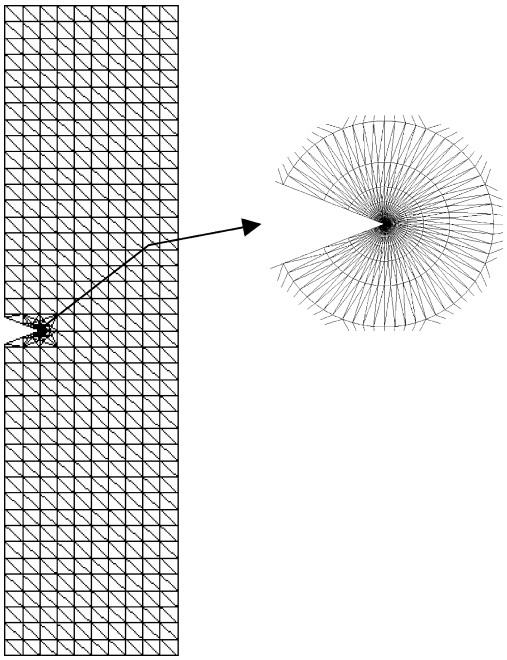

Fig. 12. The FE mesh used for the analyses of double-edge- and centre-notched plates.

Table 7
Mode I SIFs ($K_I/\sigma\sqrt{\pi}a^{1-\lambda^I}$) of central double-edge-notched plate for various notch lengths and notch opening angles ($h/2w = 2$).

γ (°)	a/w				
		0.2	0.4	0.6	0.8
0	FFEM	1.111	1.132	1.236	1.573
	Tada [40]	1.118	1.132	1.226	1.567
30	FFEM	1.122	1.143	1.248	1.586
	Chen [19]	1.123	1.145	1.251	1.604
45	FFEM	1.125	1.153	1.261	1.602
	–	–	–	–	–
60	FFEM	1.165	1.191	1.300	1.650
	Chen [19]	1.176	1.199	1.309	1.672
90	FFEM	1.302	1.323	1.442	1.850
	Chen [19]	1.298	1.323	1.445	1.864

Table 8
Mode I SIFs ($K_I/\sigma\sqrt{\pi}a^{1-\lambda^I}$) of centre-notched plate for various notch lengths and notch opening angles ($h/2w = 2$).

γ (°)	a/w				
		0.2	0.4	0.6	0.8
0	FFEM	1.024	1.109	1.303	1.814
	Tada [29]	1.024	1.109	1.303	1.814
30	FFEM	1.053	1.151	1.375	1.959
45	FFEM	1.067	1.184	1.433	2.072
60	FFEM	1.131	1.261	1.547	2.283
90	FFEM	1.321	1.497	1.923	3.018

The SIF values for central double-edge- and centre-notched plates compared to the available published results are tabulated in Tables 7 and 8, respectively. The SIFs presented in those tables increase with increasing ratios of notch length to plate width and with increasing notch opening angles. Also, it can be seen that the FFEM results are in very good agreement with the published results.

4.2.4. Examples of off-central double-edge-notched and off-centre-notched plates subject to tension load conditions

Many problems of off-central double-edge-notched plates and off-centre-notched plates shown in Fig. 13 are analysed for different notch opening angles and different notch positions. Only half of the off-central double-edge- or off-centre-notched plate is analysed after applying the appropriate boundary conditions along the symmetry line in a similar way to those

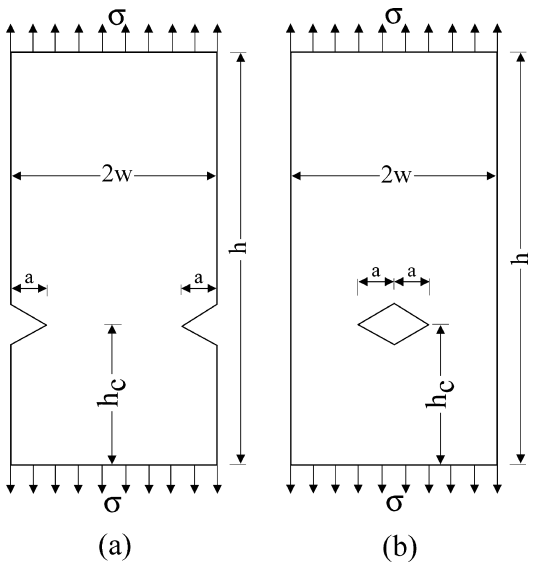

Fig. 13. (a) Off-central double-edge-notched and (b) off-centre-notched plate under tension.

Table 9
Normalised modes I and II SIFs of off-central double-edge-notched plate for various notch positions and notch opening angles ($h/2w = 2$, $a/w = 0.4$).

γ (°)	h_c/h									
	0.1		0.2		0.3		0.4		0.5	
	K_I	K_{II}	K_I	K_{II}	K_I	K_{II}	K_I	K_{II}	K_I	K_{II}
0	1.930	0.377	1.295	0.096	1.163	0.023	1.136	0.004	1.132	0.000
30	1.949	0.511	1.306	0.131	1.174	0.031	1.147	0.006	1.143	0.001
45	1.993	0.599	1.321	0.154	1.184	0.037	1.157	0.007	1.153	0.001
60	2.047	0.703	1.361	0.180	1.223	0.044	1.195	0.009	1.191	0.001
90	2.250	1.023	1.503	0.248	1.355	0.059	1.327	0.012	1.323	0.002

Table 10
Normalised modes I and II SIFs of off-centre-notched plate for various notch positions and notch opening angles ($h/2w = 2$, $a/w = 0.4$).

γ (°)	h_c/h									
	0.1		0.2		0.3		0.4		0.5	
	K_I	K_{II}	K_I	K_{II}	K_I	K_{II}	K_I	K_{II}	K_I	K_{II}
0	1.564	0.174	1.219	0.039	1.132	0.011	1.112	0.003	1.109	0.000
30	1.677	0.333	1.285	0.072	1.181	0.021	1.155	0.005	1.151	0.001
45	1.763	0.446	1.337	0.098	1.219	0.029	1.189	0.007	1.184	0.001
60	1.880	0.577	1.440	0.132	1.304	0.042	1.267	0.011	1.261	0.002
90	2.185	0.835	1.759	0.228	1.572	0.081	1.510	0.022	1.499	0.003

shown in Fig. 4b and d. The number of terms of the eigenfunction series, the number of layers in the singular region, the similarity ratio, the aspect ratio, and the ratio of the notch length to the plate half width are $nt = 20$, $nl = 16$, $\rho = 0.6$, $h/2w = 2$, and $a/w = 0.4$, respectively. Six-node triangle elements are used to model the notched plates in a similar way to that shown in Fig. 12.

Tables 9 and 10 show the SIF values computed by the FFEM for the off-central double-edge-notched and off-centre-notched plates, respectively. The values of the SIFs increase as the notch opening angle increases and as the notches move closer to the bottom/top boundary of the plate. The minimum values occur when the notches are on the horizontal symmetry line and the notch opening angle $\gamma = 0°$. The mode II occurs in these examples because of the asymmetry of the plate geometry.

5. Conclusions

In this paper, the Fractal-like Finite Element Method was extended to analyse double-edge- and centre-notched plates under anti-plane shear (mode III) or tension (mode I) loading conditions. In the FFEM, the large number of unknowns in the singular region is reduced significantly by using global interpolation functions. Exact analytical solutions of the displacement field around a notch tip are employed as the global interpolation functions; consequently, the stress intensity factors and the coefficients of the higher order terms of a notch tip asymptotic field become primary unknowns of the problem. Therefore, no post-processing technique to extract the stress intensity factors is needed. Moreover, special singular finite elements to model the singular region are not required.

The accuracy and the robustness of the method were tested via many examples of notch/crack problems. The stress intensity factor values produced in this study for cases for which published results exist were in very good agreement with those available corresponding published data. Many new results of notched plate problems were also presented.

References

[1] Seweryn A. Brittle fracture criterion for structures with sharp notches. Engng Fract Mech 1994;47:673–81.
[2] Dunn ML, Suwito W, Cunningham S. Stress intensities at notch singularities. Engng Fract Mech 1997;57(4):417–30.
[3] Knésl Z. A criterion of V-notch stability. Int J Fract 1991;48:R79–83.
[4] Gómez FJ, Elices M. A fracture criterion for sharp V-notched samples. Int J Fract 2003;123:163–75.
[5] Carpinteri A, Cornetti P, Pugno N, Sapora A, Taylor D. A finite fracture mechanics approach to structures with sharp V-notches. Engng Fract Mech 2008;75:1736–52.
[6] Gross B, Mendelson A. Plane elastostatic analysis of V-notched plates. Int J Fract 1972;8:267–76.
[7] Williams ML. Stress singularities resulting from various boundary conditions in angular corners of plates in extension. ASME J Appl Mech 1952;19:526–8.
[8] Tong P, Pian THH. On the convergence of the FEM for problems with singularity. Int J Solids Struct 1973;9:313–21.
[9] Lin KY, Tong P. Singular finite elements for the fracture analysis of V-notched plates. Int J Numer Meth Engng 1980;15:1343–54.
[10] Sinclair GB, Okajima M, Griffin JH. Path independent integrals for computing stress intensity factors at sharp notches in elastic plates. Int J Numer Meth Engng 1984;20:999–1008.

[11] Stern M, Soni ML. On the computation of stress intensities at fixed-free corners. Int J Solids Struct 1976;12:331–7.
[12] Stern M, Becker EB, Dunham RS. A contour integral computation of mixed-mode stress intensity factors. Int J Fract 1976;12:359–68.
[13] Carpenter WC. A collocation procedure for determining fracture mechanics parameters at a corner. Int J Fract 1984;24:255–66.
[14] Carpenter WC. The eigenvector solution for a general comer or finite opening crack with further studies on the collocation procedure. Int J Fract 1985;27:63–74.
[15] Babuška I, Miller A. The post-processing approach in the finite element method – part 1: calculation of displacements stresses and other higher derivatives of displacements. Int J Numer Meth Engng 1984;20:1085–109.
[16] Babuška I, Miller A. The post-processing approach in the finite element method-part 2 calculation of the stress intensity factors. Int J Numer Meth Engng 1984;20:1111–29.
[17] Portela A, Aliabadi MH, Rooke DP. Efficient boundary element analysis of sharp notched plates. Int J Numer Meth Engng 1991;32:445–70.
[18] Zhao Z, Hahn HG. Determining the SIF of a v-notch from the results of a mixed-mode crack. Engng Fract Mech 1992;43(4):511–8.
[19] Chen D-H. Stress intensity factors for V-notched strip under tension or in-plane bending. Int J Fract 1995;70:81–97.
[20] Zhang XS. The general solution of an edge crack off the center line of a rectangular sheet for mode III. Engng Fract Mech 1988;31(5):847–55.
[21] Leung AYT, Tsang KL. Mode III two-dimensional crack problem by two-level finite element method. Int J Fract 2000;102:245–58.
[22] Noda N-A, Takase Y. Generalized stress intensity factors of V-shaped notch in a round bar under torsion, tension, and bending. Engng Fract Mech 2003;70:1447–66.
[23] Mote CD. Global-local finite element. Int J Numer Meth Engng 1971;3:565–74.
[24] Leung AYT, Su RKL. Mode I crack problems by fractal two level finite element method. Engng Fract Mech 1994;48(6):847–56.
[25] Leung AYT, Su RKL. Mixed-mode two-dimensional crack problem by fractal two level finite element method. Engng Fract Mech 1995;51(6):889–95.
[26] Leung AYT, Su RKL. Two-level finite element study of axisymmetric cracks. Int J Fract 1998;89:193–203.
[27] Leung AYT, Su RKL. Eigenfunction expansion for penny-shaped and circumferential cracks. Int J Fract 1998;89:205–22.
[28] Treifi M, Tsang DKL, Oyadiji SO. Applications of the fractal-like finite element method to sharp notched plates. In: Proceedings of the ASME 2007 international design engineering technical conferences and computers and information in engineering conference IDETC/CIE, Las Vegas, Nevada, USA; 2007.
[29] Treifi M, Oyadiji SO, Tsang DKL. Computation of the stress intensity factors of sharp notched plates by the fractal-like finite element method. Int J Numer Meth Engng 2009;77:558–80.
[30] Treifi M, Oyadiji SO, Tsang DKL. Computations of modes I and II stress intensity factors of sharp notched plates under in-plane shear and bending loading by the fractal-like finite element method. Int J Solids Struct 2008;45:6468–84.
[31] Karihaloo BL, Xiao QZ. Accurate determination of the coefficient of elastic crack tip asymptotic field by a hybrid crack element with p-adaptivity. Engng Fract Mech 2001;68:1609–30.
[32] Tong P, Pian THH, Lasry SJ. A hybrid-element approach to crack problems in plane elasticity. Int J Numer Meth Engng 1973;7:297–308.
[33] Xiao QZ, Karihaloo BL, Liu XY. Direct determination of SIF and higher order terms of mixed mode cracks by a hybrid crack element. Int J Fract 2004;125:207–25.
[34] Xiao QZ, Karihaloo BL. An overview of a hybrid crack element and determination of its complete displacement field. Engng Fract Mech 2007;74:1107–17.
[35] Wolf JP. The scaled boundary finite element method. Chichester: Wiley; 2003.
[36] Chidgzey SR, Deeks AJ. Determination of coefficients of crack tip asymptotic fields sing the scaled boundary finite element method. Engng Fract Mech 2005;72:2019–36.
[37] Vasilopoulos D. On the determination of higher order terms of singular elastic stress fields near corners. Numer Math 1988;53:51–95.
[38] Murakami Y. Stress intensity factors handbook. Oxford: Pergamon Press; 1987.
[39] Fett T. T-stress solutions and stress intensity factors for 1-D cracks. Düsseldorf: VDI Verlag; 2002.
[40] Tada H, Paris PC, Irwin GR. The stress analysis of cracks handbook. 3rd ed. New York: ASME; 2000.

Chapter 9

Evaluation of Mode III Stress Intensity Factors for Bi-material Notched Bodies Using the Fractal-like Finite Element Method

Computers and Structures 2013;

http://dx.doi.org/10.1016/j.compstruc.2013.02.015

ARTICLE IN PRESS

Computers and Structures xxx (2013) xxx–xxx

Contents lists available at SciVerse ScienceDirect

Computers and Structures

journal homepage: www.elsevier.com/locate/compstruc

Evaluation of mode III stress intensity factors for bi-material notched bodies using the fractal-like finite element method

Muhammad Treifi, S. Olutunde Oyadiji *

School of Mechanical, Aerospace and Civil Engineering, University of Manchester, Manchester M13 9PL, UK

ARTICLE INFO

Article history:
Received 5 October 2012
Accepted 18 February 2013
Available online xxxx

Keywords:
Stress intensity factors
Strain energy
Bi-material
V-notch
Fractal-like finite element method
Fracture mechanics

ABSTRACT

The fractal-like finite element method (FFEM) is extended to compute the stress intensity factors (SIFs) for bi-material notched bodies subject to anti-plane shear loading. The notched bodies are formed by bonding two materials together (isotropic-isotropic/isotropic-orthotropic). Also, a strain energy-based approach is developed and used to compute mode III SIFs for a bi-material notch using standard finite element (FE) commercial packages for comparison with corresponding data produced using the FFEM. Various numerical results for bi-material cracked/notched bodies under anti-plane shear are presented to demonstrate the accuracy and efficiency of the FFEM. Many new results for bi-material notched bodies are also introduced.

1. Introduction

Stress intensity factors (SIFs) characterise the stress, strain, and displacement fields in the crack/notch tip region and have a significant function in virtually all fracture problems. For example, in failure design studies, it is necessary to accurately evaluate SIFs in order to determine fracture parameters such as the critical crack length, the fracture loads and the service life of a structural component. Fast, reliable and accurate computations of SIFs are often necessary in practical applications such as in the design of new structures or in the assessment of the integrity of existing structures. This is especially true for high integrity structures such as nuclear reactor cores, aircraft, submarines and spacecraft. Another area of major application is in welded structures.

The study of stress intensities at a corner/notch is of high importance, because the presence of corners in a structure may result in crack initiation leading to a structural failure or shortening of the service life of the structure. The importance is even higher in the case of composite bodies, which comprise isotropic materials joined together, because it could be used to evaluate the adhesive strength. Therefore, much effort and research has been devoted to the analysis of sharp notch problems. However, most of the cases available in the literature are about in-plane homogeneous notch problems.

In linear elastic fracture mechanics, it is well known that the stresses around a notch tip are singular. Williams [1] investigated the analytical form of these singularities. He found that the stresses in a homogeneous notched body become infinite at the notch tip under any boundary conditions. Seweryn [2] demonstrated that simple failure criteria based on the notch SIFs exist, at least for brittle fracture. Failure occurs when the notch SIFs reach critical values. Other researchers who tried to establish a failure criterion for a notch are Knésl [3], Gómez and Elices [4], and Carpinteri et al. [5].

Many researchers have developed various methods and procedures to compute the SIFs for a notch. Gross and Mendelson [6] calculated the SIFs for many notch cases of modes I and II by means of a boundary collocation method. Lin and Tong [7] developed singular finite elements for the analysis of V-notched plates. Carpenter [8] presented a collocation procedure to compute SIFs for notch problems based on the contour integral of Stern et al. [9]. Babuška and Miller [10] developed post-processing approaches to extract the generalised SIFs near corner points from a finite element solution. Zhao and Hahn [11] predicted the SIFs of a notch problem from the SIFs of a crack problem. Chen [12] computed the SIFs of notched plates by means of the body force method.

Other researchers developed semi-analytical methods such as the hybrid crack element (HCE), the scaled boundary finite element method (SBFEM), and the fractal-like finite element method (FFEM). The HCE was developed by Tong et al. [13] to compute the SIFs for plane cracks. Wolf [14] developed the SBFEM, which is a numerical finite element-based procedure in the circumferential directions and an analytical procedure in the radial direction. The FFEM is based on the concept of global–local interpolation functions [15]. Su and co-authors [16–19] developed the FFEM to

* Corresponding author. Tel.: +44 161 275 4348.
E-mail addresses: m.treifi@mmu.ac.uk (M. Treifi), s.o.oyadiji@manchester.ac.uk (S.O. Oyadiji).

0045-7949/$ - see front matter © 2013 Elsevier Ltd. All rights reserved.
http://dx.doi.org/10.1016/j.compstruc.2013.02.015

compute the SIFs for various crack problems only. Recently Treifi et al. [20–24] have extended the FFEM to analyse homogeneous notch problems. They presented many results concerning homogeneous notched plates subjected to mode I, mode II, or mode III loading conditions.

Most of the aforementioned research work was concerned only with homogeneous crack and/or notch problems. For bi-material cases, which are more complicated, researchers such as Theocaris [25], Dempsey and Sinclair [26], and Hein and Erdogan [27], among others, studied the stress and displacement fields and investigated the behaviour of the singular eigenvalues for bi-material notches. The case of an interfacial crack problem, which is a special case of a bi-material notch problem, has been investigated by many researchers. Lin and Mar [28] constructed a hybrid crack element to compute SIFs for cracks in bi-materials. Yau and Wang [29] used a procedure that involves known auxiliary solutions and evaluation of conservation integrals along a suitably selected remote path. Lee and Choi [30] computed the SIFs for interfacial cracks using a boundary element method which employed the multi-region technique and the double-point concept. Matsumto et al. [31] evaluated the SIFs of interface cracks using a concept based on the interaction energy release rates.

Results for stress intensities for bi-material notch problems were reported by few researchers, due to their complexity. Carpenter and Byers [32] investigated bi-material notch problems by using the reciprocal work contour integral method. Tan and Meguid [33] presented a singular finite element to compute the SIFs of a notch formulated by using explicit expressions for the singular stress and displacement fields of a general bi-material wedge. Chen and Sze [34] developed a hybrid-stress finite element model in which the asymptotic stress and displacement fields embedded into the wedge-tip element were numerically obtained. All of this research work was concerned with only the in-plane problems, i.e. modes I and II.

The most general case of loading on a notched body can be described by means of superposition of the results of modes I, II and III. Therefore, the case of anti-plane shear, i.e. mode III, in bi-material crack/notch problems is necessary to describe the most general case of loading on a notched body. Wu and Chiu [35] computed the SIFs for interface cracks in bi-materials under anti-plane shear by using a complex-variable formulation based on the solutions of a dislocation and a body force in an infinite composite body. Other researchers who studied the case of a bi-material crack under anti-plane shear loading conditions are, among others, Lee and Earmme [36], Li [37], and Li and Duan [38]. The general case of anti-plane notch was investigated by Jun and Yuqiu [39] by using a Sub-Region Mixed FEM. They provided very limited examples of a notch in a disk. Liu and Chue [40] examined the stress singularity orders in dissimilar anisotropic wedges. Ma and Hour [41] concluded that the order of singularity for the anti-plane dissimilar anisotropic notch problem is always real.

In this paper, the mode III stress and displacement expressions around a bi-material notch tip are derived analytically and employed as global interpolation functions to extend the FFEM to compute the SIFs for anti-plane bi-material notch problems. The FFEM brings together the agility of the finite element method (FEM) and the accuracy of the exact analytical solutions. It is well known that in order to improve the convergence of finite element solutions for problems with singularities, it is necessary to discretise the singular regions around the singular points using very fine meshes. This leads to a large number of unknowns and a considerable increase of the computational cost. In the FFEM, the employment of the exact analytical solutions of the displacement field around a notch tip as global interpolation functions to transform the large number of nodal displacements around a notch tip into a small set of generalised co-ordinates reduces the computational cost significantly. Also, the SIFs and the coefficients of the higher order terms of the notch tip asymptotic field are generalised co-ordinates and are computed directly. Therefore, no post-processing is required to extract them. Moreover, no special singular finite elements are needed to model the singular region around a notch tip—conventional finite elements can be used to model the whole of the cracked/notched body. The implementation of the FFEM involves simple matrix multiplication. No complicated mathematics is involved.

Various numerical examples of bi-material notch problems subject to anti-plane shear loading conditions are presented. The accuracy of the FFEM results is demonstrated by comparison with available results for anti-plane bi-material crack problems, as crack problems are special cases of notch problems. Also, many bi-material crack problems results are compared to values predicted by the commercial FE package ABAQUS [42]. Results for bi-material notch problems are not available and current commercial FE packages are generally not able to predict the SIFs for a notch. Therefore, an approach based on the strain energy (SE) of a finite volume surrounding the notch tip is developed and used to predict the SIF values for a notch subject to mode III loading conditions. ABAQUS is used to compute the strain energy, and the approach presented in Section 4 is used to extract the SIFs for notch problems. The FFEM results are in very good agreement with the available published results and the numerical results computed and/or extracted using commercial FE packages. Most of the results for anti-plane bi-material notch cases presented in this paper appear to be new.

2. Formulation of the FFEM

For the sake of brevity and completeness, only a short description of the FFEM formulation is presented in this section. One may refer to Leung and Su [16–19] or Treifi et al. [21–23] for a detailed description. In the FFEM, a notched/cracked body is divided into singular and regular regions as shown in Fig. 1. The whole body is modelled using any conventional finite elements. However, the singular region is discretised using a very fine mesh generated layer by layer in a fractal-like self-similar manner as illustrated in Fig. 2. It should be noted from this figure that the fractal self-similar nature of the mesh applies to the radial direction towards the notch/crack tip but not to the hoop direction. For this reason, the topology is referred to as being fractal-like. Also, the fractals used are deterministic rather than stochastic as clearly shown by Fig. 2. The resulting large number of nodal displacements in the singular region is then transformed into a small set of generalised co-ordinates using global interpolation functions. This concept is based on the idea of local-cum-global interpolation. The local interpolation functions (shape functions) reduce the infinite

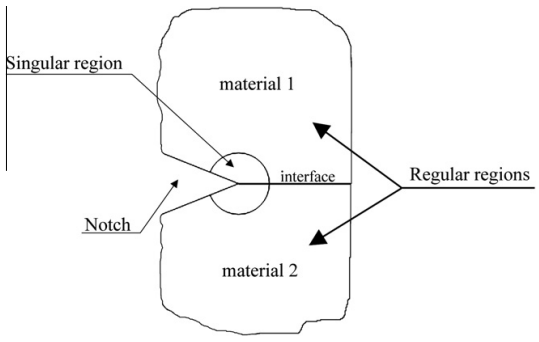

Fig. 1. Regular and singular regions of a bi-material notched body.

Please cite this article in press as: Treifi M, Oyadiji SO. Evaluation of mode III stress intensity factors for bi-material notched bodies using the fractal-like finite element method. Comput Struct (2013), http://dx.doi.org/10.1016/j.compstruc.2013.02.015

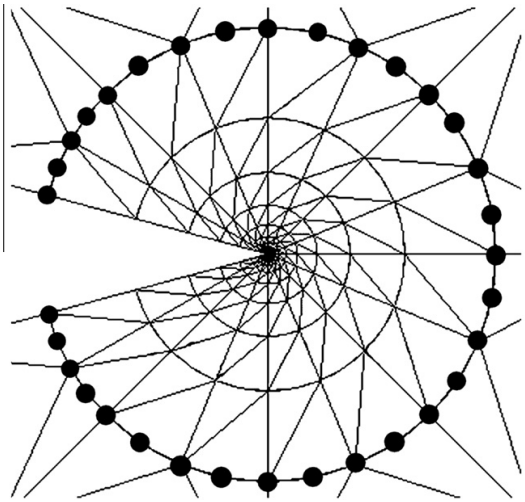

Fig. 2. Mesh in a singular region (master nodes highlighted).

number of degrees of freedom of a continuum to a finite number of degrees of freedom related to the nodes of the continuous element. Similarly, the global interpolation functions can be used to reduce the number of nodal unknowns to a small number of unknowns. This process reduces the number of unknowns of the problem significantly, and consequently the computational cost.

The layers of finite elements in the singular region are generated by using the notch/crack tip as a centre of similarity and assuming a similarity ratio (ρ). All the nodes inside the singular region are considered slave nodes, while the ones on the line that separates the regular and singular regions are considered master nodes as illustrated in Fig. 2. By utilising the properties of the self-similar two-dimensional isoparametric finite elements; i.e. the stiffness matrices of two-dimensional isoparametric finite elements of similar shapes are the same [16]; the stiffness matrices of the inner layers can be computed from only the stiffness matrix of the first layer in the singular region. Therefore, the generalised stiffness matrix of the singular region becomes a sum of a geometric series, allowing the use of theoretically infinite number of layers in the singular region [23].

The static equilibrium equation in the conventional FEM can be written as

$$\mathbf{K}\mathbf{d} = \mathbf{f} \tag{1}$$

where $\mathbf{K}$ is the stiffness matrix, $\mathbf{d}$ is the nodal displacement vector, and $\mathbf{f}$ is the nodal force vector.

The nodal displacements of the nodes in the singular region can be transformed into a small vector of generalised co-ordinates by using global interpolation functions; that is, for the nth layer:

$$\mathbf{d}_s^n = \mathbf{T}_s^n \mathbf{a} \tag{2}$$

where $\mathbf{d}_s^n$ is the nodal displacement vector of the nodes in the nth layer in the singular region, $\mathbf{T}_s^n$ is the transformation matrix of the nth layer, and $\mathbf{a}$ is the vector of generalised co-ordinates. After the transformation process is applied, Eq. (1) can be rewritten as

$$\begin{bmatrix} \mathbf{K}_{rr} & \mathbf{K}_{rm} & 0 \\ \mathbf{K}_{mr} & \mathbf{K}_{mm} + \mathbf{K}_{mm}^{1st} & \overline{\mathbf{K}}_{ms}^{1st} \\ 0 & \overline{\mathbf{K}}_{sm}^{1st} & \overline{\mathbf{K}}_{ss}^{1st} + \overline{\mathbf{K}}_{s}^{inn} \end{bmatrix} \begin{Bmatrix} \mathbf{d}_r \\ \mathbf{d}_m \\ \mathbf{a} \end{Bmatrix} = \begin{Bmatrix} \mathbf{f}_r \\ \mathbf{f}_m + \mathbf{f}_m^{1st} \\ \bar{\mathbf{f}}_s^{1st} + \bar{\mathbf{f}}_s^{inn} \end{Bmatrix} \tag{3}$$

where

$$\overline{\mathbf{K}}_{ms}^{1st} = \mathbf{K}_{ms}^{1st} \mathbf{T}_s^{1st}$$

$$\overline{\mathbf{K}}_{s}^{inn} = \sum_{n=2}^{nl} \overline{\mathbf{K}}_s^n,$$

$$\overline{\mathbf{K}}_s^n = \mathbf{T}_s^{n^T} \mathbf{K}_s^n \mathbf{T}_s^n,$$

$$\bar{\mathbf{f}}_s^{1st} = \mathbf{T}_s^{1st^T} \mathbf{f}_s^{1st},$$

$$\bar{\mathbf{f}}_s^{inn} = \sum_{n=2}^{nl} \bar{\mathbf{f}}_s^n, \text{ and}$$

$$\bar{\mathbf{f}}_s^n = \mathbf{T}_s^{n^T} \mathbf{f}_s^n.$$

The subscripts r, m, and s refer to the nodes in the regular region, master nodes, and slave nodes, respectively, the superscripts 1st and *inn* refer to the first layer and the inner layers in the singular region respectively, and *nl* is the number of layers used in the singular region.

Let $\mathbf{d}_s$ be the vector of the nodal displacements of the slave nodes. This vector is much larger than the vector of the generalised co-ordinates $\mathbf{a}$. Therefore, solving the system of equations in Eq. (3) reduces the computational cost considerably compared to solving the system of equations in Eq. (1). Also, Eq. (3) shows that the generalised co-ordinates (which are the SIFs and the coefficients of the higher order terms) are directly computed. No post-processing technique is required to extract them.

3. Global interpolation functions for mode III bi-material notch

In the FFEM, the global interpolation functions have a very important role, because they are used to transform the large number of unknowns (nodal displacements) in a singular region to a small set of generalised co-ordinates. Therefore, exact analytical solutions of the displacement field around a notch tip are employed as global interpolation functions. Those exact analytical solutions are found to be eigenfunction series expansions. A description of the derivation of the stress and displacement fields for an anti-plane bi-material notch is presented in this section. These derivations are based on Linear Elastic Fracture Mechanics (LEFM) assumptions. It should be noted that the LEFM still provides accurate predictions especially when the extent of the plastic region is not significant which is the case for many materials.

Let (r, θ) be a polar co-ordinate system centred at the tip of a bi-material notch, such that the x-axis is located at the interface of the two materials 1 and 2 as illustrated in Fig. 3. In the state of anti-plane, the only non-zero stress components are τ_{rz} and $\tau_{\theta z}$, and the only non-zero displacement component is in the z direction (w). The stress components can be expressed in terms of w as

$$\tau_{rz}^{(j)} = G_j \frac{\partial w^{(j)}}{\partial r} \tag{4}$$

$$\tau_{\theta z}^{(j)} = G_j \frac{1}{r} \frac{\partial w^{(j)}}{\partial \theta} \tag{5}$$

where G_j is the shear modulus of material j ($j = 1, 2$). The equilibrium equation can be written in terms of the stress components as

$$\frac{\partial \tau_{\theta z}^{(j)}}{\partial \theta} + r \frac{\partial \tau_{rz}^{(j)}}{\partial r} + \tau_{rz}^{(j)} = 0 \tag{6}$$

Substituting Eqs. (4) and (5) into Eq. (6), the equilibrium equation can be expressed in terms of the displacement component w as

Please cite this article in press as: Treifi M, Oyadiji SO. Evaluation of mode III stress intensity factors for bi-material notched bodies using the fractal-like finite element method. Comput Struct (2013), http://dx.doi.org/10.1016/j.compstruc.2013.02.015

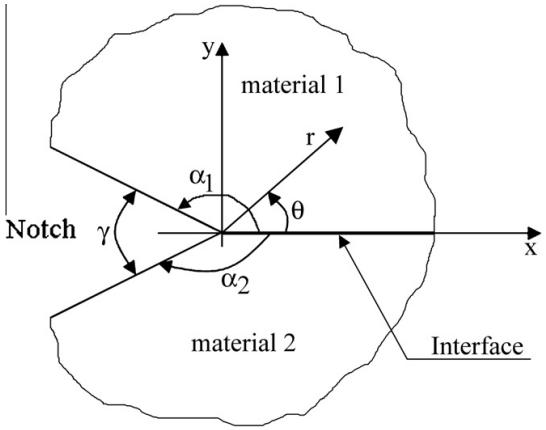

Fig. 3. Bi-material notch and co-ordinate systems.

$$\frac{1}{r}\frac{\partial^2 w^{(j)}}{\partial\theta^2}+r\frac{\partial^2 w^{(j)}}{\partial r^2}+\frac{\partial w^{(j)}}{\partial r}=0 \tag{7}$$

The displacement function $w^{(j)}$ can be assumed as

$$w^{(j)}=r^{\lambda}F_j(\theta) \tag{8}$$

where λ is an eigenvalue. After substituting $w^{(j)}$ and its derivatives into the differential Eq. (7), the general solution of the resulting equation is

$$w^{(j)}=r^{\lambda}(A_j\cos\lambda\theta+B_j\sin\lambda\theta) \tag{9}$$

where A_j and B_j are the generalised co-ordinates (the coefficients of the terms of the mode III notch asymptotic field). On substituting Eq. (9) into Eqs. (4) and (5), the stress expressions are

$$\tau_{rz}^{(j)}=G_j\lambda r^{\lambda-1}(A_j\cos\lambda\theta+B_j\sin\lambda\theta) \tag{10}$$

$$\tau_{\theta z}^{(j)}=G_j\lambda r^{\lambda-1}(-A_j\sin\lambda\theta+B_j\cos\lambda\theta) \tag{11}$$

The eigenvalues λ are obtained by imposing the following boundary and continuity conditions:

$$\tau_{\theta z}^{(1)}(r,\theta=+\alpha_1)=0 \tag{12}$$

$$\tau_{\theta z}^{(2)}(r,\theta=-\alpha_2)=0 \tag{13}$$

$$w^{(1)}(r,\theta=0)=w^{(2)}(r,\theta=0) \tag{14}$$

$$\tau_{\theta z}^{(1)}(r,\theta=0)=\tau_{\theta z}^{(2)}(r,\theta=0) \tag{15}$$

Substituting Eqs. (9) and (11) into Eqs. (12)–(15) yields

$$B_1=A_1\frac{\sin\lambda\alpha_1}{\cos\lambda\alpha_1} \tag{16}$$

$$B_2=-A_2\frac{\sin\lambda\alpha_2}{\cos\lambda\alpha_2} \tag{17}$$

$$A_2=A_1 \tag{18}$$

$$B_2=\frac{G_1}{G_2}B_1 \tag{19}$$

For non-trivial solutions of A_j *and* B_j, the determinant of Eqs. (16)–(19) must vanish. By solving the resulting determinant, the eigenvalues are obtained from

$$G_1\sin\lambda\alpha_1\cos\lambda\alpha_2+G_2\cos\lambda\alpha_1\sin\lambda\alpha_2=0 \tag{20}$$

Eq. (20) can be rewritten as

$$\left(\frac{G_1}{G_2}+1\right)\sin\lambda(\alpha_1+\alpha_2)+\left(\frac{G_1}{G_2}-1\right)\sin\lambda(\alpha_1-\alpha_2)=0 \tag{21}$$

Eq. (21) can be solved using Muller's iteration method [43]. The solution of Eq. (21) is found to be always real [41]. For the special case when $G_1 = G_2$ *and* $\alpha_1 = \alpha_2 = \alpha$, Eq. (21) is reduced to

$$\lambda=\frac{n\pi}{2\alpha} \tag{22}$$

which is the same relationship as the one derived for a symmetric homogeneous isotropic notch [23].

The displacement and stress expressions in materials 1 and 2 can be rewritten as

$$w^{(1)}=r^{\lambda}(A_1\cos\lambda\theta+B_1\sin\lambda\theta) \tag{23}$$

$$w^{(2)}=r^{\lambda}\left(A_1\cos\lambda\theta+\frac{G_1}{G_2}B_1\sin\lambda\theta\right) \tag{24}$$

$$\tau_{rz}^{(1)}=G_1\lambda r^{\lambda-1}(A_1\cos\lambda\theta+B_1\sin\lambda\theta) \tag{25}$$

$$\tau_{\theta z}^{(1)}=G_1\lambda r^{\lambda-1}(-A_1\sin\lambda\theta+B_1\cos\lambda\theta) \tag{26}$$

$$\tau_{rz}^{(2)}=G_2\lambda r^{\lambda-1}\left(A_1\cos\lambda\theta+\frac{G_1}{G_2}B_1\sin\lambda\theta\right) \tag{27}$$

$$\tau_{\theta z}^{(2)}=G_2\lambda r^{\lambda-1}\left(-A_1\sin\lambda\theta+\frac{G_1}{G_2}B_1\cos\lambda\theta\right) \tag{28}$$

The mode III SIF of an anti-plane bi-material notch is defined as

$$K_{III}^{(j)}=\sqrt{2\pi}\lim_{r\to 0}r^{1-\lambda}\tau_{\theta z}^{(j)}(\theta=0) \tag{29}$$

Substituting Eq. (26) or (28) into Eq. (29) gives

$$K_{III}^{(j)}=\sqrt{2\pi}G_j\lambda B_j=\sqrt{2\pi}G_1\lambda B_1 \tag{30}$$

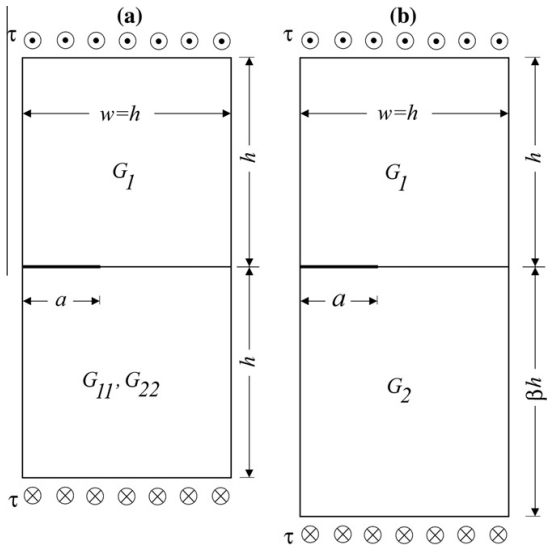

Fig. 4. Bi-material cracked body under anti-plane shear: (a) isotropic-orthotropic materials and (b) transformed isotropic-isotropic materials.

Please cite this article in press as: Treifi M, Oyadiji SO. Evaluation of mode III stress intensity factors for bi-material notched bodies using the fractal-like finite element method. Comput Struct (2013), http://dx.doi.org/10.1016/j.compstruc.2013.02.015

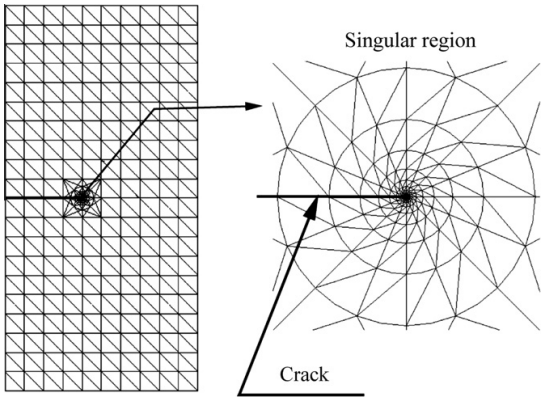

Fig. 5. The finite element mesh used in the analysis of bi-material cracked bodies.

Table 1
Normalised SIFs for a bi-material cracked body under anti-plane shear ($a/w = 0.4$).

β		G_2/G_1		
		1/4	1	4
0.1	FFEM	1.667	1.489	1.269
	ABAQUS	1.667	1.489	1.269
	SE	1.669	1.494	1.272
	Ref. [35]	1.67	1.49	1.27
0.2	FFEM	1.327	1.244	1.149
	ABAQUS	1.327	1.244	1.149
	SE	1.327	1.244	1.149
	Ref. [35]	1.33	1.24	1.15
0.5	FFEM	1.109	1.097	1.085
	ABAQUS	1.109	1.098	1.085
	SE	1.109	1.097	1.085
	Ref. [35]	1.11	1.09	1.09
1	FFEM	1.077	1.077	1.077
	ABAQUS	1.077	1.077	1.077
	SE	1.077	1.077	1.077
	Ref. [35]	1.08	1.08	1.07

The generalised co-ordinate B_1 in Eq. (30) is computed directly in the FFEM. Therefore, no-post processing technique is required to calculate the mode III SIF.

4. Relationships between mode III notch SIFS and the strain energy of a finite volume around a notch-tip

Published results for notch mode III SIFs are not available in the literature and current FE commercial packages, such as ABAQUS, are not able to compute the SIFs of notch problems. To validate the FFEM results, an approach based on strain energy is developed for the case of a mode III notch.

The strain energy of a finite volume around a notch-tip can be written as

$$E^{(e)} = \int_V W^{(e)} dV \tag{31}$$

where $W^{(e)}$ is the strain energy density and can be computed as

$$W^{(e)} = \int \boldsymbol{\sigma} : \partial \boldsymbol{\varepsilon} \tag{32}$$

where $\boldsymbol{\sigma}$ and $\boldsymbol{\varepsilon}$ are stress and strain tensors, respectively. For a mode III bi-material case, the strain energy of a finite volume of a radius R_c around a notch-tip can be computed using Eqs. (25)–(32) as follows

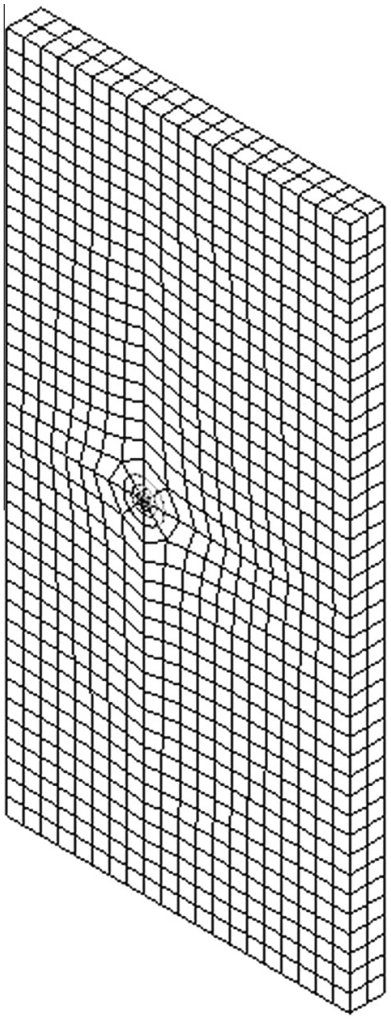

Fig. 6. The finite element mesh used in the ABAQUS analysis of bi-material cracked bodies.

Table 2
Normalised SIFs for a bi-material cracked body under anti-plane shear ($G_2/G_1 = 1/4$).

a/w		β			
		0.1	0.2	0.5	1.0
0.1	FFEM	1.127	1.039	1.007	1.004
	Ref. [35]	1.13	1.03	1.01	1.00
0.2	FFEM	1.324	1.128	1.029	1.017
	Ref. [35]	1.32	1.13	1.03	1.02
0.3	FFEM	1.504	1.228	1.064	1.041
	Ref. [35]	1.50	1.23	1.06	1.04
0.4	FFEM	1.667	1.327	1.109	1.077
	Ref. [35]	1.67	1.33	1.11	1.08
0.5	FFEM	1.817	1.423	1.168	1.130
	Ref. [35]	1.82	1.42	1.16	1.13
0.6	FFEM	1.956	1.519	1.247	1.210
	Ref. [35]	1.95	1.52	1.24	1.21
0.7	FFEM	2.091	1.626	1.368	1.337
	Ref. [35]	2.09	1.63	1.37	1.34
0.8	FFEM	2.236	1.784	1.585	1.565
	Ref. [35]	2.23	1.78	1.59	1.56

Please cite this article in press as: Treifi M, Oyadiji SO. Evaluation of mode III stress intensity factors for bi-material notched bodies using the fractal-like finite element method. Comput Struct (2013), http://dx.doi.org/10.1016/j.compstruc.2013.02.015

Table 3
Normalised SIFs for a bi-material cracked body under anti-plane shear ($G_2/G_1 = 1$).

a/w		β			
		0.1	0.2	0.5	1.0
0.1	FFEM	1.091	1.028	1.006	1.004
	Ref. [35]	1.09	1.03	1.01	1.00
0.2	FFEM	1.233	1.093	1.025	1.017
	Ref. [35]	1.23	1.09	1.03	1.02
0.3	FFEM	1.367	1.167	1.055	1.041
	Ref. [35]	1.36	1.16	1.05	1.04
0.4	FFEM	1.489	1.244	1.097	1.077
	Ref. [35]	1.49	1.24	1.09	1.08
0.5	FFEM	1.606	1.323	1.154	1.130
	Ref. [35]	1.61	1.32	1.14	1.13
0.6	FFEM	1.720	1.410	1.234	1.210
	Ref. [35]	1.72	1.41	1.23	1.21
0.7	FFEM	1.841	1.521	1.356	1.337
	Ref. [35]	1.84	1.52	1.35	1.34
0.8	FFEM	2.000	1.703	1.578	1.565
	Ref. [35]	2.00	1.70	1.57	1.56

Table 4
Normalised SIFs for a bi-material cracked body under anti-plane shear ($G_2/G_1 = 4$).

a/w		β			
		0.1	0.2	0.5	1.0
0.1	FFEM	1.045	1.015	1.005	1.004
	Ref. [35]	1.05	1.02	1.01	1.00
0.2	FFEM	1.119	1.051	1.020	1.017
	Ref. [35]	1.12	1.05	1.02	1.02
0.3	FFEM	1.194	1.096	1.047	1.041
	Ref. [35]	1.19	1.09	1.05	1.04
0.4	FFEM	1.269	1.149	1.085	1.077
	Ref. [35]	1.27	1.15	1.09	1.07
0.5	FFEM	1.347	1.212	1.140	1.130
	Ref. [35]	1.34	1.20	1.14	1.13
0.6	FFEM	1.437	1.293	1.219	1.210
	Ref. [35]	1.43	1.29	1.22	1.20
0.7	FFEM	1.555	1.412	1.345	1.337
	Ref. [35]	1.54	1.41	1.35	1.33
0.8	FFEM	1.746	1.621	1.570	1.565
	Ref. [35]	1.74	1.61	1.57	1.56

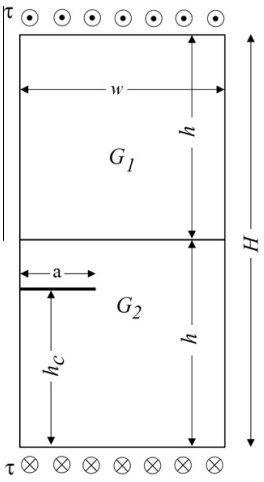

Fig. 7. Bi-material body with a crack parallel to an interface under anti-plane shear.

$$E^{(e)} = \frac{I}{8\pi G_1^2 \lambda^3} R_c^{2\lambda} K_{III}^2 \tag{33}$$

where I is an integral and its value is

$$I = G_2\lambda^2\alpha_2\left(\left(\frac{\cos\lambda\alpha_1}{\sin\lambda\alpha_1}\right)^2 + \left(\frac{G_1}{G_2}\right)^2\right) + G_1\lambda^2\alpha_1\left(\left(\frac{\cos\lambda\alpha_1}{\sin\lambda\alpha_1}\right)^2 + 1\right) \tag{34}$$

Convenient expressions for R_c are proposed based on the ultimate tensile strength σ_t and on the fracture toughness K_{IC}. Under plane strain conditions [44]

$$R_c = \frac{(1+\nu)(5-8\nu)}{4\pi}\left(\frac{K_{IC}}{\sigma_t}\right)^2 \tag{35}$$

and under plane stress conditions [45]

$$R_c = \frac{(5-3\nu)}{4\pi}\left(\frac{K_{IC}}{\sigma_t}\right)^2 \tag{36}$$

The strain energy $E^{(e)}$ can be computed using commercial FE packages such as ABAQUS. This, then, is substituted in Eq. (33) to extract the mode III SIFs of a notch.

5. Numerical examples and verification

The accuracy of the FFEM results is validated by means of comparison with published results for anti-plane bi-material crack problems and numerical results using ABAQUS for crack and notch problems. Because of the lack of published results for anti-plane bi-material notch problems, the approach based on the strain energy of a finite volume around a notch tip presented in Section 4 is used to predict the notch SIFs using the FE package ABAQUS. Crack problems are special cases of notch problems (a notch with an opening angle of zero is basically a crack). Many examples of bi-material crack problems subject to anti-plane loading conditions for which published results exist are presented first to demonstrate the accuracy of the FFEM and the standard FE-based SE approach. That is followed by examples of a crack parallel to an interface. Then, many examples of bi-material notch problems under anti-plane shear loading conditions for different notch opening angles, notch positions, notch lengths, and elastic mismatch ratios (G_2/G_1) are presented.

5.1. Numerical examples for anti-plane bi-material crack problems

A bi-material edge cracked body of a rectangular cross-section of height $2h$ and width $w = h$ subject to anti-plane shear loading conditions is analysed in this section. The bi-material cracked body is formed by bonding an isotropic material with shear modulus G_1 to an orthotropic material with shear moduli G_{11}, G_{22} as shown in Fig. 4(a). The orthotropic part of the body can be transformed into an isotropic material with shear modulus $G_2 = \sqrt{G_{11}G_{22}}$ by adjusting the height of the orthotropic part h to βh as shown in Fig. 4(b), where $\beta = G_2/G_{22}$ [35]. In the FFEM analysis, ten terms of the eigenfunction series, 16 layers in the singular region and a similarity ratio $\rho = 0.6$ are used. These values are chosen based on the convergence study presented in Ref. [23]. The size of the singular region is the same for all the examples analysed. Six-node triangular elements are used to mesh the geometries of the cross-sections in a similar manner to that shown in Fig. 5. For all the examples in this paper, seven-point integration scheme is used for the triangular elements.

First, in Table 1, the results predicted by the FFEM and by the strain energy approach presented in Section 4 are validated by

Please cite this article in press as: Treifi M, Oyadiji SO. Evaluation of mode III stress intensity factors for bi-material notched bodies using the fractal-like finite element method. Comput Struct (2013), http://dx.doi.org/10.1016/j.compstruc.2013.02.015

Table 5
Normalised SIFs for a crack parallel to an interface in a bi-material body under anti-plane shear ($a/w = 0.4$).

h_c/H	G_2/G_1															
	1		0.9		0.8		1/2		1/5		1/10		1/20		1/50		1/100	
	FFEM	ABAQUS	FFEM	ABAQUS	FFEM	ABAQUS	FFEM	ABAQUS	FFEM	ABAQUS	FFEM	ABAQUS	FFEM	ABAQUS	FFEM	ABAQUS	FFEM	ABAQUS
0.9	1.243	1.243	1.243	1.243	1.243	1.243	1.244	1.244	1.245	1.245	1.245	1.245	1.245	1.245	1.245	1.245	1.245	1.245
0.8	1.116	1.116	1.117	1.117	1.117	1.118	1.120	1.120	1.123	1.123	1.125	1.125	1.126	1.126	1.126	1.126	1.127	1.127
0.7	1.086	1.087	1.088	1.089	1.091	1.091	1.099	1.100	1.113	1.113	1.119	1.119	1.123	1.123	1.125	1.125	1.126	1.126
0.65	1.081	1.081	1.085	1.085	1.089	1.089	1.106	1.106	1.133	1.133	1.145	1.146	1.153	1.153	1.158	1.158	1.159	1.159
0.6	1.078	1.078	1.086	1.086	1.094	1.094	1.127	1.127	1.182	1.182	1.210	1.210	1.226	1.227	1.237	1.238	1.241	1.241
0.55	1.077	1.077	1.091	1.091	1.107	1.107	1.175	1.175	1.305	1.305	1.38	1.381	1.430	1.430	1.464	1.464	1.477	1.477
0.525	1.077	1.077	1.096	1.096	1.119	1.119	1.221	1.221	1.450	1.449	1.607	1.607	1.724	1.724	1.815	1.815	1.850	1.850
0.5	1.077	1.077	1.077	1.077	1.077	1.077	1.077	1.077	1.077	1.077	1.077	1.077	1.077	1.077	1.077	1.077	1.077	1.077
0.475	1.077	1.077	1.059	1.058	1.039	1.039	0.975	0.975	0.898	0.898	0.869	0.869	0.853	0.853	0.844	0.844	0.841	0.841
0.45	1.077	1.077	1.064	1.064	1.050	1.050	1.001	1.001	0.939	0.939	0.915	0.915	0.902	0.902	0.893	0.893	0.891	0.891
0.4	1.078	1.078	1.071	1.071	1.064	1.064	1.036	1.036	0.997	0.997	0.981	0.981	0.972	0.972	0.967	0.967	0.965	0.965
0.35	1.081	1.081	1.077	1.077	1.073	1.073	1.058	1.058	1.035	1.036	1.026	1.026	1.020	1.021	1.017	1.017	1.016	1.016
0.3	1.086	1.087	1.084	1.084	1.082	1.082	1.074	1.074	1.061	1.062	1.056	1.056	1.053	1.053	1.051	1.051	1.050	1.051
0.2	1.116	1.116	1.116	1.116	1.115	1.115	1.113	1.113	1.109	1.109	1.108	1.108	1.107	1.107	1.106	1.106	1.106	1.106
0.1	1.243	1.243	1.243	1.243	1.243	1.243	1.242	1.242	1.241	1.241	1.241	1.241	1.241	1.241	1.241	1.241	1.241	1.241

means of comparison with available published results predicted by Wu and Chiu [35] and those predicted by the commercial FE package ABAQUS. For the ABAQUS analysis, a three-dimensional model subject to mode III loading and boundary conditions is used. The model is meshed using C3D20 elements as shown in Fig. 6. In addition, quarter point wedge elements are used around the crack-tip. For the strain energy approach, R_c is taken equal to 0.07776 (that includes 3 layers of elements around the crack-tip for which the strain energy is computed). This value of R_c is determined after the J-integral has stabilised. Then, in Tables 2–4, the mode III SIFs computed using the FFEM compared to the values predicted by Wu and Chiu [35] are presented. The values of the SIFs of Wu and Chiu [35] presented in Tables 1–4 are interpolated from graphs, as those authors presented their results using graphs only. The SIFs are computed for different crack lengths ($a/w = 0.1, 0.2, \ldots, 0.8$), elastic mismatch ratios ($G_2/G_1 = 1/4, 1, 4$), and orthotropic material properties ($\beta = 0.1, 0.2, 0.5, 1$).

The results presented in Table 1 demonstrate the accuracy of the FFEM and the strain energy approach to predict the SIFs for mode III interfacial crack problems. Tables 1–4 show that the SIFs for a bi-material crack when both of the materials are isotropic (i.e. the crack is located on the horizontal centre line of the cross-section) are independent of the elastic mismatch ratios. This was also observed in Ref. [35]. The values of the SIFs increase with increasing crack lengths, decreasing values of β, and decreasing values of elastic mismatch ratios G_2/G_1. It can also be seen from those tables that the FFEM results are in very good agreement with the published results. This proves that the use of the global interpolation functions in the FFEM, which were derived for a general bi-material notch in Section 3, produces accurate results for mode III bi-material crack problems (when the notch opening angle $\gamma = 0°$). This means that they can be used with confidence to compute the SIFs for bi-material notch problems.

5.2. Numerical examples for an anti-plane bi-material crack parallel to an interface

Examples of a bi-material body with a crack parallel to an interface ($w = h$, $a/w = 0.4$) are analysed using the FFEM and ABAQUS. The bi-material body is formed by bonding together two isotropic materials as shown in Fig. 7. For the ABAQUS analysis, three-dimensional elements C3D20 are used to model the bi-material body. In addition, singular quarter point elements are used around the crack tip. Also, mode III loading and boundary conditions are applied. In the FFEM analysis, the body is meshed in a similar manner to that shown in Fig. 5.

The results for different elastic mismatch ratios G_2/G_1, and different crack locations h_c/H are presented in Table 5. This table shows that the mode III SIF values predicted by the FFEM and ABAQUS are in very good agreement. Also, it demonstrates a very interesting behaviour of the values of the SIFs as the crack location gets closer or farther from the interface. When the crack location is far from the interface, the SIF values are close to the SIF values of a homogeneous body. As the crack location gets closer to the interface, the values of the SIFs are affected in different ways depending on which material the crack is located in. If the crack is in the stiffer material, the values of the SIFs increase, but their values decrease if the crack is in the softer material. This trend becomes more pronounced as the material properties of the two materials differ substantially. To show that clearly, the values of the mode III SIFs are plotted in Fig. 8. To help understand this behaviour of the bi-material body with a crack parallel to an interface, the deformed shapes for the cases of ($G_2/G_1 = 1, 1/2, 1/10, 1/100$) and ($h_c/H = 0.4, 0.6$) are plotted in Fig. 9. The curvatures of the deformed shapes differ considerably depending on the crack location whether it is in the stiffer or the softer material.

Please cite this article in press as: Treifi M, Oyadiji SO. Evaluation of mode III stress intensity factors for bi-material notched bodies using the fractal-like finite element method. Comput Struct (2013), http://dx.doi.org/10.1016/j.compstruc.2013.02.015

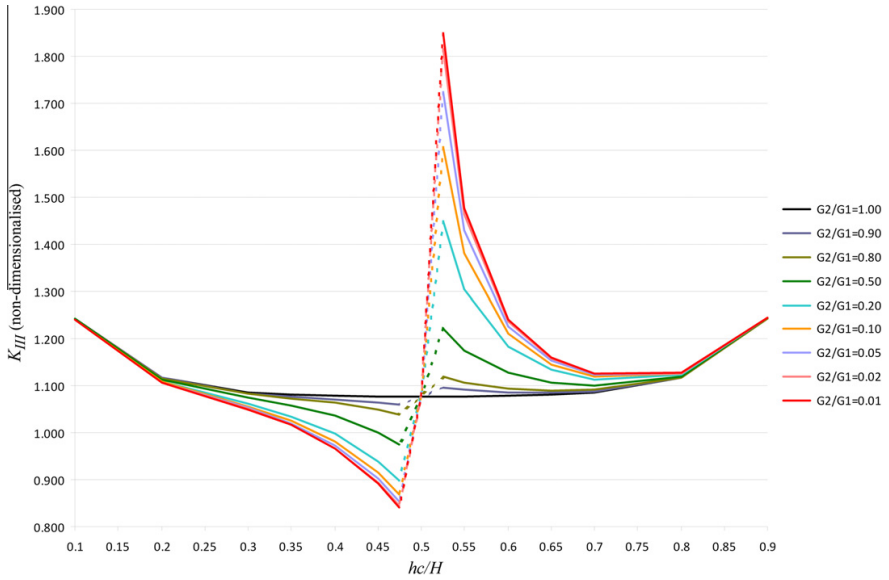

Fig. 8. SIF values for a crack parallel to an interface.

5.3. Numerical examples for anti-plane bi-material notch problems

Many examples of bi-material notched bodies of a rectangular cross-section of height H and width w where $H/w = 2$ are presented in this section. The notched bodies are subject to anti-plane shear loading conditions as shown in Fig. 10(a). The bi-material bodies are formed by bonding two isotropic materials together. In the FFEM analysis, ten terms of the eigenfunction series, 16 layers in the singular region and a similarity ratio $\rho = 0.6$ are used. Six-node triangle elements are used to mesh the geometries of the cross-sections in a similar manner to that shown in Fig. 10(b).

The mode III SIFs computed by the FFEM for $a/w = 0.4$ and for different notch opening angles ($\gamma = 0°, 10°, \ldots, 90°$), notch positions ($h_c/h = 0.1, 0.2, \ldots, 0.5$), and elastic mismatch ratios ($G_2/G_1 = 1/10, 1/4, 1, 4, 10$) are tabulated in Tables 6–10. Tables 11–15 present the mode III SIFs computed by the FFEM for a notch opening angle $\gamma = 50°$ and for different notch lengths ($a/w = 0.1, 0.2, \ldots, 0.5$), notch positions ($h_c/h = 0.1, 0.2, \ldots, 0.5$), and elastic mismatch ratios ($G_2/G_1 = 1/10, 1/4, 1, 4, 10$). The missing values in those tables are due to the fact that the geometry of the plate is no more rectangular (the top and bottom boundaries are no more equal and the notch faces have unequal lengths).

From Tables 6–10, it can be seen that the values of the SIFs increase with increasing notch opening angles, as the notch gets closer to the bottom boundary, and with decreasing elastic mismatch ratios. Tables 11–15 show that the SIFs increase with increasing notch lengths, as the notch gets closer to the bottom boundary, and with decreasing elastic mismatch ratios. From Tables 6–15, the SIFs are dependent on the elastic mismatch ratios of the bi-material notched body in general. They are only independent of the elastic mismatch ratios when the notch is located on the horizontal symmetry line; i.e. the notched body is symmetric with respect to the bisector of the notch opening angle which coincides with the interface. This can be proven analytically [35]. Assume a symmetrical notched body consisting of one material only ($G_2/G_1 = 1$). The displacement and the stresses for this case can be referred to as w' and τ', respectively. For a general case of an elastic mismatch ratio of a symmetrical bi-material notched body, the displacements vanish along the interface, due to the symmetry conditions. From Eqs. (23)–(28), it can be shown that the displacement and the stresses are $w^{(1)} = w'$ and $\tau^{(1)} = \tau'$ in material 1 and $w^{(2)} = \frac{G_1}{G_2} w'$ and $\tau^{(2)} = \tau'$ in material 2. This demonstrates the stresses are independent of the elastic mismatch ratio. Therefore, the SIFs are independent of the elastic mismatch ratio of a symmetrical bi-material notched body under mode III loading conditions.

It should be noted that most of the results in Tables 6–15 appear to be new and that there are no published SIF values available with which to compare them. To validate those results, a comparison with the strain energy approach presented in Section 4 is carried out. Again, R_c is taken equal to 0.07776 (that includes 3 layers of elements around the notch-tip for which the strain energy is computed). ABAQUS is used to compute the strain energy. A three-dimensional model subject to mode III loading and boundary conditions is analysed. The model is meshed using C3D20 elements as shown in Fig. 11. In addition, quarter point wedge elements are used around the notch-tip. A comparison of the SIF values predicted by the FFEM and the strain energy approach is shown in Tables 16–20. These tables show that the SIF values predicted by both approaches are in very good agreement. It was also shown in the previous sections that the use of the global interpolation functions presented in Section 3, which were derived for anti-plane bi-material notch problems, produced accurate results for anti-plane bi-material crack problems (when the notch angle $\gamma = 0°$). Consequently, it can be assumed that the FFEM results for notch problems in Tables 6–15 are valid and accurate.

To demonstrate the efficiency of the FFEM with regard to reducing the computational cost, let us consider one of the examples when the notched body is symmetrical about the interface, $\gamma = 0°$, and $a/w = 0.4$. According to the mesh used, the total number of degrees of freedom (one degree of freedom per node), which is consequently the number of equations to be solved, is 5063 in the conventional finite element method. In the FFEM analysis, because of the transformation, the total number of equations to be solved is only 1148. Those numbers depend on the mesh used to model the singular region—16 layers were used in this example as shown in Fig. 10(b). Larger numbers of layers can generally be

Please cite this article in press as: Treifi M, Oyadiji SO. Evaluation of mode III stress intensity factors for bi-material notched bodies using the fractal-like finite element method. Comput Struct (2013), http://dx.doi.org/10.1016/j.compstruc.2013.02.015

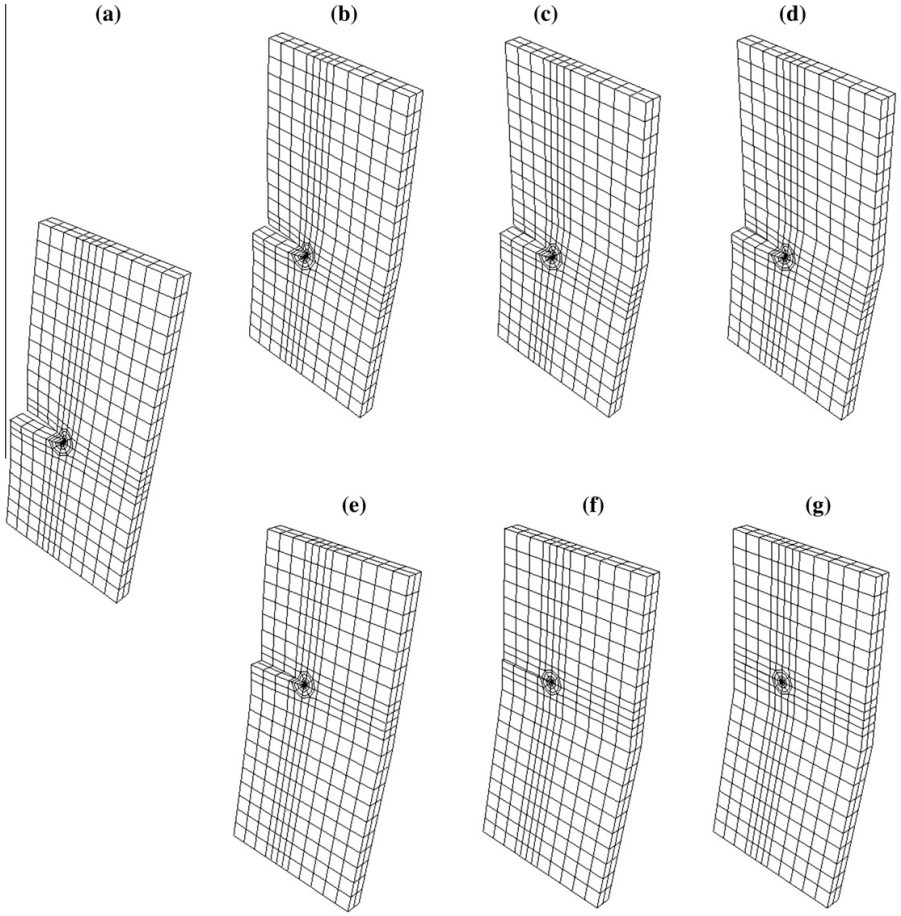

Fig. 9. Deformed shapes of a bi-material body with a crack parallel to an interface: (a) $G_2/G_1 = 1$ and $h_c/H = 0.4$, (b) $G_2/G_1 = 1/2$ and $h_c/H = 0.4$, (c) $G_2/G_1 = 1/10$ and $h_c/H = 0.4$, (d) $G_2/G_1 = 1/100$ and $h_c/H = 0.4$, (e) $G_2/G_1 = 1/2$ and $h_c/H = 0.6$, (f) $G_2/G_1 = 1/10$ and $h_c/H = 0.6$, and (g) $G_2/G_1 = 1/100$ and $h_c/H = 0.6$.

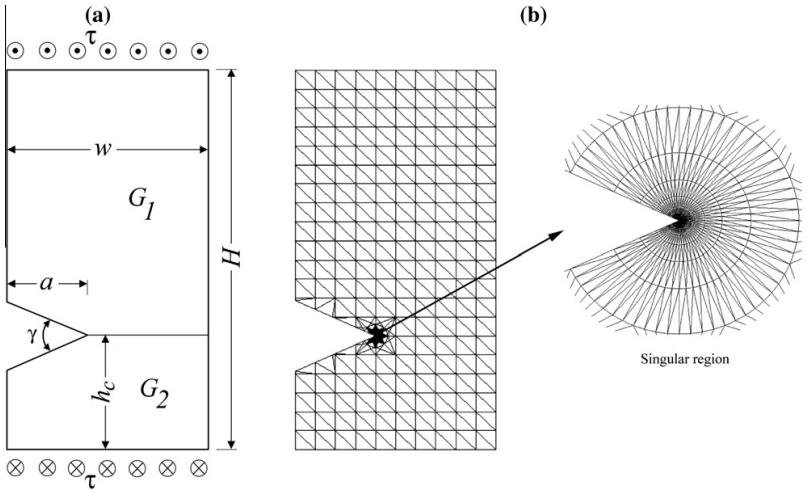

Fig. 10. (a) Bi-material notched body under anti-plane shear and (b) the finite element mesh used in the analysis.

Please cite this article in press as: Treifi M, Oyadiji SO. Evaluation of mode III stress intensity factors for bi-material notched bodies using the fractal-like finite element method. Comput Struct (2013), http://dx.doi.org/10.1016/j.compstruc.2013.02.015

Table 6
Normalised SIFs for a bi-material notched body under anti-plane shear computed by FFEM ($G_2/G_1 = 1/10$, $a/w = 0.4$).

$\gamma(^\circ)$	h_c/H				
	0.1	0.2	0.3	0.4	0.5
0	1.354	1.148	1.096	1.081	1.077
10	1.422	1.202	1.146	1.130	1.126
20	1.496	1.259	1.199	1.183	1.178
30	1.574	1.320	1.256	1.238	1.233
40	1.659	1.384	1.316	1.296	1.291
50	1.751	1.453	1.379	1.358	1.352
60	–	1.526	1.445	1.423	1.417
70	–	1.603	1.515	1.491	1.484
80	–	1.686	1.589	1.562	1.555
90	–	–	1.666	1.636	1.628

Table 7
Normalised SIFs for a bi-material notched body under anti-plane shear computed by FFEM ($G_2/G_1 = 1/4$, $a/w = 0.4$).

$\gamma(^\circ)$	h_c/H				
	0.1	0.2	0.3	0.4	0.5
0	1.326	1.140	1.093	1.080	1.077
10	1.393	1.193	1.143	1.130	1.126
20	1.464	1.250	1.197	1.182	1.178
30	1.540	1.310	1.253	1.237	1.233
40	1.622	1.373	1.312	1.296	1.291
50	1.711	1.441	1.375	1.357	1.352
60	–	1.513	1.442	1.422	1.417
70	–	1.589	1.511	1.490	1.484
80	–	1.670	1.584	1.561	1.555
90	–	–	1.661	1.635	1.628

Table 8
Normalised SIFs for a bi-material notched body under anti-plane shear computed by FFEM ($G_2/G_1 = 1$, $a/w = 0.4$).

$\gamma(^\circ)$	h_c/H				
	0.1	0.2	0.3	0.4	0.5
0	1.243	1.116	1.086	1.079	1.077
10	1.303	1.168	1.136	1.128	1.126
20	1.368	1.223	1.189	1.180	1.178
30	1.437	1.281	1.245	1.235	1.233
40	1.511	1.343	1.304	1.293	1.291
50	1.590	1.408	1.366	1.355	1.352
60	–	1.477	1.431	1.419	1.417
70	–	1.550	1.500	1.487	1.484
80	–	1.627	1.572	1.558	1.555
90	–	–	1.647	1.631	1.628

Table 9
Normalised SIFs for a bi-material notched body under anti-plane shear computed by FFEM ($G_2/G_1 = 4$, $a/w = 0.4$).

$\gamma(^\circ)$	h_c/H				
	0.1	0.2	0.3	0.4	0.5
0	1.148	1.092	1.080	1.077	1.077
10	1.201	1.142	1.129	1.126	1.126
20	1.259	1.195	1.181	1.178	1.178
30	1.320	1.251	1.237	1.233	1.233
40	1.384	1.311	1.295	1.291	1.291
50	1.453	1.374	1.356	1.352	1.352
60	–	1.440	1.421	1.417	1.417
70	–	1.509	1.489	1.484	1.484
80	–	1.582	1.560	1.554	1.555
90	–	–	1.633	1.627	1.628

Table 10
Normalised SIFs for a bi-material notched body under anti-plane shear computed by FFEM ($G_2/G_1 = 10$, $a/w = 0.4$).

$\gamma(^\circ)$	h_c/H				
	0.1	0.2	0.3	0.4	0.5
0	1.109	1.083	1.077	1.076	1.077
10	1.160	1.132	1.126	1.125	1.126
20	1.215	1.185	1.179	1.177	1.178
30	1.272	1.240	1.234	1.232	1.233
40	1.334	1.299	1.292	1.290	1.291
50	1.398	1.361	1.353	1.351	1.352
60	–	1.426	1.417	1.416	1.417
70	–	1.494	1.485	1.483	1.484
80	–	1.565	1.555	1.553	1.555
90	–	–	1.628	1.626	1.628

Table 11
Normalised SIFs for a bi-material notched body under anti-plane shear computed by FFEM ($G_2/G_1 = 1/10$, $\gamma = 50^\circ$).

a/w	h_c/H				
	0.1	0.2	0.3	0.4	0.5
0.1	1.303	1.258	1.250	1.248	1.247
0.2	1.441	1.305	1.276	1.268	1.266
0.3	1.596	1.372	1.319	1.304	1.300
0.4	1.751	1.453	1.379	1.358	1.352
0.5	–	1.548	1.461	1.438	1.431

Table 12
Normalised SIFs for a bi-material notched body under anti-plane shear computed by FFEM ($G_2/G_1 = 1/4$, $\gamma = 50^\circ$).

a/w	h_c/H				
	0.1	0.2	0.3	0.4	0.5
0.1	1.298	1.257	1.249	1.247	1.247
0.2	1.424	1.300	1.275	1.268	1.266
0.3	1.567	1.364	1.316	1.303	1.300
0.4	1.711	1.441	1.375	1.357	1.352
0.5	–	1.534	1.457	1.437	1.431

Table 13
Normalised SIFs for a bi-material notched body under anti-plane shear computed by FFEM ($G_2/G_1 = 1$, $\gamma = 50^\circ$).

a/w	h_c/H				
	0.1	0.2	0.3	0.4	0.5
0.1	1.282	1.253	1.248	1.247	1.247
0.2	1.373	1.288	1.271	1.267	1.266
0.3	1.479	1.340	1.310	1.302	1.300
0.4	1.590	1.408	1.366	1.355	1.352
0.5	–	1.495	1.447	1.434	1.431

Table 14
Normalised SIFs for a bi-material notched body under anti-plane shear computed by FFEM ($G_2/G_1 = 4$, $\gamma = 50^\circ$).

a/w	h_c/H				
	0.1	0.2	0.3	0.4	0.5
0.1	1.262	1.249	1.247	1.247	1.247
0.2	1.313	1.275	1.268	1.266	1.266
0.3	1.377	1.315	1.303	1.300	1.300
0.4	1.453	1.374	1.356	1.352	1.352
0.5	–	1.455	1.436	1.431	1.431

Please cite this article in press as: Treifi M, Oyadiji SO. Evaluation of mode III stress intensity factors for bi-material notched bodies using the fractal-like finite element method. Comput Struct (2013), http://dx.doi.org/10.1016/j.compstruc.2013.02.015

Table 15
Normalised SIFs for a bi-material notched body under anti-plane shear computed by FFEM ($G_2/G_1 = 10$, $\gamma = 50°$).

a/w	h_c/H				
	0.1	0.2	0.3	0.4	0.5
0.1	1.254	1.248	1.247	1.247	1.247
0.2	1.288	1.270	1.267	1.266	1.266
0.3	1.335	1.306	1.300	1.299	1.300
0.4	1.398	1.361	1.353	1.351	1.352
0.5	–	1.441	1.432	1.430	1.431

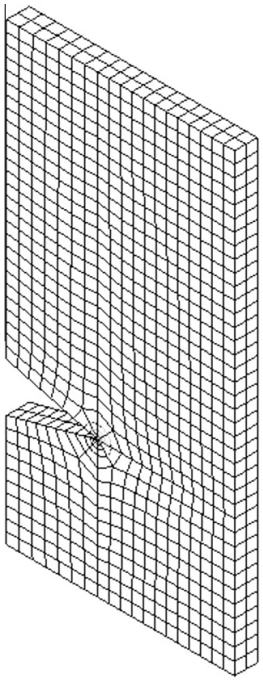

Fig. 11. The finite element mesh used in the ABAQUS analysis of bi-material notched bodies.

Table 16
Normalised SIFs for a bi-material notched body under anti-plane shear ($G_2/G_1 = 1/10$, $a/w = 0.4$).

$\gamma(°)$	h_c/H					
	0.2		0.3		0.5	
	FFEM	SE	FFEM	SE	FFEM	SE
0	1.148	1.148	1.096	1.095	1.077	1.077
30	1.320	1.320	1.256	1.256	1.233	1.233
60	1.526	1.526	1.445	1.445	1.417	1.417
90	–	–	1.666	1.665	1.628	1.628

used, and theoretically an infinite number of layers can also be used as mentioned in Section 2 without increasing the number of equations to be solved in the FFEM. This shows the computational cost reduction that can potentially be achieved by using the FFEM. This is in addition to the fact that post-processing techniques or special singular elements are not needed as is the case in other finite element approaches.

Table 17
Normalised SIFs for a bi-material notched body under anti-plane shear ($G_2/G_1 = 1/4$, $a/w = 0.4$).

$\gamma(°)$	h_c/H					
	0.2		0.3		0.5	
	FFEM	SE	FFEM	SE	FFEM	SE
0	1.140	1.140	1.093	1.093	1.077	1.077
30	1.310	1.310	1.253	1.253	1.233	1.233
60	1.513	1.513	1.442	1.442	1.417	1.417
90	–	–	1.661	1.661	1.628	1.628

Table 18
Normalised SIFs for a bi-material notched body under anti-plane shear ($G_2/G_1 = 1$, $a/w = 0.4$).

$\gamma(°)$	h_c/H					
	0.2		0.3		0.5	
	FFEM	SE	FFEM	SE	FFEM	SE
0	1.116	1.116	1.086	1.086	1.077	1.077
30	1.281	1.281	1.245	1.245	1.233	1.233
60	1.477	1.477	1.431	1.432	1.417	1.417
90	–	–	1.647	1.647	1.628	1.628

Table 19
Normalised SIFs for a bi-material notched body under anti-plane shear ($G_2/G_1 = 4$, $a/w = 0.4$).

$\gamma(°)$	h_c/H					
	0.2		0.3		0.5	
	FFEM	SE	FFEM	SE	FFEM	SE
0	1.092	1.092	1.080	1.080	1.077	1.077
30	1.251	1.252	1.237	1.237	1.233	1.233
60	1.440	1.440	1.421	1.421	1.417	1.417
90	–	–	1.633	1.633	1.628	1.628

Table 20
Normalised SIFs for a bi-material notched body under anti-plane shear ($G_2/G_1 = 10$, $a/w = 0.4$).

$\gamma(°)$	h_c/H					
	0.2		0.3		0.5	
	FFEM	SE	FFEM	SE	FFEM	SE
0	1.083	1.083	1.077	1.077	1.077	1.077
30	1.240	1.241	1.234	1.234	1.233	1.233
60	1.426	1.426	1.417	1.417	1.417	1.417
90	–	–	1.628	1.628	1.628	1.628

6. Conclusion

In this paper, the FFEM was extended to compute the SIFs for bi-material notch problems under anti-plane shear loading conditions. Exact analytical solutions of the asymptotic field around a notch tip were derived for an anti-plane bi-material notch and were used as global interpolation functions in the FFEM to transform the large number of nodal displacements of the slave nodes in the singular region to a small number of generalised co-ordinates. The SIFs are computed directly, as they are directly related to the generalised co-ordinates, which are primary unknowns of the problem. Therefore, no post processing technique is needed to extract them. Also, no special singular elements are needed to model the singular region. Any conventional finite elements can be used.

Please cite this article in press as: Treifi M, Oyadiji SO. Evaluation of mode III stress intensity factors for bi-material notched bodies using the fractal-like finite element method. Comput Struct (2013), http://dx.doi.org/10.1016/j.compstruc.2013.02.015

Due to the lack of available data for mode III bi-material notch problems, an approach based on the strain energy of a finite region around a notch-tip was developed to extract the notch SIF values for a notched body subject to mode III loading conditions using commercial FE packages.

Many numerical examples of anti-plane bi-material crack and notch problems were presented to demonstrate the accuracy and efficiency of the FFEM. The results were verified and validated via comparison with available published data and numerical results. Most of the bi-material notch cases analysed in this paper appear to be new. The numerical values of the mode III SIFs showed that they are dependent on the material properties of the bi-material notched body in general, but they are independent of them when the bi-material notched body is composed of isotropic materials and is symmetrical with respect to the bisector of the notch opening angle which coincides with the interface.

References

[1] Williams ML. Stress singularities resulting from various boundary conditions in angular corners of plates in extension. ASME J Appl Mech 1952;19:526–8.
[2] Seweryn A. Brittle fracture criterion for structures with sharp notches. Eng Fract Mech 1994;47:673–81.
[3] Knésl Z. A criterion of V-notch stability. Int J Fract 1991;48:R79–83.
[4] Gómez FJ, Elices M. A fracture criterion for sharp V-notched samples. Int J Fract 2003;123:163–75.
[5] Carpinteri A, Cornetti P, Pugno N, Sapora A, Taylor D. A finite fracture mechanics approach to structures with sharp V-notches. Eng Fract Mech 2008;75:1736–52.
[6] Gross B, Mendelson A. Plane elastostatic analysis of V-notched plates. Int J Fract 1972;8:267–76.
[7] Lin KY, Tong P. Singular finite elements for the fracture analysis of V-notched plates. Int J Numer Methods Eng 1980;15:1343–54.
[8] Carpenter WC. A collocation procedure for determining fracture mechanics parameters at a corner. Int J Fract 1984;24:255–66.
[9] Stern M, Becker EB, Dunham RS. A contour integral computation of mixed-mode stress intensity factors. Int J Fract 1976;12:359–68.
[10] Babuška I, Miller A. The post-processing approach in the finite element method-part 2: calculation of the stress intensity factors. Int J Numer Methods Eng 1984;20:1111–29.
[11] Zhao Z, Hahn HG. Determining the SIF of a V-notch from the results of a mixed-mode crack. Eng Fract Mech 1992;43:511–8.
[12] Chen D-H. Stress intensity factors for V-notched strip under tension or in-plane bending. Int J Fract 1995;70:81–97.
[13] Tong P, Pian THH, Lasry SJ. A hybrid-element approach to crack problems in plane elasticity. Int J Numer Methods Eng 1973;7:297–308.
[14] Wolf JP. The Scaled Boundary Finite Element Method. Chichester: Wiley; 2003.
[15] Mote CD. Global-local finite element. Int J Numer Methods Eng 1971;3:565–74.
[16] Leung AYT, Su RKL. Mode I crack problems by fractal two level finite element method. Eng Fract Mech 1994;48:847–56.
[17] Leung AYT, Su RKL. Mixed-mode two-dimensional crack problem by fractal two level finite element method. Eng Fract Mech 1995;51:889–95.
[18] Su RKL, Sun HY. Numerical solution of cracked thin plates subjected to bending, twisting and shear loads. Int J Fract 2002;117:323–35.
[19] Su RKL, Sun HY. Numerical solutions of two-dimensional anisotropic crack problems. Int J Solids Struct 2003;40:4615–35.
[20] Treifi M, Tsang DKL, Oyadiji SO. Applications of the fractal-like finite element method to sharp notched plates. In: ASME Conf. Proc. IDETC/CIE2007; September 4, 2007. p. 399–405.
[21] Treifi M, Oyadiji SO, Tsang DKL. Computations of modes I and II stress intensity factors of sharp notched plates under in-plane shear and bending loading by the fractal-like finite element method. Int J Solids Struct 2008;45:6468–84.
[22] Treifi M, Oyadiji SO, Tsang DKL. Computation of the stress intensity factors of sharp notched plates by the fractal-like finite element method. Int J Numer Methods Eng 2009;77:558–80.
[23] Treifi M, Oyadiji SO, Tsang DKL. Computations of the stress intensity factors of double-edge and centre V-notched plates under tension and anti-plane shear by the fractal-like finite element method. Eng Fract Mech 2009;76:2091–108.
[24] Treifi M, Oyadiji SO. Computations of SIFs for non-symmetric V-notched plates by the FFEM. In: ASME Conf. Proc. IDETC/CIE2009, no. 3; 2009. p. 711–17.
[25] Theocaris PS. The order of singularity at a multi-wedge corner of a composite plate. Int J Eng Sci 1974;12:107–20.
[26] Dempsey JP, Sinclair GB. On the singular behavior at the vertex of a bi-material wedge. J Elast 1981;11:317–27.
[27] Hein VL, Erdogan F. Stress singularities in a two-material wedge. Int J Fract 1971;7:317–30.
[28] Lin KY, Mar JW. Finite element analysis of stress intensity factors for cracks at a bi-material interface. Int J Fract 1976;12:521–31.
[29] Yau JF, Wang SS. An analysis of interface cracks between dissimilar isotropic materials using conservation integrals in elasticity. Eng Fract Mech 1984;20:423–32.
[30] Lee KY, Choi HJ. Boundary element analysis of stress intensity factors for bimaterial interface cracks. Eng Fract Mech 1988;29:461–72.
[31] Matsumto T, Tanaka M, Obara R. Computation of stress intensity factors of interface cracks based on interaction energy release rates and BEM sensitivity analysis. Eng Fract Mech 2000;65:683–702.
[32] Carpenter WC, Byers C. A path independent integral for computing stress intensities for V-notched cracks in a bi-material. Int J Fract 1987;35:245–68.
[33] Tan MA, Meguid SA. Analysis of bimaterial wedges using a new singular finite element. Int J Fract 1997;88:373–91.
[34] Chen MC, Sze KY. A novel hybrid finite element analysis of bimaterial wedge problems. Eng Fract Mech 2001;68:1463–76.
[35] Wu K-C, Chiu Y-T. Antiplane shear interface cracks in anisotropic bimaterials. J Appl Mech 1991;58:399–403.
[36] Lee KW, Earmme YY. An interfacial edge crack in anisotropic bimaterial under anti-plane singularity. Int J Fract 2000;104:15–22.
[37] Li X-F. Closed-form solution for a mode-III interface crack between two bonded dissimilar elastic layers. Int J Fract 2001;109:L3–8.
[38] Li X-F, Duan X-Y. An interfacially-cracked orthotropic rectangular bi-material subjected to antiplane shear loading. Appl Math Comput 2006;174:1060–79.
[39] Jun Q, Yuqiu L. Sub-region mixed fem for calculating stress intensity factor of antiplane notch in bi-material. Eng Fract Mech 1992;43:1003–7.
[40] Liu C-I, Chue C-H. On the stress singularity of dissimilar anisotropic wedges and junctions in antiplane shear. Compos Struct 2006;73:432–42.
[41] Ma C-C, Hour B-L. Analysis of dissimilar anisotropic wedges subjected to antiplane shear deformation. Int J Solids Struct 1989;25:1295–309.
[42] ABAQUS Documentation: Version 6.5, ABAQUS, Inc.; 2004.
[43] Press WH, Flannery BP, Teukolsky SA, Vetterling WT. Numerical Recipes: The Art of Scientific Computing. Cambridge University Press; 1986.
[44] Yosibash Z, Bussiba AR, Gilad I. Failure criteria for brittle elastic materials. Int J Fract 2004;125:307–33.
[45] Lazzarin P, Berto F. From Neuber's elementary volume to Kitagawa and Atzori's diagrams: an interpretation based on local energy. Int J Fract 2005;135:L33–8.

Please cite this article in press as: Treifi M, Oyadiji SO. Evaluation of mode III stress intensity factors for bi-material notched bodies using the fractal-like finite element method. Comput Struct (2013), http://dx.doi.org/10.1016/j.compstruc.2013.02.015

Chapter 10

Strain Energy Approach to Compute Stress Intensity Factors for Isotropic Homogeneous and Bi-material V-notches

International Journal of Solids and Structures 2013; 50: 2196-2212

http://dx.doi.org/10.1016/j.ijsolstr.2013.03.011

ARTICLE IN PRESS

International Journal of Solids and Structures xxx (2013) xxx–xxx

Contents lists available at SciVerse ScienceDirect

International Journal of Solids and Structures

journal homepage: www.elsevier.com/locate/ijsolstr

Strain energy approach to compute stress intensity factors for isotropic homogeneous and bi-material V-notches

Muhammad Treifi, S. Olutunde Oyadiji *

School of Mechanical, Aerospace and Civil Engineering, University of Manchester, Manchester M13 9PL, UK

ARTICLE INFO

Article history:
Received 18 October 2012
Received in revised form 8 March 2013
Available online xxxx

Keywords:
Strain energy
Stress intensity factor
Notch
Finite element method
Bi-material
Fracture mechanics

ABSTRACT

A strain energy approach (SEA) is developed to compute the general stress intensity factors (SIFs) for isotropic homogeneous and bi-material plates containing cracks and notches subject to mode I, II and III loading conditions. The approach is based on the strain energy of a control volume around the notch tip, which may be computed by using commercial finite element packages. The formulae are simple and easy to implement. Various numerical examples are presented and compared to corresponding published results or results that are computed using different numerical methods to demonstrate the accuracy of the SEA. Many of those results are new, especially for the cases of bi-material notches where the problem is quite complicated.

1. Introduction

The importance of studying stress intensities caused by the presence of sharp corners/notches has led to much research devoted to the analysis of sharp notches. The presence of sharp notches causes stress intensities around the notch tip. This area is vulnerable to a crack initiation that may lead to structural failure or shortening of the service life of a structure. Most of the research in literature is for isotropic homogeneous cases. Very little is done for bi-material notch problems, due to its complexity.

It is well known that, in linear elastic fracture mechanics, the stresses at a notch tip become infinite (singular) (Williams, 1952, 1957). Based on experimental findings by Seweryn (1994), it was demonstrated that simple failure criteria based on the notch SIFs exist. Therefore, some researchers tried to establish a failure criterion for notch problems, such as Knésl (1991), Gómez and Elices (2003) and Carpinteri et al. (2008). Other researchers developed different methods and procedures to compute the notch SIFs such as the boundary collocation method (Gross and Mendelson, 1972), the boundary element singularity subtraction technique (Portela et al., 1991), singular finite elements (Lin and Tong, 1980) and finite element post-processing approaches (Babuška and Miller, 1984). Semi-analytical methods are also developed to compute the SIFs of a notch such as the hybrid crack element (HCE) (Tong et al., 1973), the scaled boundary finite element method (SBFEM) (Wolf, 2003), and the fractal-like finite element method (FFEM) (Leung and Su, 1994; Treifi et al., 2008, 2009a,b, 2007; Treifi and Oyadiji, 2009). Those methods are capable of computing not only the SIFs but also the higher order terms of the notch tip asymptotic field.

Most of the work mentioned above dealt only with homogeneous crack/notch problems. For bi-material problems, published results are available mainly for interfacial crack problems. For bi-material notches, published SIFs are rare, because the problem is quite complicated. For interface crack cases, Williams (1959) investigated configurations of dissimilar materials containing interface cracks. Lin and Mar (1976) developed a hybrid crack element. Lee and Choi (1988) used a boundary element method which employed the multi-region technique and the double-point concept. Yau and Wang (1984) developed a procedure based on the evaluation of conservation integrals. Matsumto et al. (2000) used an approach based on the interaction energy release rates to compute the SIFs of interface cracks. Researchers who dealt with bi-material notch problems are few, and their research work was more about studying the stress and displacement fields and the behaviour of the singular eigenvalues. Early work was carried out by Bogy (1968, 1970) and Bogy and Wang (1971). Carpenter and Byers (1987) used a reciprocal work contour integral method. Tan and Meguid (1997) developed a singular finite element formulated using expressions of the singular stress and displacement fields of a bi-material notch. Chen and Sze (2001) developed a hybrid finite element formulated using numerically obtained asymptotic stress and displacement fields. Carpinteri et al. (2006) presented an approximate analytical model based on the theory of multi-layered beams to compute mode I SIFs for a general notch perpendicular to a bi-material interface. Paggi and Carpinteri (2008) presented a comprehensive review of interface mechanical problems leading to stress singularities.

* Corresponding author. Tel.: +44 161 2754348.
E-mail addresses: m.treifi@mmu.ac.uk (M. Treifi), s.o.oyadiji@manchester.ac.uk (S.O. Oyadiji).

0020-7683/$ - see front matter © 2013 Elsevier Ltd. All rights reserved.
http://dx.doi.org/10.1016/j.ijsolstr.2013.03.011

Please cite this article in press as: Treifi, M., Oyadiji, S.O. Strain energy approach to compute stress intensity factors for isotropic homogeneous and bi-material V-notches. Int. J. Solids Struct. (2013), http://dx.doi.org/10.1016/j.ijsolstr.2013.03.011

In this paper, we present a strain energy based approach to compute the SIF values for homogeneous and bi-material notch problems subject to mode I, II and III loading conditions. The approach is based on the work of Lazzarin and Zambardi (2001), Lazzarin and Berto (2005), Lazzarin and Filippi (2006), Lazzarin and Zappalorto (2008), Lazzarin et al. (2010), Berto and Lazzarin (2007), Radaj et al. (2009), Zappalorto and Lazzarin (2011) and Zappalorto et al. (2008) who developed the idea of using averaged strain energy over a control volume around a notch tip to compute the SIFs for sharp and rounded notches. They dealt mainly with homogeneous pure mode I, II or III cases. For mixed mode I and II cases, they usually neglected the effect of mode II SIF (Lazzarin and Zambardi, 2001) where they used examples with non-singular mode II stress components, but in a recent publication (Lazzarin et al., 2010) they suggested using two concentric volumes to compute mode I and II notch SIFs. However, this approach does not always work as will be discussed later. In the current work, we simply partition the control volume and the integral accordingly to compute mode I and II SIFs for homogeneous mixed-mode and bi-material notch problems. This new strategy is operationally very simple to implement. It involves simple mathematical operations that can be carried out numerically. The strain energy for the control volume could be computed by using commercial finite element packages. In most of these packages, it is not possible to compute notch SIFs, but the SEA empowers analysts to compute notch SIFs. The accuracy of the approach is tested via many examples of isotropic homogeneous and bi-material notches under different loading conditions. The results are compared to available published results and results computed numerically using different numerical methods; the agreement is very good. Also, new results are presented.

2. Strain energy approach

The strain energy of a finite volume around a notch-tip can be written as (Bower, 2010)

$$E^{(e)} = \int_V W^{(e)} dV \tag{1}$$

where $W^{(e)}$ is the strain energy density and can be computed as follows

$$W^{(e)} = \int \sigma : \partial\varepsilon \tag{2}$$

where σ and ε are stress and strain tensors, respectively. For an isotropic material, the strain energy density $W^{(e)}$ for a generalised state of stress can be written as

$$W^{(e)} = \frac{1}{2}[\sigma_{xx}\varepsilon_{xx} + \sigma_{yy}\varepsilon_{yy} + \sigma_{zz}\varepsilon_{zz} + \tau_{xy}\gamma_{xy} + \tau_{xz}\gamma_{xz} + \tau_{yz}\gamma_{yz}] \tag{3}$$

The strains can be written in terms of the stresses by using Hooke's law

$$\begin{aligned}
\varepsilon_{xx} &= \frac{1}{E}[\sigma_{xx} - \nu(\sigma_{yy} + \sigma_{zz})] \\
\varepsilon_{yy} &= \frac{1}{E}[\sigma_{yy} - \nu(\sigma_{xx} + \sigma_{zz})] \\
\varepsilon_{zz} &= \frac{1}{E}[\sigma_{zz} - \nu(\sigma_{xx} + \sigma_{yy})] \\
\gamma_{xy} &= \frac{1}{G}\tau_{xy} \\
\gamma_{yz} &= \frac{1}{G}\tau_{yz} \\
\gamma_{xz} &= \frac{1}{G}\tau_{xz} \\
G &= \frac{E}{2(1+\nu)}
\end{aligned} \tag{4}$$

where E, G, ν are Young's modulus, shear modulus and Poisson's ratio, respectively. For simplicity the stresses can be expressed as

$$\sigma_{ij} = f(K_I, K_{II}, K_{III}, r, \theta) \tag{5}$$

where K_I, K_{II} and K_{III} are the mode I, II and III SIFs, respectively. By substituting the stress expressions into Eq. (1) and carrying out the integration over a finite volume around the notch tip, Eq. (1) becomes a representation of a direct relation between the strain energy for a finite volume and the SIFs. The strain energy could be easily computed using a commercial finite element package. Most FE packages are not, to our knowledge, capable of computing the SIFs for general notches. Therefore, this approach is quite useful to extract SIFs for general notches by using current commercial FE packages. Eq. (1) could be partitioned to deal with bi-material or mixed mode cases where two equations are needed to compute mode I and mode II SIFs. This will be discussed in detail in the next sections.

2.1. Isotropic homogeneous notch

2.1.1. Relationships between stress intensity factors and strain energy of a finite volume around a notch tip under in-plane loading conditions (mode I, II and mixed mode)

For the in-plane problem, the strain energy density is

$$W^{(e)} = \frac{1}{2E}\left[\sigma_{xx}^2 + \sigma_{yy}^2 + \sigma_{zz}^2 - 2\nu(\sigma_{xx}\sigma_{yy} + \sigma_{xx}\sigma_{zz} + \sigma_{yy}\sigma_{zz}) + 2(1+\nu)\tau_{xy}^2\right] \tag{6}$$

where $\sigma_{zz} = 0$ under plane-stress and $\sigma_{zz} = \nu(\sigma_{xx} + \sigma_{yy})$ under plane-strain.

The stress expressions for a general homogeneous notch as seen in Fig. 1 are (Williams, 1952; Portela et al., 1991)

$$\begin{aligned}
\sigma_{xx} = {} & \lambda^I r^{\lambda^I - 1} A_1 [(2 + \lambda^I \cos 2\alpha + \cos 2\lambda^I \alpha) \cos(\lambda^I - 1)\theta \\
& - (\lambda^I - 1)\cos(\lambda^I - 3)\theta] \\
& + \lambda^{II} r^{\lambda^{II} - 1} A_2 [-(2 + \lambda^{II} \cos 2\alpha - \cos 2\lambda^{II}\alpha) \sin(\lambda^{II} - 1)\theta \\
& + (\lambda^{II} - 1)\sin(\lambda^{II} - 3)\theta]
\end{aligned} \tag{7}$$

$$\begin{aligned}
\sigma_{yy} = {} & \lambda^I r^{\lambda^I - 1} A_1 [(2 - \lambda^I \cos 2\alpha - \cos 2\lambda^I \alpha) \cos(\lambda^I - 1)\theta \\
& + (\lambda^I - 1)\cos(\lambda^I - 3)\theta] + \lambda^{II} r^{\lambda^{II} - 1} A_2 [(-2 + \lambda^{II} \cos 2\alpha \\
& - \cos 2\lambda^{II}\alpha) \sin(\lambda^{II} - 1)\theta - (\lambda^{II} - 1)\sin(\lambda^{II} - 3)\theta]
\end{aligned} \tag{8}$$

$$\begin{aligned}
\tau_{xy} = {} & \lambda^I r^{\lambda^I - 1} A_1 [-(\lambda^I \cos 2\alpha + \cos 2\lambda^I \alpha) \sin(\lambda^I - 1)\theta \\
& + (\lambda^I - 1)\sin(\lambda^I - 3)\theta] \\
& + \lambda^{II} r^{\lambda^{II} - 1} A_2 [-(\lambda^{II} \cos 2\alpha - \cos 2\lambda^{II}\alpha) \cos(\lambda^{II} - 1)\theta \\
& + (\lambda^{II} - 1)\cos(\lambda^{II} - 3)\theta]
\end{aligned} \tag{9}$$

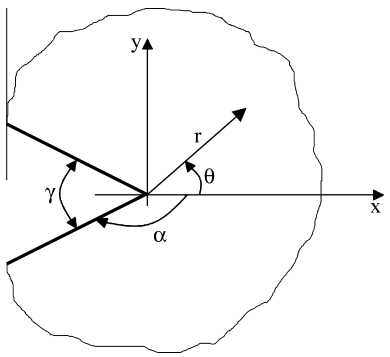

Fig. 1. Isotropic homogeneous notch geometry.

Please cite this article in press as: Treifi, M., Oyadiji, S.O. Strain energy approach to compute stress intensity factors for isotropic homogeneous and bi-material V-notches. Int. J. Solids Struct. (2013), http://dx.doi.org/10.1016/j.ijsolstr.2013.03.011

where λ^I and λ^{II} are eigenvalues and are computed using the following characteristic equations

$$\lambda^I \sin 2\alpha + \sin 2\lambda^I\alpha = 0 \tag{10}$$

$$\lambda^{II} \sin 2\alpha - \sin 2\lambda^{II}\alpha = 0 \tag{11}$$

A_1 and A_2 are constants related to the mode I and mode II SIFs

$$K_I = \sqrt{2\pi}\lambda^I\left(1 + \lambda^I - \lambda^I \cos 2\alpha - \cos 2\lambda^I\alpha\right)A_1 \tag{12}$$

$$K_{II} = \sqrt{2\pi}\lambda^{II}\left(-1 + \lambda^{II} - \lambda^{II} \cos 2\alpha + \cos 2\lambda^{II}\alpha\right)A_2 \tag{13}$$

Eqs. (7)–(9) are eigenfunction series expansions (the Σ symbol is dropped for simplicity). In the SEA, only the singular terms are considered. The stress expressions in Eqs. (7)–(9) can be rewritten for simplicity as

$$\sigma_{xx} = A_1 r^{\lambda^I-1} f_x(\theta) + A_2 r^{\lambda^{II}-1} g_x(\theta) = A_1 r^{\lambda^I-1} f_x + A_2 r^{\lambda^{II}-1} g_x \tag{14}$$

$$\sigma_{yy} = A_1 r^{\lambda^I-1} f_y(\theta) + A_2 r^{\lambda^{II}-1} g_y(\theta) = A_1 r^{\lambda^I-1} f_y + A_2 r^{\lambda^{II}-1} g_y \tag{15}$$

$$\tau_{xy} = A_1 r^{\lambda^I-1} f_{xy}(\theta) + A_2 r^{\lambda^{II}-1} g_{xy}(\theta) = A_1 r^{\lambda^I-1} f_{xy} + A_2 r^{\lambda^{II}-1} g_{xy} \tag{16}$$

Under plane-stress, substituting the above equations into Eq. (6) gives

$$\begin{aligned} W^{(e)} = \frac{1}{2E}\Big[& A_1^2 r^{2(\lambda^I-1)}\left(f_x^2 + f_y^2 - 2\nu f_x f_y + 2(1+\nu)f_{xy}^2\right) \\ & + A_2^2 r^{2(\lambda^{II}-1)}\left(g_x^2 + g_y^2 - 2\nu g_x g_y + 2(1+\nu)g_{xy}^2\right) \\ & + A_1 A_2 r^{(\lambda^I+\lambda^{II}-2)}\left(2f_x g_x + 2f_y g_y - 2\nu(f_x g_y + f_y g_x)\right. \\ & \left. + 4(1+\nu)f_{xy}g_{xy}\right)\Big] \end{aligned} \tag{17}$$

By substituting Eq. (17) into Eq. (1), the strain energy for a finite volume of a radius R_c around a notch tip is

$$\begin{aligned} E^{(e)} &= \int_0^{R_c}\int_{-\alpha}^{+\alpha} W^{(e)} r dr d\theta \\ &= \frac{1}{2E}\left\{ A_1^2 \frac{R_c^{2\lambda^I}}{2\lambda^I}\int_{-\alpha}^{+\alpha}\left(f_x^2 + f_y^2 - 2\nu f_x f_y + 2(1+\nu)f_{xy}^2\right)d\theta \right. \\ &\quad + A_2^2 \frac{R_c^{2\lambda^{II}}}{2\lambda^{II}}\int_{-\alpha}^{+\alpha}\left(g_x^2 + g_y^2 - 2\nu g_x g_y + 2(1+\nu)g_{xy}^2\right)d\theta \\ &\quad + A_1 A_2 \frac{R_c^{(\lambda^I+\lambda^{II})}}{(\lambda^I+\lambda^{II})}\int_{-\alpha}^{+\alpha}\left(2f_x g_x + 2f_y g_y - 2\nu(f_x g_y + f_y g_x)\right. \\ &\quad \left.\left. + 4(1+\nu)f_{xy}g_{xy}\right)d\theta \right\} \end{aligned} \tag{18}$$

Substituting Eqs. (12) and (13) into Eq. (18) gives a quadratic equation with two unknowns

$$E^{(e)} = MK_I^2 + NK_{II}^2 + QK_I K_{II} \tag{19}$$

It should be noted that the coefficients M, N and Q have different dimensional units. Sih (1974) reported a similar expression relating the strain energy density to the crack SIFs when he introduced a strain energy density factor as a fracture parameter for crack problems. The integration could be carried out numerically by using, for example, Composite Simpson's rule. Eq. (19) illustrates a direct relation between the SIFs and the strain energy of a finite volume around the notch tip. For pure mode I or pure mode II, Eq. (19) can be used to compute mode I SIF, K_I, or mode II SIF, K_{II} ($E^{(e)} = MK_I^2$ for pure mode I and $E^{(e)} = NK_{II}^2$ for pure mode II). However, in the case of mixed mode problems, Eq. (19) represents an equation that contains two unknowns K_I and K_{II}. To overcome this, Eq. (19) could be partitioned into two regions: one below the bisector ($-\alpha$ to 0) and the other above the bisector (0 to $+\alpha$) as shown in Fig. 2. This leads to the following two quadratic equations with two unknowns

$$E_1^{(e)} = \int_0^{R_c}\int_{-\alpha}^{0} W^{(e)} r dr d\theta = M_1 K_I^2 + N_1 K_{II}^2 + Q_1 K_I K_{II} \tag{20}$$

$$E_2^{(e)} = \int_0^{R_c}\int_{0}^{+\alpha} W^{(e)} r dr d\theta = M_2 K_I^2 + N_2 K_{II}^2 + Q_2 K_I K_{II} \tag{21}$$

Due to the symmetry, the following relations hold

$$\begin{aligned} M_1 &= M_2 \\ N_1 &= N_2 \\ Q_1 &= -Q_2 \end{aligned} \tag{22}$$

After some simple algebraic manipulations, the mode I and II SIFs can be computed using the following equations

$$K_{II} = \frac{E_1^{(e)} - E_2^{(e)}}{2Q_1 K_I} \tag{23}$$

$$2M_1 K_I^4 - \left(E_1^{(e)} + E_2^{(e)}\right)K_I^2 + \frac{N_1\left(E_1^{(e)} - E_2^{(e)}\right)^2}{2Q_1^2} = 0 \tag{24}$$

Obviously, Eqs. (23) and (24) would give more than one set of answers. Usually it is easy to determine the correct set. However, for less experienced analysts, the ratio of the relative displacements of the notch faces could be used to determine the right set of answers. For a crack problem, the following equation holds

$$\frac{K_I}{K_{II}} = \frac{\Delta_y}{\Delta_x} \tag{25}$$

where $\Delta_y = v_1(r_0, \alpha_1) - v_2(r_0, \alpha_2)$ and $\Delta_x = u_1(r_0, \alpha_2) - u_2(r_0, \alpha_2)$ are the relative displacements of the crack faces. Eq. (25) could be used as an approximation for notch cases too i.e. $\frac{K_I}{K_{II}} \approx \frac{\Delta_y}{\Delta_x}$. Because Δ_x and Δ_y are computed numerically using finite element analysis, Eq. (25) is better considered as an approximation rather than an equality. The displacements of two nodes facing each other on the notch faces such as the nodes 1 and 2 as shown in Fig. 2 could be used. It is advisable to consider nodes that are reasonably far from the notch tip.

Lazzarin et al. (2010) suggested using two concentric circles with different radii to deal with mixed mode cases, but their suggestion cannot be used for the special case of a notch with an opening angle of zero, i.e. a crack.

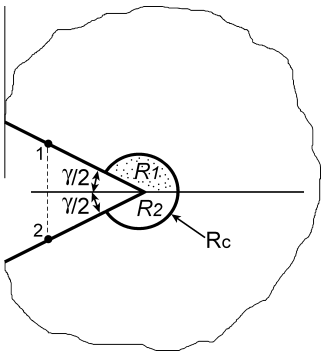

Fig. 2. Partitioning of the control volume.

Please cite this article in press as: Treifi, M., Oyadiji, S.O. Strain energy approach to compute stress intensity factors for isotropic homogeneous and bi-material V-notches. Int. J. Solids Struct. (2013), http://dx.doi.org/10.1016/j.ijsolstr.2013.03.011

2.1.2. Relationships between stress intensity factors and strain energy of a finite volume around a notch tip under out-of-plane loading conditions (mode III)

For the out-of-plane problem, the strain energy density is

$$W^{(e)} = \frac{1}{2G}\left[\tau_{rz}^2 + \tau_{\theta z}^2\right] \tag{26}$$

The stress expressions for a general homogeneous notch under mode III loading conditions are

$$\tau_{rZ} = G\lambda^{III} r^{\lambda^{III}-1} B \sin\lambda^{III}\theta \tag{27}$$

$$\tau_{\theta Z} = G\lambda^{III} r^{\lambda^{III}-1} B \cos\lambda^{III}\theta \tag{28}$$

where $\lambda^{III} = \frac{n\pi}{2\alpha}; n = 1, 2, 3, \ldots$ and B is a constant. For detailed derivations, one may refer to Seweryn and Molski (1996). Eqs. (27) and (28) are eigenfunction series expansions (the Σ symbol is dropped for simplicity). In the SEA, only the singular term is considered, i.e. $n = 1$. The constant B associated with the singular eigenvalue is related to the mode III SIF

$$K_{III} = \sqrt{2\pi} G\lambda^{III} B \tag{29}$$

By substituting Eqs. (27)–(29) into Eqs. (26) and (1), and after some algebraic manipulations, the strain energy of a finite volume under mode III conditions can be written as

$$E^{(e)} = \frac{R_c^{2\lambda^{III}} K_{III}^2 \alpha}{4\pi G \lambda^{III}} \tag{30}$$

This equation is in agreement with an expression presented by Lazzarin and Zappalorto (2008) relating the strain energy density to the mode III SIF. Eq. (30) represents a simple analytical formula that links the mode III SIF to the strain energy of a finite volume around and a notch tip.

2.2. Bi-material notch

2.2.1. Relationships between stress intensity factors and strain energy of a finite volume around a notch tip under in-plane loading conditions (mode I, II and mixed mode)

For the in-plane bi-material problem, the expression for the strain energy density is

$$W^{j(e)} = \frac{1}{2E_j}\left[\left(\sigma_{xx}^j\right)^2 + \left(\sigma_{yy}^j\right)^2 + \left(\sigma_{zz}^j\right)^2 - 2\nu_j\left(\sigma_{xx}^j\sigma_{yy}^j + \sigma_{xx}^j\sigma_{zz}^j + \sigma_{yy}^j\sigma_{zz}^j\right) + 2\left(1+\nu_j\right)\left(\tau_{xy}^j\right)^2\right] \tag{31}$$

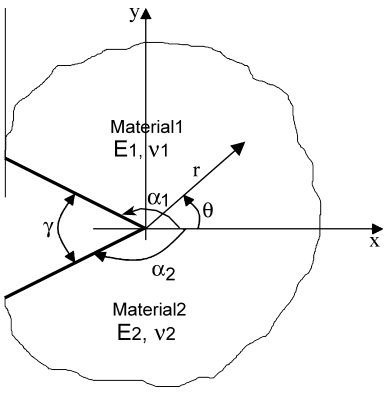

Fig. 3. Bi-material notch geometry.

where j refers to the material. Under plane-stress conditions $\sigma_{zz} = 0$, and under plane-strain conditions $\sigma_{zz} = \nu(\sigma_{xx} + \sigma_{yy})$.

The stress expressions for a general bi-material notch as seen in Fig. 3 are (Carpenter and Byers, 1987)

$$\begin{aligned}2\sigma_{xx}^{(1)} = {} & \lambda r^{\lambda-1} A_1\left[3e^{i\theta(\lambda-1)} - e^{-i\theta(1-\lambda)}\left(e^{-2i\theta}-1\right)(\lambda-1)\right.\\ & \left.+Y_2\left(3e^{-i\theta(\lambda-1)} - e^{i\theta(1-\lambda)}\left(e^{2i\theta}-1\right)(\lambda-1)\right) - S_1 e^{i\theta(1-\lambda)} - \overline{S}_2 e^{-i\theta(1-\lambda)}\right]\\ & +\overline{\lambda} r^{\overline{\lambda}-1}\overline{A}_1\left[\overline{Y}_2\left(3e^{i\theta(\overline{\lambda}-1)} - e^{-i\theta\left(1-\overline{\lambda}\right)}\left(e^{-2i\theta}-1\right)(\overline{\lambda}-1)\right)\right.\\ & \left.+3e^{-i\theta\left(\overline{\lambda}-1\right)} - e^{i\theta(1-\overline{\lambda})}\left(e^{2i\theta}-1\right)(\overline{\lambda}-1) - S_2 e^{i\theta(1-\overline{\lambda})} - \overline{S}_1 e^{-i\theta(1-\overline{\lambda})}\right]\end{aligned} \tag{32}$$

$$\begin{aligned}2\sigma_{xx}^{(2)} = {} & \lambda r^{\lambda-1} A_1\left[Y_1\left(3e^{i\theta(\lambda-1)} - e^{-i\theta(1-\lambda)}\left(e^{-2i\theta}-1\right)(\lambda-1)\right)\right.\\ & +Y_3\left(3e^{-i\theta(\lambda-1)} - e^{i\theta(1-\lambda)}\left(e^{2i\theta}-1\right)(\lambda-1)\right)\\ & \left.-S_3 e^{i\theta(1-\lambda)} - \overline{S}_4 e^{-i\theta(1-\lambda)}\right]\\ & +\overline{\lambda} r^{\overline{\lambda}-1}\overline{A}_1\left[\overline{Y}_3\left(3e^{i\theta(\overline{\lambda}-1)} - e^{-i\theta(1-\overline{\lambda})}\left(e^{-2i\theta}-1\right)(\overline{\lambda}-1)\right)\right.\\ & \left.+\overline{Y}_1\left(3e^{-i\theta(\overline{\lambda}-1)} - e^{i\theta(1-\overline{\lambda})}\left(e^{2i\theta}-1\right)(\overline{\lambda}-1)\right) - S_4 e^{i\theta(1-\overline{\lambda})} - \overline{S}_3 e^{-i\theta(1-\overline{\lambda})}\right]\end{aligned} \tag{33}$$

$$\begin{aligned}2\sigma_{yy}^{(1)} = {} & \lambda r^{\lambda-1} A_1\left[e^{i\theta(\lambda-1)} + e^{-i\theta(1-\lambda)}\left(e^{-2i\theta}-1\right)(\lambda-1)\right.\\ & \left.+Y_2\left(e^{-i\theta(\lambda-1)} + e^{i\theta(1-\lambda)}\left(e^{2i\theta}-1\right)(\lambda-1)\right) + S_1 e^{i\theta(1-\lambda)} + \overline{S}_2 e^{-i\theta(1-\lambda)}\right]\\ & +\overline{\lambda} r^{\overline{\lambda}-1}\overline{A}_1\left[\overline{Y}_2\left(e^{i\theta(\overline{\lambda}-1)} + e^{-i\theta(1-\overline{\lambda})}\left(e^{-2i\theta}-1\right)(\overline{\lambda}-1)\right)\right.\\ & \left.+e^{-i\theta(\overline{\lambda}-1)} + e^{i\theta(1-\overline{\lambda})}\left(e^{2i\theta}-1\right)(\overline{\lambda}-1) + S_2 e^{i\theta(1-\overline{\lambda})} + \overline{S}_1 e^{-i\theta(1-\overline{\lambda})}\right]\end{aligned} \tag{34}$$

$$\begin{aligned}2\sigma_{yy}^{(2)} = {} & \lambda r^{\lambda-1} A_1\left[Y_1\left(e^{i\theta(\lambda-1)} + e^{-i\theta(1-\lambda)}\left(e^{-2i\theta}-1\right)(\lambda-1)\right)\right.\\ & \left.+Y_3\left(e^{-i\theta(\lambda-1)} + e^{i\theta(1-\lambda)}\left(e^{2i\theta}-1\right)(\lambda-1)\right) + S_3 e^{i\theta(1-\lambda)} + \overline{S}_4 e^{-i\theta(1-\lambda)}\right]\\ & +\overline{\lambda} r^{\overline{\lambda}-1}\overline{A}_1\left[\overline{Y}_3\left(e^{i\theta(\overline{\lambda}-1)} + e^{-i\theta(1-\overline{\lambda})}\left(e^{-2i\theta}-1\right)(\overline{\lambda}-1)\right)\right.\\ & \left.+\overline{Y}_1\left(e^{-i\theta(\overline{\lambda}-1)} + e^{i\theta(1-\overline{\lambda})}\left(e^{2i\theta}-1\right)(\overline{\lambda}-1)\right) + S_4 e^{i\theta(1-\overline{\lambda})} + \overline{S}_3 e^{-i\theta(1-\overline{\lambda})}\right]\end{aligned} \tag{35}$$

$$\begin{aligned}2i\tau_{xy}^{(1)} = {} & \lambda r^{\lambda-1} A_1\left[Y_2\left(e^{-i\theta(\lambda-1)} - e^{i\theta(1-\lambda)}\left(e^{2i\theta}-1\right)(\lambda-1)\right)\right.\\ & \left.+e^{-i\theta(1-\lambda)}\left(e^{-2i\theta}-1\right)(\lambda-1) - e^{i\theta(\lambda-1)} + \overline{S}_2 e^{-i\theta(1-\lambda)} - S_1 e^{i\theta(1-\lambda)}\right]\\ & +\overline{\lambda} r^{\overline{\lambda}-1}\overline{A}_1\left[e^{-i\theta(\overline{\lambda}-1)} - e^{i\theta(1-\overline{\lambda})}\left(e^{2i\theta}-1\right)(\overline{\lambda}-1)\right.\\ & \left.+\overline{Y}_2\left(e^{-i\theta(1-\overline{\lambda})}\left(e^{-2i\theta}-1\right)(\overline{\lambda}-1) - e^{i\theta(\overline{\lambda}-1)}\right) + \overline{S}_1 e^{i\theta(1-\overline{\lambda})} - S_2 e^{i\theta(1-\overline{\lambda})}\right]\end{aligned} \tag{36}$$

$$\begin{aligned}2i\tau_{xy}^{(2)} = {} & \lambda r^{\lambda-1} A_1\left[Y_3\left(e^{-i\theta(\lambda-1)} - e^{i\theta(1-\lambda)}\left(e^{2i\theta}-1\right)(\lambda-1)\right)\right.\\ & \left.+Y_1\left(e^{-i\theta(1-\lambda)}\left(e^{-2i\theta}-1\right)(\lambda-1) - e^{i\theta(\lambda-1)}\right) + \overline{S}_4 e^{-i\theta(1-\lambda)} - S_3 e^{i\theta(1-\lambda)}\right]\\ & +\overline{\lambda} r^{\overline{\lambda}-1}\overline{A}_1\left[\overline{Y}_1\left(e^{-i\theta(\overline{\lambda}-1)} - e^{i\theta(1-\overline{\lambda})}\left(e^{2i\theta}-1\right)(\overline{\lambda}-1)\right)\right.\\ & \left.+\overline{Y}_3\left(e^{-i\theta(1-\overline{\lambda})}\left(e^{-2i\theta}-1\right)(\overline{\lambda}-1) - e^{i\theta(\overline{\lambda}-1)}\right) + \overline{S}_3 e^{-i\theta(1-\overline{\lambda})} - S_4 e^{i\theta(1-\overline{\lambda})}\right]\end{aligned} \tag{37}$$

where

$$S_1 = -e^{2i\lambda\alpha_1} - \left(e^{2i\alpha_1} - 1\right)\lambda Y_2$$

$$S_2 = -\overline{Y}_2 e^{2i\overline{\lambda}\alpha_1} - \left(e^{2i\alpha_1} - 1\right)\overline{\lambda}$$

$$S_3 = -Y_1 e^{-2i\lambda\alpha_2} - \left(e^{-2i\alpha_2} - 1\right)\lambda Y_3$$

Please cite this article in press as: Treifi, M., Oyadiji, S.O. Strain energy approach to compute stress intensity factors for isotropic homogeneous and bi-material V-notches. Int. J. Solids Struct. (2013), http://dx.doi.org/10.1016/j.ijsolstr.2013.03.011

$$S_4 = -\overline{Y}_3 e^{-2i\overline{\lambda}\alpha_2} - \left(e^{-2i\alpha_2} - 1\right)\overline{\lambda}\overline{Y}_1$$

$$\mathbf{Y} = \begin{Bmatrix} Y_1 \\ Y_2 \\ Y_3 \end{Bmatrix} = -\mathbf{D}_{\mathbf{22}}^{-1}\mathbf{D}_{\mathbf{21}}$$

$$\mathbf{D_{22}} = \begin{bmatrix} -\kappa_2 + e^{-2i\lambda\alpha_2} & \frac{G_2}{G_1}\lambda\left(e^{2i\alpha_1} - 1\right) & \lambda\left(1 - e^{-2i\alpha_2}\right) \\ \lambda\left(e^{2i\alpha_2} - 1\right) & 1 - e^{-2i\lambda\alpha_1} & e^{2i\lambda\alpha_2} - 1 \\ \lambda\left(1 - e^{2i\alpha_2}\right) & \frac{G_2}{G_1}\left(\kappa_1 + e^{-2i\lambda\alpha_1}\right) & -\left(\kappa_2 + e^{2i\lambda\alpha_2}\right) \end{bmatrix}$$

$$\mathbf{D_{21}} = \begin{bmatrix} \frac{G_2}{G_1}\left(\kappa_1 + e^{2i\lambda\alpha_1}\right) \\ \lambda\left(1 - e^{-2i\alpha_1}\right) \\ \frac{G_2}{G_1}\lambda\left(e^{-2i\alpha_1} - 1\right) \end{bmatrix}$$

and $\kappa_j = 3 - 4\nu_j$ for plane-strain and $\kappa_j = 3 - 4\nu_j/(1+\nu_j)$ for plane-stress. λ is an eigenvalue and can be determined numerically using Muller's method from the following equation

$$\det\left(\begin{bmatrix} 1 - e^{2i\lambda\alpha_1} & e^{-2i\lambda\alpha_2} - 1 & \lambda\left(1 - e^{2i\alpha_1}\right) & \lambda\left(e^{-2i\alpha_2} - 1\right) \\ \frac{G_2}{G_1}\left(\kappa_1 + e^{2i\lambda\alpha_1}\right) & -\kappa_2 + e^{-2i\lambda\alpha_2} & \frac{G_2}{G_1}\lambda\left(e^{2i\alpha_1} - 1\right) & \lambda\left(1 - e^{-2i\alpha_2}\right) \\ \lambda\left(1 - e^{-2i\alpha_1}\right) & \lambda\left(e^{2i\alpha_2} - 1\right) & 1 - e^{-2i\lambda\alpha_1} & e^{2i\lambda\alpha_2} - 1 \\ \frac{G_2}{G_1}\lambda\left(e^{-2i\alpha_1} - 1\right) & \lambda\left(1 - e^{2i\alpha_2}\right) & \frac{G_2}{G_1}\left(\kappa_1 + e^{-2i\lambda\alpha_1}\right) & -\left(\kappa_2 + e^{2i\lambda\alpha_2}\right) \end{bmatrix}\right) = 0 \tag{38}$$

Eq. (38) gives either one singular complex singular eigenvalue where $real(\lambda) < 1$ or two singular real eigenvalues $\lambda_I < 1$ and $\lambda_{II} < 1$ (in some cases only one real eigenvalue exists). An alternative matrix formulation of the stress field around a notch tip could be used as presented by Paggi and Carpinteri (2008).

For a complex eigenvalue, the complex SIF for a bi-material notch can be computed using one of the following equations

$$K_c = \sqrt{2\pi}\lambda A_1\left[Y_2\left(1 - e^{-2i\lambda\alpha_1}\right) - \lambda\left(e^{-2i\alpha_1} - 1\right)\right] \tag{39}$$

$$K_c = \sqrt{2\pi}\overline{\lambda}\overline{A}_1\left[1 - e^{-2i\overline{\lambda}\alpha_1} - \overline{\lambda}\overline{Y}_2\left(e^{-2i\alpha_1} - 1\right)\right] \tag{40}$$

Eqs. (32) and (37) are eigenfunction series expansions (the Σ symbol is dropped for simplicity). In the SEA, only the singular terms are considered. The stress expressions in Eqs. (32)–(37) can be rewritten for simplicity as

$$\sigma^j_{xx} = A_1 r^{\lambda-1} f^j_x(\theta) + \overline{A}_1 r^{\overline{\lambda}-1} g^j_x(\theta) = A_1 r^{\lambda-1} f^j_x + \overline{A}_1 r^{\overline{\lambda}-1} g^j_x \tag{41}$$

$$\sigma^j_{yy} = A_1 r^{\lambda-1} f^j_y(\theta) + \overline{A}_1 r^{\overline{\lambda}-1} g^j_y(\theta) = A_1 r^{\lambda-1} f^j_y + \overline{A}_1 r^{\overline{\lambda}-1} g^j_y \tag{42}$$

$$\tau^j_{xy} = A_1 r^{\lambda-1} f^j_{xy}(\theta) + \overline{A}_1 r^{\overline{\lambda}-1} g^j_{xy}(\theta) = A_1 r^{\lambda-1} f^j_{xy} + \overline{A}_1 r^{\overline{\lambda}-1} g^j_{xy} \tag{43}$$

Under plane-stress, substituting the above equations into Eq. (31) gives

$$\begin{aligned} W^{j(e)} = \frac{1}{2E_j}\Big[& A_1^2 r^{2(\lambda-1)}\left(f^{j\,2}_x + f^{j\,2}_y - 2\nu_j f^j_x f^j_y + 2(1+\nu_j) f^{j\,2}_{xy}\right) \\ & + \overline{A}_1^2 r^{2(\overline{\lambda}-1)}\left(g^{j\,2}_x + g^{j\,2}_y - 2\nu_j g^j_x g^j_y + 2(1+\nu_j) g^{j\,2}_{xy}\right) \\ & + A_1\overline{A}_1 r^{(\lambda+\overline{\lambda}-2)}\left(2f^j_x g^j_x + 2f^j_y g^j_y - 2\nu_j\left(f^j_x g^j_y + f^j_y g^j_x\right) + 4(1+\nu_j) f^j_{xy} g^j_{xy}\right)\Big] \end{aligned} \tag{44}$$

The strain energy for a finite volume of a radius R_c around a notch tip is obtained by substituting the above equation into Eq. (1),

$$\begin{aligned} E^{j(e)} = \int_0^{R_c}\int_\theta W^{j(e)} r dr d\theta = \frac{1}{2E_j}\Bigg\{ & A_1^2 \frac{R_c^{2\lambda}}{2\lambda}\int_\theta \left(f^{j\,2}_x + f^{j\,2}_y - 2\nu_j f^j_x f^j_y + 2(1+\nu_j) f^{j\,2}_{xy}\right) d\theta \\ & + \overline{A}_1^2 \frac{R_c^{2\overline{\lambda}}}{2\overline{\lambda}}\int_\theta \left(g^{j\,2}_x + g^{j\,2}_y - 2\nu_j g^j_x g^j_y + 2(1+\nu_j) g^{j\,2}_{xy}\right) d\theta \\ & + A_1\overline{A}_1 \frac{R_c^{(\lambda+\overline{\lambda})}}{(\lambda+\overline{\lambda})}\int_\theta \left(2f^j_x g^j_x + 2f^j_y g^j_y - 2\nu_j\left(f^j_x g^j_y + f^j_y g^j_x\right) + 4(1+\nu_j) f^j_{xy} g^j_{xy}\right) d\theta \Bigg\} \end{aligned} \tag{45}$$

The integration over θ is from $-\alpha_2$ to 0 for $j = 2$ (material 2) and from 0 to α_1 for $j = 1$ (material 1).

Equation (45) gives one equation per material in terms of two unknowns which are the real and imaginary parts of A_1 (or K_c). For brevity and simplicity Eq. (45) can be rewritten as

$$E^{j(e)} = A_1^2 M_j + \overline{A}_1^2 N_j + A_1\overline{A}_1 Q_j \tag{46}$$

Eq. (46) could be simplified further, because $N_j = \overline{M}_j$ and Q_j is a real number, as

$$a^2\left(2M_1^{Real} + Q_1\right) + b^2\left(Q_1 - 2M_1^{Real}\right) - 4abM_1^{Imaginary} - E^{1(e)} = 0 \tag{47}$$

for material 1, and

$$a^2\left(2M_2^{Real} + Q_2\right) + b^2\left(Q_2 - 2M_2^{Real}\right) - 4abM_2^{Imaginary} - E^{2(e)} = 0 \tag{48}$$

for material 2, where $A_1 = a + ib$. The bi-material SIFs can be computed using Eqs. (47) and (48) after computing the strain energy in material 1 and material 2 within a finite region around the notch tip of radius R_c.

For real eigenvalues λ_I and λ_{II}, the stress expressions are

$$\begin{aligned} 2\sigma^{(1)}_{xx} = \sum_k \lambda_k r^{\lambda_k - 1} a_k \Big\{ & (p_{k1} + ip_{k2})\left[e^{i\theta(\lambda_k-1)}\left(2 + \lambda_k\left(e^{-2i\alpha_1} - e^{-2i\theta}\right) + e^{-2i\theta}\right)\right. \\ & \left. + e^{2i\lambda_k\alpha_1} e^{-i\theta(\lambda_k-1)}\right] \\ & + (p_{k1} - ip_{k2})\left[e^{-i\theta(\lambda_k-1)}\left(2 + \lambda_k\left(e^{2i\alpha_1} - e^{2i\theta}\right) + e^{2i\theta}\right)\right. \\ & \left. + e^{-2i\lambda_k\alpha_1} e^{i\theta(\lambda_k-1)}\right]\Big\} \end{aligned} \tag{49}$$

$$\begin{aligned} 2\sigma^{(2)}_{xx} = \sum_k \lambda_k r^{\lambda_k - 1} a_k \{ & (s_{k1}(p_{k1} + ip_{k2}) + s_{k2}(p_{k1} - ip_{k2})) \\ & \times\left[e^{i\theta(\lambda_k-1)}\left(2 + \lambda_k\left(e^{2i\alpha_2} - e^{-2i\theta}\right) + e^{-2i\theta}\right) + e^{-2i\lambda_k\alpha_2} e^{-i\theta(\lambda_k-1)}\right] \\ & + (\overline{s}_{k1}(p_{k1} - ip_{k2}) + \overline{s}_{k2}(p_{k1} + ip_{k2})) \\ & \times\left[e^{-i\theta(\lambda_k-1)}\left(2 + \lambda_k\left(e^{-2i\alpha_2} - e^{2i\theta}\right) + e^{2i\theta}\right) + e^{2i\lambda_k\alpha_2} e^{i\theta(\lambda_k-1)}\right]\} \end{aligned} \tag{50}$$

$$\begin{aligned} 2\sigma^{(1)}_{yy} = \sum_k \lambda_k r^{\lambda_k - 1} a_k \Big\{ & (p_{k1} + ip_{k2})\left[e^{i\theta(\lambda_k-1)}\left(2 + \lambda_k\left(e^{-2i\theta} - e^{-2i\alpha_1}\right) - e^{-2i\theta}\right)\right. \\ & \left. - e^{2i\lambda_k\alpha_1} e^{-i\theta(\lambda_k-1)}\right] \\ & + (p_{k1} - ip_{k2})\left[e^{-i\theta(\lambda_k-1)}\left(2 + \lambda_k\left(e^{2i\theta} - e^{2i\alpha_1}\right) - e^{2i\theta}\right)\right. \\ & \left. - e^{-2i\lambda_k\alpha_1} e^{i\theta(\lambda_k-1)}\right]\Big\} \end{aligned} \tag{51}$$

$$\begin{aligned} 2\sigma^{(2)}_{yy} = \sum_k \lambda_k r^{\lambda_k - 1} a_k \{ & (s_{k1}(p_{k1} + ip_{k2}) + s_{k2}(p_{k1} - ip_{k2})) \\ & \times\left[e^{i\theta(\lambda_k-1)}\left(2 + \lambda_k\left(e^{-2i\theta} - e^{2i\alpha_2}\right) - e^{-2i\theta}\right) - e^{-2i\lambda_k\alpha_2} e^{-i\theta(\lambda_k-1)}\right] \\ & + (\overline{s}_{k1}(p_{k1} - ip_{k2}) + \overline{s}_{k2}(p_{k1} + ip_{k2})) \\ & \times\left[e^{-i\theta(\lambda_k-1)}\left(2 + \lambda_k\left(e^{2i\theta} - e^{-2i\alpha_2}\right) - e^{2i\theta}\right) - e^{2i\lambda_k\alpha_2} e^{i\theta(\lambda_k-1)}\right]\} \end{aligned} \tag{52}$$

$$\begin{aligned} 2i\tau^{(1)}_{xy} = \sum_k \lambda_k r^{\lambda_k - 1} a_k \Big\{ & (p_{k1} + ip_{k2})\left[e^{i\theta(\lambda_k-1)}\left(\lambda_k\left(e^{-2i\theta} - e^{-2i\alpha_1}\right) - e^{-2i\theta}\right)\right. \\ & \left. + e^{2i\lambda_k\alpha_1} e^{-i\theta(\lambda_k-1)}\right] + (p_{k1} - ip_{k2})\left[e^{-i\theta(\lambda_k-1)}\left(\lambda_k\left(e^{2i\alpha_1} - e^{2i\theta}\right) + e^{2i\theta}\right)\right. \\ & \left. - e^{-2i\lambda_k\alpha_1} e^{i\theta(\lambda_k-1)}\right]\Big\} \end{aligned} \tag{53}$$

$$\begin{aligned} 2i\tau^{(2)}_{xy} = \sum_k \lambda_k r^{\lambda_k - 1} a_k \{ & (s_{k1}(p_{k1} + ip_{k2}) + s_{k2}(p_{k1} - ip_{k2})) \\ & \times\left[e^{i\theta(\lambda_k-1)}\left(\lambda_k\left(e^{-2i\theta} - e^{2i\alpha_2}\right) - e^{-2i\theta}\right) + e^{-2i\lambda_k\alpha_2} e^{-i\theta(\lambda_k-1)}\right] \\ & + (\overline{s}_{k1}(p_{k1} - ip_{k2}) + \overline{s}_{k2}(p_{k1} + ip_{k2})) \\ & \times\left[e^{-i\theta(\lambda_k-1)}\left(\lambda_k\left(e^{-2i\alpha_2} - e^{2i\theta}\right) + e^{2i\theta}\right) - e^{2i\lambda_k\alpha_2} e^{i\theta(\lambda_k-1)}\right]\} \end{aligned} \tag{54}$$

Please cite this article in press as: Treifi, M., Oyadiji, S.O. Strain energy approach to compute stress intensity factors for isotropic homogeneous and bi-material V-notches. Int. J. Solids Struct. (2013), http://dx.doi.org/10.1016/j.ijsolstr.2013.03.011

where $k = I, II$, $s_{k1} = \frac{d_{k4}d_{k5} - d_{k1}d_{k8}}{d_{k3}d_{k8} - d_{k7}d_{k4}}$, $s_{k2} = \frac{d_{k6}d_{k4} - d_{k2}d_{k8}}{d_{k3}d_{k8} - d_{k7}d_{k4}}$, and to avoid division by zero, p_{k1} and p_{k2} can be computed using the expressions stated in Table 1 where

$$q_{k11} = \mathrm{Re}(t_{k1}) + \mathrm{Re}(t_{k2}), \quad q_{k12} = \mathrm{Im}(t_{k2}) - \mathrm{Im}(t_{k1})$$

$$q_{k21} = \mathrm{Im}(t_{k1}) + \mathrm{Im}(t_{k2}), \quad q_{k22} = \mathrm{Re}(t_{k1}) - \mathrm{Re}(t_{k2})$$

$$t_{k1} = \bar{s}_{k2} - s_{k3}, \quad t_{k2} = \bar{s}_{k1} - s_{k4}$$

Table 1
Definition of p_{k1} and p_{k2}.

Largest $\lvert q_{kij}\rvert$	p_{k1}	p_{k2}
q_{k11}	$-q_{k12}/q_{k11}$	1
q_{k12}	1	$-q_{k11}/q_{k12}$
q_{k21}	$-q_{k22}/q_{k21}$	1
q_{k22}	1	$-q_{k21}/q_{k22}$

$$s_{k3} = \frac{d_{k5}d_{k3} - d_{k1}d_{k7}}{d_{k4}d_{k7} - d_{k8}d_{k3}}, \quad s_{k4} = \frac{d_{k6}d_{k3} - d_{k2}d_{k7}}{d_{k4}d_{k7} - d_{k8}d_{k3}}$$

$$d_{k1} = G_2(\kappa_1 + e^{2i\lambda_k\alpha_1}), \quad d_{k2} = G_2\lambda_k(e^{2i\alpha_1} - 1),$$
$$d_{k3} = -G_1(\kappa_2 + e^{-2i\lambda_k\alpha_2}), \quad d_{k4} = -G_1\lambda_k(e^{-2i\alpha_2} - 1),$$
$$d_{k5} = 1 - e^{2i\lambda_k\alpha_1}, \quad d_{k6} = -\lambda_k(e^{2i\alpha_1} - 1), \quad d_{k7} = e^{-2i\lambda_k\alpha_2} - 1,$$
$$d_{k8} = \lambda_k(e^{-2i\alpha_2} - 1)$$

To determine p_{k1} and p_{k2} from Table 1, it should be noted that the first step is to determine the largest absolute value of the q_{kij}'s, this is $|q_{kij}|$. The corresponding expressions for p_{k1} and p_{k2} are obtained from the row containing this largest absolute value of q_{kij}.

The SIFs expressions are

$$K_I = \sqrt{2\pi}\frac{\lambda_I a_I}{2}\left[(p_{I1} + ip_{I2})(1 + \lambda_I(1 - e^{-2i\alpha_1}) - e^{2i\lambda_I\alpha_1}) + (p_{I1} - ip_{I2})(1 + \lambda_I(1 - e^{2i\alpha_1}) - e^{-2i\lambda_I\alpha_1})\right] \quad (55)$$

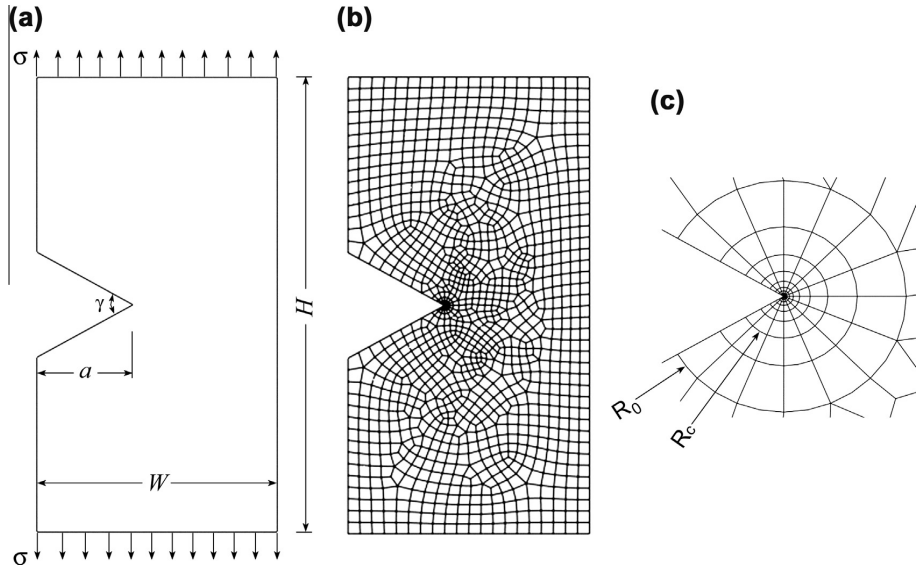

Fig. 4. (a) Notched plate subject to tension loading conditions (b) the plate FE mesh (c) control volume.

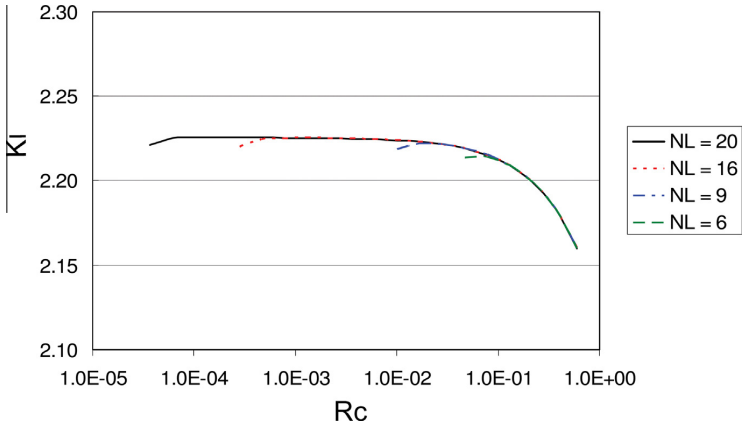

Fig. 5. SIFs for Notched plate $\gamma = 60^{\circ}$ under tension loading conditions.

Please cite this article in press as: Treifi, M., Oyadiji, S.O. Strain energy approach to compute stress intensity factors for isotropic homogeneous and bi-material V-notches. Int. J. Solids Struct. (2013), http://dx.doi.org/10.1016/j.ijsolstr.2013.03.011

$$K_{II} = \sqrt{2\pi}\frac{\lambda_{II}a_{II}}{2i}\left[(p_{II1}+ip_{II2})\left(\lambda_{II}\left(1-e^{-2i\alpha_1}\right)+e^{2i\lambda_{II}\alpha_1}-1\right)\right.$$
$$\left.+(p_{II1}-ip_{II2})\left(\lambda_{II}\left(e^{2i\alpha_1}-1\right)-e^{-2i\lambda_I\alpha_1}+1\right)\right] \quad (56)$$

The stress expressions in Eqs. (49)–(54) can be rewritten as

$$\sigma^j_{xx} = a_I r^{\lambda_I-1}f^j_x(\theta)+a_{II}r^{\lambda_{II}-1}g^j_x(\theta) = a_I r^{\lambda_I-1}f^j_x + a_{II}r^{\lambda_{II}-1}g^j_x \quad (57)$$

$$\sigma^j_{yy} = a_I r^{\lambda_I-1}f^j_y(\theta)+a_{II}r^{\lambda_{II}-1}g^j_y(\theta) = a_I r^{\lambda_I-1}f^j_y + a_{II}r^{\lambda_{II}-1}g^j_y \quad (58)$$

$$\tau^j_{xy} = a_I r^{\lambda_I-1}f^j_{xy}(\theta)+a_{II}r^{\lambda_{II}-1}g^j_{xy}(\theta) = a_I r^{\lambda_I-1}f^j_{xy} + a_{II}r^{\lambda_{II}-1}g^j_{xy} \quad (59)$$

Assuming plane-stress state, substituting the above equations into Eq. (31) gives

$$W^{j(e)} = \frac{1}{2E_j}\left[a_I^2 r^{2(\lambda_I-1)}\left(f_x^{j\,2}+f_y^{j\,2}-2\nu_j f^j_x f^j_y+2(1+\nu_j)f_{xy}^{j\,2}\right)\right.$$
$$+a_{II}^2 r^{2(\lambda_{II}-1)}\left(g_x^{j\,2}+g_y^{j\,2}-2\nu_j g^j_x g^j_y+2(1+\nu_j)g_{xy}^{j\,2}\right)$$
$$\left.+a_I a_{II} r^{(\lambda_I+\lambda_{II}-2)}\left(2f^j_x g^j_x+2f^j_y g^j_y-2\nu_j\left(f^j_x g^j_y+f^j_y g^j_x\right)+4(1+\nu_j)f^j_{xy}g^j_{xy}\right)\right] \quad (60)$$

by substituting the above equation into Eq. (1), the strain energy for a finite volume of a radius R_c around a bi-material notch tip with real singular eigenvalues is obtained

$$E^{j(e)} = \int_0^{R_c}\int_\theta W^{j(e)} r\,dr\,d\theta$$
$$= \frac{1}{2E_j}\left\{a_I^2\frac{R_c^{2\lambda_I}}{2\lambda_I}\int_\theta\left(f_x^{j\,2}+f_y^{j\,2}-2\nu_j f^j_x f^j_y+2(1+\nu_j)f_{xy}^{j\,2}\right)d\theta\right.$$
$$+a_{II}^2\frac{R_c^{2\lambda_{II}}}{2\lambda_{II}}\int_\theta\left(g_x^{j\,2}+g_y^{j\,2}-2\nu_j g^j_x g^j_y+2(1+\nu_j)g_{xy}^{j\,2}\right)d\theta$$
$$+a_I a_{II}\frac{R_c^{(\lambda_I+\lambda_{II})}}{(\lambda_I+\lambda_{II})}\int_\theta\left(2f^j_x g^j_x+2f^j_y g^j_y-2\nu_j\left(f^j_x g^j_y+f^j_y g^j_x\right)\right.$$
$$\left.\left.+4(1+\nu_j)f^j_{xy}g^j_{xy}\right)d\theta\right\} \quad (61)$$

The integration over θ is from $-\alpha_2$ to 0 for $j=2$ (material 2) and from 0 to α_1 for $j=1$ (material 1). Computing the strain energy for each region using a commercial FE package, and substituting it back into Eq. (60) gives

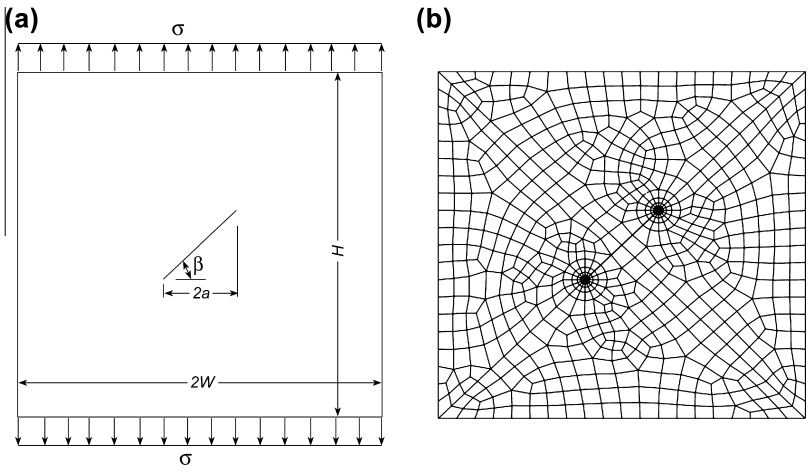

Fig. 6. (a) A slant centre cracked plate (b) the plate FE mesh.

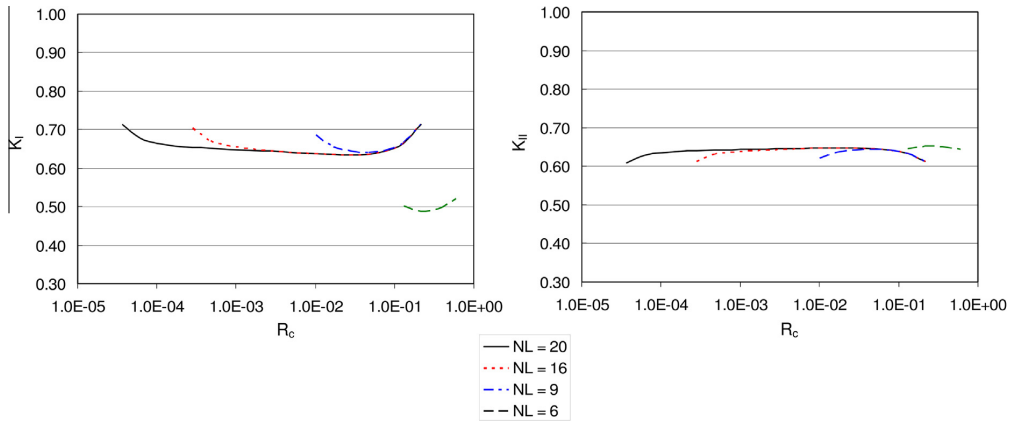

Fig. 7. Mode I and II SIFs for the slant centre cracked plate.

Please cite this article in press as: Treifi, M., Oyadiji, S.O. Strain energy approach to compute stress intensity factors for isotropic homogeneous and bi-material V-notches. Int. J. Solids Struct. (2013), http://dx.doi.org/10.1016/j.ijsolstr.2013.03.011

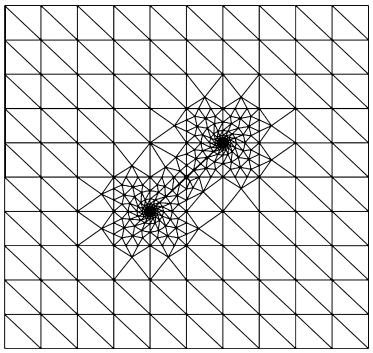

Fig. 8. The FE mesh used in the FFEM of the slant centre cracked plate.

$$E^{j(e)} = M_j K_I^2 + N_j K_{II}^2 + Q_j K_I K_{II} \tag{62}$$

Eq. (62) represents two quadratic equations with two unknowns, K_I and K_{II}, which can be solved easily using a programming software such as the MATLAB program.

2.2.2. Relationships between stress intensity factors and strain energy of a finite volume around a notch tip under out-of-plane loading conditions (mode III)

For the out-of-plane bi-material problem, the strain energy density in cylindrical-polar coordinates is

$$W^{j(e)} = \frac{1}{2G}\left[{\tau^j_{rz}}^2 + {\tau^j_{\theta z}}^2\right] \tag{63}$$

The stress expressions for a general bi-material notch under mode III loading conditions are

$$\tau^{(1)}_{rz} = G_1 \lambda^{III} r^{\lambda^{III}-1} B\left(\frac{\cos\lambda^{III}\alpha_1}{\sin\lambda^{III}\alpha_1}\cos\lambda^{III}\theta + \sin\lambda^{III}\theta\right) \tag{64}$$

$$\tau^{(1)}_{\theta z} = G_1 \lambda^{III} r^{\lambda^{III}-1} B\left(-\frac{\cos\lambda^{III}\alpha_1}{\sin\lambda^{III}\alpha_1}\sin\lambda^{III}\theta + \cos\lambda^{III}\theta\right) \tag{65}$$

for material 1 and

$$\tau^{(2)}_{rz} = G_2 \lambda^{III} r^{\lambda^{III}-1} B\left(\frac{\cos\lambda^{III}\alpha_1}{\sin\lambda^{III}\alpha_1}\cos\lambda^{III}\theta + \frac{G_1}{G_2}\sin\lambda^{III}\theta\right) \tag{66}$$

$$\tau^{(2)}_{\theta z} = G_2 \lambda^{III} r^{\lambda^{III}-1} B\left(-\frac{\cos\lambda^{III}\alpha_1}{\sin\lambda^{III}\alpha_1}\sin\lambda^{III}\theta + \frac{G_1}{G_2}\cos\lambda^{III}\theta\right) \tag{67}$$

for material, 2 where λ^{III} is an eigenvalue that can be computed from

$$\left(\frac{G_1}{G_2}+1\right)\sin\lambda^{III}(\alpha_1+\alpha_2) + \left(\frac{G_1}{G_2}-1\right)\sin\lambda^{III}(\alpha_1-\alpha_2) = 0 \tag{68}$$

and B is a constant. Eqs. (64) and (67) are eigenfunction series expansions (the Σ symbol is dropped for simplicity). In the SEA, only the singular term is considered. The constant B associated with the singular eigenvalue is related to the mode III SIF

$$K_{III} = \sqrt{2\pi} G_1 \lambda^{III} B \tag{69}$$

For detailed derivations, one may refer to Qian and Hasebe (1997). By substituting Eqs. (64)–(67) into Eqs. (63) and (1), and after some algebraic manipulations, the strain energy of a finite volume under mode III conditions can be written as

$$E^{(e)} = \int_0^{R_c}\left(\int_{-\alpha_2}^{0} W^{2(e)} d\theta + \int_0^{\alpha_1} W^{1(e)} d\theta\right) r dr = \frac{I}{8\pi G_1^2 {\lambda^{III}}^3} R_c^{2\lambda^{III}} K_{III}^2 \tag{70}$$

where I is an integral and its value is

$$I = G_2 {\lambda^{III}}^2 \alpha_2 \left(\left(\frac{\cos\lambda^{III}\alpha_1}{\sin\lambda^{III}\alpha_1}\right)^2 + \left(\frac{G_1}{G_2}\right)^2\right) + G_1 {\lambda^{III}}^2 \alpha_1 \left(\left(\frac{\cos\lambda^{III}\alpha_1}{\sin\lambda^{III}\alpha_1}\right)^2 + 1\right) \tag{71}$$

Eq. (70) represents a simple analytical formula that can be used to determine mode III SIF values of bi-material notches after computing the strain energy of a finite volume of radius R_c around and a notch tip using available commercial FE packages.

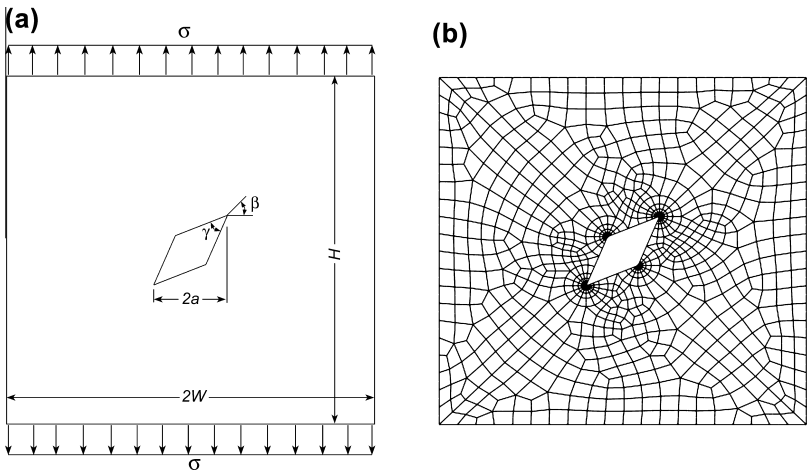

Fig. 9. (a) A slant centre notched plate $\gamma = 45^\circ$ (b) the plate FE mesh.

Please cite this article in press as: Treifi, M., Oyadiji, S.O. Strain energy approach to compute stress intensity factors for isotropic homogeneous and bi-material V-notches. Int. J. Solids Struct. (2013), http://dx.doi.org/10.1016/j.ijsolstr.2013.03.011

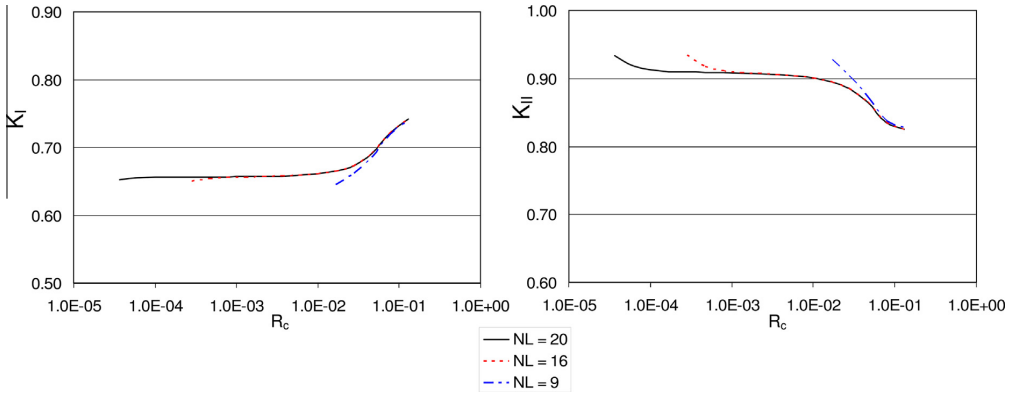

Fig. 10. Mode I and II SIFs for the slant centre notched plate.

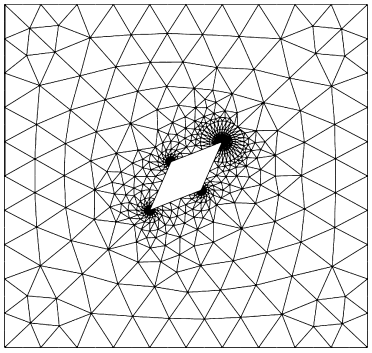

Fig. 11. The FE mesh used in the FFEM of the slant centre notched plate.

3. Numerical examples and verification

The proposed approach is verified by means of comparison with available published results and numerical results computed using the ABAQUS FEA commercial software and/or the software developed by the authors using FFEM. The numerical examples are presented in sub-groups corresponding to the sub-sections in Section 2 starting with isotropic homogeneous and then bi-material examples. Some discussion on the choice of R_c is also presented for each case. In all the examples the strain energy values for a finite volume around the notch tip are predicted using ABAQUS version 6.8. In the FEA, it is well known that the mesh of a body has an effect on the results, and that good meshes should be used for the analysis. Here, too, a good mesh should be used to achieve accurate results. By 'good mesh' we mean that large and small elements should not be adjacent, but there should be a transitional change in size.

3.1. Isotropic homogeneous notch

3.1.1. Mode I, II and mixed mode

The effect of the radius R_c on the accuracy of the SEA to predict SIF values for isotropic notch cases subject to in-plane loading conditions is demonstrated through different examples. For all the examples the global mesh used is more or less the same, but the local mesh around the notch tip is different. For example, different numbers of finite elements are used to discretise the small region around the notch/crack tip.A notched plate with a notch opening angle of $\gamma = 60^{\circ}$ under pure mode I loading conditions shown in Fig. 4(a) is considered first. The plate is of height $H = 20$ and width $W = 10$. The notch length is a where $a/w = 0.4$. Quadrilateral elements (which are designated as CPS8 in the ABAQUS FEA software) are used to model the plate as shown in Fig. 4(b). The small region around the notch tip is meshed layer by layer with a similarity ratio $\rho = 0.6$ as illustrated in Fig. 4(c). The radius of the first layer is

Table 2
Scaled SIFs under tension loading conditions.

γ (λ_I, λ_{II})		h_c/H									
		0.1		0.2		0.3		0.4		0.5	
		K_I	K_{II}	K_I	K_{II}	K_I	K_{II}	K_I	K_{II}	K_I	K_{II}
0	SEA	3.508	1.048	2.352	0.234	2.158	0.053	2.120	0.010	2.115	0.000
	FFE	3.490	1.040	2.344	0.232	2.151	0.054	2.114	0.011	2.109	0.001
(0.5,0.5)	ABAQUS	3.504	1.045	2.349	0.232	2.155	0.054	2.119	0.010	2.113	0.000
30	SEA	3.557	1.439	2.369	0.308	2.174	0.073	2.137	0.011	2.132	0.000
	FFE	3.544	1.448	2.361	0.307	2.167	0.07	2.131	0.014	2.125	0.001
(0.5014,0.5982)	ABAQUS	–	–	–	–	–	–	–	–	–	–
60	SEA	–	–	2.464	0.423	2.265	0.091	2.230	0.016	2.226	0.000
	FFE	–	–	2.472	0.404	2.263	0.090	2.226	0.018	2.221	0.003
(0.5122,0.7309)	ABAQUS	–	–	–	–	–	–	–	–	–	–
90	SEA	–	–	–	–	2.514	0.125	2.478	0.021	2.474	0.000
	FFE	–	–	–	–	2.511	0.127	2.477	0.026	2.473	0.005
(0.5445,0.9085)	ABAQUS	–	–	–	–	–	–	–	–	–	–

Please cite this article in press as: Treifi, M., Oyadiji, S.O. Strain energy approach to compute stress intensity factors for isotropic homogeneous and bi-material V-notches. Int. J. Solids Struct. (2013), http://dx.doi.org/10.1016/j.ijsolstr.2013.03.011

$R_0 = 0.6$. This is an arbitrary choice to provide transitional change in the size of the finite elements used to model the plate. R_0 has no significance other than to indicate the relative size of the mesh used around the notch tip with respect to the mesh size in the domain far from the notch tip. Initially, six layers are used within R_0. The mode I SIF values are computed based on the energy values for control volumes of sizes ranging from 1 layer to 6 layers (that is, the control radius is $R_c = 0.046656–0.6$). The same is repeated for 9 ($R_c = 0.0100777–0.6$), 16 ($R_c = 0.000282168–0.6$) and 20 ($R_c = 0.0000365376–0.6$) layers. The value of R_0 is not changed. Only the number of layers within R_0 and the radius of the control volume R_c are changed. The results are plotted in Fig. 5. The graph shows clearly that convergence is achieved with increasing number of layers within R_0; that is, using smaller sizes of the control volume R_c allowed by finer meshes within R_0. The converged SIF value (scaled by $\sigma\sqrt{\pi}a^{1-\lambda}$) achieved is $K_I = 2.225$. Published results for this case are reported to be $K_I = 2.223$ by Gross and Mendelson (1972) and $K_I = 2.222$ by Portela et al. (1991). In this example, accurate results are achieved when computing the strain energy value for values of R_c between 0.000101566 and 0.046656. In other words, the strain energy is computed for a control volume of size ranging from 3 to 15 layers out of the 20 layers that are used to model the region around the notch tip. Fig. 5 also shows that the size of the control volume R_c has an important role and results are less dependent on the mesh within R_c. In this figure, the different curves mean that different meshes (number of layers within R_c) are used for each value of R_c. Considering a value of $R_c = 0.046656$ in Fig. 5, its projection on the green dashed curve shows that only

Table 3
Scaled SIFs under shear loading conditions.

γ (λ_I, λ_{II})		h_c/H									
		0.1		0.2		0.3		0.4		0.5	
		K_I	K_{II}	K_I	K_{II}	K_I	K_{II}	K_I	K_{II}	K_I	K_{II}
0	SEA	10.275	5.798	4.963	1.971	3.055	1.325	1.572	1.162	0.000	1.180
	FFE	10.465	5.568	4.981	1.926	3.064	1.306	1.513	1.194	0.000	1.180
(0.5,0.5)	ABAQUS	10.505	5.591	4.993	1.927	3.069	1.306	1.516	1.194	0.000	1.181
30	SEA	10.754	7.681	5.035	2.601	3.085	1.807	1.521	1.665	0.000	1.636
	FFE	10.732	7.716	5.020	2.582	3.077	1.787	1.519	1.651	0.000	1.635
(0.5014,0.5982)	ABAQUS	–	–	–	–	–	–	–	–	–	–
60	SEA	–	–	5.198	3.557	3.183	2.483	1.574	2.325	0.000	2.301
	FFE	–	–	5.268	3.448	3.207	2.468	1.584	2.323	0.000	2.307
(0.5122,0.7309)	ABAQUS	–	–	–	–	–	–	–	–	–	–
90	SEA	–	–	–	–	3.476	3.422	1.720	3.229	0.000	3.208
	FFE	–	–	–	–	3.462	3.389	1.716	3.195	0.000	3.175
(0.5445,0.9085)	ABAQUS	–	–	–	–	–	–	–	–	–	–

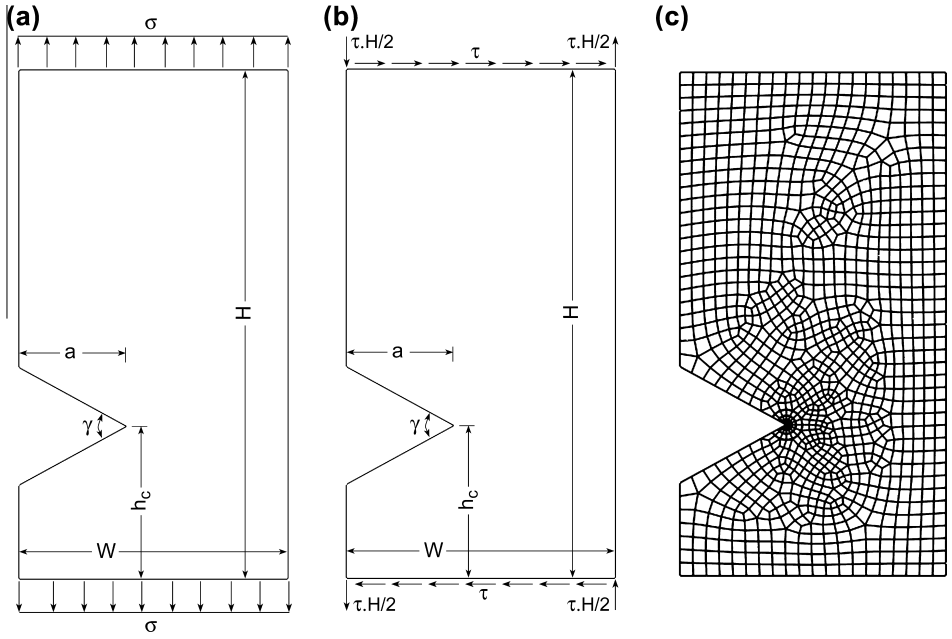

Fig. 12. (a) Notched plate subject to tension loading conditions (b) notched plate subject to in-plane shear loading conditions (c) the plate FE mesh.

Please cite this article in press as: Treifi, M., Oyadiji, S.O. Strain energy approach to compute stress intensity factors for isotropic homogeneous and bi-material V-notches. Int. J. Solids Struct. (2013), http://dx.doi.org/10.1016/j.ijsolstr.2013.03.011

one layer of FE elements is used within R_c. Its projection on the blue line shows that more layers, 4 layers of elements, are used within $R_c = 0.046656$, and so on for the red (11 layers) and black (15 layers) lines.

For mixed-mode problems, two examples, one of a slant crack and another of a slant notch, are considered. Fig. 6(a) illustrates a plate with a slant centre crack at angle of $\beta = 45^\circ$ subject to tensile loading. The plate dimensions are $H = 2W = 10$. The crack length is $2a = 2$. To compute the strain energy the plate is meshed using quadrilateral elements (CPS8) in ABAQUS as shown in Fig. 6(b). Like the previous example, the SIFs values are computed using the strain energy of different volumes around the crack tip. Coarse and fine meshes are used within $R_0 = 0.6$. The results are plotted in Fig. 7. It is clear again that better convergence is achieved by using finer meshes within R_0, i.e. smaller sizes of the control volume $R_c < 0.1$. This observation is in line with the general accepted size of the region governed by the singular terms around a crack tip, which is about $a/10$. The scaled SIFs predicted using the strain energy for a control volume of radius $R_c = 0.00047019$ (6 layers) when using 20 layers within $R_0 = 0.6$ (fine mesh) are $K_I = 0.651$ and $K_{II} = 0.641$. The SIFs values for this problem computed using the ABAQUS package are $K_I = 0.655$ and $K_{II} = 0.640$. In ABAQUS, quarter-point elements are used around the crack tip, and the plate mesh is the same as in Fig. 6(b). By using the fractal-like finite element method (FFEM), a method extended by the current authors to compute the notch SIFs, the SIFs values for this problem are $K_I = 0.650$ and $K_{II} = 0.636$. In FFEM, the plate is meshed using six-node triangular elements as shown in Fig. 8.

Now, a plate similar to the last example containing an inclined centre notch as shown in Fig. 9(a) is analysed. The notch opening angle is $\gamma = 45^\circ$ and its length is $2a = 2$. The plate dimensions are $H = 2W = 10$. The plate is meshed using CPS8 elements in ABAQUS as shown in Fig. 9(b). The SIFs values computed based on the strain energy values for different enclosed volumes around

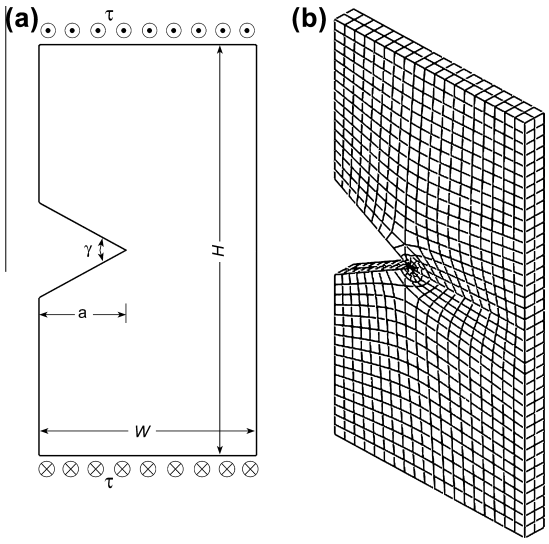

Fig. 13. (a) Notched plate subject to anti-plane shear loading conditions $\gamma = 60^\circ$ (b) the plate FE mesh.

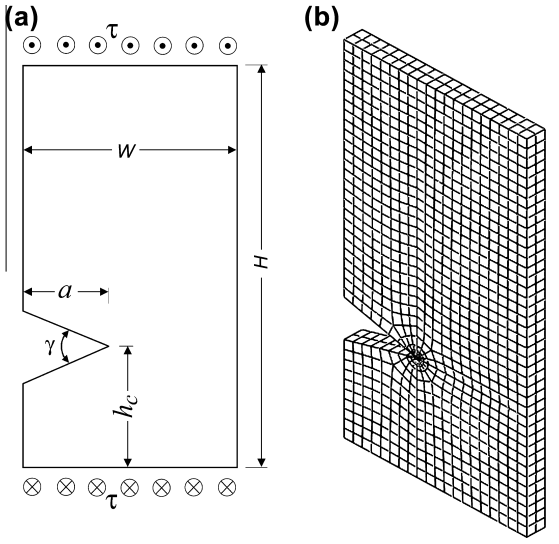

Fig. 15. (a) Off-centre notched plate subject to anti-plane shear loading conditions (b) the plate FE mesh.

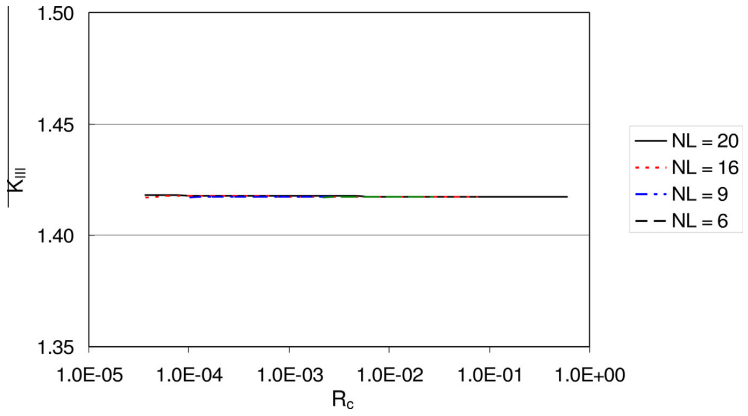

Fig. 14. Mode III SIFs for the notched plate $\gamma = 60^\circ$.

Please cite this article in press as: Treifi, M., Oyadiji, S.O. Strain energy approach to compute stress intensity factors for isotropic homogeneous and bi-material V-notches. Int. J. Solids Struct. (2013), http://dx.doi.org/10.1016/j.ijsolstr.2013.03.011

the notch tip (different R_c's) are plotted in Fig. 10. Like the previous examples, using a finer mesh (and therefore smaller R_c) gives better convergence. The scaled SIFs predicted using the strain energy for a control volume of 4 layers ($R_c = 0.000169262$) and 20 layers within $R_0 = 0.6$ are $K_I = 0.657, K_{II} = 0.910$. For this problem, Lazzarin et al. (2010)[1] reported the following SIFs values $K_I = 355, K_{II} = 325$ not scaled ($K_I = 0.641, K_{II} = 0.838$ scaled). Lazzarin et al. (2010) computed the mode I and II SIFs based on the strain energy density of two concentric circles. Using their approach, the authors computed the SIF values based on the strain energy of two concentric circles of radii $R_c = 0.000169262$ (3 layers) and $R_c = 0.000282047$ (5 layers). The SIFs values obtained are $K_I = 0.657, K_{II} = 0.910$ which are in good agreement with our computed values using the SEA. The difference between the current results and those reported by Lazzarin et al. (2010) could be attributed to using different sizes of control volumes compared to the ones used in this paper.

Using the FFEM (Treifi et al., 2009a), the SIFs values for this example are $K_I = 0.646, K_{II} = 0.912$. In the FFEM, the plate is meshed as shown in Fig. 11 using six-node triangle elements. In the singular region, twenty layers of elements are used. The SIFs values predicted using the strain energy approach as described in Section 2.1.1 and the FFEM are in very good agreement. This proves that the current results are correct.

The approach based on two concentric circles is not always applicable, as the current authors did a test using two circles to compute the mixed mode SIFs for the previous crack example. The results obtained were totally unrealistic. This is due to the fact that the two concentric circles approach leads to an indeterminate system of equations in the case of a crack problem, i.e. a notch with a zero opening angle. However, the approach presented in this paper does not have this limitation. Therefore, the current procedure is a more general approach to compute mixed mode SIFs of a general notch including the special case of a crack. It should also be noted that Lazzarin et al. (2010) did not mention that their approach is applicable to mixed mode crack problems explicitly.

Different examples of notched plates with different notch opening angles and different locations under tension or shear loading conditions are presented in Tables 2 and 3. The notched plates and their FE meshes are similar to the ones shown in Fig. 12. The results are compared to those predicted by ABAQUS for the crack cases using the same mesh and the FFEM results reported by Treifi et al. (2008, 2009a) for crack and notch cases. The plate dimensions are $H = 2W = 20$, and the notch length is a where $a/w = 0.4$. Fine mesh of 20 layers of elements is used within $R_0 = 0.6$, and the strain energy used to predict the SIF values is computed for a volume of radius $R_c = 0.000101566$ (that is for 3 layers). The results are presented in Tables 2 and 3 and are in good agreement with the results predicted using the other numerical approaches. The accuracy of the SEA could be improved by computing the strain energy for different volumes and then looking at the converged regions as demonstrated in the previous examples.

3.1.2. Mode III

A convergence study of an edge notched plate subject to mode III loading conditions as shown in Fig. 13 is presented to demonstrate the effect of R_c on the accuracy of the SEA. The plate is modelled and analysed using different meshes within the region around the notch-tip. The plate dimensions are: $H = 2W = 20$, the plate thickness $t = 1$, the notch length is a where $a/W = 0.4$, and the notch opening angle $\gamma = 60^\circ$. Three dimensional FE elements (C3D20) are used to model the plate in ABAQUS in order to compute the strain energy, and anti-plane conditions are applied.The small region around the notch tip is meshed layer by layer with a similarity ratio $\rho = 0.6$. The radius of the first layer is taken as $R_0 = 0.6$. Initially, six layers are used within R_0. The mode I SIF values are computed based on the energy values for control volumes of sizes ranging from 1 layer to 6 layers (that is, the control radius is R_c = 0.046656–0.6). The same is repeated for 9 (R_c = 0.0100777–0.6), 16 (R_c = 0.000282168–0.6) and 20 (R_c = 0.0000365376–0.6) layers. The value of R_0 is not changed. The mode III SIF values are plotted in Fig. 14. For the parameters considered ($NL = 6, 9, 16, 20$), this figure shows clearly that convergence is achieved regardless of the mesh around the notch tip (within R_0) and radius of the control volume (R_c). The converged SIF value (scaled by $\tau\sqrt{\pi}a^{1-\lambda_{III}}$) predicted by the SEA is $K_{III} = 1.418$. The mode III SIF for this case reported by Treifi et al. (2009b) using the FFEM is $K_{III} = 1.417$.

Different examples of notched plates with different notch opening angles and different locations under anti-plane loading conditions are analysed. The notched plates and their FE meshes are similar to the ones shown in Fig. 15. The results are compared in Table 4 to those predicted by ABAQUS for the crack cases using the same mesh and the FFEM results for the crack and notch cases reported by Treifi et al. (2009b) (the values are scaled by $\tau\sqrt{\pi}a^{1-\lambda_{III}}$). In the FFEM, the plate is meshed using 6-node triangular elements similar to the mesh shown in Fig. 16. The plate dimen-

Table 4
Scaled SIFs ($K_{III}/\tau\sqrt{\pi}a^{1-\lambda_{III}}$) under anti-plane shear loading conditions.

$\gamma(\lambda_{III})$		h_c/H		
		0.2	0.3	0.5
0	SEA	1.117	1.087	1.077
	FFE	1.116	1.086	1.077
(0.5)	ABAQUS	1.117	1.087	1.077
30	SEA	1.282	1.245	1.234
	FFE	1.281	1.245	1.233
(0.545455)	ABAQUS	–	–	–
60	SEA	1.478	1.432	1.417
	FFE	1.477	1.431	1.417
(0.6)	ABAQUS	–	–	–
90	SEA	–	1.648	1.628
	FFE	–	1.647	1.628
(0.666667)	ABAQUS	–	–	–

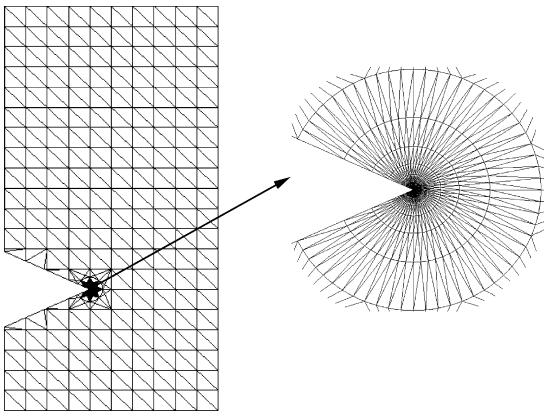

Fig. 16. The FE mesh used in the FFEM of off-centre notched plate subject to anti-plane shear loading conditions.

[1] It seems there is a typographical error in Lazzarin et al. (2010); in Table 5: λ_2^{45} value is 0.660 and not 0.624.

Please cite this article in press as: Treifi, M., Oyadiji, S.O. Strain energy approach to compute stress intensity factors for isotropic homogeneous and bimaterial V-notches. Int. J. Solids Struct. (2013), http://dx.doi.org/10.1016/j.ijsolstr.2013.03.011

sions are $H = 2W = 20$ and the notch length is a where $a/w = 0.4$. A coarse mesh of 7 layers of elements is used within $R_0 = 0.6$, and the strain energy used to predict the SIF values is computed for a volume of radius $R_c = 0.07776$ (that is for 3 layers). The SEA results presented in Table 4 are in good agreement with the results predicted using ABAQUS for crack cases and the FFEM for crack and notch cases. The accuracy of the SEA is excellent when dealing with pure mode cases, so for those cases finer meshes are not necessary.

3.2. Bi-material notch

3.2.1. Mode I, II and mixed mode

To demonstrate the effect of R_c on the accuracy of SIFs values predicted using the SEA relationships presented in Section 2.2.1 for a bi-material notch, an edge cracked plate consisting of two parts as shown in Fig. 17(a) is analysed for different material property ratios. The convergence study presented in Section 3.1.1 for single material notch cases demonstrated the need for a fine mesh around the notch-tip to obtain high accuracy results for mixed-mode I and II cases. Therefore, 20 layers will be used within the small region ($R_0 = 0.6$) containing the crack tip. The plate is meshed using CPS8 elements in ABAQUS as shown in Fig. 17(b). The cracked plate dimensions are $H = 3W = 30$, and the crack length a is given as $a/W = 0.4$. The Poisson's ratios of both materials are taken as $\nu_1 = \nu_2 = 0.3$. The Young Modulus ratios considered are $E_1/E_2 = 1, 2, 4, 10, 100$. The real and imaginary parts of the complex SIF, representing Mode I and II SIFs, are computed

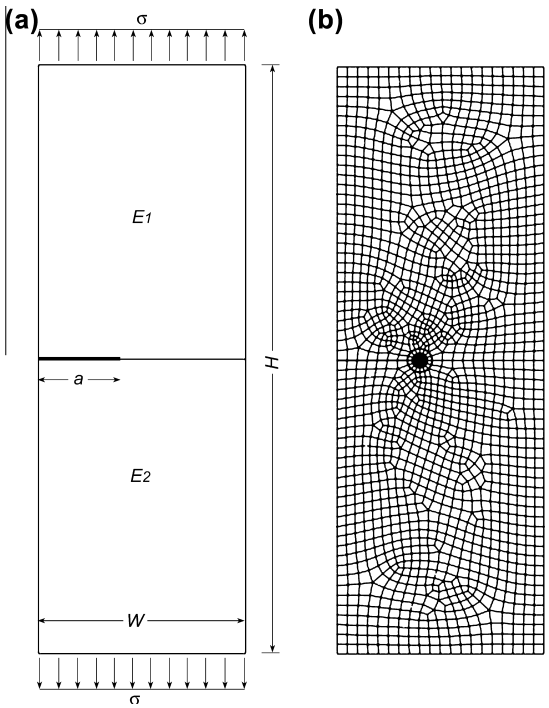

Fig. 17. (a) A bi-material cracked plate subject to tension (b) the plate FE mesh.

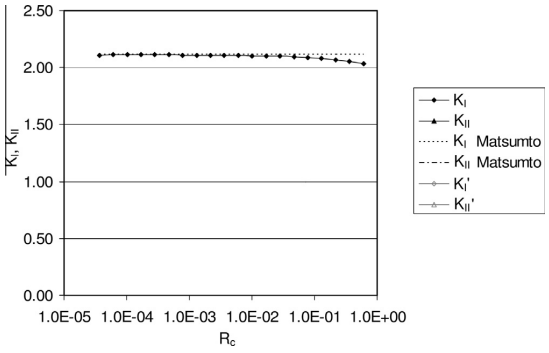

Fig. 18. SIFs for the bi-material cracked plate $E_1/E_2 = 1$.

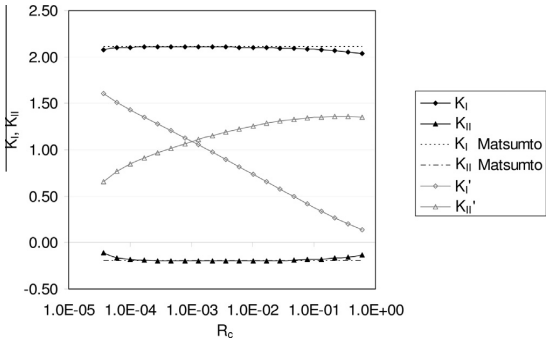

Fig. 19. SIFs for the bi-material cracked plate $E_1/E_2 = 2$.

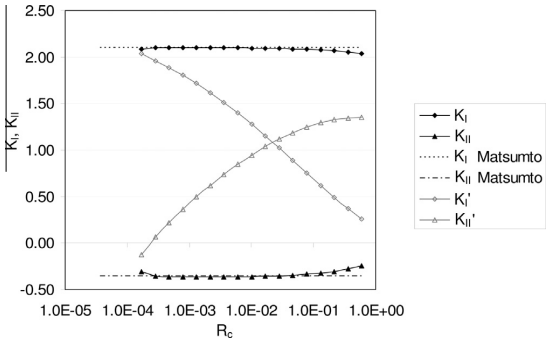

Fig. 20. SIFs for the bi-material cracked plate $E_1/E_2 = 4$.

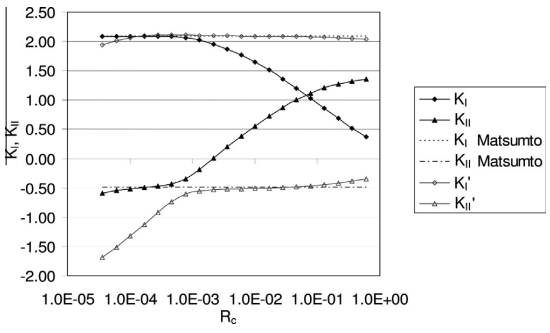

Fig. 21. SIFs for the bi-material cracked plate $E_1/E_2 = 10$.

Please cite this article in press as: Treifi, M., Oyadiji, S.O. Strain energy approach to compute stress intensity factors for isotropic homogeneous and bi-material V-notches. Int. J. Solids Struct. (2013), http://dx.doi.org/10.1016/j.ijsolstr.2013.03.011

using different values of R_c ranging from $R_c = 0.0000365376$ to 0.6 (that is, for 1 layer to 20 layers). The SIF values are plotted in Figs. 18–22. Because Eq. (62) gives two sets of valid roots, both sets are plotted. Corresponding SIFs values predicted by Matsumto et al. (2000) are also plotted for comparison. Those figures show that convergence is achieved for only one set of the roots for $E_1/E_2 = 1, 2, 4$ (small differences in material properties). However, for large differences in material properties as is the case in $E_1/E_2 = 10, 100$, both sets of roots converge within different regions. When one of the sets converges, the other diverges. In addition, for small material property differences $E_1/E_2 = 1, 2$, convergence is achieved using small R_c, but for large material property differences $E_1/E_2 = 10, 100$ convergence is achieved using large R_c. In the cases studied here, good accuracy is achieved using $R_c = 0.000282109$ (that is, the control volume containing 5 layers) for the cases of small material property differences. For the cases of large material property differences, better convergence is achieved using $R_c = 0.0167961$ (that is, the control volume containing 13 layers).

Based on the above discussion, the SIFs for an edge-crack bi-material plate are computed for different crack lengths and different material property ratios. The cracked plate and its FE mesh are similar to those shown in Fig. 17. The plate dimensions are the same as of the previous example. 20 layers are used within the small region ($R_0 = 0.6$) containing the crack tip. The scaled SIF values ($K_c/\sigma\sqrt{\pi}a^{1-\mathrm{Re}(\lambda)}(2a)^{i\mathrm{Im}(\lambda)}$) computed using the SEA are tabulated in Table 5. Corresponding published results by Matsumto et al. (2000) and computed results using ABAQUS are also tabulated for comparison. In ABAQUS, the same mesh is used to compute the SIFs. The control volume radius is taken as $R_c = 0.000282$ (5 layers), $R_c = 0.001306$ (8 layers), $R_c = 0.006047$ (11 layers) and $R_c = 0.016796$ (13 layers) for $E_1/E_2 = 1$, $E_1/E_2 = 2$, $E_1/E_2 = 4$ and $E_1/E_2 = 10, 100$, respectively. The singular eigenvalues for a bi-material crack of $E_1/E_2 = 1, 2, 4, 10, 100$ are $\lambda = 0.5$, $\lambda = 0.5 + i0.037306$, $\lambda = 0.5 + i0.0678545$, $\lambda = 0.5 + i0.0937743$ and $\lambda = 0.5 + i0.113817$, respectively. Table 5 shows that the SEA results are in good agreement with the numerical results computed using ABAQUS and with those reported by Matsumto et al. (2000).

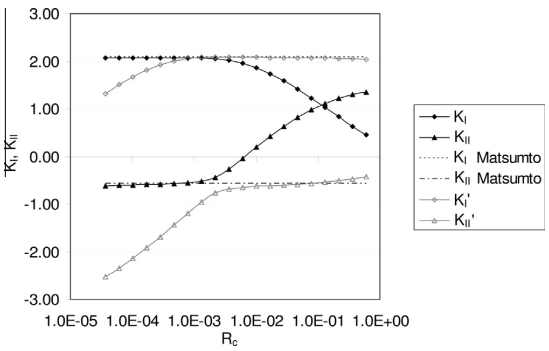

Fig. 22. SIFs for the bi-material cracked plate $E_1/E_2 = 100$.

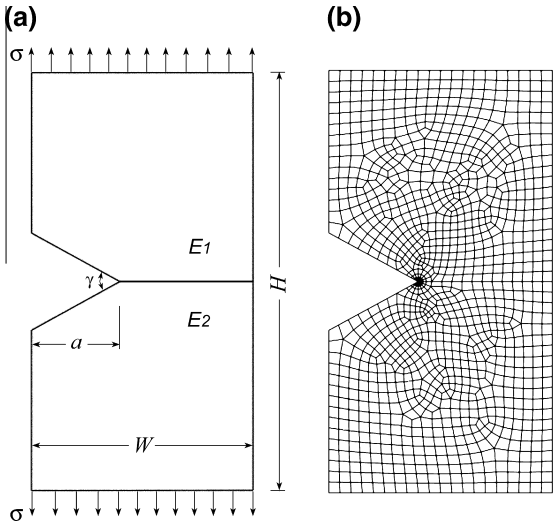

Fig. 23. (a) A bi-material notched plate subject to tension (b) the plate FE mesh.

Table 5
Scaled SIFs for a bi-material cracked plate.

a/W		E_1/E_2									
		1		2		4		10		100	
		K_I	K_{II}	K_I	K_{II}	K_I	K_{II}	K_I	K_{II}	K_I	K_{II}
0.2	SEA	1.367	0.000	1.365	−0.138	1.364	−0.250	1.365	−0.339	1.370	−0.418
	ABAQUS	1.368	0.000	1.368	−0.137	1.368	−0.251	1.369	−0.350	1.371	−0.430
	Matsumto	–	–	1.367	−0.137	1.368	−0.251	1.366	−0.348	1.376	−0.429
0.3	SEA	1.660	0.000	1.657	−0.160	1.652	−0.292	1.646	−0.397	1.644	−0.488
	ABAQUS	1.661	0.000	1.659	−0.159	1.654	−0.289	1.649	−0.400	1.643	−0.487
	Matsumto	–	–	1.657	−0.156	1.655	−0.288	1.648	−0.394	1.647	−0.470
0.4	SEA	2.112	0.000	2.107	−0.199	2.099	−0.364	2.088	−0.498	2.080	−0.609
	ABAQUS	2.112	0.000	2.109	−0.198	2.101	−0.360	2.090	−0.496	2.079	−0.600
	Matsumto	–	–	2.109	−0.195	2.102	−0.358	2.090	−0.491	2.083	−0.569
0.5	SEA	2.827	0.000	2.819	−0.268	2.805	−0.489	2.787	−0.669	2.771	−0.812
	ABAQUS	2.826	0.000	2.821	−0.268	2.807	−0.485	2.788	−0.665	2.771	−0.801
	Matsumto	–	–	2.819	−0.268	2.806	−0.483	2.789	−0.661	2.772	−0.793
0.6	SEA	4.037	0.000	4.024	−0.396	4.000	−0.718	3.967	−0.983	3.937	−1.180
	ABAQUS	4.035	0.000	4.025	−0.398	4.002	−0.718	3.971	−0.982	3.940	−1.177
	Matsumto	–	–	4.024	−0.398	4.001	−0.714	3.968	−0.973	3.906	−1.171
0.7	SEA	6.363	0.000	6.338	−0.665	6.288	−1.202	6.220	−1.647	6.157	−1.956
	ABAQUS	6.357	0.000	6.336	−0.671	6.291	−1.210	6.230	−1.651	6.168	−1.974
	Matsumto	–	–	6.348	−0.668	6.298	−1.204	6.227	−1.634	6.157	−1.957

Please cite this article in press as: Treifi, M., Oyadiji, S.O. Strain energy approach to compute stress intensity factors for isotropic homogeneous and bi-material V-notches. Int. J. Solids Struct. (2013), http://dx.doi.org/10.1016/j.ijsolstr.2013.03.011

For a notch case, a bi-material notched plate with an opening angle of $\gamma = 60^{\circ}$ as shown in Fig. 23(a) is analysed. The plate dimensions are $H = 2W = 20$, and the crack length a is taken as $a/W = 0.4$. The Poisson's ratios of both material are taken as $v_1 = v_2 = 0.3$. The SIFs are computed for different material property ratios $E_1/E_2 = 1, 2, 4, 10, 100$. The plate is meshed using CPS8 elements in ABAQUS as shown in Fig. 23(b) to compute the strain energy. 20 layers are used within the small region ($R_0 = 0.6$) containing the crack tip. The results are tabulated in Table 6. The control volume radius for which the strain energy is computed is taken as $R_c = 0.000282$ (5 layers), $R_c = 0.001306$ (8 layers), $R_c = 0.006047$ (11 layers) and $R_c = 0.016796$ (13 layers) for $E_1/E_2 = 1$, $E_1/E_2 = 2$, $E_1/E_2 = 4$ and $E_1/E_2 = 10, 100$, respectively. Table 6 shows that the singular eigenvalues ($\mathrm{Re}(\lambda) < 1$) for each case are either two real eigenvalues or one complex eigenvalue. The cases of two singular real eigenvalues give two real SIFs K_I and K_{II} for mode I and II, respectively. The cases of one singular complex eigenvalue give complex SIFs $K_c = K_1 + iK_2$. The results in Table 6 are new and there are no available published results to compare with. However, the previous validation for crack cases, which are special cases of notch problems with opening angle of $\gamma = 0^{\circ}$, shows that the SEA gives accurate results. Therefore, the results in Table 6 are valid. It should be noted that the ABAQUS software only computes SIF values when the notch opening angle is zero, i.e. a crack, but for true notches it cannot compute the notch SIFs.

3.2.2. Mode III

The mode III SIFs for different cases of a bi-material notched plate subject to out-of-plane shear loading conditions as shown in Fig. 24 are computed using the SEA. The plate dimensions are: $H = 2W = 20$, the plate thickness $t = 1$, the notch length is a where $a/W = 0.4$. Three dimensional FE elements (C3D20) are used to model the plate in ABAQUS in a similar way to that in Fig. 15(b) in order to compute the strain energy, and anti-plane conditions are applied. The results are compared to those predicted by ABAQUS for the crack cases and the FFEM (Treifi and Oyadiji, 2013) for the crack and notch cases. In the ABAQUS analysis for the crack cases, the same mesh as for the SEA is used. For the notch cases where ABAQUS cannot predict the notch SIFs, the results are compared to those predicted by the FFEM. In the FFEM, the plate is meshed using 6-node triangular elements similar to the mesh shown in Fig. 16. Based on the convergence study presented for

Table 6
Scaled SIFs for a bi-material notched plate ($\gamma = 60^{\circ}$).

E_1/E_2	λ_I	λ_{II}	K_I or K_1	K_{II} or K_2
1	0.51222136	0.73090074	2.226	0.000
2	0.52425299	0.71632272	2.430	−0.666
4	0.56267468	0.67219769	3.633	−1.980
10	0.61388523 + i0.07040375		2.881	−2.549
100	0.61052742 + i0.11267322		2.365	−1.940

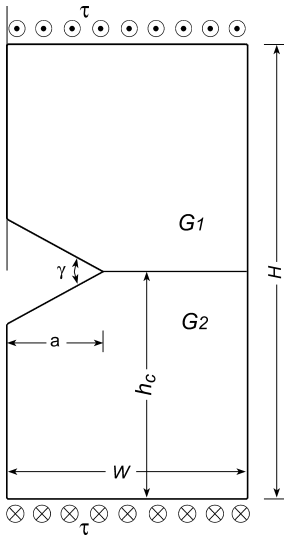

Fig. 24. A bi-material notched plate subject to anti-plane shear loading conditions.

Table 7
Scaled SIFs ($K_{III}/\tau\sqrt{\pi}a^{1-\lambda_{III}}$) under anti-plane shear loading conditions ($G_1/G_2 = 10$).

γ		h_c/H		
		0.2	0.3	0.5
0	SEA	1.148	1.096	1.077
	FFE	1.148	1.096	1.077
	ABAQUS	1.148	1.096	1.077
30	SEA	1.320	1.256	1.234
	FFE	1.320	1.256	1.233
	ABAQUS	–	–	–
60	SEA	1.527	1.446	1.417
	FFE	1.526	1.445	1.417
	ABAQUS	–	–	–
90	SEA	–	1.666	1.628
	FFE	–	1.666	1.628
	ABAQUS	–	–	–

Table 8
Scaled SIFs ($K_{III}/\tau\sqrt{\pi}a^{1-\lambda_{III}}$) under anti-plane shear loading conditions ($G_1/G_2 = 4$).

γ		h_c/H		
		0.2	0.3	0.5
0	SEA	1.140	1.094	1.077
	FFE	1.140	1.093	1.077
	ABAQUS	1.140	1.093	1.077
30	SEA	1.310	1.253	1.234
	FFE	1.310	1.253	1.233
	ABAQUS	–	–	–
60	SEA	1.514	1.442	1.417
	FFE	1.513	1.442	1.417
	ABAQUS	–	–	–
90	SEA	–	1.661	1.628
	FFE	–	1.661	1.628
	ABAQUS	–	–	–

Table 9
Scaled SIFs ($K_{III}/\tau\sqrt{\pi}a^{1-\lambda_{III}}$) under anti-plane shear loading conditions ($G_1/G_2 = 1/4$).

γ		h_c/H		
		0.2	0.3	0.5
0	SEA	1.092	1.080	1.077
	FFE	1.092	1.080	1.077
	ABAQUS	1.092	1.080	1.077
30	SEA	1.252	1.237	1.234
	FFE	1.251	1.237	1.233
	ABAQUS	–	–	–
60	SEA	1.440	1.422	1.417
	FFE	1.440	1.421	1.417
	ABAQUS	–	–	–
90	SEA	–	1.634	1.628
	FFE	–	1.633	1.628
	ABAQUS	–	–	–

Please cite this article in press as: Treifi, M., Oyadiji, S.O. Strain energy approach to compute stress intensity factors for isotropic homogeneous and bi-material V-notches. Int. J. Solids Struct. (2013), http://dx.doi.org/10.1016/j.ijsolstr.2013.03.011

Table 10
Scaled SIFs ($K_{III}/\tau\sqrt{\pi}a^{1-\lambda_{III}}$) under anti-plane shear loading conditions ($G_1/G_2 = 1/10$).

γ		h_c/H		
		0.2	0.3	0.5
0	SEA	1.083	1.078	1.077
	FFE	1.083	1.077	1.077
	ABAQUS	1.083	1.078	1.077
30	SEA	1.241	1.234	1.234
	FFE	1.240	1.234	1.233
	ABAQUS	–	–	–
60	SEA	1.426	1.418	1.417
	FFE	1.426	1.417	1.417
	ABAQUS	–	–	–
90	SEA	–	1.629	1.628
	FFE	–	1.628	1.628
	ABAQUS	–	–	–

the mode III isotropic cases, a coarse mesh of 7 layers of elements is used within $R_0 = 0.6$, and the strain energy used to predict the SIF values is computed for a volume of radius $R_c = 0.07776$ (3 layers). The SEA results compared to corresponding results predicted using ABAQUS and the FFEM are presented in Tables 7–10. The results of the three different approaches are in excellent agreement.

4. Conclusions

In this paper, a simple approach based on the strain energy of a control volume was developed to compute the mode I, II and III SIFs for isotropic homogeneous and bi-material crack/notch problems. The approach is simple to employ numerically. It relates the SIFs to the strain energy that may be computed using commercial FE packages; thus, enabling those packages to compute notch SIFs. The accuracy of the SEA was demonstrated via many different numerical examples of homogeneous and bi-material cracked and notched plates. For pure mode conditions, a coarse mesh (and therefore a larger size of the control volume) may be used to model the region around the notch tip, but it is recommended using finer meshes (and therefore a smaller size of the control volume) when dealing with mixed mode cases. The results generated using the SEA are in very good agreement with existing published results and numerical solutions.

References

Babuška, I., Miller, A., 1984. The post-processing approach in the finite element method-part 2: Calculation of the stress intensity factors. International Journal for Numerical Methods in Engineering 20, 1111–1129.
Berto, F., Lazzarin, P., 2007. Relationships between J-integral and the strain energy evaluated in a finite volume surrounding the tip of sharp and blunt V-notches. International Journal of Solids and Structures 44, 4621–4645.
Bogy, D.B., 1968. Edge-bonded dissimilar orthogonal elastic wedges under normal and shear loading. ASME Journal of Applied Mechanics 35, 460–466.
Bogy, D.B., 1970. On the problem of edge-bonded elastic quarter-planes loaded at the boundary. International Journal of Solids and Structures 6, 1287–1313.
Bogy, D.B., Wang, K.C., 1971. Stress singularities at interface corners in bonded dissimilar isotropic elastic materials. International Journal of Solids and Structures 7, 993–1005.
Bower, A.F., 2010. Applied Mechanics of Solids. CRC Press.
Carpenter, W.C., Byers, C., 1987. A path independent integral for computing stress intensities for V-notched cracks in a bi-material. International Journal of Fracture 35, 245–268.
Carpinteri, A., Cornetti, P., Pugno, N., Sapora, A., Taylor, D., 2008. A finite fracture mechanics approach to structures with sharp V-notches. Engineering Fracture Mechanics 75, 1736–1752.
Carpinteri, A., Paggi, M., Pugno, N., 2006. Numerical evaluation of generalized stress-intensity factors in multi-layered composites. International Journal of Solids and Structures 43, 627–641.
Chen, M.C., Sze, K.Y., 2001. A novel hybrid finite element analysis of bimaterial wedge problems. Engineering Fracture Mechanics 68, 1463–1476.
Gómez, F.J., Elices, M., 2003. A fracture criterion for sharp V-notched samples. International Journal of Fracture 123, 163–175.
Gross, B., Mendelson, A., 1972. Plane elastostatic analysis of V-notched plates. International Journal of Fracture 8, 267–276.
Knésl, Z., 1991. A criterion of V-notch stability. International Journal of Fracture 48, R79–R83.
Lazzarin, P., Berto, F., Zappalorto, M., 2010. Rapid calculations of notch stress intensity factors based on averaged strain energy density from coarse meshes: Theoretical bases and applications. International Journal of Fatigue 32, 1559–1567.
Lazzarin, P., Berto, F., 2005. Some expressions for the strain energy in a finite volume surrounding the root of blunt V-notches. International Journal of Fracture 135, 161–185.
Lazzarin, P., Filippi, S., 2006. A generalized stress intensity factor to be applied to rounded V-shaped notches. International Journal of Solids and Structures 43, 2461–2478.
Lazzarin, P., Zambardi, R., 2001. A finite-volume-energy based approach to predict the static and fatigue behavior of components with sharp V-shaped notches. International Journal of Fracture 112, 275–298.
Lazzarin, P., Zappalorto, M., 2008. Plastic notch stress intensity factors for pointed V-notches under antiplane shear loading. International Journal of Fracture 152, 1–25.
Lee, K.Y., Choi, H.J., 1988. Boundary element analysis of stress intensity factors for bimaterial interface cracks. Engineering Fracture Mechanics 29, 461–472.
Leung, A.Y.T., Su, R.K.L., 1994. Mode I crack problems by fractal two level finite element method. Engineering Fracture Mechanics 48, 847–856.
Lin, K.Y., Mar, J.W., 1976. Finite element analysis of stress intensity factors for cracks at a bi-material interface. International Journal of Fracture 12, 521–531.
Lin, K.Y., Tong, P., 1980. Singular finite elements for the fracture analysis of V-notched plates. International Journal for Numerical Methods in Engineering 15, 1343–1354.
Matsumto, T., Tanaka, M., Obara, R., 2000. Computation of stress intensity factors of interface cracks based on interaction energy release rates and BEM sensitivity analysis. Engineering Fracture Mechanics 65, 683–702.
Paggi, M., Carpinteri, A., 2008. On the stress singularities at multimaterial interfaces and related analogies with fluid dynamics and diffusion. ASME Applied Mechanics Reviews 61, 1–22.
Portela, A., Aliabadi, M.H., Rooke, D.P., 1991. Efficient boundary element analysis of sharp notched plates. International Journal for Numerical Methods in Engineering 32, 445–470.
Qian, J., Hasebe, N., 1997. Property of eigenvalues and eigenfunctions for an interface V-notch in antiplane elasticity. Engineering Fracture Mechanics 56, 729–734.
Radaj, D., Berto, F., Lazzarin, P., 2009. Local fatigue strength parameters for welded joints based on strain energy density with inclusion of small-size notches. Engineering Fracture Mechanics 76, 1109–1130.
Seweryn, A., 1994. Brittle fracture criterion for structures with sharp notches. Engineering Fracture Mechanics 47, 673–681.
Seweryn, A., Molski, K., 1996. Elastic stress singularities and corresponding generalized stress intensity factors for angular corners under various boundary conditions. Engineering Fracture Mechanics 55, 529–556.
Sih, G.C., 1974. Strain-energy-density factor applied to mixed mode crack problems. International Journal of Fracture 10, 305–321.
Tan, M.A., Meguid, S.A., 1997. Analysis of bimaterial wedges using a new singular finite element. International Journal of Fracture 88, 373–391.
Tong, P., Pian, T.H.H., Lasry, S.J., 1973. A hybrid-element approach to crack problems in plane elasticity. International Journal for Numerical Methods in Engineering 7, 297–308.
Treifi, M., Oyadiji, S.O., 2009. Computations of SIFs for non-symmetric V-notched plates by the FFEM. In: Proceedings of ASME Conference IDETC/CIE2009, vol. 3. ASME, pp. 711–717. http://dx.doi.org/10.1115/DETC2009-86585.
Treifi, M., Oyadiji, S.O., 2013. Evaluation of mode III stress intensity factors for bi-material notched bodies using the fractal-like finite element method. Computers and Structures, http://dx.doi.org/10.1016/j.compstruc.2013.02.015.
Treifi, M., Oyadiji, S.O., Tsang, D.K.L., 2008. Computations of modes I and II stress intensity factors of sharp notched plates under in-plane shear and bending loading by the fractal-like finite element method. International Journal of Solids and Structures 45, 6468–6484.
Treifi, M., Oyadiji, S.O., Tsang, D.K.L., 2009a. Computation of the stress intensity factors of sharp notched plates by the fractal-like finite element method. International Journal for Numerical Methods in Engineering 77, 558–580.
Treifi, M., Oyadiji, S.O., Tsang, D.K.L., 2009b. Computations of the stress intensity factors of double-edge and centre V-notched plates under tension and anti-plane shear by the fractal-like finite element method. Engineering Fracture Mechanics 76, 2091–2108.
Treifi, M., Tsang, D.K.L., Oyadiji, S.O., 2007. Applications of the fractal-like finite element method to sharp notched plates. In: Proceedings of ASME Conference IDETC/CIE2007, vol. 4, pp. 399–405.
Williams, M.L., 1952. Stress singularities resulting from various boundary conditions in angular corners of plates in extension. ASME Journal of Applied Mechanics 19, 526–528.
Williams, M.L., 1957. On the stress distribution at the base of a stationary crack. ASME Journal of Applied Mechanics 24, 109–114.
Williams, M.L., 1959. The stresses around a fault or crack in dissimilar media. Bulletin of the Seismological Society of America 49, 199–204.
Wolf, J.P., 2003. The Scaled Boundary Finite Element Method. Wiley, Chichester.

Please cite this article in press as: Treifi, M., Oyadiji, S.O. Strain energy approach to compute stress intensity factors for isotropic homogeneous and bi-material V-notches. Int. J. Solids Struct. (2013), http://dx.doi.org/10.1016/j.ijsolstr.2013.03.011

Yau, J.F., Wang, S.S., 1984. An analysis of interface cracks between dissimilar isotropic materials using conservation integrals in elasticity. Engineering Fracture Mechanics 20, 423–432.

Zappalorto, M., Lazzarin, P., 2011. Strain energy-based evaluations of plastic notch stress intensity factors at pointed V-notches under tension. Engineering Fracture Mechanics 78, 2691–2706.

Zappalorto, M., Lazzarin, P., Yates, J.R., 2008. Elastic stress distributions for hyperbolic and parabolic notches in round shafts under torsion and uniform antiplane shear loadings. International Journal of Solids and Structures 45, 4879–4901.

Please cite this article in press as: Treifi, M., Oyadiji, S.O. Strain energy approach to compute stress intensity factors for isotropic homogeneous and bi-material V-notches. Int. J. Solids Struct. (2013), http://dx.doi.org/10.1016/j.ijsolstr.2013.03.011

Chapter 11

Bi-material V-notch Stress Intensity Factors by the Fractal-like Finite Element Method

Engineering Fracture Mechanics 2013;

http://dx.doi.org/10.1016/j.engfracmech.2013.04.006

ARTICLE IN PRESS

Engineering Fracture Mechanics xxx (2013) xxx–xxx

Contents lists available at SciVerse ScienceDirect

Engineering Fracture Mechanics

journal homepage: www.elsevier.com/locate/engfracmech

Bi-material V-notch stress intensity factors by the fractal-like finite element method

Muhammad Treifi, S. Olutunde Oyadiji *

School of Mechanical, Aerospace and Civil Engineering, University of Manchester, Manchester M13 9PL, UK

ARTICLE INFO

Article history:
Received 20 November 2012
Received in revised form 9 April 2013
Accepted 11 April 2013
Available online xxxx

Keywords:
Stress intensity factor
Bi-material
Notch
Finite element method
Fracture mechanics
Crack

ABSTRACT

The fractal-like finite element method (FFEM) is developed to provide stress intensity factor (SIF) values for bi-material notches. The displacement fields around a bi-material notch tip are derived and employed as global interpolation functions in the FFEM to transform the large number of nodal displacements in the singular region to a small set of generalised co-ordinates leading to direct computation of the SIFs and the coefficients of the higher order terms. Various numerical examples for bi-material crack and notch cases are presented. New results for bi-material notches are reported.

1. Introduction

In recent years, there has been a lot of interest in computing the SIFs for a general notch (or corner), because the presence of notches may lead to crack initiation and sudden failure. Most of the research reported in the literature [1–5] deals only with isotropic homogenous notches based on the pioneering work presented by Williams [6]. For bi-material notches, there are hardly any results reported. Most research is about the behaviour of the eigenvalues and its computation rather than computing the SIFs [7–9]. That is simply due to the complexity of the bi-material case. However, SIFs were reported for a bi-material crack, which is a special case of a notch (the notch opening angle is zero) by some authors, such as Matsumto et al. [10], Yuuki and Cho [11] and Miyazaki et al. [12]. Williams [6] showed that the stress and displacement expressions around a notch tip can be written as eigenfunction series expansions. For a single material (isotropic homogenous) notch, the singular eigenvalues are always real. The singular eigenvalues are those which are less than one and they result in unbounded stresses. In the case of a two material (bi-material) notch, the singular eigenvalues could be real or complex numbers. This means that different eigenfunction series expansions have to be used for each case.

The FFEM was originally developed to compute the SIFs for crack problems [13,14]. Reddy and Rao [15] extended the method to analyse the shape sensitivity for a homogeneous isotropic crack. The current authors successfully developed the FFEM to compute the SIFs for an isotropic homogenous notch [16–20]. It should be noted that the two-level finite element method [13], the fractal two level finite element methods [14], the fractal finite element mixed-mode method [15], and the fractal-like finite element method [16–20] are identically the same. In fact, they are all fractal-like because the finite elements are truly fractal in the radial direction from the point of singularity, whereas in the circumferential direction in a layer, the elements are not fractal in nature. Therefore, the fractal self-similar nature of the mesh applies to the radial direction

* Corresponding author. Tel.: +44 161 2754348.
E-mail addresses: m.treifi@mmu.ac.uk (M. Treifi), s.o.oyadiji@manchester.ac.uk (S.O. Oyadiji).

0013-7944/$ - see front matter © 2013 Elsevier Ltd. All rights reserved.
http://dx.doi.org/10.1016/j.engfracmech.2013.04.006

Nomenclature

a	crack/notch length
$\mathbf{a}$	set of generalised co-ordinates
A, B, a, b	generalised co-ordinates
$\mathbf{d}$	nodal displacement vector
$\mathbf{d}_r$, $\mathbf{d}_m$, and $\mathbf{d}_s$	nodal displacement vectors of nodes in regular region, master nodes, and in singular region
$\mathbf{d}_s^{1st,2nd,\ldots}$	nodal displacements of the nodes in the first layer, second layer, ... in the singular region
E	Young's modulus
$\mathbf{f}$	nodal force vector
$\mathbf{f}_r$, $\mathbf{f}_m$, and $\mathbf{f}_s$	nodal force vectors of nodes in regular region, master nodes, and in singular region
$\bar{\mathbf{f}}_s^{1st,inn}$	transformed nodal force vectors of the first layer and the inner layers in the singular region
G	shear modulus
H	plate height
$\mathbf{K}$	stiffness matrix
$\mathbf{K}_{rr}$, $\mathbf{K}_{mr}$, $\mathbf{K}_{mm}$, $\mathbf{K}_{ss,\ldots}$	partitioned stiffness matrices (r refers to regular region, m to master nodes, and s to slave nodes)
$\mathbf{K}_s^n$	partitioned stiffness matrix of the nth layer in the singular region
$\overline{\mathbf{K}}_s^{1st}$, $\overline{\mathbf{K}}_s^{inn}$	transformed partitioned stiffness matrices of the first layer and the inner layers in the singular region
K_I, K_{II}	stress intensity factors of mode I, II
K_c	complex stress intensity factor
i	complex unit $\left(\sqrt{-1}\right)$
j	integer variables
NL	number of layers in the singular region
NT	number of terms of eigenfunction series expansion
P_x, P_y	forces
R_s	radius of singular region
r, θ	polar co-ordinates
$\mathbf{T}_s^n$	transformation matrix of the nodal displacements of the nth layer in the singular region
$\mathbf{T}_s^{1st}$	transformation matrix of the nodal displacements of the first layer in the singular region
W	width of single-edge-notched plate
u_x, u_y	displacements in x and y directions
x, y	cartesian co-ordinates
z	complex variable
α	angle between notch face and x-axis
γ	notch opening angle
ϕ, ω	complex potentials
λ	eigenvalue
ν	Poisson's ratio
ρ	similarity ratio
σ	normal stress
τ	shear stress

towards the notch/crack tip but not necessarily to the hoop direction. For this reason, the authors prefer to refer to the topology as being fractal-like.

In this paper, the authors develop the FFEM to compute the SIFs for a bi-material notch. The stress and displacement fields are derived for real and complex eigenvalues. Then, the FFEM is developed by employing the displacement expressions as global interpolation functions to compute the SIFs for bi-material notch problems. To demonstrate the accuracy of the FFEM to compute bi-material notch SIFs, the SIF values for various bi-material notch examples are computed and compared to available published results and results computed using different numerical approaches.

2. Global interpolation functions for a bi-material notch

The stress and displacement functions of a bi-material notch as shown in Fig. 1 can be expressed using a complex variable approach as [21]:

$$\sigma_{xx}^j + \sigma_{yy}^j = 4\mathrm{Re}(\phi^{j\prime}(z)) \tag{1}$$

$$\sigma_{yy}^j - i\tau_{xy}^j = \phi^{j\prime}(z) + (z-\bar{z})\overline{\phi^{j\prime\prime}(z)} + \overline{\omega^{j\prime}(z)} \tag{2}$$

Please cite this article in press as: Treifi M, Oyadiji SO. Bi-material V-notch stress intensity factors by the fractal-like finite element method. Engng Fract Mech (2013), http://dx.doi.org/10.1016/j.engfracmech.2013.04.006

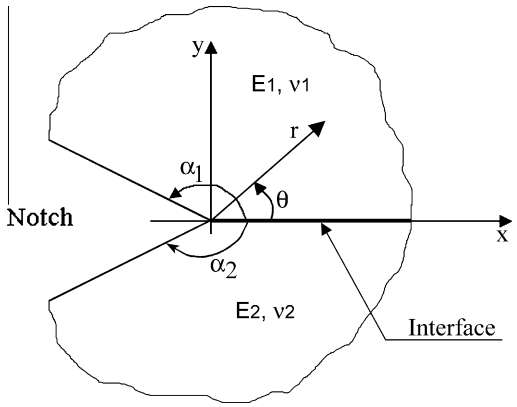

Fig. 1. Bi-material notch geometry.

$$-P_y^j + iP_x^j = \phi^j(z) + (z-\bar{z})\overline{\phi^{j\prime}(z)} + \overline{\omega^j(z)} \tag{3}$$

$$u_x^j + iu_y^j = \frac{1}{2G_j}[\kappa_j\phi^j(z) - (z-\bar{z})\overline{\phi^{j\prime}(z)} - \overline{\omega^j(z)}] \tag{4}$$

where j refers to material j, G_j is the shear modulus of material j, $\kappa_j = 3-4\nu_j$ for plane-strain or $\kappa_j = 3-4\nu_j/(1+\nu_j)$ for plane-stress and ν_j is the Poisson's ratio of material j. $\phi^j(z)$ and $\omega^j(z)$ are complex potentials and are assumed to be

$$\phi^j(z) = A_j z^\lambda + a_j z^{\bar{\lambda}} \text{ and } \omega^j(z) = B_j z^\lambda + b_j z^{\bar{\lambda}} \tag{5}$$

Substituting Eq. (5) into Eqs. (2)–(4) gives

$$\sigma_{yy}^j - i\tau_{xy}^j = \lambda r^{\lambda-1}e^{i\theta(1-\lambda)}[A_j e^{2i\theta(\lambda-1)} + \bar{a}_j(e^{2i\theta}-1)(\lambda-1) + \bar{b}_j] + \bar{\lambda}r^{\bar{\lambda}-1}e^{i\theta(1-\bar{\lambda})}[a_j e^{2i\theta(\bar{\lambda}-1)} + \overline{A}_j(e^{2i\theta}-1)(\bar{\lambda}-1) + \overline{B}_j] \tag{6}$$

$$-P_y^j + iP_x^j = r^\lambda e^{-i\theta\lambda}[A_j e^{2i\theta\lambda} + \bar{a}_j\lambda(e^{2i\theta}-1) + \bar{b}_j] + r^{\bar{\lambda}}e^{-i\theta\bar{\lambda}}[a_j e^{2i\theta\bar{\lambda}} + \overline{A}_j\bar{\lambda}(e^{2i\theta}-1) + \overline{B}_j] \tag{7}$$

$$2G_j\left(u_x^j + iu_y^j\right) = r^\lambda e^{-i\theta\lambda}[\kappa_j A_j e^{2i\theta\lambda} - \bar{a}_j\lambda(e^{2i\theta}-1) - \bar{b}_j] + r^{\bar{\lambda}}e^{-i\theta\bar{\lambda}}[\kappa_j a_j e^{2i\theta\lambda} - \overline{A}_j\bar{\lambda}(e^{2i\theta}-1) - \overline{B}_j] \tag{8}$$

The complex potentials must satisfy the following continuity and boundary conditions

$$\begin{aligned} &-P_y^1 + iP_x^1\big|_{\theta=0} = -P_y^2 + iP_x^2\big|_{\theta=0} \\ &u_x^1 + iu_y^1\big|_{\theta=0} = u_x^2 + iu_y^2\big|_{\theta=0} \\ &-P_y^1 + iP_x^1\big|_{\theta=\alpha_1} = 0 \\ &-P_y^2 + iP_x^2\big|_{\theta=-\alpha_2} = 0 \end{aligned} \tag{9}$$

Substituting Eqs. (7) and (8) into (9) gives, after simplification,

$$\begin{bmatrix} 1-e^{2i\lambda\alpha_1} & e^{-2i\lambda\alpha_2}-1 & \lambda(1-e^{2i\alpha_1}) & \lambda(e^{-2i\alpha_2}-1) \\ \frac{G_2}{G_1}(\kappa_1+e^{2i\lambda\alpha_1}) & -\kappa_2+e^{-2i\lambda\alpha_2} & \frac{G_2}{G_1}\lambda(e^{2i\alpha_1}-1) & \lambda(1-e^{-2i\alpha_2}) \\ \lambda(1-e^{-2i\alpha_1}) & \lambda(e^{2i\alpha_2}-1) & 1-e^{-2i\lambda\alpha_1} & e^{2i\lambda\alpha_2}-1 \\ \frac{G_2}{G_1}\lambda(e^{-2i\alpha_1}-1) & \lambda(1-e^{2i\alpha_2}) & \frac{G_2}{G_1}(\kappa_1+e^{-2i\lambda\alpha_1}) & -(\kappa_2+e^{2i\lambda\alpha_2}) \end{bmatrix} \begin{Bmatrix} A_1 \\ A_2 \\ \bar{a}_1 \\ \bar{a}_2 \end{Bmatrix} = \{0\} \tag{10}$$

or

$$[\mathbf{D}][A_1 \quad A_2 \quad \bar{a}_1 \quad \bar{a}_2]^T = \{0\} \tag{11}$$

For non-trivial solution the determinant of $[D]$ should be zero, i.e.

$$\det[\mathbf{D}] = 0 \tag{12}$$

Solving Eq. (12) gives the values of λ, the eigenvalues, that make the determinant zero. Muller's method is used to solve this equation using the technique presented in Ref. [22]. The values of λ may be real or complex.

Please cite this article in press as: Treifi M, Oyadiji SO. Bi-material V-notch stress intensity factors by the fractal-like finite element method. Engng Fract Mech (2013), http://dx.doi.org/10.1016/j.engfracmech.2013.04.006

2.1. Complex eigenvalues

For complex eigenvalues, Eq. (11) could be partitioned as follows

$$\begin{bmatrix} [\mathbf{D}_{11}] & \vdots & [\mathbf{D}_{12}] \\ \cdots & \cdots\cdots & \cdots \\ [\mathbf{D}_{21}] & \vdots & [\mathbf{D}_{22}] \end{bmatrix} \begin{Bmatrix} A_1 \\ \cdots \\ A_2 \\ \bar{a}_1 \\ \bar{a}_2 \end{Bmatrix} = \begin{Bmatrix} 0 \\ \cdots \\ 0 \\ 0 \\ 0 \end{Bmatrix} \tag{13}$$

From Eq. (13)

$$\begin{Bmatrix} A_2 \\ \bar{a}_1 \\ \bar{a}_2 \end{Bmatrix} = -[\mathbf{D}_{22}]^{-1}[\mathbf{D}_{21}]A_1 = \{\mathbf{S}\}A_1 \tag{14}$$

Using Eq. (14) and the boundary conditions, the coefficients of the complex potentials can be written in terms of A_1 and its conjugate $\bar{A}_1$ as

$$\begin{Bmatrix} A_1 \\ \bar{A}_1 \\ a_1 \\ \bar{a}_1 \\ B_1 \\ \bar{B}_1 \\ b_1 \\ \bar{b}_1 \end{Bmatrix} = \begin{bmatrix} 1 & 0 \\ 0 & 1 \\ 0 & \overline{\mathbf{S}(2)} \\ \mathbf{S}(2) & 0 \\ -\mathbf{S}(2)e^{-2i\lambda\alpha_1} - \lambda(e^{-2i\alpha_1} - 1) & 0 \\ 0 & -\overline{\mathbf{S}(2)}e^{2i\bar{\lambda}\alpha_1} - \bar{\lambda}(e^{2i\alpha_1} - 1) \\ 0 & -e^{-2i\bar{\lambda}\alpha_1} - \bar{\lambda}\overline{\mathbf{S}(2)}(e^{-2i\alpha_1} - 1) \\ -e^{2i\lambda\alpha_1} - \lambda\mathbf{S}(2)(e^{2i\alpha_1} - 1) & 0 \end{bmatrix} \begin{Bmatrix} A_1 \\ \bar{A}_1 \end{Bmatrix} = [\mathbf{H}_1]\begin{Bmatrix} A_1 \\ \bar{A}_1 \end{Bmatrix} \tag{15}$$

for material 1 and

$$\begin{Bmatrix} A_2 \\ \bar{A}_2 \\ a_2 \\ \bar{a}_2 \\ B_2 \\ \bar{B}_2 \\ b_2 \\ \bar{b}_2 \end{Bmatrix} = \begin{bmatrix} \mathbf{S}(1) & 0 \\ 0 & \overline{\mathbf{S}(1)} \\ 0 & \overline{\mathbf{S}(3)} \\ \mathbf{S}(3) & 0 \\ -\mathbf{S}(3)e^{2i\lambda\alpha_2} - \lambda\mathbf{S}(1)(e^{2i\alpha_2} - 1) & 0 \\ 0 & -\overline{\mathbf{S}(3)}e^{-2i\bar{\lambda}\alpha_2} - \bar{\lambda}\overline{\mathbf{S}(1)}(e^{-2i\alpha_2} - 1) \\ 0 & -\overline{\mathbf{S}(1)}e^{2i\bar{\lambda}\alpha_2} - \bar{\lambda}\overline{\mathbf{S}(3)}(e^{2i\alpha_2} - 1) \\ -\mathbf{S}(1)e^{-2i\lambda\alpha_2} - \lambda\mathbf{S}(3)(e^{-2i\alpha_2} - 1) & 0 \end{bmatrix} \begin{Bmatrix} A_1 \\ \bar{A}_1 \end{Bmatrix} = [\mathbf{H}_2]\begin{Bmatrix} A_1 \\ \bar{A}_1 \end{Bmatrix} \tag{16}$$

for material 2.

A_1 and its conjugate $\bar{A}_1$ can be written in terms of the real and imaginary parts of A_1 as

$$\begin{Bmatrix} A_1 \\ \bar{A}_1 \end{Bmatrix} = \begin{bmatrix} 1 & i \\ 1 & -i \end{bmatrix} \begin{Bmatrix} \mathrm{Re}(A_1) \\ \mathrm{Im}(A_1) \end{Bmatrix} = [\mathbf{N}] \begin{Bmatrix} \mathbf{Re}(A_1) \\ \mathbf{Im}(A_1) \end{Bmatrix} \tag{17}$$

If we let

$$[\mathbf{L}_j] = \begin{bmatrix} r^{\lambda}\kappa_j e^{-i\lambda\theta}e^{2i\lambda\theta} \\ \bar{\lambda}r^{\bar{\lambda}}e^{-i\bar{\lambda}\theta}(1 - e^{2i\theta}) \\ r^{\bar{\lambda}}\kappa_j e^{-i\bar{\lambda}\theta}e^{2i\bar{\lambda}\theta} \\ \lambda r^{\lambda}e^{-i\lambda\theta}(1 - e^{2i\theta}) \\ 0 \\ -r^{\bar{\lambda}}e^{-i\bar{\lambda}\theta} \\ 0 \\ -r^{\lambda}e^{-i\lambda\theta} \end{bmatrix}^T \tag{18}$$

then Eq. (8), the displacement expression, could be rewritten as

$$2G_j\left(u_x^j + iu_y^j\right) = [\mathbf{L}_j][\mathbf{H}_j][\mathbf{N}] \begin{Bmatrix} \mathrm{Re}(A_1) \\ \mathrm{Im}(A_1) \end{Bmatrix} = [\mathbf{J}_j] \begin{Bmatrix} \mathrm{Re}(A_1) \\ \mathrm{Im}(A_1) \end{Bmatrix} \tag{19}$$

Please cite this article in press as: Treifi M, Oyadiji SO. Bi-material V-notch stress intensity factors by the fractal-like finite element method. Engng Fract Mech (2013), http://dx.doi.org/10.1016/j.engfracmech.2013.04.006

Equating the real and imaginary parts of both sides of Eq. (19) leads to

$$\begin{Bmatrix} u_x^j \\ u_y^j \end{Bmatrix} = \frac{1}{2G_j} \begin{bmatrix} \mathrm{Re}(\mathbf{J}_j(1,1)) & \mathrm{Re}(\mathbf{J}_j(1,2)) \\ \mathrm{Im}(\mathbf{J}_j(1,1)) & \mathrm{Im}(\mathbf{J}_j(1,2)) \end{bmatrix} \begin{Bmatrix} \mathrm{Re}(A_1) \\ \mathrm{Im}(A_1) \end{Bmatrix} \tag{20}$$

Eq. (20) shows that the displacement expressions for each complex eigenvalue can be written in terms of a complex coefficient with real and imaginary parts.

2.2. Real eigenvalues

For real eigenvalues, the complex potentials $\phi^j(z)$ and $\omega^j(z)$ are reduced to

$$\phi^j(z) = A_j z^\lambda \text{ and } \omega^j(z) = B_j z^\lambda \tag{21}$$

Substituting Eq. (21) into Eqs. (2)–(4) gives

$$\sigma_{yy}^j - i\tau_{xy}^j = \lambda r^{\lambda-1} e^{i\theta(1-\lambda)} [A_j e^{2i\theta(\lambda-1)} + \overline{A}_j (e^{2i\theta} - 1)(\lambda - 1) + \overline{B}_j] \tag{22}$$

$$-P_y^j + iP_x^j = r^\lambda e^{-i\theta\lambda} [A_j e^{2i\theta\lambda} + \overline{A}_j \lambda (e^{2i\theta} - 1) + \overline{B}_j] \tag{23}$$

$$2G_j \left(u_x^j + iu_y^j \right) = r^\lambda e^{-i\theta\lambda} [\kappa_j A_j e^{2i\theta\lambda} - \overline{A}_j \lambda (e^{2i\theta} - 1) - \overline{B}_j] \tag{24}$$

By making use of the continuity and boundary conditions of Eq. (9), the following relation must hold

$$\begin{bmatrix} q_{11} & q_{12} \\ q_{21} & q_{22} \end{bmatrix} \begin{Bmatrix} \mathrm{Re}(A_1) \\ \mathrm{Im}(A_1) \end{Bmatrix} = \{0\} \tag{25}$$

where

$$q_{11} = \mathrm{Re}(t_1) + \mathrm{Re}(t_2), \quad q_{12} = \mathrm{Im}(t_2) - \mathrm{Im}(t_1)$$
$$q_{21} = \mathrm{Im}(t_1) + \mathrm{Im}(t_2), \quad q_{22} = \mathrm{Re}(t_1) - \mathrm{Re}(t_2)$$
$$t_1 = \bar{s}_2 - s_3, \quad t_2 = \bar{s}_1 - s_4$$
$$s_1 = \frac{d_4 d_5 - d_1 d_8}{d_3 d_8 - d_7 d_4}, \quad s_2 = \frac{d_6 d_4 - d_2 d_8}{d_3 d_8 - d_7 d_4}, \quad s_3 = \frac{d_5 d_3 - d_1 d_7}{d_4 d_7 - d_8 d_3}, \quad s_4 = \frac{d_6 d_3 - d_2 d_7}{d_4 d_7 - d_8 d_3}$$
$$d_1 = G_2(\kappa_1 + e^{2i\lambda\alpha_1}), \quad d_2 = G_2\lambda(e^{2i\alpha_1} - 1), \quad d_3 = -G_1(\kappa_2 + e^{-2i\lambda\alpha_2}), \quad d_4 = -G_1\lambda(e^{-2i\alpha_2} - 1),$$
$$d_5 = 1 - e^{2i\lambda\alpha_1}, \quad d_6 = -\lambda(e^{2i\alpha_1} - 1), \quad d_7 = e^{-2i\lambda\alpha_2} - 1, \quad d_8 = \lambda(e^{-2i\alpha_2} - 1)$$

Eq. (25) shows that Im (A_1) can be determined in terms of Re (A_1) or vice versa, i.e.,

$$\begin{Bmatrix} \mathrm{Re}(A_1) \\ \mathrm{Im}(A_1) \end{Bmatrix} = \begin{Bmatrix} p_1 \\ p_2 \end{Bmatrix} c = [\mathbf{P}]c \tag{26}$$

where c is either Re (A_1) or Im (A_1). To avoid division by zero, p_1 and p_2 may be computed from Table 1 depending on the largest absolute value of q_{ij}.

From Eqs. (17) and (26), A_1 and its conjugate $\overline{A}_1$ can be written in terms of c as

$$\begin{Bmatrix} A_1 \\ \overline{A}_1 \end{Bmatrix} = \begin{bmatrix} 1 & i \\ 1 & -i \end{bmatrix} \begin{Bmatrix} \mathrm{Re}(A_1) \\ \mathrm{Im}(A_1) \end{Bmatrix} = [\mathbf{N}] \begin{Bmatrix} \mathrm{Re}(A_1) \\ \mathrm{Im}(A_1) \end{Bmatrix} = [\mathbf{N}][\mathbf{P}]c \tag{27}$$

and A_2 and its conjugate $\overline{A}_2$ can be written in terms of A_1 and $\overline{A}_1$ and therefore in terms of c as

$$\begin{Bmatrix} A_2 \\ \overline{A}_2 \end{Bmatrix} = \begin{bmatrix} s_1 & s_2 \\ s_3 & s_4 \end{bmatrix} \begin{Bmatrix} A_1 \\ \overline{A}_1 \end{Bmatrix} = [\mathbf{S}] \begin{Bmatrix} A_1 \\ \overline{A}_1 \end{Bmatrix} = [\mathbf{S}][\mathbf{N}][\mathbf{P}]c \tag{28}$$

Table 1
Definition of p_1 and p_2.

Largest $\lvert q_{ij} \rvert$	p_1	p_2
q_{11}	$-q_{12}/q_{11}$	1
q_{12}	1	$-q_{11}/q_{12}$
q_{21}	$-q_{22}/q_{21}$	1
q_{22}	1	$-q_{21}/q_{22}$

Please cite this article in press as: Treifi M, Oyadiji SO. Bi-material V-notch stress intensity factors by the fractal-like finite element method. Engng Fract Mech (2013), http://dx.doi.org/10.1016/j.engfracmech.2013.04.006

Using Eqs. (27) and (28) in addition to the boundary conditions, the coefficients of the complex potentials in Eqs. (22)–(24) can be written as

$$\begin{Bmatrix} A_1 \\ \overline{A}_1 \\ \overline{B}_1 \end{Bmatrix} = \begin{bmatrix} 1 & 0 \\ 0 & 1 \\ -e^{2i\lambda\alpha_1} & -\lambda(e^{2i\alpha_1}-1) \end{bmatrix} \begin{Bmatrix} A_1 \\ \overline{A}_1 \end{Bmatrix} = [\mathbf{H}_1][\mathbf{N}][\mathbf{P}]c = [\mathbf{R}_1]c \tag{29}$$

for material 1 and

$$\begin{Bmatrix} A_2 \\ \overline{A}_2 \\ \overline{B}_2 \end{Bmatrix} = \begin{bmatrix} 1 & 0 \\ 0 & 1 \\ -e^{-2i\lambda\alpha_2} & -\lambda(e^{-2i\alpha_2}-1) \end{bmatrix} \begin{Bmatrix} A_2 \\ \overline{A}_2 \end{Bmatrix} = [\mathbf{H}_2][\mathbf{S}][\mathbf{N}][\mathbf{P}]c = [\mathbf{R}_2]c \tag{30}$$

for material 2. If we let

$$[\mathbf{L}_j] = r^{\lambda}e^{-i\lambda\theta}\begin{bmatrix} \kappa_j e^{2i\lambda\theta} & -\lambda(e^{2i\theta}-1) & -1 \end{bmatrix} \tag{31}$$

then Eq. (24), the displacement expression for real eigenvalues, could be rewritten as

$$2G_j\left(u_x^j + iu_y^j\right) = [\mathbf{L}_j][\mathbf{R}_j]c = [\mathbf{J}_j]c \tag{32}$$

Equating the real and imaginary parts of both sides of Eq. (32) leads to

$$\begin{Bmatrix} u_x^j \\ u_y^j \end{Bmatrix} = \frac{1}{2G_j}\begin{bmatrix} \mathrm{Re}(\mathbf{J}_j(1,1)) \\ \mathrm{Im}(\mathbf{J}_j(1,1)) \end{bmatrix} c \tag{33}$$

Eq. (33) shows that the displacement expressions for each real eigenvalue can be written in terms of a real coefficient Similar formulation was presented in polar coordinates in Ref. [22].

2.3. Generalised coordinates

The displacement expressions around a notch tip are the sum of terms of Eqs. (20) and (33) repeated for as many eigenvalues considered (those equations are series expansions. The $\sum$ symbol is dropped for simplicity). The coefficients c in Eq. (33) and the real and imaginary parts of the coefficients A_1 in Eq. (20) are called generalised coordinates and will be computed directly in the FFEM. The ones associated with the singular eigenvalues ($\mathrm{Re}(\lambda) < 1$) are related directly to the SIFs of a general notch. The rest are the constants of the higher order terms.

3. Stress intensity factors

The eigenvalues computed using Eq. (12) could be real or complex. For a general bi-material notch, the singular eigenvalues ($\mathrm{Re}(\lambda) < 1$) are either two real singular eigenvalues associated with mode I and mode II (λ_I,λ_{II}) or a single complex singular eigenvalue with real and imaginary parts (in some cases only one real singular eigenvalue exists). A complex singular eigenvalue is associated with a complex SIF that can be computed using one of the following equations

$$\boldsymbol{K}_c = \sqrt{2\pi}\lambda A_1[\mathbf{S}(2)(1-e^{-2i\lambda\alpha_1}) - \lambda(e^{-2i\alpha_1}-1)] \tag{34}$$

$$\boldsymbol{K}_c = \sqrt{2\pi}\bar{\lambda}\overline{A}_1\lfloor 1 - e^{-2i\bar{\lambda}\alpha_1} - \bar{\lambda}\overline{\mathbf{S}(2)}(e^{-2i\alpha_1}-1)\rfloor \tag{35}$$

The real and imaginary parts of $\boldsymbol{K}_c$ represent mode I and mode II SIFs. For the case of two real singular eigenvalues, where one eigenvalue is associated with mode I while the other is associated with mode II, the SIFs expressions are

$$\boldsymbol{K}_I = \sqrt{2\pi}\frac{\lambda_I c_I}{2}[(p_{I1}+ip_{I2})(1+\lambda_I(1-e^{-2i\alpha_1}) - e^{2i\lambda_I\alpha_1}) + (p_{I1}-ip_{I2})(1+\lambda_I(1-e^{2i\alpha_1}) - e^{-2i\lambda_I\alpha_1})] \tag{36}$$

for mode I, and

$$\boldsymbol{K}_{II} = \sqrt{2\pi}\frac{\lambda_{II} c_{II}}{2i}[(p_{II1}+ip_{II2})(\lambda_{II}(1-e^{-2i\alpha_1}) + e^{2i\lambda_{II}\alpha_1} - 1) + (p_{II1}-ip_{II2})(\lambda_{II}(e^{2i\alpha_1}-1) - e^{-2i\lambda_I\alpha_1} + 1)] \tag{37}$$

for mode II.

4. Fractal-like finite element method for a bi-material notch

The FFEM is a semi-analytical method that incorporates the agility of the finite element method (FEM) and the accuracy of the analytical solutions. A bi-material notched body is divided into regular and singular regions as shown in Fig. 2. The analytical expressions of the displacement field around a notch tip are used as global interpolation functions to transform the

Please cite this article in press as: Treifi M, Oyadiji SO. Bi-material V-notch stress intensity factors by the fractal-like finite element method. Engng Fract Mech (2013), http://dx.doi.org/10.1016/j.engfracmech.2013.04.006

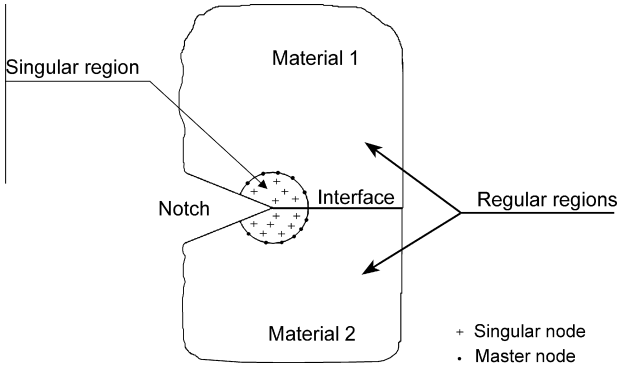

Fig. 2. Singular and regular regions of a notched plate.

large number of nodal displacements $\mathbf{d}_s$ of the nodes in the singular region containing the notch tip to a small set of generalised coordinates $\mathbf{a}$ as follows

$$\mathbf{d}_s = \mathbf{T}\mathbf{a} \tag{38}$$

where $\mathbf{T}$ is a transformation matrix and is computed using the displacement expressions in Eqs. (20) and (33) depending on the type of the eigenvalue. The idea of the global interpolation functions is similar to the idea of the local interpolation functions (shape functions) of a finite element. For a complex eigenvalue, Eq. (20) is used, while for a real eigenvalue Eq. (33) is used. In the reported literature of the FFEM, such as Treifi et al. [17,20], the transformation matrix $\mathbf{T}$ of any layer in the singular region can be computed in terms of the transformation matrix of the first layer when the layers of elements in the singular region are constructed using a similarity ratio. This leads to a transformed stiffness matrix of the inner layers being written as a sum of a geometric series allowing virtually the use of an infinite number of layers in the singular region based only on the stiffness matrix of the first layer. However, for the case of a bi-material notch where eigenvalues may be complex, this is not simple because λ and its conjugate $\bar{\lambda}$ appear in the displacement expressions. Therefore, a finite number of layers will be used in the singular region instead of using the sum of a geometric series. It should be noted that the fractal self-similar nature of the mesh applies to the radial direction towards the notch/crack tip but not necessarily to the hoop direction. For this reason, the topology is referred to as being fractal-like.

In the FFEM, the equilibrium equation in the conventional FEM can be partitioned and transformed as follows

$$\begin{bmatrix} \mathbf{K}_{rr} & \mathbf{K}_{rm} & 0 \\ \mathbf{K}_{mr} & \mathbf{K}_{mm}+\mathbf{K}_{mm}^{1st} & \overline{\mathbf{K}}_{ms}^{1st} \\ 0 & \overline{\mathbf{K}}_{sm}^{1st} & \overline{\mathbf{K}}_{ss}^{1st}+\overline{\mathbf{K}}_{s}^{inn} \end{bmatrix} \begin{Bmatrix} \mathbf{d}_r \\ \mathbf{d}_m \\ \mathbf{a} \end{Bmatrix} = \begin{Bmatrix} \mathbf{f}_r \\ \mathbf{f}_m+\mathbf{f}_m^{1st} \\ \bar{\mathbf{f}}_s^{1st}+\bar{\mathbf{f}}_s^{inn} \end{Bmatrix} \tag{39}$$

where r refers to regular nodes, m master nodes located on the border encompassing the singular region, and s singular nodes. Only the over-barred components (the over-bar here does not refer to the complex conjugate) are transformed:

$$\overline{\mathbf{K}}_{ms}^{1st} = \mathbf{K}_{ms}^{1st}\mathbf{T}_s^{1st}$$
$$\overline{\mathbf{K}}_{ss}^{1st} = \mathbf{T}_s^{1st^T}\mathbf{K}_{ss}^{1st}\mathbf{T}_s^{1st}$$
$$\overline{\mathbf{K}}_{s}^{inn} = \sum_{n=2}^{nl}\overline{\mathbf{K}}_{s}^{n}$$
$$\overline{\mathbf{K}}_{s}^{n} = \mathbf{T}_s^{n^T}\mathbf{K}_s^{n}\mathbf{T}_s^{n}$$
$$\bar{\mathbf{f}}_s^{1st} = \mathbf{T}_s^{1st^T}\mathbf{f}_s^{1st}$$
$$\bar{\mathbf{f}}_s^{inn} = \sum_{n=2}^{nl}\bar{\mathbf{f}}_s^{n}$$
$$\bar{\mathbf{f}}_s^{n} = \mathbf{T}_s^{n^T}\mathbf{f}_s^{n}$$

where $\mathbf{T}_s^{1st}$ and $\mathbf{T}_s^{n}$ refer to the transformation matrices for the first and n^{th} layers of the singular region.

The eigenvalues for a bi-material notch may be a combination of real and complex numbers. Each real eigenvalue is associated with a single element of the vector of generalised coordinates, but each complex eigenvalue is associated with two elements (real and imaginary parts of a complex generalised coordinate) of that vector. Therefore, the FFEM code is rewritten to invoke the appropriate expressions derived in Section 2 according to the type of each eigenvalue.

Please cite this article in press as: Treifi M, Oyadiji SO. Bi-material V-notch stress intensity factors by the fractal-like finite element method. Engng Fract Mech (2013), http://dx.doi.org/10.1016/j.engfracmech.2013.04.006

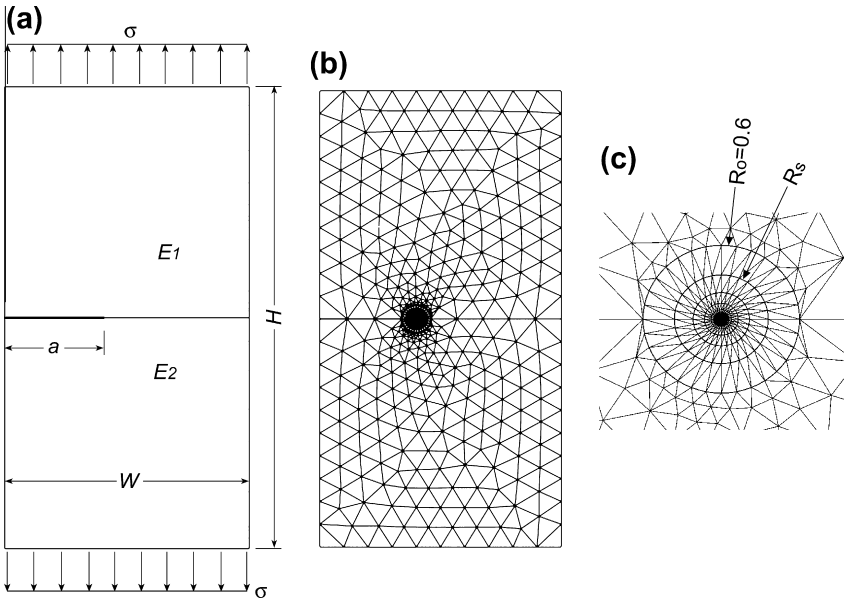

Fig. 3. (a) Bi-material cracked plate ($H/W = 2$) subject to tension loading conditions (b) and (c) the plate FE mesh used in the FFEM.

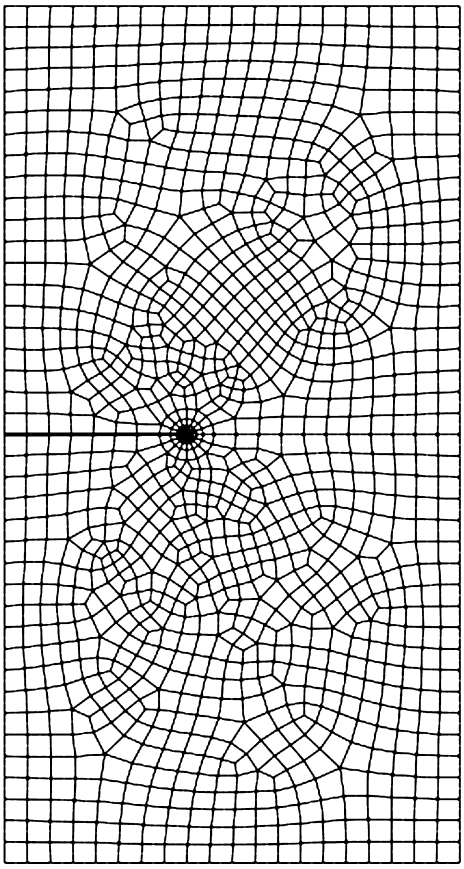

Fig. 4. The FE mesh of the cracked plate ($H/W = 2$) used to compute the SIFs in the ABAQUS software.

Please cite this article in press as: Treifi M, Oyadiji SO. Bi-material V-notch stress intensity factors by the fractal-like finite element method. Engng Fract Mech (2013), http://dx.doi.org/10.1016/j.engfracmech.2013.04.006

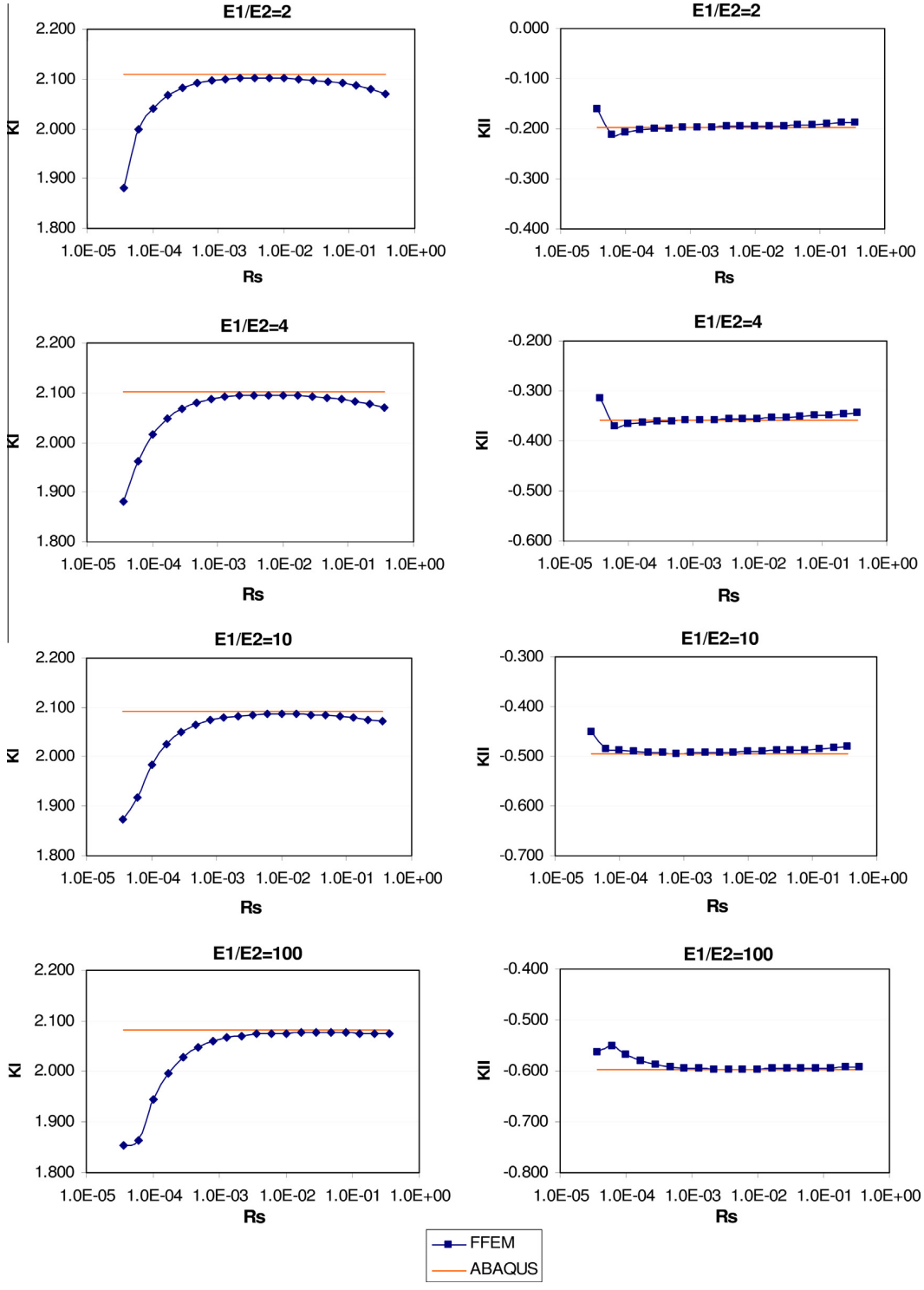

Fig. 5. Variations of bi-material crack SIFs with size of the singular region for different material property ratios compared to those obtained using ABAQUS ($a/w = 0.4$).

Please cite this article in press as: Treifi M, Oyadiji SO. Bi-material V-notch stress intensity factors by the fractal-like finite element method. Engng Fract Mech (2013), http://dx.doi.org/10.1016/j.engfracmech.2013.04.006

As $\mathbf{d}_s$ is much larger than $\mathbf{a}$, solving the equilibrium equation for $\mathbf{a}$ instead of $\mathbf{d}_s$ reduces the computational cost dramatically. Also, in the FFEM the SIFs are computed directly without any need for special singular elements or post-processing technique, because the SIFs are directly related to $\mathbf{a}$ as shown in Eqs. (34)–(37).

5. Numerical examples and verifications

5.1. Convergence study

The size of the singular region is determined through a convergence study of examples of bi-material crack and bi-material notch cases with different material property ratios and different crack lengths. The choice of the number of terms of the global interpolation functions NT, the similarity ratio ρ and the number of layers NL to model the singular region are based on previous convergence studies [17,18,20].

A bi-material edge cracked plate subjected to tension loading conditions, as shown in Fig. 3a, is considered first. The plate is of height $H = 20$ and width $W = 10$. The crack length a is taken as $a/w = 0.4$. Six node triangular elements (seven-point integration scheme) are used to model the plate as shown in Fig. 3b. For this example and all the examples in this paper, the region around the notch/crack tip is modelled using 20 layers starting with a radius of 0.6 down to 0.00003656 as shown in Fig. 3c. The layers are constructed using a similarity ratio of $\rho = 0.6$. The number of terms of the global interpolation functions to be used in the transformation is taken as $NT = 21$. The Poisson's ratios are taken to be $v_1 = v_2 = 0.3$.

The SIF values are computed for different material property ratios (2, 4, 10 and 100) using the FFEM. The results are compared to those computed using ABAQUS finite element analysis (FEA) commercial package. In ABAQUS, the cracked plate is modelled using quadrilateral elements (which are designated as CPS8 in the ABAQUS FEA software) as shown in Fig. 4. Also, the region around the crack tip is modelled using the same number of layers as in the FFEM. In addition, quarter-point singular elements are used in the ABAQUS FEA software to model the first layer around the crack tip.

Fig. 5 shows the SIFs computed for different sizes of the singular region and different material property ratios. The sizes and corresponding number of layers are taken as: the first radius considered is $R_s = 0.36$ containing 19 layers, the second radius is $R_s = 0.216$ containing 18 layers, and so on down to the nineteenth radius $R_s = 0.00003656$ containing only one layer.

The same analysis as above is repeated for a bi-material edge notched plate as shown in Fig. 6a. The plate is meshed using six node triangular elements as shown in Fig. 6b. The opening angle of the notch is taken to be $\gamma = 60°$. No published results are available for this case and current commercial FEA packages, such as the ABAQUS software, are not capable of computing the SIFs for a true notch. However, the current authors have developed a strain energy approach (SEA) to compute the SIFs for a notch, which is based on the strain energy of a finite volume around the notch tip [23]. The strain energy, which may be computed using commercial FEA packages, is used to compute the notch SIFs by using the formulae presented in Ref. [23]. The ABAQUS software is used to compute the strain energy for this case. The plate is meshed as shown in Fig. 6c using quadrilateral elements (CPS8). The notch SIFs computed using the FFEM for different sizes of the singular region and different material property ratios compared to the SIF values computed using the SEA are plotted in Fig. 7.

From Figs. 5 and 7, it can be seen that the size of the singular region has an effect on the results. Convergence is achieved within a limited region ($R_s = 0.001$–0.03) for a bi-material crack with a material property ratio of $E_1/E_2 = 10$ or less. For larger

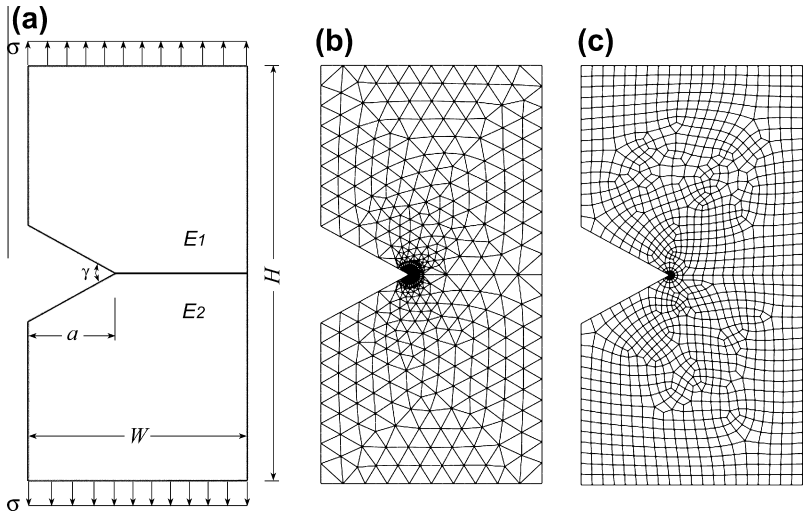

Fig. 6. (a) Bi-material V-notched plate ($H/W = 2$) subject to tension loading conditions, (b) the plate FE mesh used in the FFEM, and (c) the plate FE mesh used in the ABAQUS software to compute the strain energy.

Please cite this article in press as: Treifi M, Oyadiji SO. Bi-material V-notch stress intensity factors by the fractal-like finite element method. Engng Fract Mech (2013), http://dx.doi.org/10.1016/j.engfracmech.2013.04.006

values of material property ratios and for the notch cases, convergence is achieved within a larger region of the size of the singular region ($R_s > 0.001$). The larger the size of the singular region, the more the nodal displacements that are transformed leading to less computational cost.

Now, the relation between the crack length and the size of the singular region is examined. A bi-material cracked plate as shown in Fig. 8a is considered. The material property ratio is taken as $E_1/E_2 = 4$. The plate is of height $H = 30$ and width

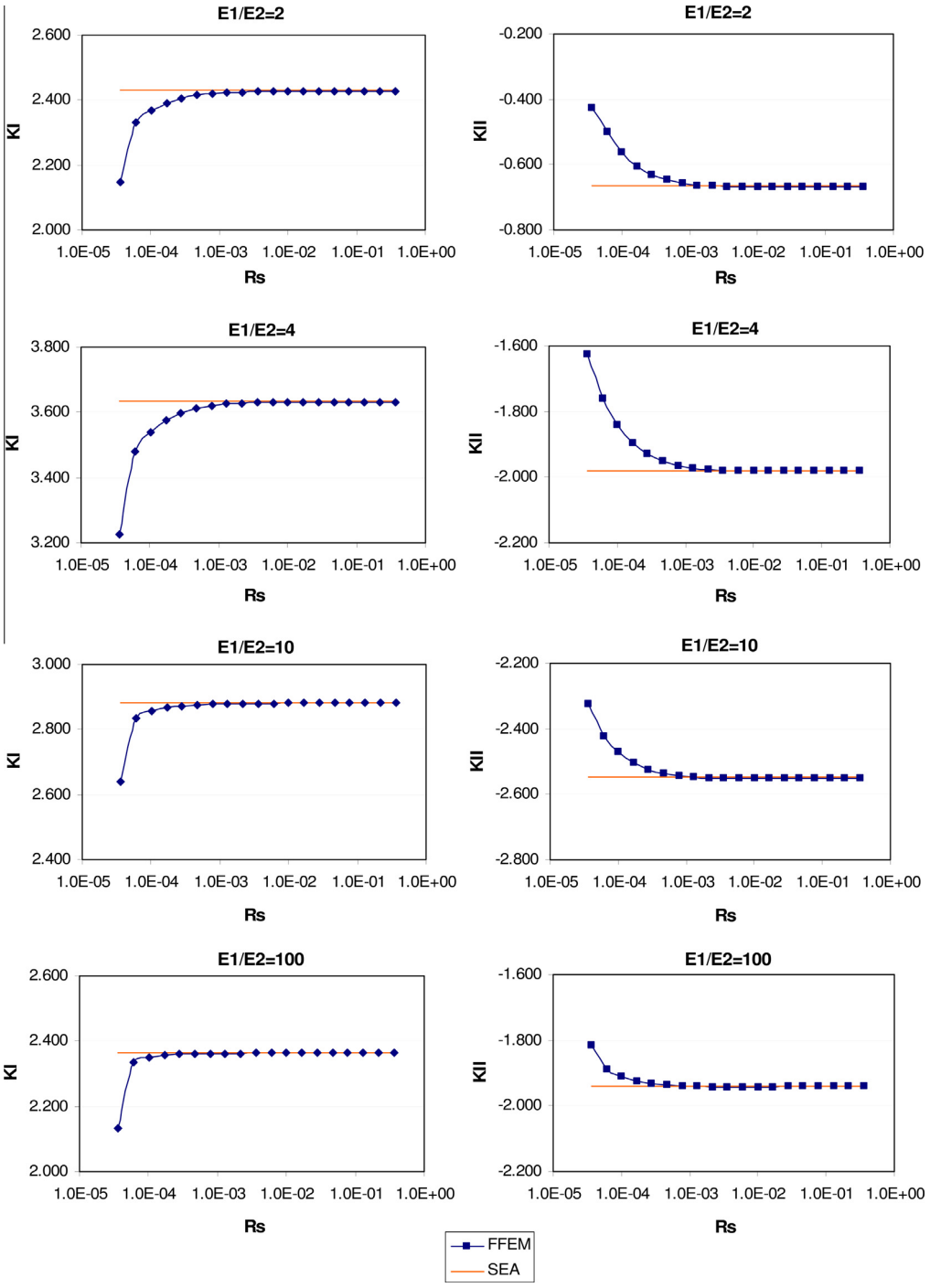

Fig. 7. Variations of bi-material notch SIFs with size of the singular region for different material property ratios compared to those obtained using the SEA ($a/w = 0.4$).

Please cite this article in press as: Treifi M, Oyadiji SO. Bi-material V-notch stress intensity factors by the fractal-like finite element method. Engng Fract Mech (2013), http://dx.doi.org/10.1016/j.engfracmech.2013.04.006

$W = 10$. Six node triangular elements are used to mesh the plate as shown in Fig. 8b and c. The SIF values are computed for different crack lengths ($a/w = 0.2, 0.3, 0.4, 0.5, 0.6$ and 0.7). The volumes of the singular region and corresponding number of layers are taken as follows: the first radius considered is $R_s = 0.36$ containing 19 layers, the second radius is $R_s = 0.216$ containing 18 layers, and so on down to the twelfth radius $R_s = 0.00047$ containing six layers. Smaller radii are not considered because they will not give results with good accuracy as we found from the previous two examples. The FFEM results are plotted in Figs. 9–14 and are compared to those reported by Matsumto et al. [10]. It can be seen from those figures that convergence is achieved with smaller sizes of the singular region when the crack length is short. As the crack length increases, convergence is achieved when using larger sizes of the singular region.

Based on the above discussion, the radius of the singular region for a crack problem may be taken as $R_s = 0.0036$ when the crack length is $a/W \leqslant 0.5$ and the material property ratio is $E_1/E_2 \leqslant 10$, $R_s = 0.0467$ when the crack length is $a/W \leqslant 0.5$ and the material property ratio is $E_1/E_2 > 10$, and $R_s = 0.0467$when the crack length is $a/W > 0.5$ for all material property ratios. For notch problems where convergence is achievable for a wider range of values of the radius of the singular region, the radius of the singular region may be taken as $R_s = 0.0467$ for all cases. These values of R_s are used for the rest of the examples presented in this paper.

5.2. Bi-material crack

A bi-material cracked plate subjected to tension loading conditions as shown in Fig. 8a is analysed. The plate is of height $H = 30$ and width $W = 10$. Six node triangular elements are used to mesh the plate as shown in Fig. 8b and c. Different crack lengths ($a/w = 0.2, 0.3, 0.4, 0.5, 0.6$ and 0.7) and different material property ratios ($E_1/E_2 = 2, 4, 10$ and 100) are considered. The scaled SIF values $\left(K_c/\sigma\sqrt{\pi}a^{1-\mathrm{Re}(\lambda)}(2a)^{i\mathrm{Im}(\lambda)}\right)$ computed using the FFEM are tabulated in Table 2. Corresponding published results by Matsumto et al. [10] and computed results using the ABAQUS software and the SEA are also tabulated for comparison. In ABAQUS and the SEA, the plate is meshed using quadrilateral elements (CPS8) as shown in Fig. 15 and singular quarter-point elements are used around the crack tip. The singular eigenvalues for a bi-material crack of a material property ratio of $E_1/E_2 = 2$, 4, 10 and 100 are $\lambda = 0.5 + i0.037306$, $\lambda = 0.5 + i0.0678545$, $\lambda = 0.5 + i0.0937743$ and $\lambda = 0.5 + i0.113817$, respectively. Table 2 shows that the FFEM results are in good agreement with the numerical results computed using ABAQUS and the SEA and with those reported by Matsumto et al. [10].

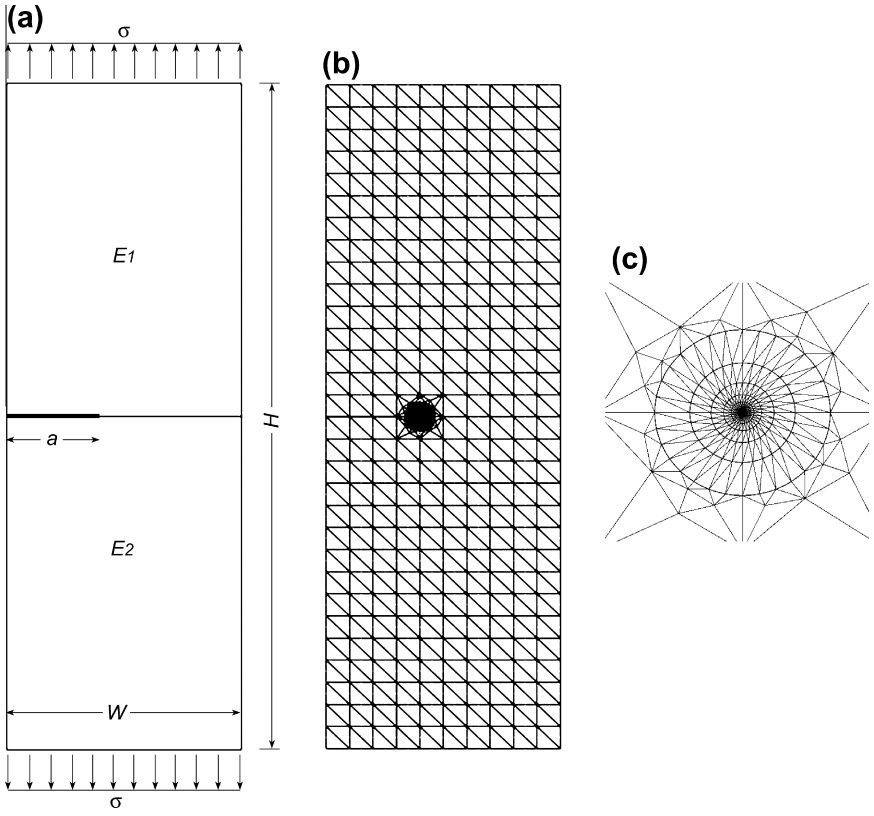

Fig. 8. (a) Bi-material cracked plate ($H/W = 3$) subject to tension loading conditions (b) and (c) the plate FE mesh used in the FFEM.

Please cite this article in press as: Treifi M, Oyadiji SO. Bi-material V-notch stress intensity factors by the fractal-like finite element method. Engng Fract Mech (2013), http://dx.doi.org/10.1016/j.engfracmech.2013.04.006

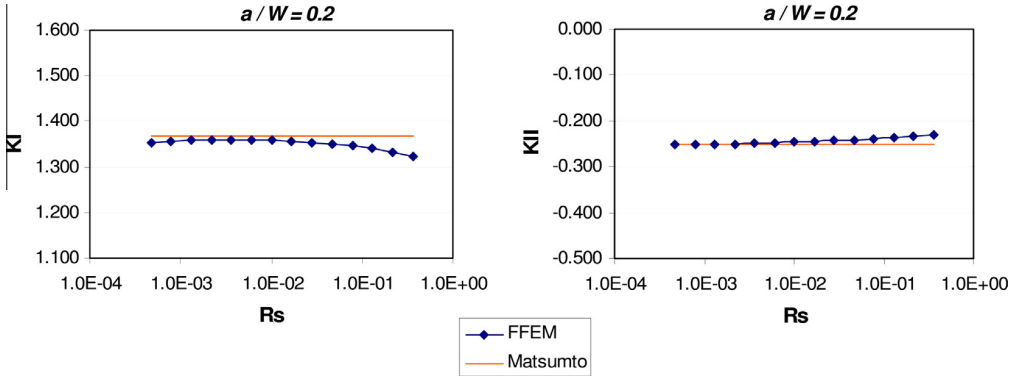

Fig. 9. Variations of bi-material crack SIFs with size of the singular region compared to those obtained Matsumto ($a/w = 0.2, E_1/E_2 = 4$).

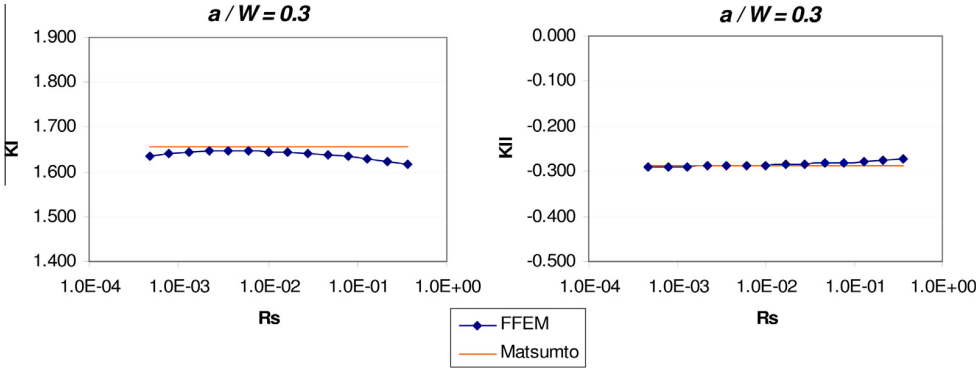

Fig. 10. Variations of bi-material crack SIFs with size of the singular region compared to those obtained Matsumto ($a/w = 0.3, E_1/E_2 = 4$).

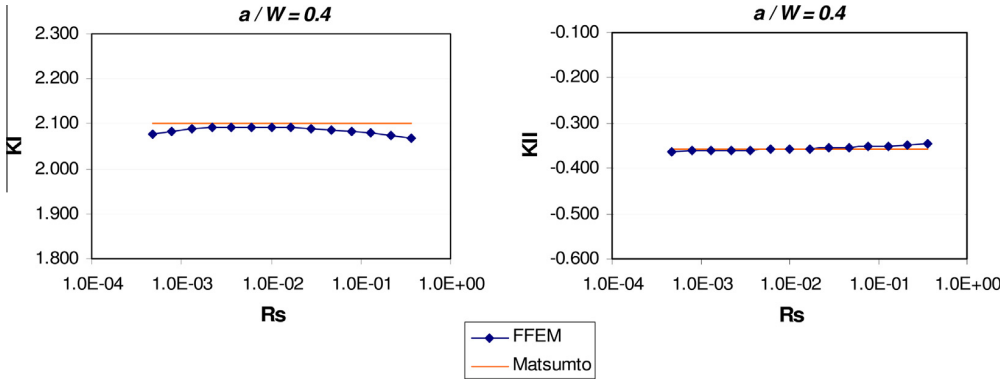

Fig. 11. Variations of bi-material crack SIFs with size of the singular region compared to those obtained Matsumto ($a/w = 0.4, E_1/E_2 = 4$).

5.3. Bi-material notch

A bi-material V-notched plate subjected to tension loading conditions as shown in Fig. 6a is analysed for different notch opening angles ($\gamma = 0°$, 30°, 45°, 60° and 90°) and different material property ratios ($E_1/E_2 = 2$, 4, 10 and 100). The plate dimensions are $H = 20$ and $W = 10$. The notch length is taken as $a/W = 0.4$. Six node triangular elements are used to mesh the plate in a similar way to that shown in Fig. 6b. No available published results exist to compare with for the notch cases, and current FEA software, such as the ABAQUS software, cannot compute the SIFs for a true notch; i.e. the notch opening

Please cite this article in press as: Treifi M, Oyadiji SO. Bi-material V-notch stress intensity factors by the fractal-like finite element method. Engng Fract Mech (2013), http://dx.doi.org/10.1016/j.engfracmech.2013.04.006

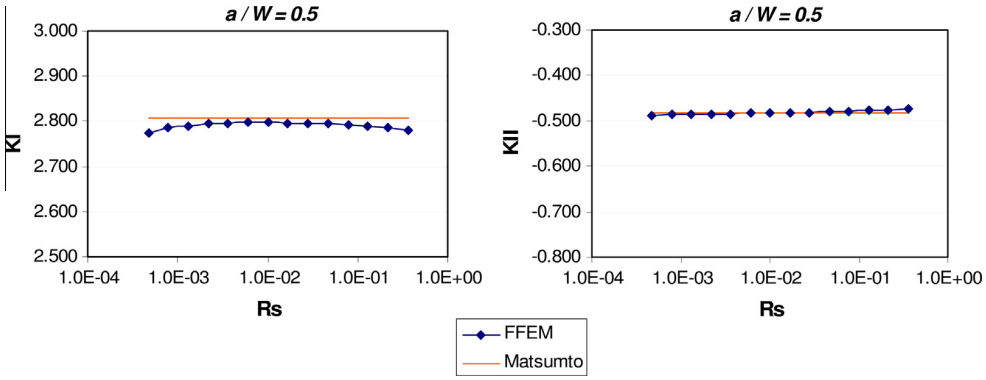

Fig. 12. Variations of bi-material crack SIFs with size of the singular region compared to those obtained Matsumto ($a/w = 0.5, E_1/E_2 = 4$).

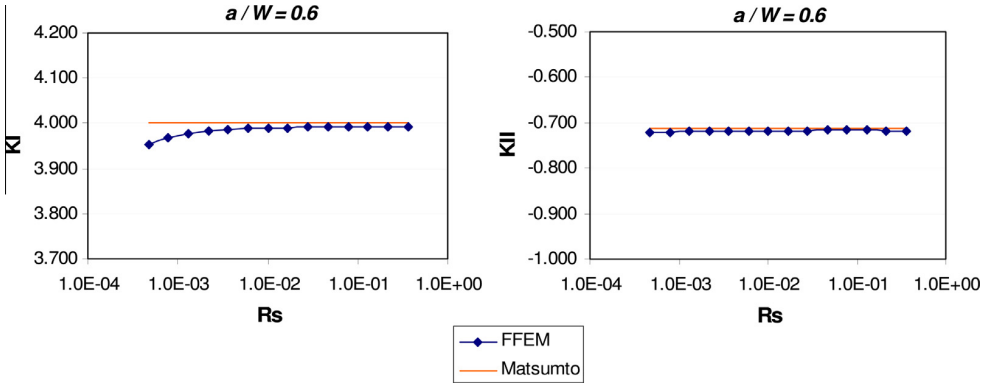

Fig. 13. Variations of bi-material crack SIFs with size of the singular region compared to those obtained Matsumto ($a/w = 0.6, E_1/E_2 = 4$).

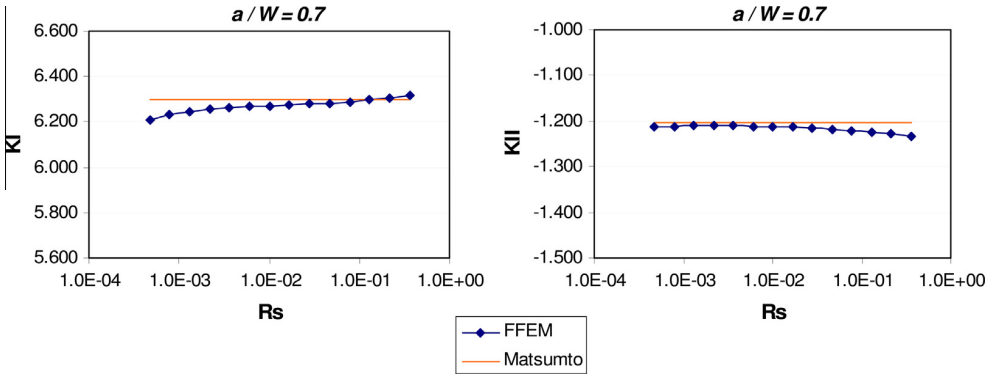

Fig. 14. Variations of bi-material crack SIFs with size of the singular region compared to those obtained Matsumto ($a/w = 0.7, E_1/E_2 = 4$).

angle is not zero. It is only capable of computing the SIF values for crack problems. Therefore, the SEA is used to compare the results for the true notch cases. In the SEA, the plate is meshed in a similar way to that shown in Fig. 6c to compute the strain energy.

The scaled SIF values computed using the FFEM and SEA are tabulated in Table 3. The singular eigenvalues ($\mathrm{Re}(\lambda) < 1$) for each case are also tabulated in Table 3. For each case, the singular eigenvalues are either two real eigenvalues or a single complex eigenvalue. Each case with two singular real eigenvalues gives two real SIFs K_I and K_{II} for mode I and II, respectively, while each case with a single complex singular eigenvalue gives a complex SIF $K_c = K_1 + iK_2$. The real and imaginary parts of a

Please cite this article in press as: Treifi M, Oyadiji SO. Bi-material V-notch stress intensity factors by the fractal-like finite element method. Engng Fract Mech (2013), http://dx.doi.org/10.1016/j.engfracmech.2013.04.006

Table 2
Scaled SIFs for bi-material cracked plates under tension.

a/W		E_1/E_2							
		2		4		10		100	
		K_I	K_{II}	K_I	K_{II}	K_I	K_{II}	K_I	K_{II}
0.2	FFEM	1.358	−0.135	1.360	−0.249	1.363	−0.349	1.367	−0.429
	SEA	1.365	−0.138	1.364	−0.250	1.365	−0.339	1.370	−0.418
	ABAQUS	1.368	−0.137	1.368	−0.251	1.369	−0.350	1.371	−0.430
	Matsumto	1.367	−0.137	1.368	−0.251	1.366	−0.348	1.376	−0.429
0.3	FFEM	1.649	−0.157	1.646	−0.287	1.642	−0.400	1.639	−0.487
	SEA	1.657	−0.160	1.652	−0.292	1.646	−0.397	1.644	−0.488
	ABAQUS	1.659	−0.159	1.654	−0.289	1.649	−0.400	1.643	−0.487
	Matsumto	1.657	−0.156	1.655	−0.288	1.648	−0.394	1.647	−0.470
0.4	FFEM	2.099	−0.197	2.092	−0.359	2.082	−0.496	2.074	−0.600
	SEA	2.107	−0.199	2.099	−0.364	2.088	−0.498	2.080	−0.609
	ABAQUS	2.109	−0.198	2.101	−0.360	2.090	−0.496	2.079	−0.600
	Matsumto	2.109	−0.195	2.102	−0.358	2.090	−0.491	2.083	−0.569
0.5	FFEM	2.808	−0.267	2.796	−0.485	2.779	−0.666	2.764	−0.802
	SEA	2.819	−0.268	2.805	−0.489	2.787	−0.669	2.771	−0.812
	ABAQUS	2.821	−0.268	2.807	−0.485	2.788	−0.665	2.771	−0.801
	Matsumto	2.819	−0.268	2.806	−0.483	2.789	−0.661	2.772	−0.793
0.6	FFEM	4.014	−0.396	3.991	−0.717	3.961	−0.982	3.929	−1.177
	SEA	4.024	−0.396	4.000	−0.718	3.967	−0.983	3.937	−1.180
	ABAQUS	4.025	−0.398	4.002	−0.718	3.971	−0.982	3.940	−1.177
	Matsumto	4.024	−0.398	4.001	−0.714	3.968	−0.973	3.906	−1.171
0.7	FFEM	6.336	−0.676	6.283	−1.218	6.214	−1.656	6.145	−1.969
	SEA	6.338	−0.665	6.288	−1.202	6.220	−1.647	6.157	−1.956
	ABAQUS	6.336	−0.671	6.291	−1.210	6.230	−1.651	6.168	−1.974
	Matsumto	6.348	−0.668	6.298	−1.204	6.227	−1.634	6.157	−1.957

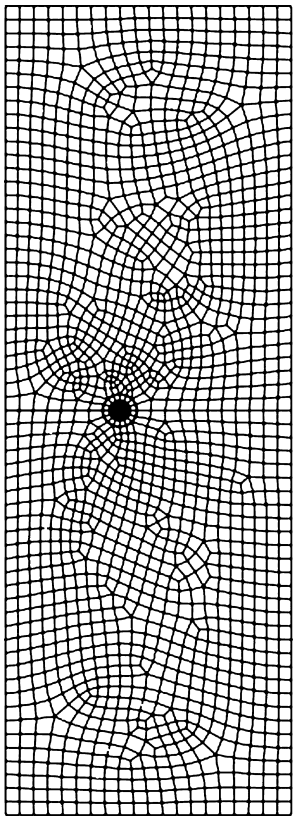

Fig. 15. The FE mesh of the cracked plate ($H/W = 3$) used to compute the SIFs in the ABAQUS software.

Please cite this article in press as: Treifi M, Oyadiji SO. Bi-material V-notch stress intensity factors by the fractal-like finite element method. Engng Fract Mech (2013), http://dx.doi.org/10.1016/j.engfracmech.2013.04.006

Table 3
Scaled SIFs for bi-material V-notched plates under tension ($a/W = 0.4$).

$\gamma(^\circ)$		E_1/E_2							
		2		4		10		100	
		K_I	K_{II}	K_I	K_{II}	K_I	K_{II}	K_I	K_{II}
0	FFEM	2.102	−0.196	2.095	−0.357	2.085	−0.493	2.077	−0.595
	SEA	2.109	−0.199	2.100	−0.363	2.089	−0.496	2.082	−0.607
	ABAQUS	2.110	−0.198	2.102	−0.359	2.092	−0.495	2.081	−0.598
	λ	0.5 + i0.0373		0.5 + i0.0679		0.5 + i0.0938		0.5 + i0.1138	
30	FFEM	3.447	−2.187	2.469	−1.315	2.264	−1.146	2.192	−1.148
	SEA	3.449	−2.188	2.470	−1.315	2.264	−1.143	2.193	−1.149
	ABAQUS	–	–	–	–	–	–	–	–
	λ	0.5265	0.5727	0.5490 + i0.0602		0.5482 + i0.0950		0.5475 + i0.1198	
45	FFEM	2.508	−0.943	3.688	−3.043	2.446	−1.636	2.260	−1.493
	SEA	2.510	−0.941	3.689	−3.042	2.446	−1.633	2.261	−1.490
	ABAQUS	–	–	–	–	–	–	–	–
	λ	0.5202	0.6433	0.5802 + i0.0352		0.5784 + i0.0879		0.5767 + i0.1187	
60	FFEM	2.428	−0.668	3.632	−1.980	2.881	−2.552	2.364	−1.942
	SEA	2.430	−0.666	3.633	−1.980	2.881	−2.549	2.365	−1.940
	ABAQUS	–	–	–	–	–	–	–	–
	λ	0.5243	0.7163	0.5627	0.6722	0.6139 + i0.0704		0.6105 + i0.1127	
90	FFEM	2.587	−0.394	2.967	−0.825	4.202	−1.680	3.465	−4.887
	SEA	2.590	−0.391	2.969	−0.826	4.201	−1.677	3.466	−4.888
	ABAQUS	–	–	–	–	–	–	–	–
	λ	0.5532	0.8929	0.5765	0.8545	0.6197	0.7927	0.6975 + i0.0609	

complex SIF correspond to mode I and II. From Table 3, it can be seen that the notch SIF values predicted using the FFEM and the SEA are in very good agreement.

Zuccarello and Ferrante [24] reported an experimental SIF for a V-notched bi-material plate subjected to tension loading conditions as shown in Fig. 6a. The plate dimensions are $H = 30$ cm, $W = 7.5$ cm, the thickness $t = 1$ cm, and the notch opening angle is $\gamma = 135^\circ$. The plate is made of two parts: Aluminium ($E_1 = 63{,}300$ MPa, $\nu_1 = 0.33$) and PSM-1 ($E_2 = 2990$ MPa, $\nu_2 = 0.39$). The adhesive chosen to bond the two materials together has practically the same material properties as PSM-1. The experimental SIF for this case is $K_I/\sigma a^{1-\lambda_I} = 1.55$. Zuccarello and Ferrante did not include the factor $\sqrt{2\pi}$ in the definition of SIFs. Modelling the plate in a similar way to that shown in Fig. 6b, the SIF computed using the FFEM is $K_I/\sqrt{2\pi}\sigma a^{1-\lambda_I} = 1.54$ (the mode I eigenvalue for this case is $\lambda_I = 0.6515$, mode II eigenvalue is not singular). The published experimental and the computed FFEM SIF values for this problem are in very good agreement.

6. Conclusions

In this paper, the FFEM was developed to compute the mode I and II SIFs for bi-material V-notch problems. Exact analytical solutions of the asymptotic field around a bi-material notch tip were derived and used as global interpolation functions in the FFEM to transform the large number of nodal displacements in the singular region to a small number of generalised coordinates. This enables the computation of the SIFs and the coefficients of the higher order terms directly without the need for a post processing technique to extract them. Also, no special singular elements are needed to model the singular region. Any conventional finite elements can be used. Various bi-material V-notch problems were analysed and compared to available published results and numerical solutions to demonstrate the accuracy of the method. New results for bi-material notch cases were also introduced.

References

[1] Gross B, Mendelson A. Plane elastostatic analysis of V-notched plates. Int J Fract 1972;8:267–76.
[2] Lin KY, Tong P. Singular finite elements for the fracture analysis of V-notched plates. Int J Numer Methods Engng 1980;15:1343–54.
[3] Carpenter WC. A collocation procedure for determining fracture mechanics parameters at a corner. Int J Fract 1984;24:255–66.
[4] Chen D-H. Stress intensity factors for V-notched strip under tension or in-plane bending. Int J Fract 1995;70:81–97.
[5] Tong P, Pian THH, Lasry SJ. A hybrid-element approach to crack problems in plane elasticity. Int J Numer Methods Engng 1973;7:297–308.
[6] Williams ML. Stress singularities resulting from various boundary conditions in angular corners of plates in extension. ASME J Appl Mech 1952;19:526–8.
[7] Theocaris PS. The order of singularity at a multi-wedge corner of a composite plate. Int J Engng Sci 1974;12:107–20.
[8] Dempsey JP, Sinclair GB. On the singular behavior at the vertex of a bi-material wedge. J Elasticity 1981;11:317–27.
[9] Hein VL, Erdogan F. Stress singularities in a two-material wedge. Int J Fract 1971;7:317–30.
[10] Matsumto T, Tanaka M, Obara R. Computation of stress intensity factors of interface cracks based on interaction energy release rates and BEM sensitivity analysis. Engng Fract Mech 2000;65:683–702.

Please cite this article in press as: Treifi M, Oyadiji SO. Bi-material V-notch stress intensity factors by the fractal-like finite element method. Engng Fract Mech (2013), http://dx.doi.org/10.1016/j.engfracmech.2013.04.006

[11] Yuuki R, Cho SB. Efficient boundary element analysis of stress intensity factors for interface cracks in dissimilar materials. Engng Fract Mech 1989;34:179–88.
[12] Miyazaki N, Ikeda T, Soda T, Munakata T. Stress intensity factor analysis of interface crack using boundary elemental method application of contour-integral method. Engng Fract Mech 1993;45:599–610.
[13] Leung AYT, Wong SC. Two-level finite element method for plane cracks. Commun Appl Numer Methods 1989;5:263–74.
[14] Leung AYT, SU RKL. Mode I crack problems by fractal two level finite element methods. Engng Fract Mech 1994;48:847–56.
[15] Reddy RN, Rao BN. Continuum shape sensitivity analysis of fracture using fractal finite element mixed-mode method. Engng Fract Mech 2008;75:2860–906.
[16] Treifi M, Tsang DKL, Oyadiji SO. Applications of the fractal-like finite element method to sharp notched plates. ASME Conf Proc IDETC/CIE 2007;4:399–405.
[17] Treifi M, Oyadiji SO, Tsang DKL. Computations of modes I and II stress intensity factors of sharp notched plates under in-plane shear and bending loading by the fractal-like finite element method. Int J Solids Struct 2008;45:6468–84.
[18] Treifi M, Oyadiji SO, Tsang DKL. Computation of the stress intensity factors of sharp notched plates by the fractal-like finite element method. Int J Numer Methods Engng 2009;77:558–80.
[19] Treifi M, Oyadiji SO. Computations of SIFs for non-symmetric V-notched plates by the FFEM. ASME Conf Proc IDETC/CIE 2009;3:711–7.
[20] Treifi M, Oyadiji SO, Tsang DKL. Computations of the stress intensity factors of double-edge and centre V-notched plates under tension and anti-plane shear by the fractal-like finite element method. Engng Fract Mech 2009;76:2091–108.
[21] England AH. Complex variable methods in elasticity. New York: Wiley; 1971.
[22] Carpenter WC, Byers C. A path independent integral for computing stress intensities for V-notched cracks in a bi-material. Int J Fract 1987;35:245–68.
[23] Treifi M, Oyadiji SO. Strain energy approach to compute stress intensity factors for isotropic homogeneous and bi-material V-notches. Int J Solids Struct 2013. http://dx.doi.org/10.1016/j.ijsolstr.2013.03.011.
[24] Zuccarello B, Ferrante S. Use of automated photoelasticity to determine stress intensity factors of bimaterial joints. J Strain Anal Engng Des 2005;40:785–800.

Please cite this article in press as: Treifi M, Oyadiji SO. Bi-material V-notch stress intensity factors by the fractal-like finite element method. Engng Fract Mech (2013), http://dx.doi.org/10.1016/j.engfracmech.2013.04.006

Chapter 12

Discussions, Conclusions and Recommendations

12. Discussions, Conclusions and Recommendations

12.1. Discussions

In the course of this research, the FFEM was extended to evaluate the SIFs for isotropic homogeneous and bi-material V-notches under mode I, II and III loading conditions. This development regards a crack simply as a special case, because a crack is just a notch with a zero opening angle. This development has made the method more general because its applications were extended to compute SIFs resulting at singularity points for a wider range of engineering problems.

The FFEM is a semi-analytical method. It brings together the agility of the FEM and the accuracy of the exact analytical solutions. The necessity to use very fine meshes to model the singular regions around singular points leads to a large number of unknowns and a considerable increase of the computational cost of FE solutions. In the FFEM this is avoided by the employment of exact analytical expressions of a displacement field as global interpolation functions to transform the large number of nodal displacements of a singular region into a small set of generalised co-ordinates. This reduces the computational cost significantly. The SIFs and the coefficients of the higher order terms of the notch tip asymptotic field are the generalised co-ordinates that are computed directly in the FFEM. Therefore, no post-processing is required to extract them. Moreover, no special singular finite elements are needed to model the singular region around a notch tip as conventional finite elements can be used to model the whole of the cracked/notched body. As the transformation involves only simple matrix multiplications, the implementation of the FFEM into existing FEM codes is rather easy.

To extend the FFEM to computing SIFs for notches, the stress and displacement expressions were analytically derived for a homogeneous notch under in-plane conditions (mode I and II). The displacement expressions were used as GIFs in the FFEM to carry out the transformation of the nodal displacements of the nodes within a singular region. The accuracy of the results obtained for different single V-notched plates subjected to tension, shear, or bending loading conditions was very good compared to available published data or data obtained using numerical methods such as the FEM

The encouraging results obtained for the in-plane cases (modes I and II) demonstrated the potential of developing the method further to evaluate SIFs for other notch problems. Therefore, the stress and displacement expressions were analytically derived for a homogeneous notch under out-of-plane shear conditions (mode III). These were used as GIFs in the FFEM. The method was used to generate results for mode III SIFs and the accuracy of those was shown to be very good.

For both the in-plane and out-of-plane cases, the results were compared to available published results. When results were not available the results were compared to those obtained using the commercial FE software package ABAQUS. However, this was done only for crack problems because commercial FE packages are generally not capable of computing the SIFs for a general notch, and ABAQUS is no exception. In the ABAQUS simulation, similar meshes to the one used in the FFEM were used. Also, the elements around the crack tip were modelled using quarter-point crack-tip elements. Although similar meshes (and therefore similar numbers of nodes) were used in the FFEM and in the ABAQUS software, the number of equations that needed to be solved in the FFEM

was much smaller than that in ABAQUS, because of the transformation process of the nodal displacements of the singular nodes applied in the FFEM. This demonstrates an advantage of the FFEM.

In the FFEM, the property of self-similar elements was exploited too. It was shown that the element matrices of isoparametric two-dimensional FE elements are the same. Also, the transformation matrix of an inner layer in the singular region could be computed from that of the first layer. These two properties were exploited in the FFEM. Only the first layer of elements in the singular region is needed to generate all the inner layers of the singular region by using the sum of geometrical series. This property permits the discretisation of the singular region using virtually infinite number of layers of elements.

For bi-material notches the stress and displacement fields were derived for the out-of-plane case (mode III) and were used as GIFs in the FFEM. Different examples of different notch geometries and different material properties were analysed to validate the FFEM results. The mode III SIFs computed using the FFEM were compared to available published data or numerical solutions. Availability of published data is limited to crack problems only, and current commercial FE packages are also limited to crack problems. Therefore, the comparison was limited to bi-material crack problems only. Although this comparison proves sufficiently, to a certain degree, that the FFEM provides accurate results, the necessity to compare FFEM results, especially for the bi-material cases, with another method seemed advantageous to validate clearly the accuracy of the FFEM for analysing bi-material notches. Therefore, the SEA was developed. As it is based on the strain energy, it was used in conjunction with a commercial FE package, i.e., the ABAQUS software, to compute the SIFs for bi-material notches. This approach is quite

appealing, as it is easy to use in order to extract notch SIFs using commercial FE packages, which are not capable of computing SIFs of a general notch. The results for mode III SIFs of a general notch computed using the SEA agreed well with the corresponding values computed using the FFEM.

The encouraging results of the SEA led to exploring this approach further. It was extended and presented as a complete technique to compute SIFs for a general notch in isotropic or bi-material bodies under mode I, II and III conditions from FE solutions obtained using commercial FE packages. The accuracy of the approach was proven to very good.

Armed with a new approach to compute SIFs for bi-material notches, the FFEM was extended to analyse bi-material notches under mode I and II conditions (the in-plane case), following the analytical derivations of the stress and displacement expressions for a bi-material notch. The mode I and II SIFs computed for bi-material notches were compared to available published data and values computed using the ABAQUS software for crack problems and to SEA results for notch problems. The agreement between the results was very good.

For the in-plane problem of a bi-material notch, the transformation matrix for the inner layers in the singular region cannot be computed in terms of the transformation matrix of the first layer when the layers of elements in the singular region are constructed using a similarity ratio as is the case for all the previous cases. This is because the complex eigenvalues and their conjugates appear in the transformation matrix. Therefore, a finite

number of layers were used in the singular region instead of using the sum of a geometric series.

It was also shown that the size of the singular region has an effect on the results for the in-plane bi-material notch. For the other cases, it did not have any considerable effect. Similarly for the SEA, it was also shown that the size of the control volume (singular) has an effect on the results especially for mixed mode cases. Recommendations were made on the size of the singular region in the relevant chapters by carrying out convergence studies. Also, convergence studies were presented to determine the similarity ratio, the number of layers of elements to be used to model the singular region and the number of terms of the displacement series expansion to be used as GIFs in the FFEM.

Because the FFEM is based on the FEM, its results are mesh dependent as is the case in the FEM. Following the general advice for constructing good meshes in the FEM is sufficient to produce good results in the FFEM. The FFEM could be used to address other problems whether singular or not, especially when the conventional FEM has convergence problems or when the model is too large. The only limitation to the use of the FFEM is the availability of "good" global interpolation functions.

The SEA depends on the strain energy computed using FE software packages. Therefore, its results are mesh dependent, too. In addition, it is recommended to use fine meshes around the singular points especially for mixed mode cases.

To sum up, two procedures were developed to compute the SIFs for a general notch in isotropic and bi-material bodies. The first is a stand alone method, i.e., the FFEM, and the

second is a post-processing technique, i.e., the SEA, which can be used to extract the SIFs for a general notch from FE solutions produced using commercial FE packages. Both procedures produced accurate and new results.

12.2. Conclusions

The main findings of the research are as follows:

1. The analytical expressions of the stress and displacement fields around a notch tip in an isotropic homogeneous plate under mode I, II and III loading conditions were derived and used as global interpolation functions in the FFEM. The FFEM code was successfully extended to compute the SIFs for isotropic homogeneous notch. The accuracy of the results was shown to be very good compared to available publish data and numerical solutions.
2. Using a simple coordinate transformation, the FFEM code was extended to compute the SIFs for asymmetric isotropic homogeneous without the need for deriving new GIFs.
3. The analytical expressions of the stress and displacement fields around a notch tip in a bi-material body under mode I, II and III conditions were derived. It was found that the singular eigenvalues can assume real or complex values. The eigenvalues were computed successfully using a modified version of Muller's method to avoid Muller's method convergence to the same root at every step by using an incremental technique.
4. Using the displacement expressions of a bi-material notch as GIFs, the FFEM code was extended successfully to compute the SIFs for bi-material notch under

mode I, II and III conditions. The results obtained demonstrated very good accuracy with available published data and with numerical solutions.

5. A SEA was developed to extract the mode I, II and III SIFs values for isotropic homogeneous and bi-material notches from FE solutions computed using a commercial FE software package.
6. The results obtained using the FFEM agree well with corresponding results computed using the SEA. This gives more confidence of the accuracy of the FFEM, and also the SEA, to compute the SIFs values specifically for bi-material notches where published results were not available and current commercial FE packages are not capable of computing the SIFs of a general notch.

12.3. Recommendations for Future Work

1. The FFEM and the SEA could be extended to compute the plastic SIFs for notches.
2. As notches/corners are not always sharp, considering extending the FFEM and the SEA to compute the SIFs for blunt (rounded) notch is of high relevance.
3. It would be beneficial to extend the application of the FFEM to compute notch SIFs for bodies subject to dynamic loading. The SEA could also be used to compute dynamic SIFs.
4. As materials are not always isotropic, it would be good development to extend the FFEM and SEA to compute SIFs for an anisotropic notch.
5. A significant development of the FFEM would be its extension to compute the SIFs for three dimensional notched bodies.

6. The FFEM method is not limited to singularity problems. Other problems whether singular or not can be addressed, especially when the conventional FEM has convergence problems or when the model is too large, provided the availability of good global interpolation functions.

References

Aliabadi, M.H., Rooke, D.P., 1991. Numerical Fracture Mechanics. Kluwer Academic Publishers, Dordrecht.

Anderson, T.L., 1995. Fracture Mechanics: Fundamentals and Applications, 2nd ed. CRC Press LLC, London.

Atluri, S.N., 1986. Computational Methods in the Mechanics of Fracture. Elsevier Science Publishers, Oxford.

Babuška, I., Miller, A., 1984. The post-processing approach in the finite element method-part 2: calculation of the stress intensity factors. International Journal for Numerical Methods in Engineering; 20: 1111–1129.

Barenblatt, G.I., 1962. The mathematical theory of equilibrium cracks in brittle fracture. Advances in Applied Mechanics; 7: 55-129.

Barsoum, R.S., 1976a. On the use of isoparametric finite elements in linear fracture mechanics. International Journal for Numerical Methods in Engineering; 10(1): 25-37.

Barsoum, R.S., 1976b. A degenerate solid element for linear fracture analysis of plate bending and general shells. International Journal for Numerical Methods in Engineering; 10: 551-564.

Berto, F., Lazzarin, P., 2007. Relationships between J-integral and the strain energy evaluated in a finite volume surrounding the tip of sharp and blunt V-notches. International Journal of Solids and Structures; 44: 4621–4645.

Carpenter, W.C., 1984. A collocation procedure for determining fracture mechanics parameters at a corner. International Journal of Fracture; 24: 255–266.

Carpenter, W.C., Byers, C., 1987. A path independent integral for computing stress intensities for V-notched cracks in a bi-material. International Journal of Fracture; 35: 245-268.

Carpinteri, A., Cornetti, P., Pugno, N., Sapora, A., Taylor, D., 2008. A finite fracture mechanics approach to structures with sharp V-notches. Engineering Fracture Mechanics; 75: 1736–1752.

Chen, D.-H., 1995. Stress intensity factors for V-notched strip under tension or in-plane bending. International Journal of Fracture; 70: 81–97.

Chen, M.C., Sze, K.Y., 2001. A novel hybrid finite element analysis of bimaterial wedge problems. Engineering Fracture Mechanics; 68: 1463-1476.

Chidgzey, S.R., Deeks, A.J., 2005. Determination of coefficients of crack tip asymptotic fields sing the scaled boundary finite element method. Engineering Fracture Mechanics; 72: 2019–2036.

Coker, E.G., Filon, L.G.N., 1931. A Treatise on Photoelasticity. Cambridge University Press, London.

Cotterell, B., Rice, J. R., 1980. Slightly curved or kinked cracks. International Journal of Fracture; 16(2): 155-169.

Dempsey, J.P., Sinclair, G.B., 1981. On the singular behavior at the vertex of a bi-material wedge. Journal of Elasticity; 11: 317–327.

Dhondt, G., 1994. Stability of collapsed 8-node 2-D and 20-node 3-D isoparametric finite elements. International Journal for Numerical Methods in Engineering; 37: 475-496.

Dugdale, D.S., 1960. Yielding in steel sheets containing slits. Journal of the Mechanics and Physics of Solids; 8: 100-104.

England, A.H., 1971. Complex Variable Methods in Elasticity. Wiley, New York.

Gómez, F.J., Elices, M., 2003. A fracture criterion for sharp V-notched samples. International Journal of Fracture; 123: 163–175.

Griffith, A.A., 1920. The phenomena of rupture and flow in solids. Philosophical Transactions of the Royal Society of London. Series A; 221: 163-198.

Gross, B., Mendelson, A., 1972. Plane elastostatic analysis of V-notched plates. International Journal of Fracture; 8: 267–276.

Hein, V.L., Erdogan, F., 1971. Stress singularities in a two-material wedge. International Journal of Fracture; 7: 317–330.

Hellen, T.K., 1975. On the method of virtual crack extensions. International Journal for Numerical Methods in Engineering; 9: 187-207.

Hui, C.Y., Ruina, A., 1995. Why K? High order singularities and small scale yielding. International Journal of Fracture; 72: 97–120.

Inglis, C.E., 1913. Stresses in a plate due to the presence of cracks and sharp comers. Transactions of the Institute of Naval Architects; 55: 219-241.

Irwin, G.R., 1948. Fracture dynamics, fracturing of metals. American Society for Metals. Cleveland; 147-166.

Irwin, G.R., 1957. Analysis of stresses and strains near the end of a crack transversing a plate. ASME Journal of Applied Mechanics; 24: 361-364.

Irwin, G.R., 1961. Plastic zone near a crack and fracture toughness. Sagamore Research Conference Proceedings. Syracuse University Research Institute, Syracuse, NY; 4: 63-78.

Jun, Q., Yuqiu, L., 1992. Sub-region mixed fem for calculating stress intensity factor of antiplane notch in bi-material. Engineering Fracture Mechanics; 43: 1003-1007.

Karihaloo, B.L., Xiao, Q.Z., 2001. Accurate determination of the coefficient of elastic crack tip asymptotic field by a hybrid crack element with p-adaptivity. Engineering Fracture Mechanics; 68: 1609–1630.

Knésl, Z., 1991. A criterion of V-notch stability. International Journal of Fracture; 48: R79–83.

Kobayashi, A.S., 1973. Experimental Techniques in Fracture Mechanics. SESA.

Lazzarin, P., Zambardi, R., 2001. A finite-volume-energy based approach to predict the static and fatigue behavior of components with sharp V-shaped notches. International Journal of Fracture; 112: 275–298.

Lazzarin, P., Berto, F., Zappalorto, M., 2010. Rapid calculations of notch stress intensity factors based on averaged strain energy density from coarse meshes: Theoretical bases and applications. International Journal of Fatigue; 32: 1559–1567.

Lee, K.Y., Choi, H.J., 1988. Boundary element analysis of stress intensity factors for bimaterial interface cracks. Engineering Fracture Mechanics; 29: 461-472.

Lee, K.W., Earmme, Y.Y., 2000. An interfacial edge crack in anisotropic bimaterial under anti-plane singularity. International Journal of Fracture; 104: 15–22.

Leung, A.Y.T., Cheung, Y.K., 1981. Dynamic analysis of frames by a two-level finite element method. Journal of Sound and Vibration; 74: 1-9.

Leung, A.Y.T., Su, R.K.L., 1994. Mode I crack problems by fractal two level finite element method. Engineering Fracture Mechanics; 48(6): 847-856.

Leung, A.Y.T., Su, R.K.L., 1995a. Mixed-mode two dimensional crack problem by fractal two level finite element method. Engineering Fracture Mechanics; 51(6): 889-895.

Leung, A.Y.T., Su, R.K.L., 1995b. Body-force linear elastic stress intensity factor calculation using fractal two level finite element method. Engineering Fracture Mechanics; 51(6): 879-888.

Leung, A.Y.T., Su, R.K.L., 1996a. Fractal two-level finite element method for cracked Kirchhoff's plates using DKT elements. Engineering Fracture Mechanics; 54(5): 703-711.

Leung, A.Y.T., Su, R.K.L., 1996b. Fractal two level finite element analysis of cracked Reissner's plate. Thin-Walled Structures; 24: 315-334.

Leung, A.Y.T., Su, R.K.L., 1998. Two-level finite element study of axisymmetric cracks. International Journal of Fracture; 89: 193-203.

Leung, A.Y.T., Tsang, K.L., 2000. Mode III two-dimensional crack problem by two-level finite element method. International Journal of Fracture; 102: 245-258.

Leung, A.Y.T., Wong, S.C., 1988. Two-level finite element method for plates subjected to concentrated loads. Computer-Aided Civil and Infrastructure Engineering; 3: 126-127.

Leung, A.Y.T., Wong, S.C., 1989. Two-level finite element method for plane cracks. Communications in Applied Numerical Methods; 5: 263-274.

Leung, A.Y.T., Wong, S.C., 1992. Two-level finite element method for thin plate vibration subject to concentrated harmonic loads. Journal of Sound and Vibration; 152(1): 95-105.

Li, X.-F., 2001. Closed-form solution for a mode-III interface crack between two bonded dissimilar elastic layers. International Journal of Fracture; 109: L3-L8.

Li, X.-F., Duan, X.-Y., 2006. An interfacially-cracked orthotropic rectangular bi-material subjected to antiplane shear loading. Applied Mathematics and Computation; 174: 1060–1079.

Lin, K.Y., Mar, J.W., 1976. Finite element analysis of stress intensity factors for cracks at a bi-material interface. International Journal of Fracture; 12: 521-531.

Lin, K.Y., Tong, P., 1980. Singular finite elements for the fracture analysis of V-notched plates. International Journal for Numerical Methods in Engineering; 15: 1343–1354.

Liu, C.-I., Chue, C.-H., 2006. On the stress singularity of dissimilar anisotropic wedges and junctions in antiplane shear. Computers and Structures; 73: 432–442.

Matsumto, T., Tanaka, M., Obara, R., 2000. Computation of stress intensity factors of interface cracks based on interaction energy release rates and BEM sensitivity analysis. Engineering Fracture Mechanics; 65: 683-702.

Mote, C.D., 1971. Global-local finite element. International Journal for Numerical Methods in Engineering; 3: 565–574.

Musknelishvili, N.L., 1953. Some Basic Problems of the Mathematical Theory of Elasticity. Noordhoff, Leyden.

Noda, N.-A., Takase, Y., 2003. Generalized stress intensity factors of V-shaped notch in a round bar under torsion, tension, and bending. Engineering Fracture Mechanics; 70: 1447–1466.

Portela, A., Aliabadi, M.H., Rooke, D.P., 1991. Efficient boundary element analysis of sharp notched plates. International Journal for Numerical Methods in Engineering; 32: 445–470.

Press, W.H., Teukolsky, S.A., Vetterling, W.T., Flannery, B.P., 2007. Numerical Recipes the Art of Scientific Computing, 3rd Ed. Cambridge University Press, Cambridge.

Reddy, R.M., Rao, B.N., 2008a. Stochastic fracture mechanics by fractal finite element method. Computer Methods in Applied Mechanics and Engineering; 198: 459-474.

Reddy, R.M., Rao, B.N., 2008b. Fractal. Finite element method based shape sensitivity analysis of mixed-mode fracture. Finite Elements in Analysis and Design; 44: 875-888.

Rice, J.R., 1968. A path independent integral and the approximate analysis of strain concentration by notches and cracks. ASME Journal of Applied Mechanics; 35: 379-386.

Seweryn, A., 1994. Brittle fracture criterion for structures with sharp notches. Engineering Fracture Mechanics; 47: 673–681.

Sih, G.C., 1974a. Strain-energy-density factor applied to mixed mode crack problems. International Journal of Fracture; 10(3): 305-321.

Sih, G.C., Macdonald, B., 1974b. Fracture mechanics applied to engineering problems-strain energy density fracture criterion. Engineering Fracture Mechanics; 6: 361-386.

Sih, G.C., 1981. Mechanics of Fracture 7: Experimental Evaluation of Stress Concentration and Intensity Factors. Martinus Nijhoff publishers, The Hague.

Sneddon, I.N., 1946. The distribution of stress in the neighbourhood of a crack in an elastic solid. Proceeding of the Royal Society of London; A187: 229-260.

Sneddon, I.N., Lowengrub, M., 1969. Crack problems in classical theory of elasticity. John Wiley & sons, Inc..

Stern, M., Becker, E.B., Dunham, R.S., 1976. A contour integral computation of mixed-mode stress intensity factors. International Journal of Fracture; 12: 359–368.

Tan, M.A., Meguid, S.A., 1997. Analysis of bimaterial wedges using a new singular finite element. International Journal of Fracture; 88: 373–391.

Theocaris, P.S., 1974. The order of singularity at a multi-wedge corner of a composite plate. International Journal of Engineering Science; 12: 107–120.

Tong, P., Pian, T.H.H., 1973. On the convergence of the FEM for problems with singularity. International Journal of Solids and Structures; 9: 313–321.

Tong, P., Pian, T.H.H., Lasry, S.J., 1973. A hybrid-element approach to crack problems in plane elasticity. International Journal for Numerical Methods in Engineering; 7: 297–308.

Treifi, M., Oyadiji, S.O., Tsang, D.K.L., 2008. Computations of modes I and II stress intensity factors of sharp notched plates under in-plane shear and bending loading by the fractal-like finite element method. International Journal of Solids and Structures; 45: 6468–6484.

Treifi, M., Oyadiji, S.O., Tsang, D.K.L., 2009a. Computation of the stress intensity factors of sharp notched plates by the fractal-like finite element method. International Journal for Numerical Methods in Engineering; 77: 558–580.

Treifi, M., Oyadiji, S.O., Tsang, D.K.L., 2009b. Computations of the stress intensity factors of double-edge and centre V-notched plates under tension and anti-plane shear by the fractal-like finite element method. Engineering Fracture Mechanics; 76: 2091–2108.

Treifi, M., Oyadiji, S.O., 2009c. Computations of SIFs for non-symmetric V-notched plates by the FFEM. ASME Conference Proceedings IDETC/CIE2009; 3: 711-717.

Treifi, M., Oyadiji, S.O., 2013a. Evaluation of mode III stress intensity factors for bi-material notched bodies using the fractal-like finite element method. Computers and Structures. http://dx.doi.org/10.1016/j.compstruc.2013.02.015.

Treifi, M., Oyadiji, S.O., 2013b. Strain energy approach to compute stress intensity factors for isotropic homogeneous and bi-material V-notches. International Journal of Solids and Structures; 50: 2196-2212. http://dx.doi.org/10.1016/j.ijsolstr.2013.03.011.

Treifi, M., Oyadiji, S.O., 2013c. Bi-material V-notch stress intensity factors by the fractal-like finite element method. Engineering Fracture Mechanics. http://dx.doi.org/10.1016/j.engfracmech.2013.04.006.

Tsang, D.K.L., Oyadiji, S.O., Leung, A.Y.T., 2004. Applications of numerical eigenfunctions in the fractal-like finite element method. International Journal for Numerical Methods in Engineering; 61: 475-495.

Vasilopoulos, D., 1988. On the determination of higher order terms of singular elastic stress fields near corners. Numerische Mathematik; 53: 51–95.

Wells, A.A., 1961. Unstable crack propagation in metals: cleavage and fast fracture. Proceedings of the Crack Propagation Symposium, Cranfield; 1: 210-230.

Westergaard, H.M., 1939. Bearing pressures and cracks. Journal of Applied Mechanics; 6: 49-53.

Williams, M.L., 1952. Stress singularities resulting from various boundary conditions in angular corners of plates in extension. ASME Journal of Applied Mechanics; 19: 526-528.

Williams, M.L., 1957. On the stress distribution at the base of a stationary crack. ASME Journal of Applied Mechanics; 24: 109-114.

Wolf, J.P., 2003. The Scaled Boundary Finite Element Method. Wiley, Chichester.

Wu, K.-C., Chiu, Y.-T., 1991. Antiplane shear interface cracks in anisotropic bimaterials. Journal of Applied Mechanics; 58: 399-403.

Xiao, Q.Z., Karihaloo, B.L., Liu, X.Y., 2004. Direct determination of SIF and higher order terms of mixed mode cracks by a hybrid crack element. International Journal of Fracture; 125: 207–225.

Xiao, Q.Z., Karihaloo, B.L., 2007. An overview of a hybrid crack element and determination of its complete displacement field. Engineering Fracture Mechanics; 74: 1107–1117.

Xie, J.F., Fok, S.L., Leung, A.Y.T., 2003. A parametric study of the fractal finite element method for two-dimensional crack problems. International Journal for Numerical Methods in Engineering; 58: 631-642.

Yau, J.F., Wang, S.S., 1984. An analysis of interface cracks between dissimilar isotropic materials using conservation integrals in elasticity. Engineering Fracture Mechanics; 20: 423-432.

Zhang, X.S., 1988. The general solution of an edge crack off the center line of a rectangular sheet for mode III. Engineering Fracture Mechanics; 31(5): 847–855.

Zhao, Z., Hahn, H.G., 1992. Determining the SIF of a V-notch from the results of a mixed-mode crack. Engineering Fracture Mechanics; 43: 511–518.